esa SP-1176/I

New Views of the Earth

Scientific Achievements of ERS-1

esa

esa SP-1176/I
ISBN 92-9092-141-2
April 1995

NEW VIEWS OF THE EARTH

Scientific Achievements of ERS-1

DEFENCE RESEARCH AGENCY

esa

EUROPEAN ESYS SYSTEMS

ESA SP-1176/I Scientific Achievements of ERS-1

Prepared by:	ESYS Limited, Guildford, UK
Published by:	ESA Publications Division ESTEC, Noordwijk, The Netherlands
Editor:	Tan-Duc Guyenne
Layout:	Carel Haakman

ISBN 92-9092-141-2

(Printed in The Netherlands, April 1995)

CONTENTS

Preface

On 17 July 1991, the European Space Agency (ESA) launched the first European Remote-sensing Satellite (ERS-1). ESA's original objectives for this mission were both scientific and economic. The three primary objectives were to:

- *Increase our scientific understanding* of coastal zones, global ocean processes and polar regions. Major contributions to the World Climate Research Programme were foreseen and it was anticipated that the data, used in conjunction with in situ or other satellite measurements would enable significant advances to be made in physical oceanography, glaciology and climatology;

- *Develop and promote economic and commercial applications.* Based on an improved knowledge of ocean parameters and sea-state conditions, surveillance and planning of coastal and marine activities world-wide was defined as a primary target for applications development.

- *Explore the potential of radar data* for land process studies and applications.

At the time of the ERS-2 launch, ESA has embarked on a major review of the achievements of the ERS-1 mission. These achievements are considered within the context of the original scientific and economic application objectives. The high standards of enabling engineering and technology which have been attained by European and Canadian industry are also recognised. A series of three documents presents highlights from the full range of achievements of the ERS-1 mission.

I. *Scientific achievements of ERS-1*
II. *Operational application achievements of ERS-1*
III. *Engineering and industrial achievements of ERS-1*

This first document concentrates on the scientific achievements. Its purpose is to present examples of high quality scientific work which clearly demonstrate that ERS-1 data are being used extensively within the international science community. These data have stimulated an impressive range of scientific investigations in oceanography, polar science, glaciology and atmospheric and climate research that is surpassing the original expectations. Significant progress in the use of ERS-1 data in the land and solid Earth sciences is also evident. Volumes II and III will be published during 1995-96.

The findings presented here are preliminary. The international science community continues to work with the data from the ERS missions, investigating new fields of global environmental research and consolidating existing results as a basis for future economic applications. International cooperation, which also involves researchers in developing countries and eastern Europe, is addressing key environmental concerns across the globe. I am grateful to those members of the science community who have contributed to this review and look forward confidently and with interest to the results of this ongoing activity.

Guy Duchossois
ERS-1/2 Mission Manager

1. THE SCIENTIFIC OBJECTIVES

1.1. The importance of scientific results

ENVIRONMENTAL POLICY

Mankind is facing a growing number of environmental concerns. Among these the response to global warming, changes in weather patterns, melting of the polar ice caps, rising sea levels, pollution, desertification and natural hazards are increasingly issues of concern for policy makers and the general public alike.

Our current knowledge of the global Earth system is not adequate to predict changes with the accuracy required for the development of effective response strategies. Progress has certainly been made in key areas of research, but this suffers from a lack of high quality observations. There are insufficient data to develop and test models on the underlying processes controlling the atmospheric, ocean, terrestrial, cryospheric and solid Earth systems. ERS-1 provides global and repetitive observations which are being used by scientists as they tackle many of these issues.

Government and the general public require evidence and predictions of environmental change to support national and global policies. These requirements are best served by ensuring that ERS-1 data are fully utilised by scientists to improve our understanding of the global environment.

OPERATIONAL AND ECONOMIC APPLICATIONS

The original emphasis for the ERS-1 mission was oriented towards oceans and ice monitoring. It was intended as an experimental/pre-operational system forming the basis for Europe and Canada to move towards a fully operational system, justified in the longer term on the grounds of direct economic benefit resulting from the services provided.

The primary industries which were originally expected to benefit from ERS-1 included off-shore, shipping and fisheries. With more experience in using the data, the potential markets which could benefit are much broader than this, encompassing agribusiness, utilities, oil, gas and mineral exploration, civil engineering and telecommunications. The most highly valued services are forecasts and mapping products. The development and operationalisation of the latter demands high quality information which has been reliably derived from the satellite data. In addition, improved forecasts demand a deeper understanding of processes and the development of models achieved through the normal procedures of scientific enquiry.

The long-term interests of prospective operational/commercial users are therefore best served by ensuring that the highest quality science is achieved with ERS-1 data.

FULFILLING THE NEED

To fulfil economic and environmental needs, the science community which is using ERS data is addressing a broad range of investigations across many discipline areas. However, whatever the discipline, the type of activity can be considered in three distinct areas of scientific enquiry:

- Observing, discriminating and mapping of environmental variables;
- Compiling and using datasets for process investigations and for monitoring change over time;
- Using the improved process understanding and integrating data with complementary sources to help develop, test and apply models.

A preliminary assessment of the extent to which ERS-1 is contributing to development in each of these areas can be based on the examples of work included in this document.

1.2. ERS-1 mission objectives

The key scientific disciplines which were targeted by the original ERS-1 mission objectives were:

OPEN OCEANS
- Global ocean circulation, its variability & associated transfers of energy;
- Ocean/atmosphere interactions;
- Ocean tides.

REGIONAL SEAS
- Exploratory scientific studies and the development of forecast models for the Mediterranean, North Sea and other enclosed European seas;
- Observing coastal processes and shallow water bathymetry.

POLAR OCEANS
- Coupling between the North Atlantic and Arctic Ocean;
- Marine ice sheet instabilities, particularly in the West Antarctic Ice Sheet;
- Variability in sea ice cover and its influence on climate.

LAND-ICE
- Growth, decay and dynamics of ice sheets.

Chapters 2 to 5 of this document present highlights from achievements in each of these areas. Within these chapters, and also within chapters 6 & 7, achievements in many more scientific disciplines than were originally targeted by the mission are also presented, notably:

- Measuring the structure of atmospheric phenomena including tropical cyclones, monsoons, lee waves and boundary layer rolls;
- Contributing to the generation of climatological databases;
- Providing data for terrestrial scientists involved in modelling crop growth and agricultural productivity, deforestation, hydrologic processes, geology and geomorphology;
- Measuring the shape of the Earth and the associated gravitational features;
- Detecting the shape of the ocean bed under sea ice allowing a better understanding of the tectonic history;
- Detecting surface movements associated with earthquakes and volcanoes.

Figure 1.1 provides a guide to the various scientific achievements presented in this document, against the original objectives and against additional areas of science which have emerged since the start of the ERS-1 mission.

This document presents a selection of the scientific achievements made using ERS-1. Each chapter is divided according to the parameters measured using ERS-1 data and an introduction to each chapter and each parameter is provided. The achievements are discussed through a Figure and an extended caption. More detailed results can be found in the proceedings of the First and Second ERS-1 Symposia held in Cannes, France, 4-6 November 1992 (*ESA SP-359*) and in Hamburg, Germany, 11-14 October 1993 (*ESA SP-361*).

1.3. ERS-1 observations

SENSORS

Contributing to scientific study, the ERS-1 satellite carries a number of different but complementary sensors as described below.

Active Microwave Instrumentation (AMI). This comprises two separate radars:

- Synthetic Aperture Radar (SAR). In image mode, a high-resolution imaging radar capability provides the facility for all weather, day and night imaging of the Earth's surface. In wave mode, this instrument can be used to measure two dimensional spectra of ocean surface waves;

- Scatterometer. A radar instrument designed to measure sea surface wind speed and direction at the ocean surface, which is also being used for land applications where backscatter is being correlated with surface cover.

Radar altimeter. This provides accurate sea and ice surface elevation. Information on significant wave heights, various ice parameters, an estimate of sea surface wind speed and gravity information from the seabed can also be derived.

Along-Track Scanning Radiometer (ATSR). An infrared instrument which provides measurements of sea surface temperature, as well as cloud top temperature, cloud cover, water vapour and land surface temperature.

OPERATIONAL CAPABILITIES

Some of the ERS-1 instruments can only operate for a limited time within each orbit. The SAR in image mode can only be operated for approximately 12 minutes per orbit and its profile is built around user requests, complemented with a baseline planning strategy to achieve full coverage within the visibility of ground stations. The scatterometer can only be used when the SAR is not operating. The low-bit rate instruments (radar altimeter, scatterometer and SAR in wave mode) are being operated to provide global coverage, with an observation priority of oceans, permanent ice sheets and then land. The ATSR observations are practically continuous.

The areas of the Earth's surface which are observed from each of the instruments are shown in Figure 1.2. This illustrates that for any orbital point, there is limited overlap in data collection.

Figure 1.1. An introduction to the document structure based on the original science objectives for ERS-1. Areas of scientific research which have emerged during the mission are shown in italics.

MISSION OBJECTIVES	Chapter 2 Global ocean and atmosphere	Chapter 3 Regional ocean and atmosphere	Chapter 4 Sea ice
OPEN OCEANS			
Global ocean circulation modelling	Wind stress (2.3) Topography (2.10, 2.11, 2.12, 2.13) Surface temperature (2.16)	Fronts (3.9) Eddies (3.10, 3.11, 3.12, 3.13) Internal waves (3.14, 3.15, 3.16)	
Ocean-atmosphere interactions	Surface winds (2.1, 2.2, 2.4, 2.5) Surface waves (2.6, 2.7, 2.8)		
Detection of atmospheric parameters	*Atmospheric aerosols (2.19, 2.20)* *Ocean tides (2.14, 2.15)*	*Tropical cyclones (3.1, 3.2, 3.3)* *Monsoons (3.4)* *Storm structure (3.5)* *Katabatic winds (3.6)* *Gravity waves (3.7, 3.8)* *Boundary layer rolls (3.9)*	
Contribution to climatology databases	*Surface waves (2.9)* *Surface temperature (2.17, 2.18)*		
REGIONAL SEAS			
Processes in regional seas		North Sea (3.25) Mediterranean Sea (3.26)	
Coastal zones		Tidal features (3.17, 3.18) Erosion and sedimentation (3.19, 3.20) Bathymetry (3.21, 3.22, 3.23) Slicks (3.9, 3.34)	
POLAR OCEANS			
Coupling between the North Atlantic and Arctic Oceans			Ocean ice interaction (4.2, 4.14, 4.15)
Marine ice sheet instabilities			Iceberg characteristics (4.5)
Sea ice cover			Cover and extent (4.1, 4.3, 4.4, 4.6) Fluxes (4.11, 4.12, 4.13)
Sea ice motion			*Arctic (4.7, 4.8, 4.9)* *Antarctic (4.10)*

MISSION OBJECTIVES	Chapter 5 Glacialogy and snow	Chapter 6 Land	Chapter 7 The Earth's dynamic crust
LAND ICE			
Land ice sheets	Ice margins & condition (5.1, 5.2, 5.3, 5.4) Elevation models (5.5, 5.6, 5.7, 5.8) Ice sheet dynamics (5.9, 5.10, 5.11)		
Temperate glaciers	*Small ice sheets (5.12, 5.13)* *Snow cover (5.14)*		
LAND			
Status of vegetation		*Global (6.1)* *Crops (6.2, 6.3, 6.4, 6.5, 6.6)*	
Forestry		*Change detection (6.7, 6.8, 6.9)* *Carbon cycle (6.10, 6.11)*	
Surface hydrology		*Floodwater mapping (6.12, 6.13)* *Wetlands (6.14, 6.15)* *Soil moisture (6.16)*	
Geology and geomorphology		*Mapping (6.17, 6.18, 6.19, 6.20)*	
Cartography		*Elevation models (6.21, 6.22)* *Mosaicing (6.23, 6.24, 6.25, 6.26)*	
SOLID EARTH			
The Earth's shape			*Geoid (7.1, 7.2, 7.3)*
Tectonic structures			*Under the polar ocean (7.4, 7.5, 7.6, 7.7, 7.8)*
Geological structures			*Continental spreading (7.9)* *Tectonics (7.10, 7.11, 7.12)*
Earthquakes and volcanoes			*Mapping (7.13, 7.14, 7.15, 7.16, 7.17, 7.18)*

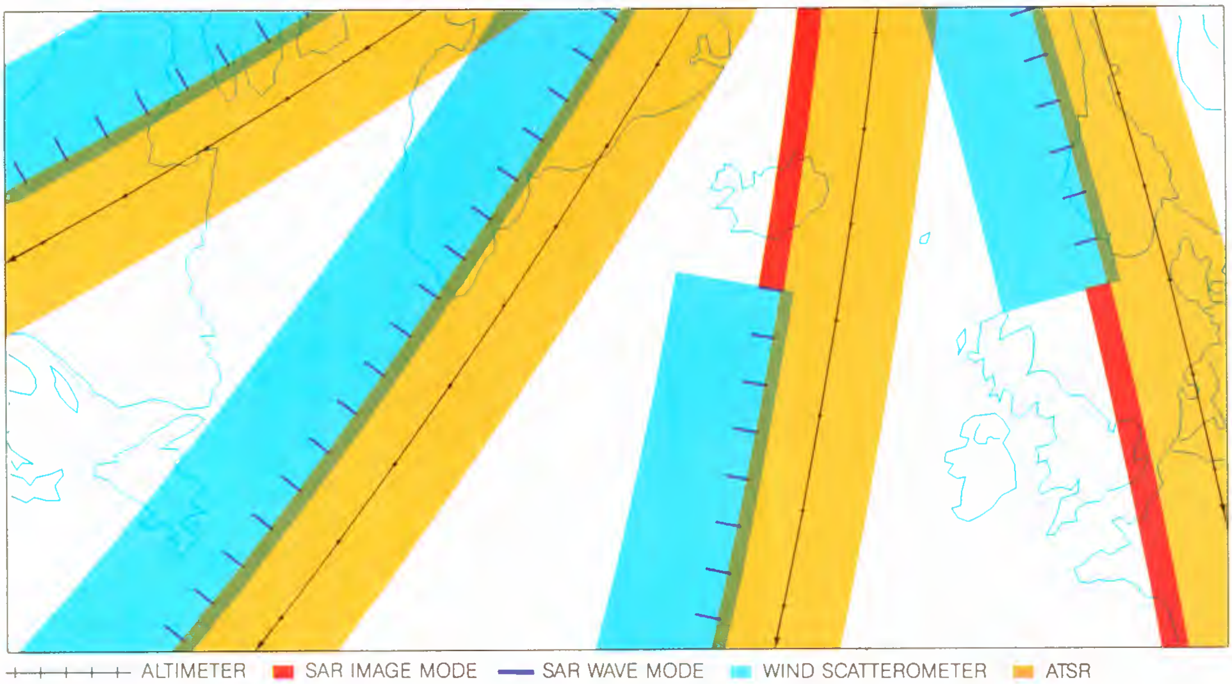

Figure 1.2. Comparison of the swath coverage for different instrument measurement modes.

MISSION PHASES

The ERS-1 mission has been divided into a number of mission phases. Each phase is a period where the orbit characteristics and priorities for sensor operations are set for a specific objective and left unchanged. These were designed to enable the various mission objectives to be achieved.

The first two phases covered the launch, early orbit and commissioning periods which were successfully completed by 12 December 1991. Since this time, the main mission phases have been as follows:

- First ice phase (December 1991 to March 1992). Optimised for Arctic ice experiments, this phase was characterised by a 3-day repeat cycle with high repetition, especially of SAR data in the polar and marginal ice zone;

- Multi-disciplinary phase (April 1992 to December 1993). This provided a 35-day repeat cycle with a much greater density of radar altimeter data and at least twice the frequency of coverage of SAR imaging at middle and high latitudes;

- Second ice phase (January to March 1994). This had the same characteristics as the first ice phase;

- Geodetic phase (April 1994 to March 1995). Two 168-day repeat cycles, one shifted 8 km from the other, allowed a high density of altimeter measurements to be recorded improving the availability of data for solid Earth applications. The SAR followed a similar profile to the multi-disciplinary phase;

- Second multi-disciplinary phase (April 1995 to the end of the mission). This has the same characteristics as the first multi-disciplinary phase.

More detailed information about the ERS-1 system can be found in *ESA SP-1146*.

2. GLOBAL OCEAN AND ATMOSPHERE

The ocean exerts a major influence on the Earth's meteorology and climate through its links with the atmosphere. Understanding the transfers of moisture and energy between ocean and atmosphere is therefore a scientific priority. Improved observations are needed to develop our understanding and thus to improve the forecasting accuracy for weather, marine conditions and also longer term climate change. The controlling processes are highly complex and fundamental discoveries about key features of the general circulation are still being made.

The scales which characterise processes at the ocean/ atmosphere boundary layer range from seconds to days and from metres to hundreds of kilometres. Still longer time and space scales govern the dynamics of ocean currents. To provide satisfactory observations using only ships, buoys and other in situ methods is therefore both difficult and expensive. For many parts of the world, data may be unavailable, inaccurate or inconsistent, causing large uncertainties to exist. Satellite observation can thus provide a valuable global data source which can be used together with the in situ data.

Consequently, ocean and ocean/atmosphere research was one of the primary objectives for the ERS-1 programme and all the sensors have contributed to our understanding in these disciplines.

In summary, ERS-1 is providing:

- Ocean surface wind field measurements at a high spatial resolution not previously available;
- Global information on two dimensional ocean surface waves and information on wave height for assimilation into wave models;
- Ocean topography data capable of mapping large-scale dynamic features such as ocean currents, the El Niño phenomena and Rossby waves;
- Sea surface temperature data at an increased accuracy compared with alternative data sources;
- Information on atmospheric aerosols;
- Measurements of total atmospheric column water vapour content.

ERS-1 data are input to operational models for short-term weather and marine forecasts. As well as providing improved spatial and temporal coverage compared with previous missions, the availability of some data products within three hours of observation has been a welcome additional capability for this user community.

ERS-1 data can also be used to support climate models whose outputs together with historical air and sea temperature observations have fostered recent concern about global warming.

2.1. Ocean surface winds

A major feature of the interaction between the ocean and the atmosphere is the creation of waves and ocean currents by surface winds. Wind stress exerted on the surface of the ocean is the major force driving ocean circulation.

Changes in the patterns of ocean current systems are known to influence regional weather and climate. They can also influence the global climate. As a result, knowing the characteristics of ocean surface winds is a fundamental requirement for research at all scales. Information on the wind stress and variations in its patterns is thus directly relevant for weather forecasting and climate prediction.

Conventional surface wind measurements are made by ships and buoys. Inevitably these are sparsely distributed, particularly in remote areas such as the Southern Ocean. Furthermore, for most applications, a regular area-averaged wind measurement is required.

ERS-1 obtains surface wind measurements from two instruments, the radar altimeter and scatterometer. The altimeter measures wind speed for areas directly below the satellite, while the scatterometer provides both wind speed and direction over a swath of 500 km width. These instruments provide complementary measurements and global coverage, both achieve a high level of consistency compared to in situ measurements because in each case, observations are made by a single instrument.

There are three areas of science in which examples of ERS-1 contributions are given below. These are:

- Improved weather analyses
- Higher quality data for ocean circulation modelling
- Identification of features not previously resolved.

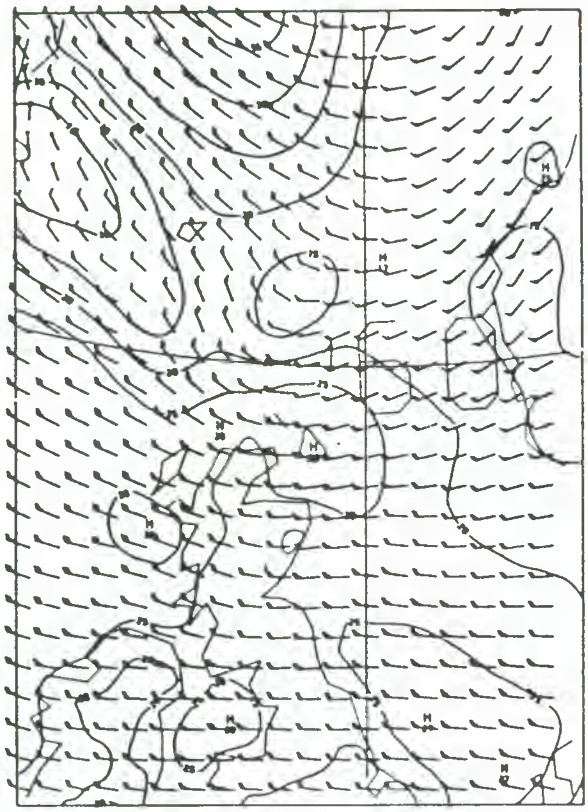

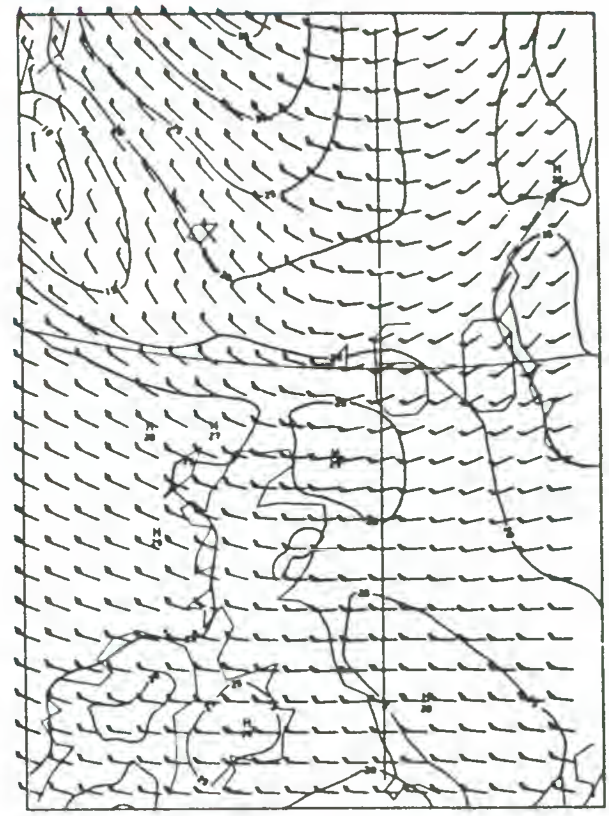

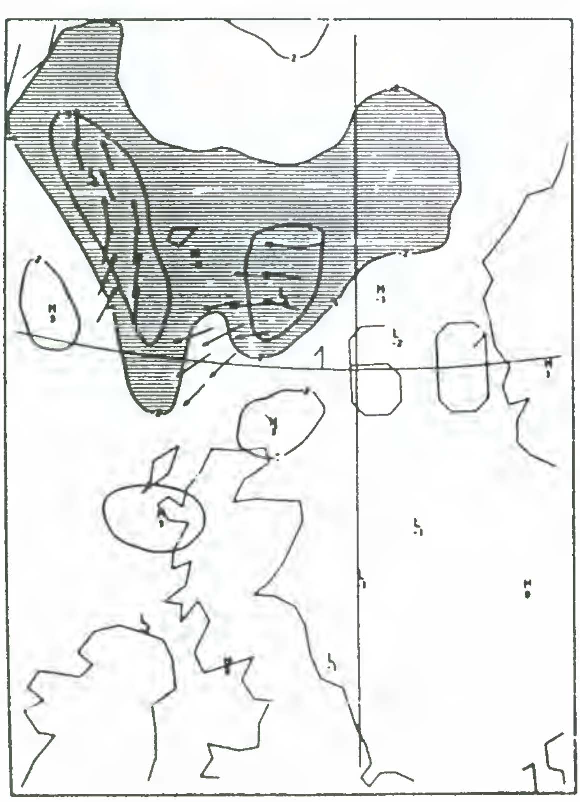

Figure 2.1 a,b,c. Data from ERS-1 are being assimilated into numerical weather forecasting models to improve the accuracy of the wind fields over the ocean. The contribution made by ERS-1 data to weather forecasting can be measured by comparing forecasts with ERS-1 data to those without. Figure a shows the winds at 10 m above the sea surface from an analysis containing ERS-1 scatterometer data while Figure b uses the same analysis without ERS-1 scatterometer data. Figure c shows the differences between the two fields. The differences represent the effects of additional resolution provided by the ERS-1 scatterometer. Small errors in the initial data fields can grow significantly over medium- and long-range forecasts. As a result, even small improvements in the initial data can give rise to significant forecast improvements.

The results of an initial assessment by the UK Meteorological Office showed that wind measurements made by the ERS-1 scatterometer have been received enthusiastically; the quality is good and de-aliasing problems are few. Small-scale low-pressure systems (both extra tropical and tropical) and trough lines (e.g. fronts) have been identified with considerable extra detail compared with model background plots. The forecasters are also confident of the wind strengths in high wind regimes. Courtesy of A Lorenc, UK Meteorological Office, Bracknell, UK.

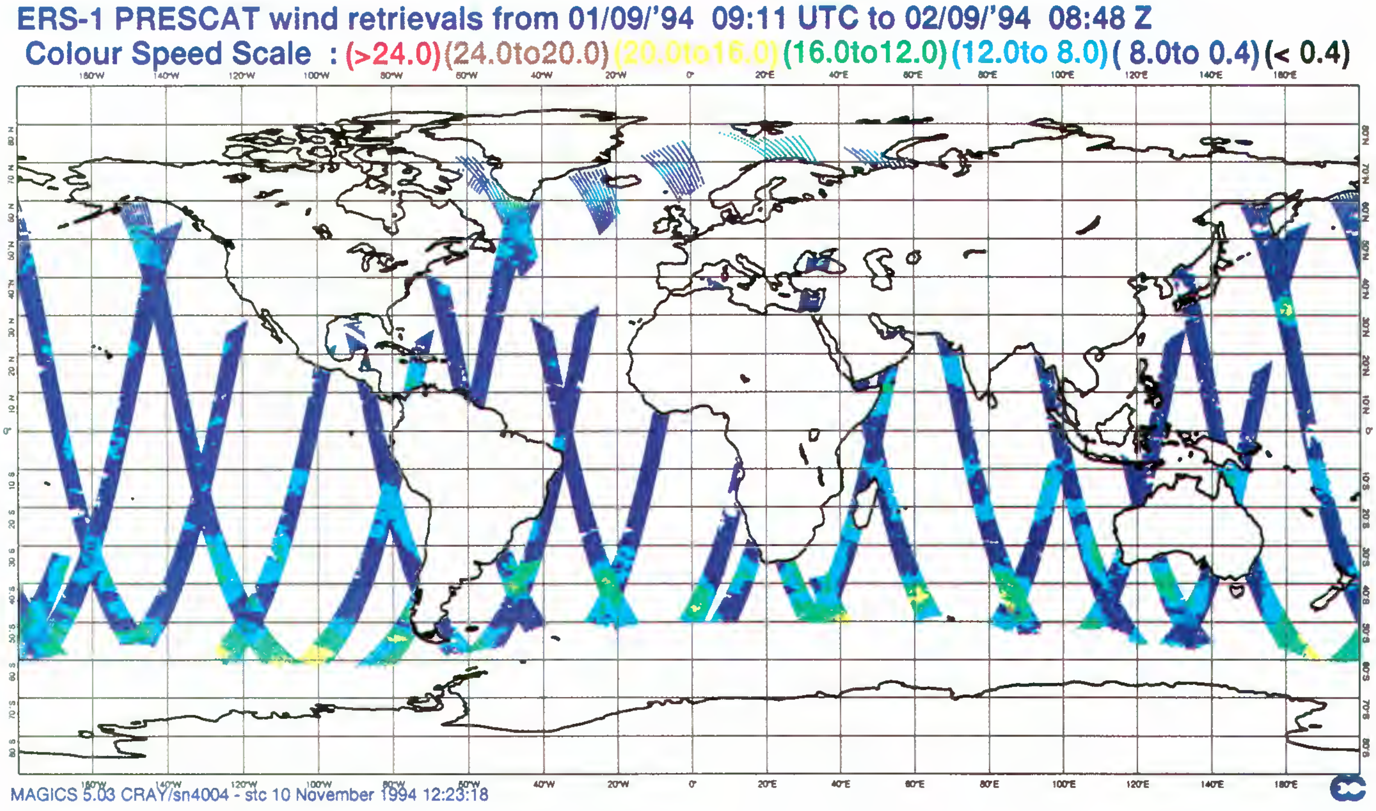

Figure 2.2. ERS-1 scatterometer data are being used in global scale numerical weather prediction at the European Centre for Medium-Range Weather Forecasts (ECMWF). This is an example of 24-hour data coverage. The colours indicate the wind speed range that was calculated at the ECMWF. Sea surface temperature data are used to exclude scatterometer data recorded over ice.

The effect of introducing the ERS-1 scatterometer data to the analysis has been to improve the specification of the boundary conditions at the surface over the oceans. Courtesy of C Gaffard, H Roquet, J Eyre, ECMWF, Reading, UK.

HIGHER QUALITY DATA FOR OCEAN CIRCULATION MODELLING

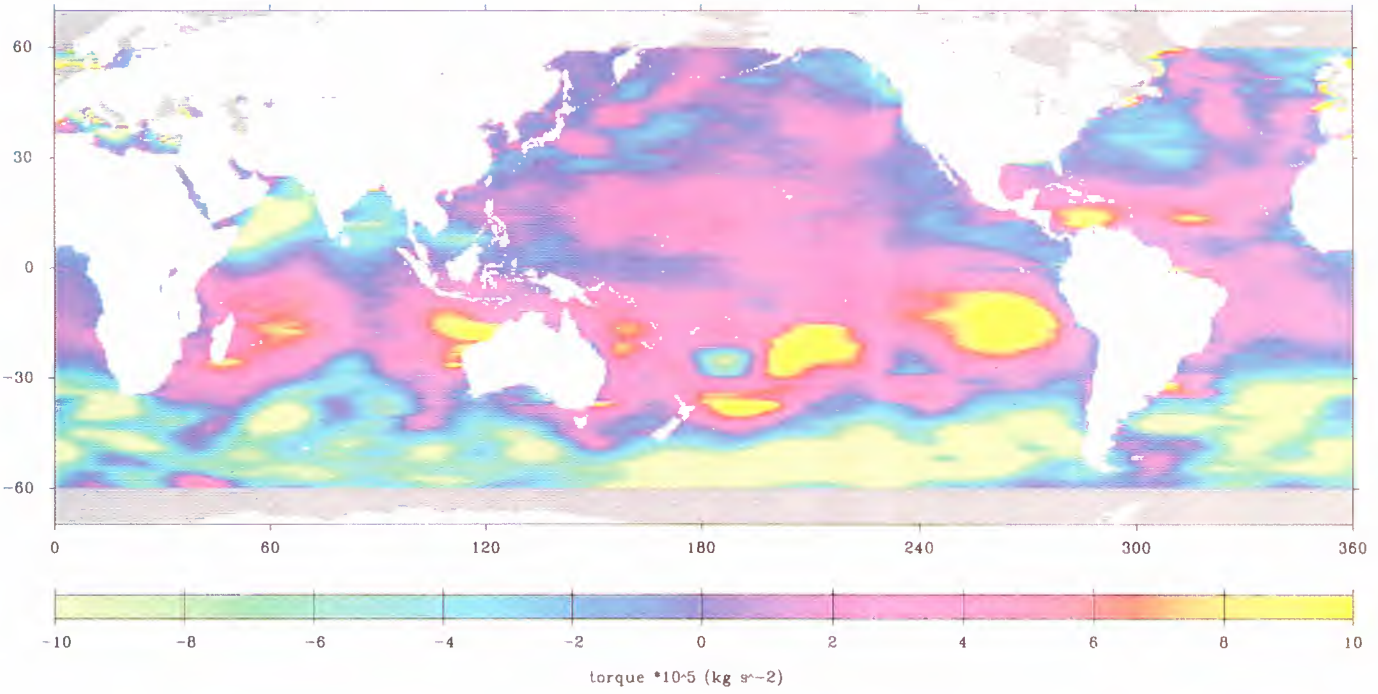

Figure 2.3. A global weekly wind stress torque has been mapped for the period 4-10 July 1993 using the ERS-1 scatterometer. Wind stress torque is the cross-product between wind stress curl and the Earth's radius vector. This Figure shows that the wind stresses are highest in the Antarctic Circumpolar Current region. During this time period the stress is also strong in the vicinity of the South Pacific coast of South America. The global wind stresses are important for understanding and modelling atmospheric and ocean circulation changes. Global wind stress curl (and torques) also provide information which can be used to compute the total angular momentum exchanges between the ocean, atmosphere and solid Earth for studies in Earth rotation and the overall Earth system dynamics. Courtesy of B Tapley, C Shum, University of Texas at Austin, USA.

IDENTIFICATION OF FEATURES NOT PREVIOUSLY RESOLVED

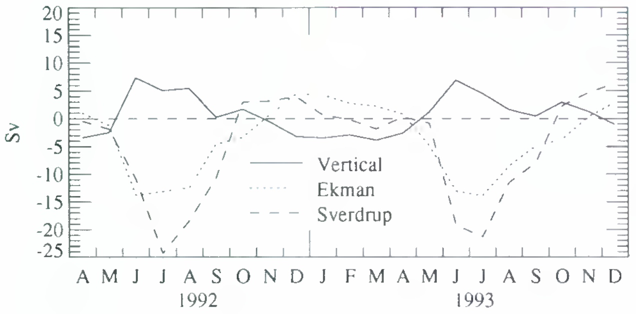

Figure 2.4. Wind-generated current variations in the Arabian Sea are representative of processes affecting global ocean circulation patterns. ERS-1 scatterometer estimates of wind speed components at a height of 10 m above the sea were used to compute:

- *The monthly mean wind-generated north-south component of the Ekman transport along the 8.5°N line of latitude (dotted line) in the Arabian Sea;*
- *The Sverdrup transport along the 8.5°N line of latitude (dashed line) in the Arabian Sea;*
- *The integrated vertical transport into and out of the Ekman layer of the Arabian Sea north of 8.5°N.*

The amount of water transported southward by the Ekman and Sverdrup transports during the monsoon of June and July was larger (34 Sv) [1 Sv = 1x10^6 m^3/s] than the amount of water transported into the Ekman layer during the summer monsoon. This additional water comes from the Somali Current and estimates of wind driven currents show that about 28 Sv were transported by the Somali Current. This value is similar to observations of the Somali Current transport at 10°N during the southwest monsoon. Courtesy of D Halpern, JPL, Pasadena, USA.

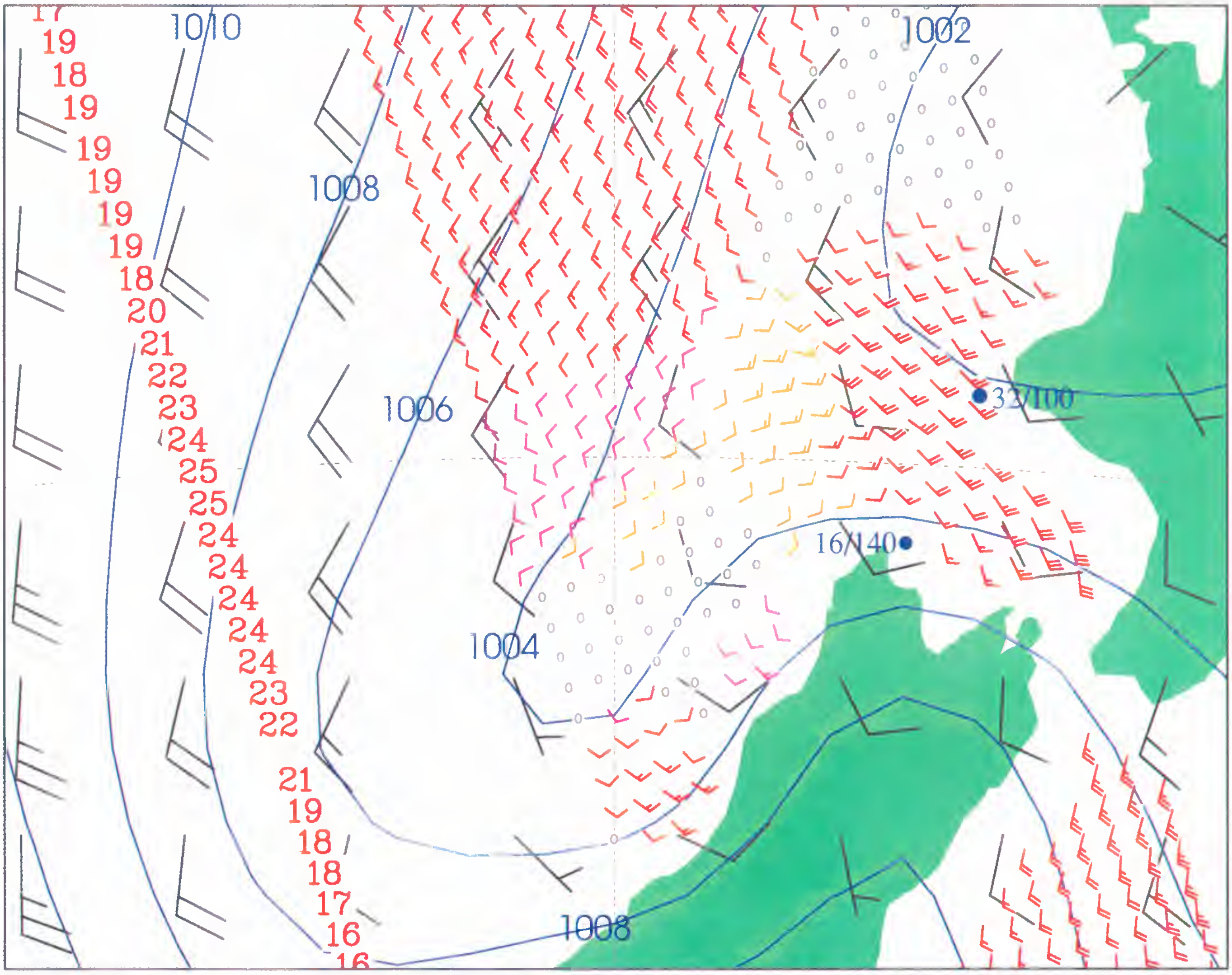

Figure 2.5. This Figure illustrates how features not evident in the conventional model forecast fields can be identified using ERS-1 scatterometer data. Wind barbs over central New Zealand from ERS-1, at 12:00 on 4 December 1992 show the flow between the North Island and South Island penetrating the lee trough to the west of the country.

Model forecast fields of ECMWF mean sea-level pressure analyses (blue isobars in hPa) and 10-m winds (black wind barbs) are plotted with the ERS-1 products from an ascending pass at 11:51 to 11:55. The ERS-1 scatterometer winds are shown as wind barbs, where those in red are less than 60° different from ECMWF 10-m wind directions, those in orange are between 60° and 120° different and those in magenta are more than 120° different and are reversed by 180°. Where no winds were provided, a grey 'o' is plotted, generally indicating light winds. ERS-1 radar altimeter winds are shown as speeds averaged over 25 m sections and shown as red numbers. Also plotted are surface wind observations at two sites with good marine exposure (blue dots with wind speed/direction). All wind speeds are in knots and directions in degrees true. The wind barbs indicate 10 knots for a full barb and 5 knots for a half barb. Courtesy of A Laing, National Institute of Water and Atmospheric Research Ltd, Wellington, New Zealand.

2.2. Ocean surface waves

As well as its full imaging mode, the ERS-1 SAR can operate in a 'wave' mode. In this mode, small SAR images (imagettes) of 10 x 5 km are acquired every 200 km (or 30 seconds) over the ocean along the satellite track. The imagettes are processed to image spectra. For the first time these allow wave modellers to obtain global information on two-dimensional wave spectra.

The data provided by ERS-1 allow wind sea evolution, swell propagation and dissipation to be studied separately. These data can be used in models through a combined wind wave data assimilation system to correct both local and non local wind and wave fields in a consistent way.

ERS-1 altimeter data have been inter-calibrated with data from Geosat, Topex/Poseidon and buoys to provide long-term global datasets on wave height. Statistical studies of wave height require large numbers of independent measurements, such as the estimation of extreme wave heights.

The scientific use of surface wave information is already leading to operational applications. This has been helped by the availability of the wave information as fast delivery products. Wave data are distributed to operational weather services within three hours of observation, allowing them to derive information on ocean wave energy, height and direction.

Two particular areas where ERS-1 is contributing to scientific development are:

- Improved description of surface waves for wave forecasting;
- Development of wave annual averages.

IMPROVED DESCRIPTION OF SURFACE WAVES FOR WAVE FORECASTING

a

b

Figure 2.6 a,b. This imagette (Fig a) of the ocean surface measured by the ERS-1 SAR in wave mode shows wave-like patterns associated with the ocean wave field. The SAR wave model spectra diagram (Fig. b) shows the directions of the waves identified in the imagette. Courtesy of S Hasselmann, Max Planck Institute for Meteorology, Hamburg, Germany.

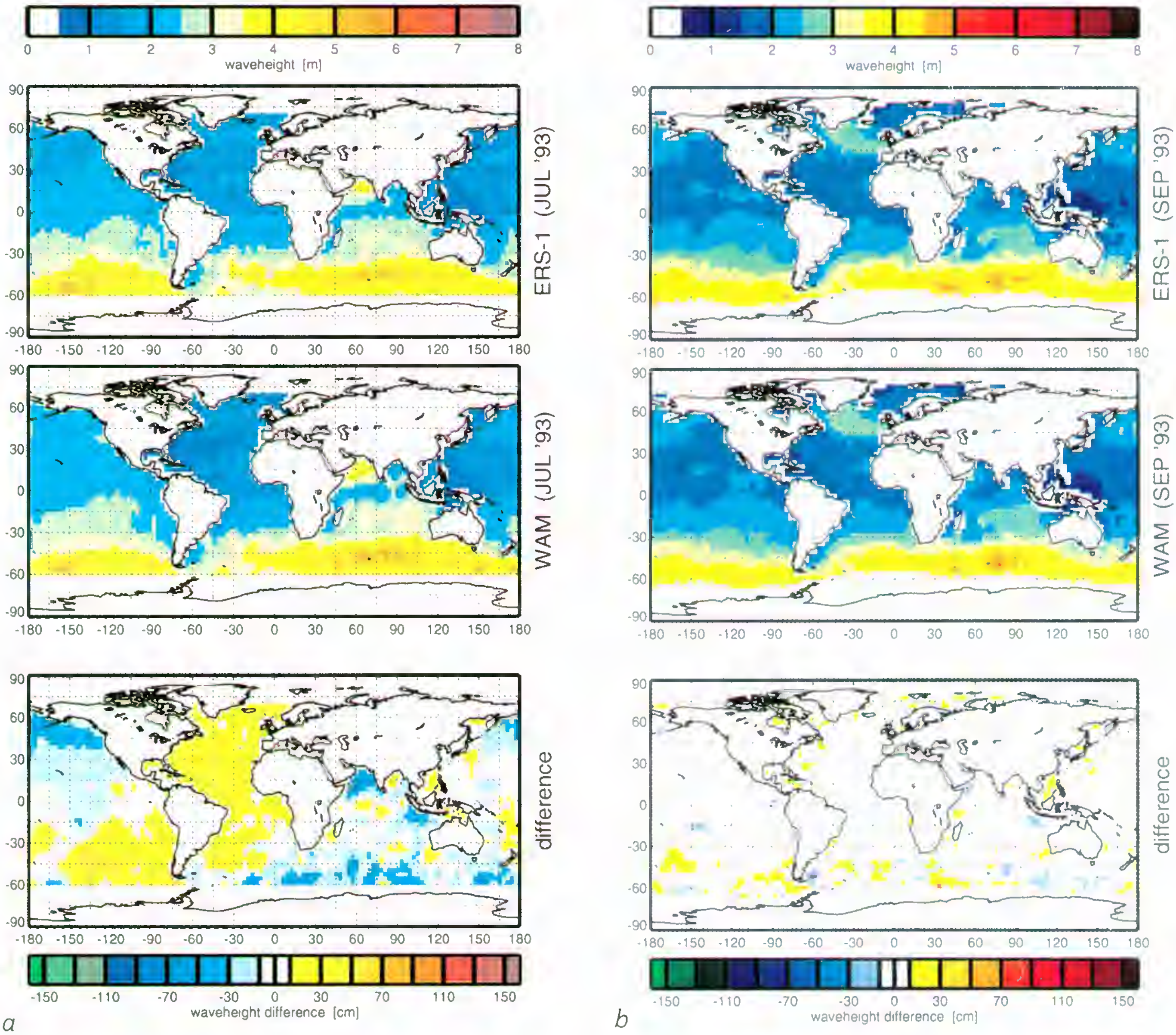

Figure 2.7 a,b. Figure a shows the distribution of significant wave height (Hs) for July 1993 measured by ERS-1 altimeter (top) and produced by the ECMWF wave prediction model (centre) for July 1993. Figure b gives the same information for September 1993. The model is driven by surface winds from the ECMWF atmospheric model. Significant differences (bottom) can be delineated in parts of the central Atlantic Ocean, North and South Pacific Ocean and in the Indian Ocean. These differences are believed to be caused mainly by erroneous wind fields used in the wave prediction models. In remote ocean areas wind measurements are sparse. This Figure clearly demonstrates the need for improved wave data and an appropriate assimilation system to optimise their use. It also shows the value of having an independent data source which allows models to be validated. Courtesy of B Hanssen, ECMWF, Reading, UK.

Figure 2.8 (see opposite page). *After the assimilation of the ERS-1 altimeter wave heights into the ECMWF wave forecasting model, the significant wave heights predicted by the model agree more closely with the buoy observations. This Figure shows there is a reduction of the standard deviation of 3% in the West Atlantic, 8% near Hawaii, 15% in the East Pacific and 23% off the coast of Peru. Apart from the West Atlantic area the bias is also reduced. The reason for the different impacts on different areas of the ocean is partly due to the different relative contributions of wind sea and swell. The improvement in the 1-day forecast is of the same order of magnitude. There is no impact on the 5-day forecasts, which will probably require improvements in the numerical models themselves.* Courtesy of A Guillaume, B Hanssen, ECMWF, Reading, UK.

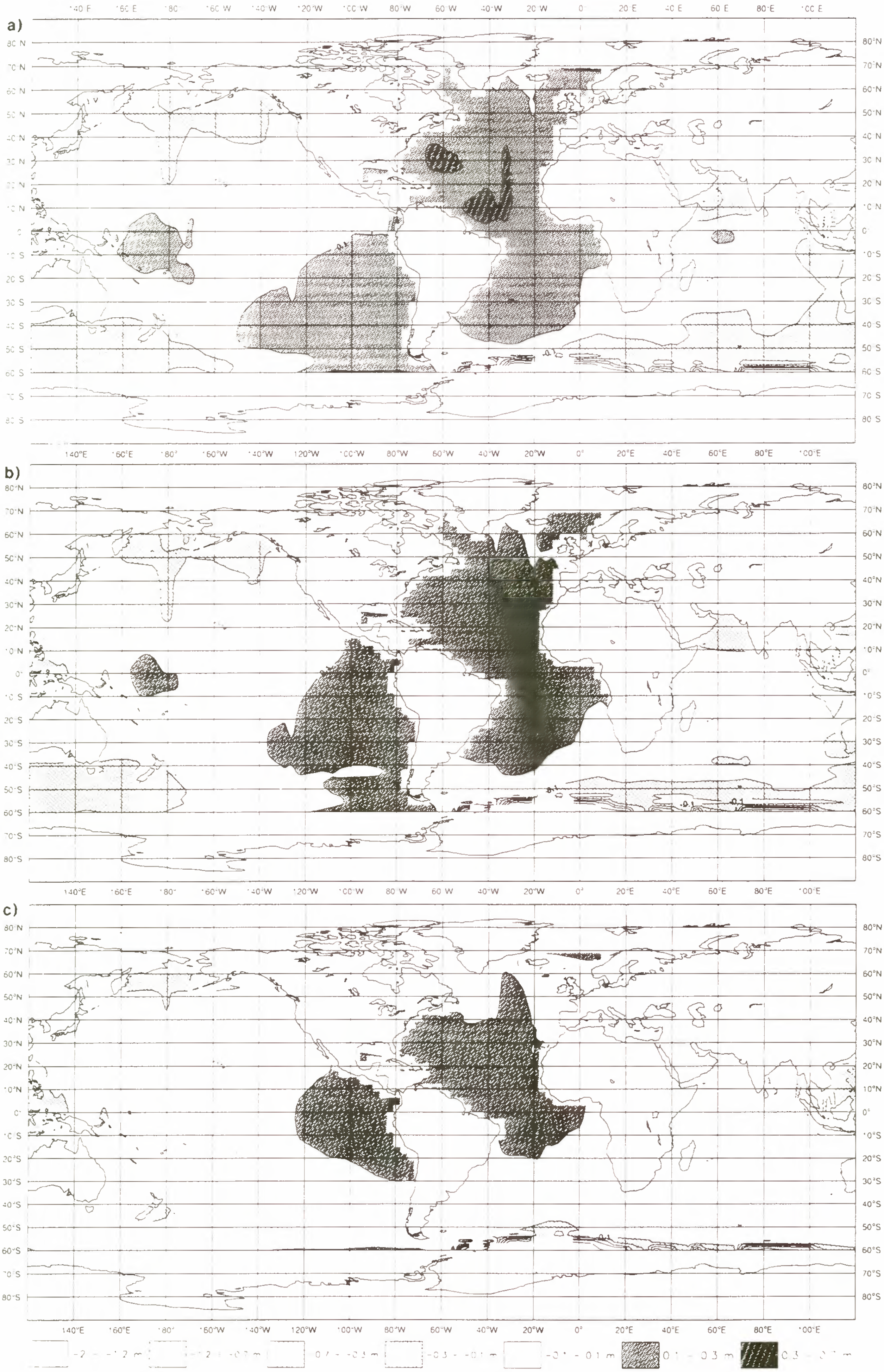
a)
b)
c)

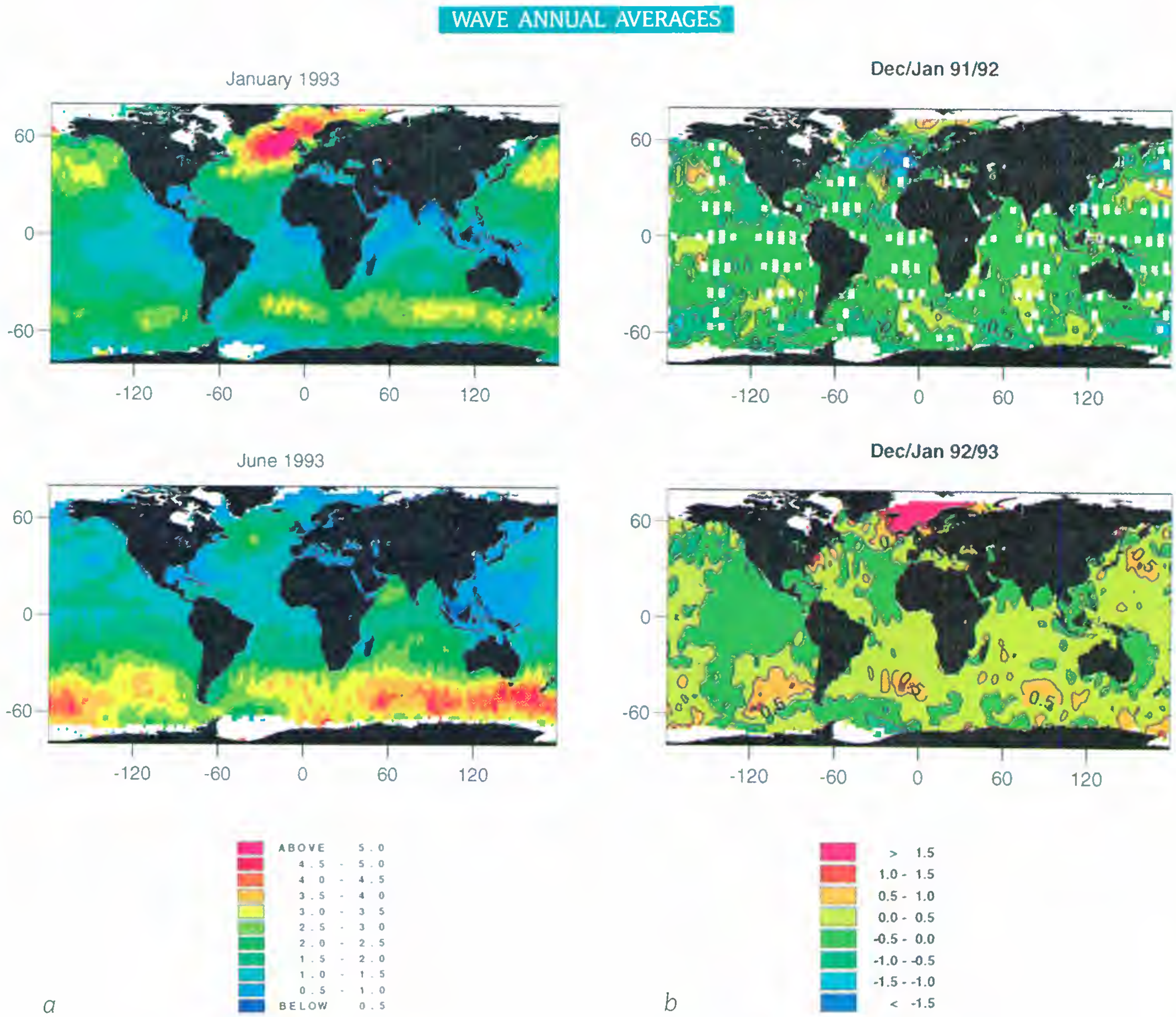

Figure 2.9 a;b. The ability of altimeters to measure ocean wave height, coupled with the world-wide coverage provided by satellite-borne instruments, now allows the study of wave climate on a global scale.

Figure a illustrates seasonal variability by comparing wave climates calculated from ERS-1 radar altimeter data for January and June 1993. In January, a large area of high waves can be identified in the North Atlantic (with a monthly mean wave height greater than 4 m), as can a narrow band of higher waves in the Southern Ocean. During June, the band of high waves in the Southern Ocean has broadened and increased, and there remains only one small area in the North Atlantic with mean wave heights greater than 3 m. In this month, higher waves were also recorded in the Arabian Sea, caused by the southwest monsoon.

Figure b illustrates how wave averages can vary between years. A climatology derived from Geosat altimeter data for a typical year (1987-88) has been subtracted from combined December and January ERS-1 altimeter wave data for two successive years (1991-92 and 1992-93). White areas in the upper image reflect gaps in coverage due to the operation of the three-day repeat cycle during this period. A clear feature is an area in the North Atlantic where significantly lower than average wave heights seen in 1991-92 are replaced by higher than average wave heights in the next year. Courtesy of D Cotton, James Rennell Centre for Ocean Circulation, Southampton, UK.

Figure 2.10 (see opposite page). *This Figure shows an averaged large-scale dynamic topography map as observed by the ERS-1 radar altimeter during a 35-day repeat orbit phase. The topography compares well with that derived using hydrographic data and reinforces the results achieved with Topex/Poseidon. The total range of the topography relative to a reference geoid is approximately 2 m and the map shows clearly the major current systems of the world's oceans (the North Atlantic Gulf Stream, the Pacific Kuroshio and the Antarctic Circumpolar Current). Knowledge of the mean dynamic topography is important for enhancing our understanding of the ocean's role in global climate changes.* Courtesy of B Tapley, C Shum, University of Texas at Austin, USA.

2.3. Ocean topography

Worldwide sea level varies significantly in space and time. Sea level is normally referenced to a geoid, a surface of the Earth which is perpendicular to the local gravity field, and which may vary from the mean Earth ellipsoid by up to 100 m. Even taking into account the irregular form of the geoid, regional variation in sea level occurs as a result of pressure differentials within the ocean resulting from momentum and heat flux exchange with the atmosphere. For example, the sea level at the centre of the Sargasso Sea is high because water is piled up by the wind stress and because the surface water is warm and thus dilated. The resulting differences in sea level are directly related to ocean currents.

Sea level can change slowly with time as a result of general climate change and associated ice sheet melting or growth, or more rapidly, due to regional variations in the ocean circulation. Ocean topography is only one expression of the overall dynamics of the ocean. As a result, topographic changes are normally associated with modifications to other observable ocean characteristics such as surface currents and associated surface temperature changes. Ocean topography can be measured directly and monitored for change using the ERS-1 radar altimeter. The ERS-1 mission follows closely the five-year Geosat mission, and taking its results with Topex/Poseidon data provides a period of almost ten years in which ocean topography has been monitored comprehensively. This information can be assimilated into ocean circulation models which transform the satellite surface information into three dimensional descriptions of ocean currents and transports.

One of the most important fluctuations of the ocean/atmosphere system is the El Niño Southern Oscillation phenomenon. Los Niños are alternating warm-cold-warm events in the tropical Pacific. During the El Niño, the warm part of the oscillation, weak trade winds result in eastward transport in the upper layer of the equatorial Pacific, causing an increase in temperature throughout the central and tropical Pacific. The cold counterpart to the El Niño is known as La Niña. These phenomena can produce dramatic changes to climate on time scales of months to several years. These events are reflected by changes in ocean topography which can be measured by the ERS-1 radar altimeter and sea surface temperature which can be measured by ERS-1 ATSR.

Finally, changes in regional or mean sea level are also of interest because of the direct impact on land, such as flooding and increased erosion as a result of a rise in sea level, or the land locking of ports as a result of falls in sea level. ERS-1 is contributing to the following areas of ocean dynamics research:

- Mapping ocean topography from the mesoscale to the global scale;
- Monitoring large scale features, such as El Niño events and associated Rossby waves;
- Modelling tides.

OCEAN TOPOGRAPHY MAPPING

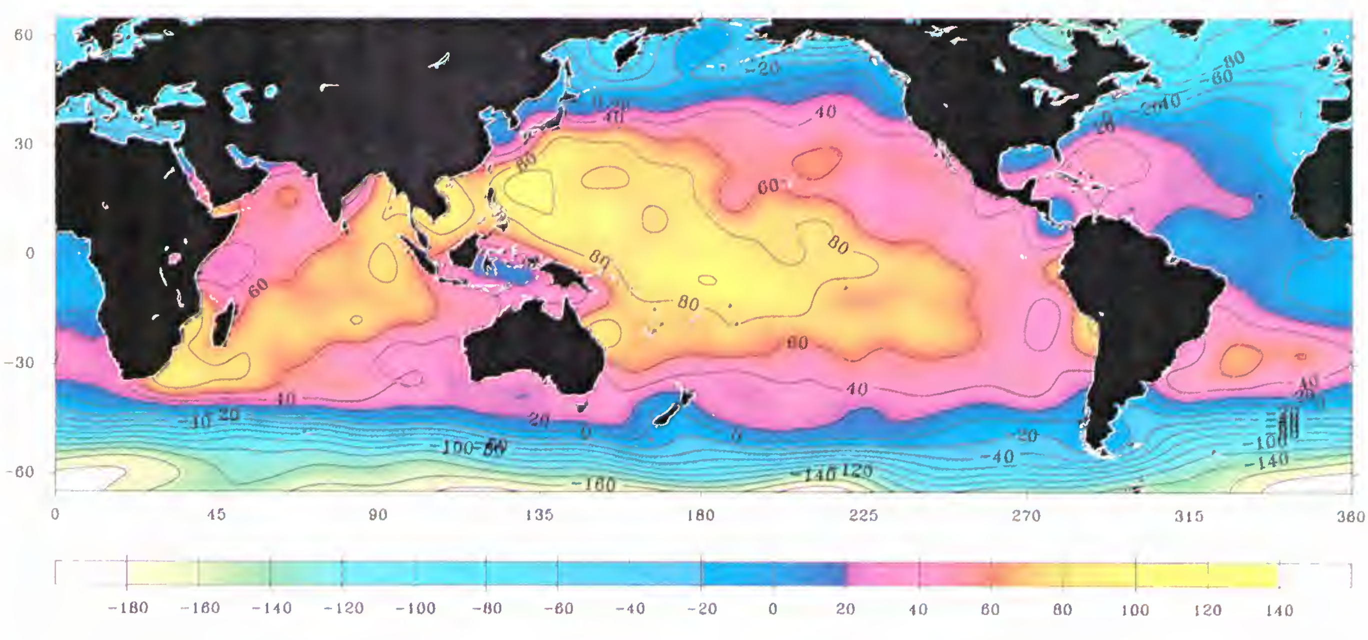

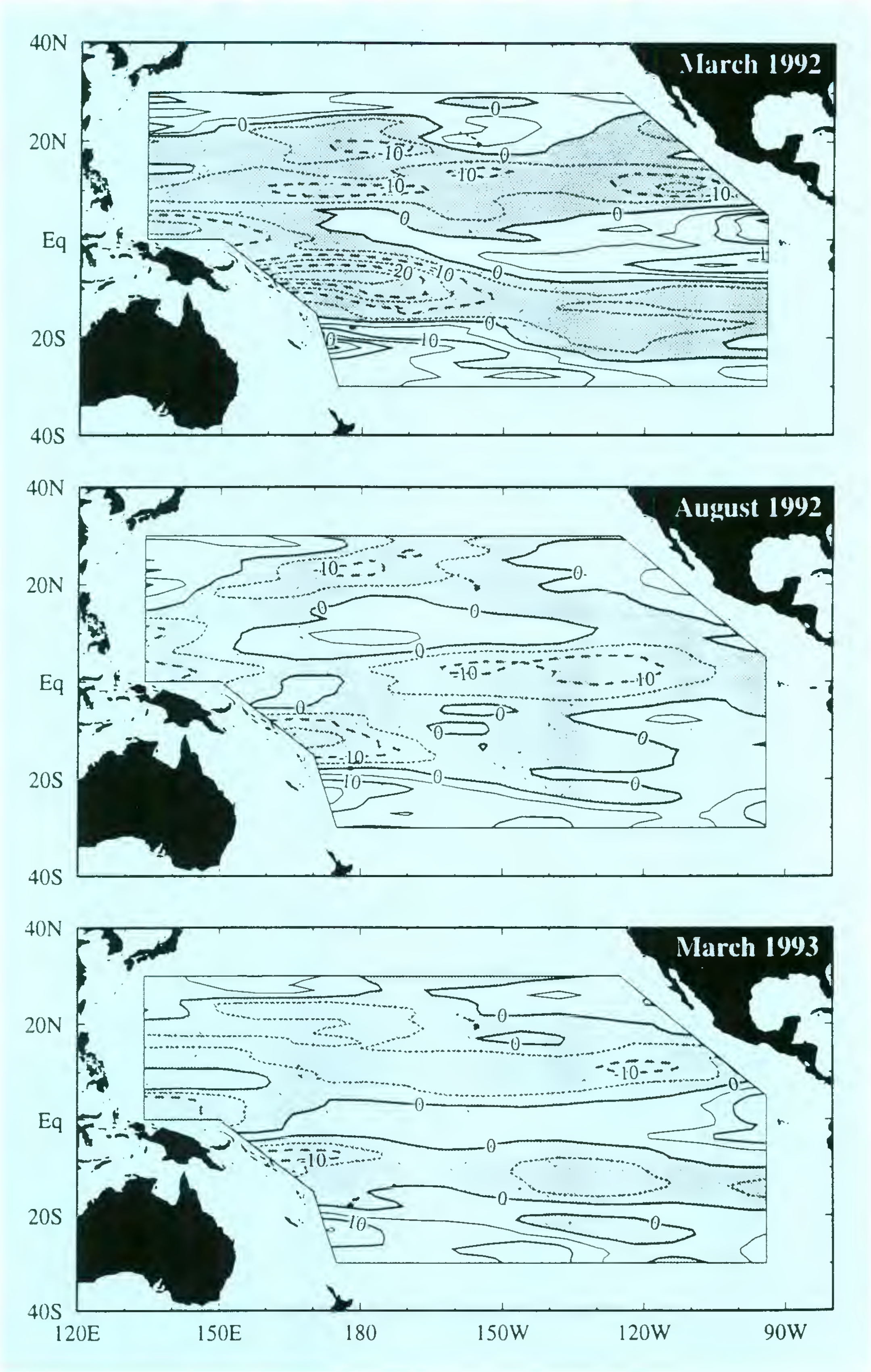

Figure 2.11. Altimetric sea level anomalies have been determined with Geosat and ERS-1 radar altimeter data. Contours are at 5-cm intervals, with negative regions shaded. Annual and semi-annual signals have been removed, leaving only the inter-annual changes relative to April 1985-86. The map shows evolution of the 1991 to 1993 Los Niños: strong El Niño (top); mild La Niña (middle); secondary weak El Niño (bottom) . The easterly position of the positive anomalies in the March images illustrates the effects of the El Niño warming on Pacific sea levels. Courtesy of R Cheney, NOAA, Silver Spring, USA.

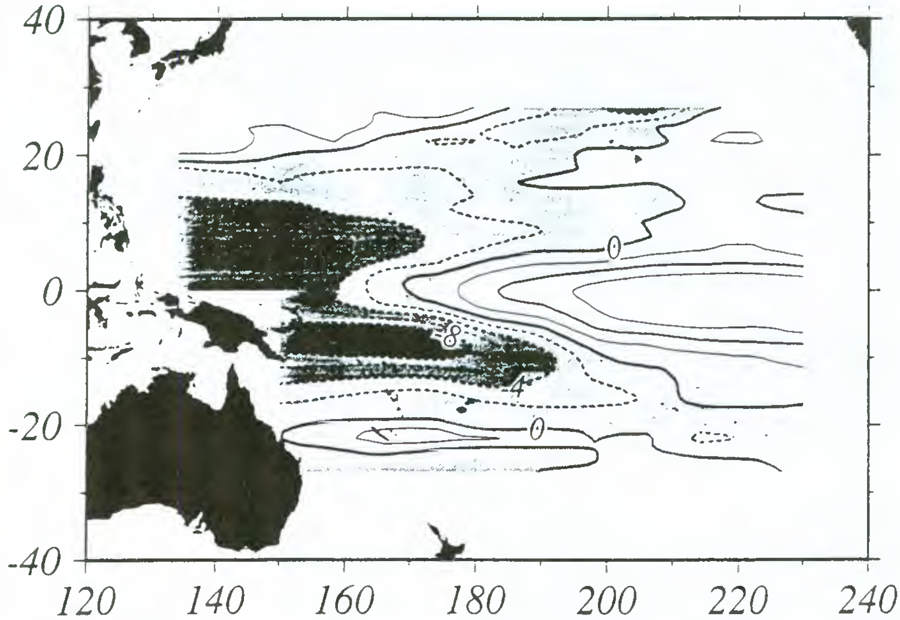

a

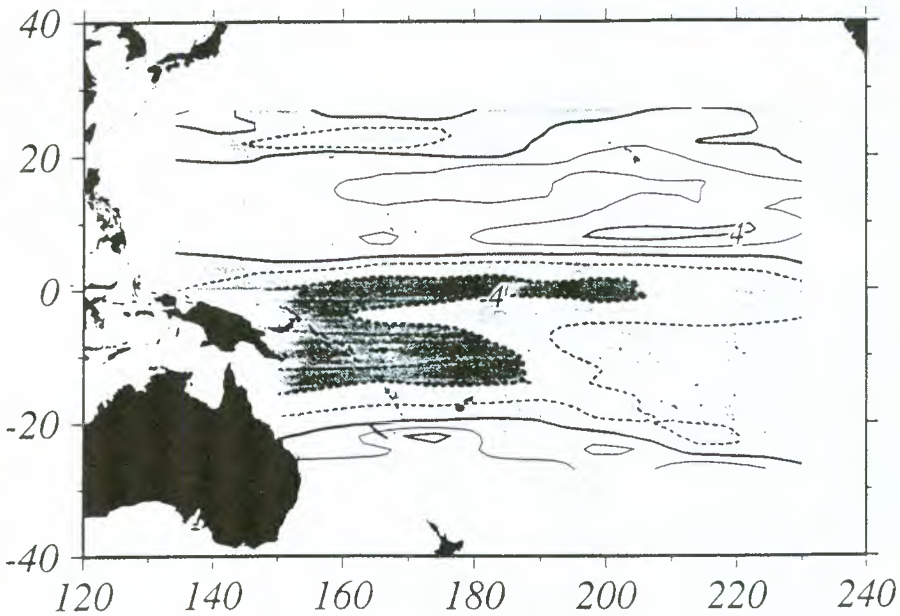

b

Figure 2.12 a,b,c. A further improvement in the Pacific ERS-1 observations has been made combining the tide gauge and altimeter data into a single analysis. These blended sea level fields combine the altimeter's high spatial resolution with the larger-scale accuracy of the tide gauge network. An analysis of the blended ERS-1 sea level anomalies reveals important similarities and differences in the evolution of the 1991-93 El Niño, compared with the 1986-87 warm event. Both events are characterised by two modes of variability which develop sequentially in time, separated by several months. The spatial structures in time and amplitude functions of these modes are presented in Figures a, b and c.

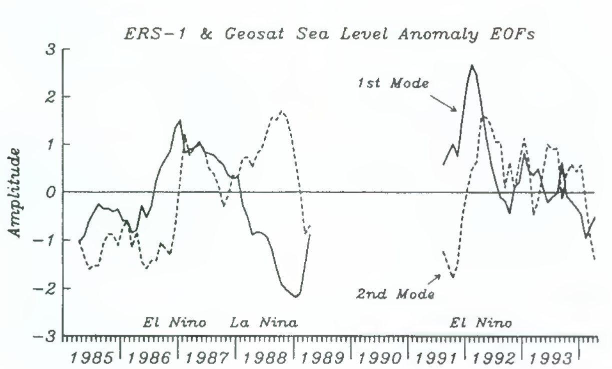

c

The time amplitude functions shown in Figure c indicate that both the 1986-87 and 1991-93 El Niños began with an abrupt increase in the first mode amplitude, followed two to six months later by a similar change in the second mode. An analysis of the surface wind field suggests that this sequence reflects changes in the zonal wind forcing. At the onset of each warm event, the wind anomalies are eastward and symmetric about the equator. As the warm event progresses, the eastward anomalies persist, but shift south of the equator. Figure c also illustrates that the sea level anomaly pattern during the late stages of the 1991-93 event did not resemble either of the two modes of the 1986-87 El Niño.
Courtesy of R Cheney, L Miller, NOAA, Silver Spring, USA.

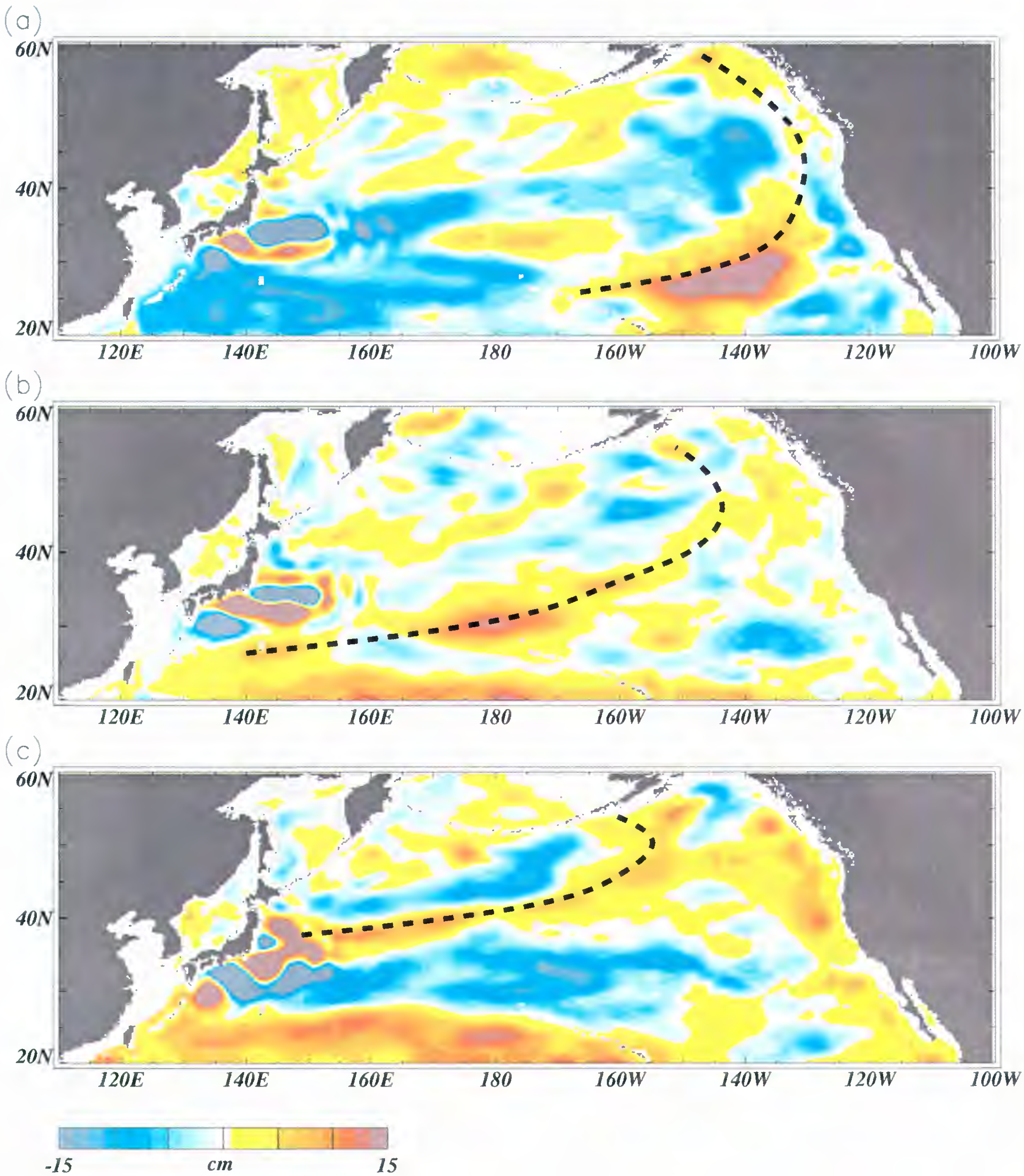

Figure 2.13. An interesting new application of ERS-1 altimeter data to large-scale oceanography is shown in this Figure. It proposes that the effects of the 1982-83 El Niño are still being felt in the North Pacific more than a decade later.

Geosat and ERS-1 altimeter data, together with satellite measurements of sea surface temperature, showed that the average position of the Kuroshio Extension (dotted line) shifted northward between 1988 and 1993. This matched similar changes seen in the output of a numerical ocean model, thus validating the model simulation. When the model was run over the 12-year period 1981-1993, it showed that the long-term effect of the 1982-83 El Niño was to produce a westward-propagating Rossby wave in the North Pacific. The remnants of this wave still exist in the Northwest Pacific Ocean and continue to exert an influence on sea surface temperature and therefore weather patterns over the North American continent. Such long-term ocean/atmosphere connections present a strong case for continued satellite monitoring of the global oceans. Courtesy of R Cheney, NOAA, Silver Spring, USA.

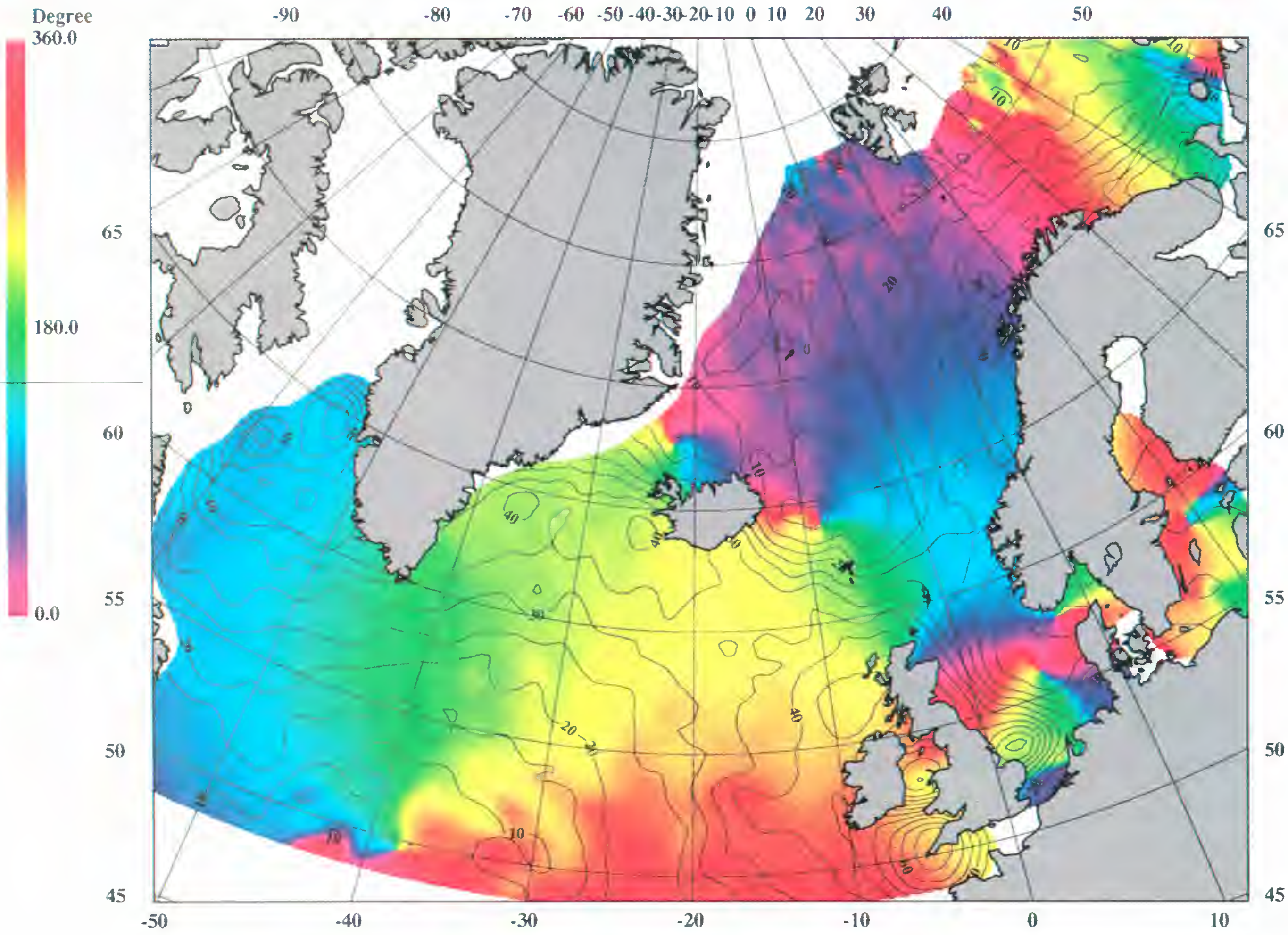

ERS1 derived S2 ocean tide model. (Amplitude, CI = 5cm)

Figure 2.14. ERS-1 is in sun-synchronous orbit. This makes it difficult to use the altimeter data for accessing ocean tides, because the satellite always sees the same phase of the solar tidal waves. However ocean tides can be derived from ERS-1 radar altimeter data by using the correlation between the tidal constituents ERS-1-derived S2 ocean tides in the North Atlantic and adjacent seas are shown here. Co-amplitude lines are shown as contours, and the phase lag with respect to Greenwich is plotted using a cyclic colour scale. The contour interval is 5 cm. Few other data are available in the polar oceans as Topex/Poseidon is limited to 66° latitude north and south, and few tide gauges exist. Tidal information derived from ERS-1 have shown that there are large errors in the currently available tidal charts. Courtesy of O Andersen, National Survey and Cadastre; C Tscherning, University of Copenhagen, Denmark.

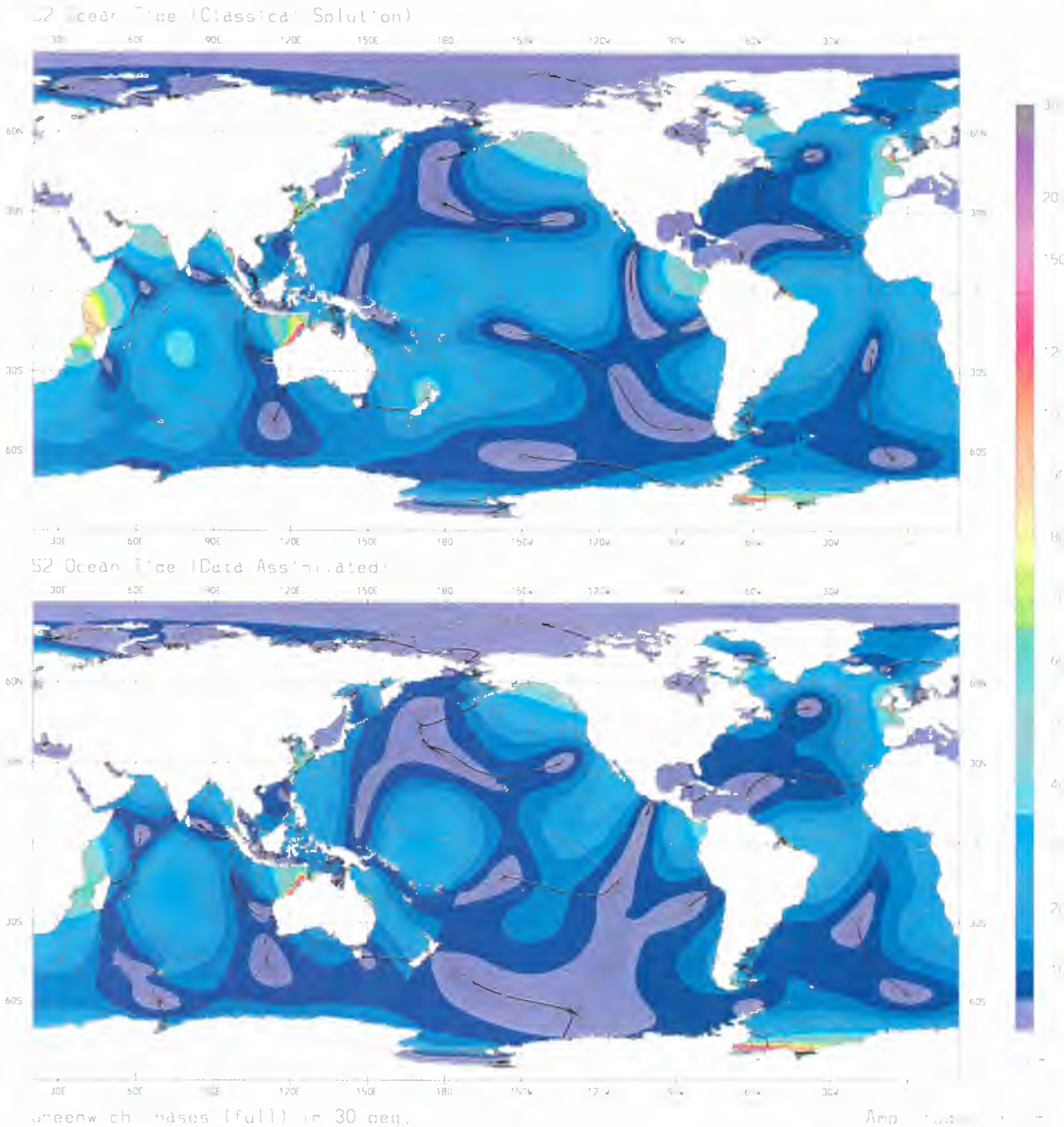

Figure 2.15. A new numerical 1/2° by 1/2° global ocean tide model, with a variational data assimilation scheme has been developed and implemented. Data on tidal elevation (e.g. ERS-1 radar altimeter data and tide gauges), tidal currents as well as gravity data can be assimilated. Maps of tidal elevation, tidal radial displacement of solid Earth and tidal gravity effect of greatly improved accuracy have been produced. This assimilation approach allows new insights into processes that are badly resolved in current numerical ocean tide models. This Figure shows two co-range/co-phase maps of tidal elevations for the principal solar tide S2 derived from a numerical, 1/2° by 1/2°, high-resolution global ocean tide model using ERS-1 radar altimeter data. Ranges are represented by colour, Greenwich phases by lines.

The upper map presents a classical model result. Application of the newly developed variational data assimilation scheme to the global ocean tide model reduces the tidal elevation error by more than 65%, when compared to more than 200 ground truth tide gauge data. The assimilation of tidal elevation data into this model results in the lower map. Courtesy of W Zahel, University of Hamburg, Germany.

Figure 2.16 (see opposite page)*. Variability in sea surface temperature has been mapped, based on ERS-1 ATSR data from 1992 and 1993 for the South Atlantic. The variability reflects the mesoscale (100 km) eddies in regions of strong current flow. The resemblance to the variability in sea surface height for the same region is striking. Such a marked correspondence has not been shown before. Areas of high oceanographic variability such as the Agulhas retroflection, and the Brazil/Falklands confluence can be clearly seen.* Courtesy of M Saunders, Mullard Space Science Laboratory, University College London; T Guymer, M Jones, James Rennell Centre for Ocean Circulation, Southampton, UK.

2.4. Ocean surface temperature

Global sea surface temperature is one of the most important parameters required for climate research. The ocean plays a major role in the Earth's climate system through its storage and transport of heat. The upper ocean has a relatively short response time (months to years) compared with the deeper ocean (decades to centuries).

If the atmosphere and upper ocean alone were responding to the increase in greenhouse heating and the cloud-radiation feedback operated according to current knowledge, the surface of the Earth would already be 1-2°C warmer than the temperatures of the 19th century. That this has not happened may be due to the thermal inertia of the ocean, determined by the slow but poorly known rate of penetration of heat in the upper 1000 m.

Modelling of the global ocean circulation is essential to determine the timing of global warming, but as with any modelling activity, it is necessary to validate the results. The availability of accurate sea surface temperature data from the ERS-1 ATSR instrument provides a means of improving the accuracy of the historical record of sea surface temperature. This allows the validation of climate models when run using historical data to reproduce the climate of the past century. It is also possible to measure the progress of specific climate variations, such as the El Niño events which have a significant effect on short-term climate as well as longer-term trends. Associated phenomena such as tropical Rossby waves can also be identified.

The ERS-1 ATSR provides a data source which is more consistent and has better coverage than in situ measurement facilities. It achieves a root mean square error of 0.3 K relative to buoy measurements without using in situ measurements. This represents at least a doubling of accuracy compared with results using previous data sources. The higher accuracies allow sea surface 'skin' temperatures to be converted to reliable 'bulk' temperatures which exhibit less high frequency variation. Bulk temperatures also provide more accurate comparisons with in situ measurements for which records exist over the past 150 years.

The data have been used to support the following:

- General monitoring of sea surface temperatures for indicators of climate change;
- Identification and tracking of specific features of ocean dynamics, such as Rossby waves and El Niño.

SEA SURFACE TEMPERATURE AND CLIMATE

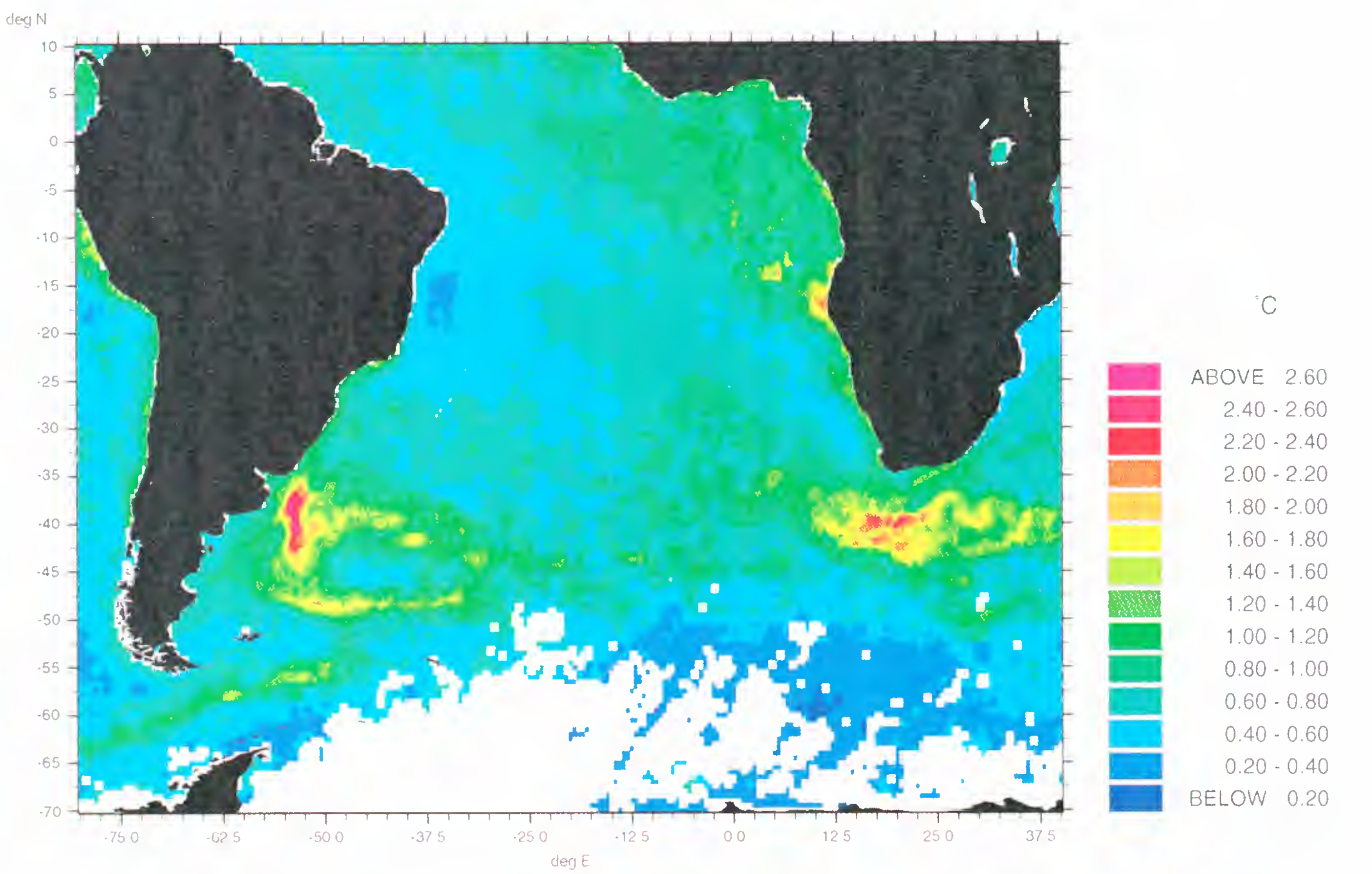

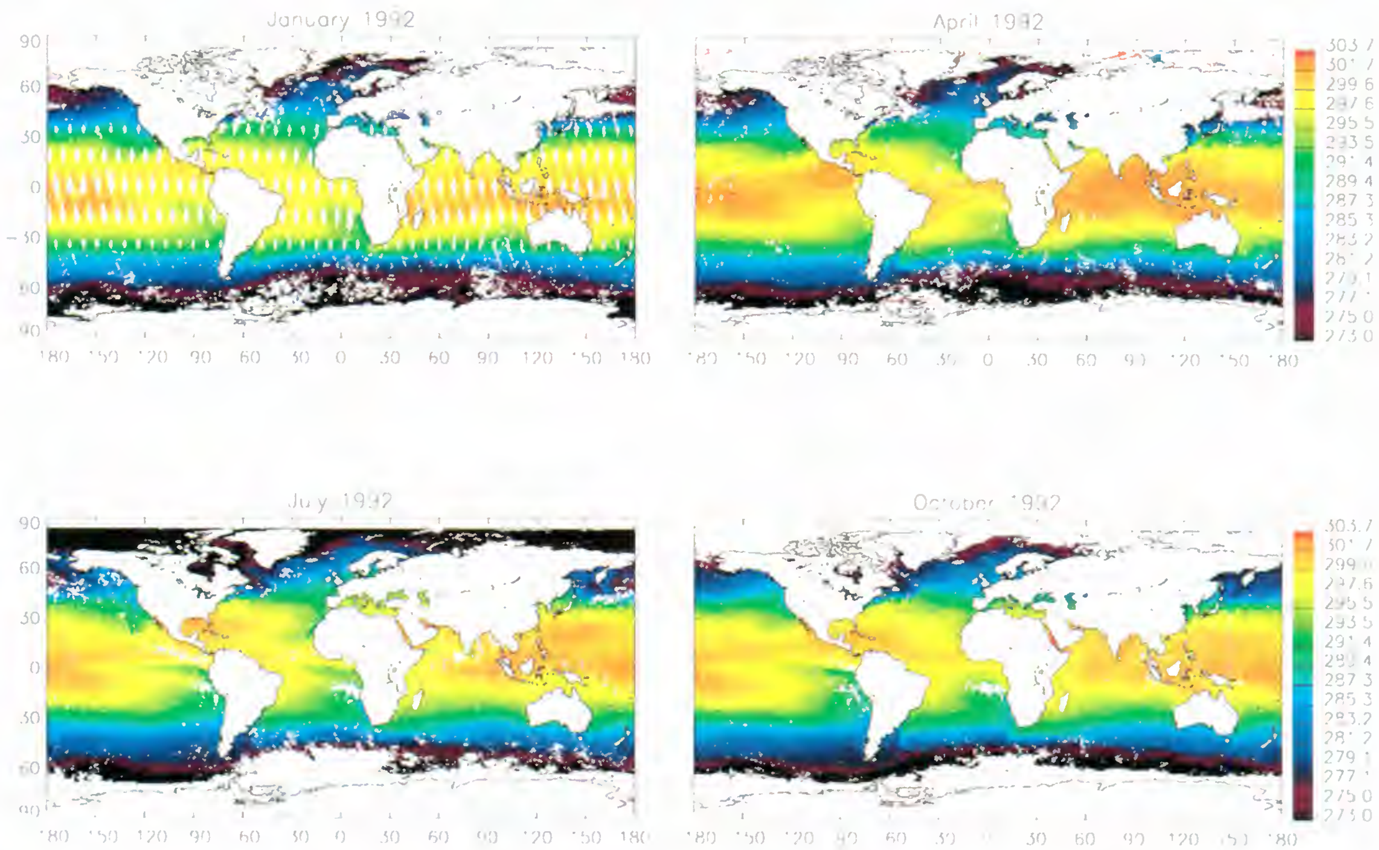

Figure 2.17. 24 monthly mean maps of global sea surface temperature have been produced using measurements from the ERS-1 ATSR. The four maps shown (January, April, July and October 1992) illustrate the evolution of many of the well-known annual features of the global sea surface temperature field with remarkable detail and clarity. For example: the East Pacific upwelling and the Equatorial 'cold tongue' between June and September; the appearance of the Gulf stream between April and June and its subsequent evolution into the North Atlantic drift in the following months; the Falklands current; the Agulhas current; and the Kuroshio.

These global data are of great importance to the climate modelling community. A number of projects are under way to use ATSR data in conjunction with coupled atmosphere-ocean models to analyse the relationship between sea surface temperature fields and important atmospheric phenomena such as the Indian monsoon. Courtesy of D Llewellyn Jones, University of Leicester; J Murray, Rutherford Appleton Laboratory, Didcot, UK.

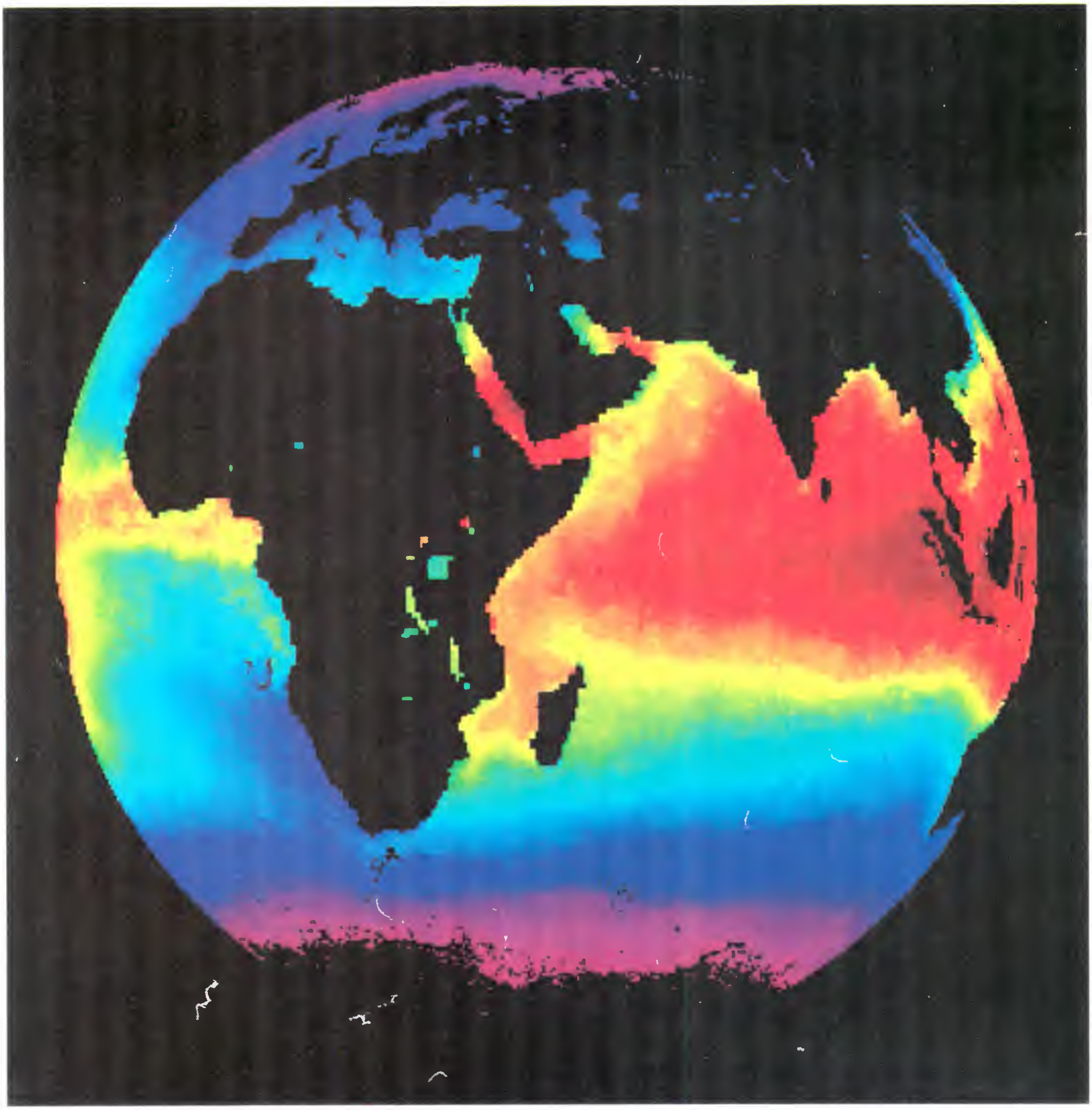

Figure 2.18. ERS-1 ATSR data for one year were averaged to create this representation of sea surface temperature in the eastern hemisphere. In the colour scheme used, temperature ranges from 271 K to 302 K through purple, blue and yellow to orange. The warmest areas with an annual mean sea surface temperature of 302 K are in the Red Sea and around the eastern coast of Sumatra. Generally temperature follows a strong latitudinal trend except in those regions where currents carry water from one latitudinal zone into another. For example, the warmth of the sea between Madagascar and Africa is due to equatorial water carried southwards by the Agulhas Current.

For a given location in the tropics, sea surface temperature usually varies by less than 2 K throughout the year, although larger differences are more likely in the Pacific. At higher latitudes, seasonal variation is much more pronounced with a difference of around 10 K between summer and winter average temperatures. Courtesy of J Murray, Rutherford Appleton Laboratory, Didcot, UK.

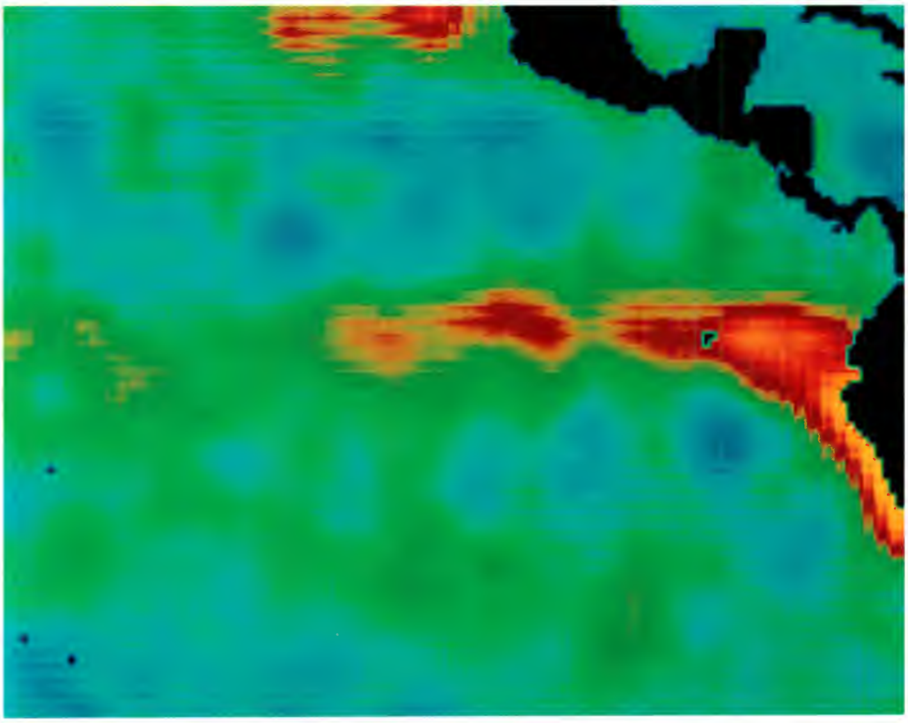

a

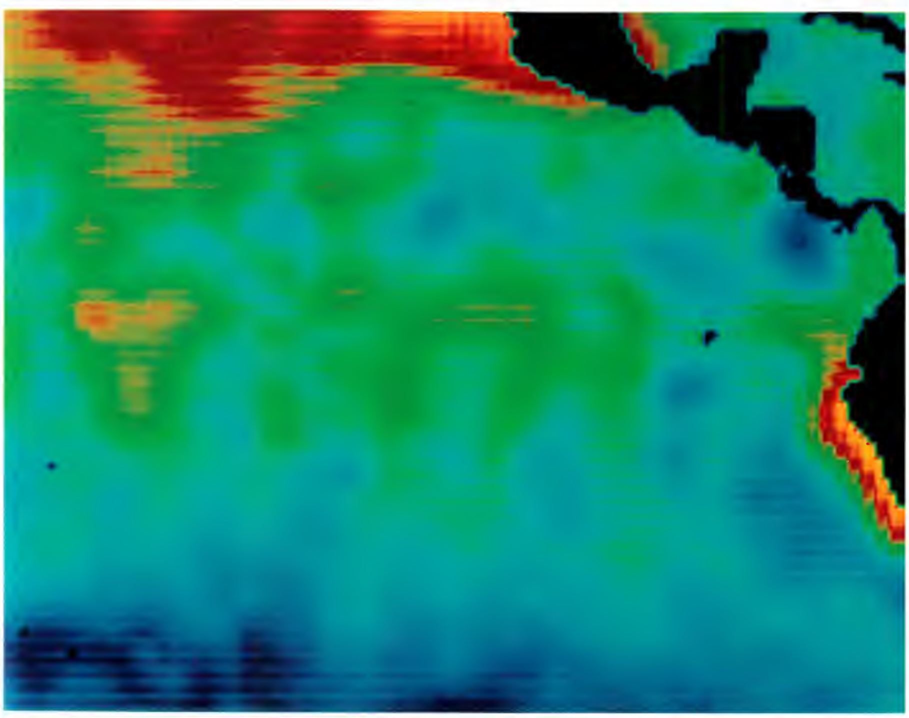

b

Figure 2.19 a,b. Sea surface temperature is a sensitive indicator of climate fluctuations. It is also a key indicator of anthropogenic change in the global climate as the thermal inertia of oceans means that high-frequency noise is filtered out. Sea surface temperature is an important factor in determining the transfer of thermal energy from the ocean to the atmosphere. It has an annual range of variation of 0.5 K to 2.0 K in the tropics and much larger variations at high latitudes.

This Figure illustrates the abrupt disappearance of the 1992 El Niño. Both of the images show the difference between seasonal averages and the actual sea surface temperature measured by the ERS-1 ATSR. The data for Figure a were acquired during the period 15-27 April 1992. The orange colour shows water about 3 K warmer than expected for the time of year. Figure b is based on data acquired only 28 days later, but almost all evidence of the anomalously warm water has disappeared. Courtesy of J Murray, Rutherford Appleton Laboratory, Didcot, UK.

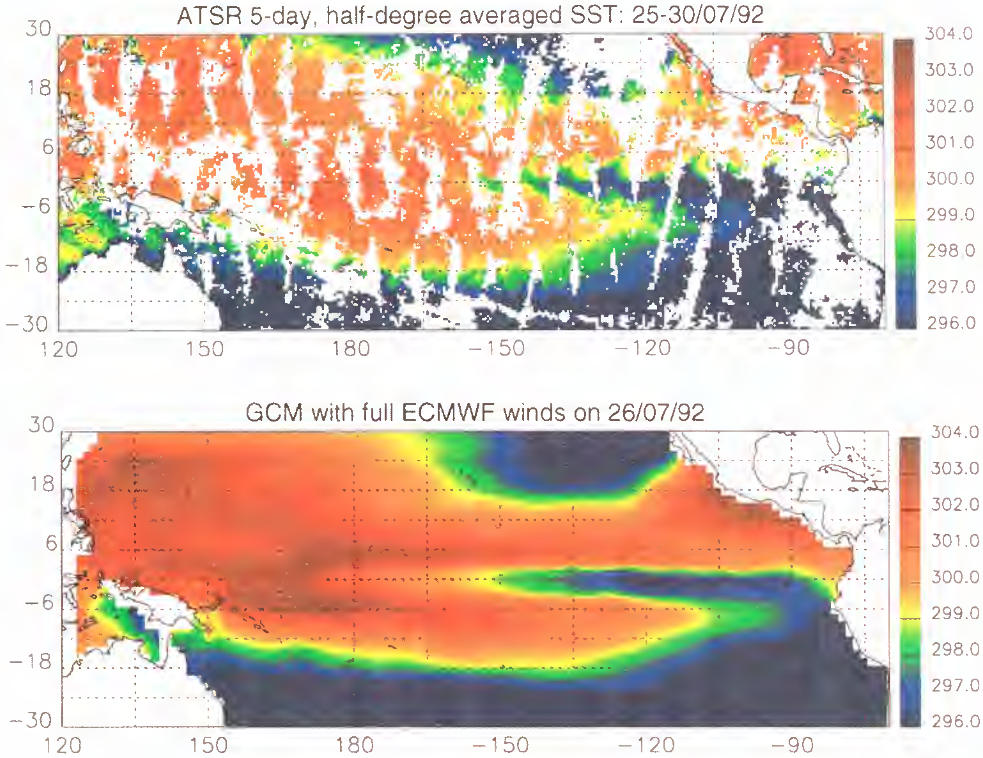

a

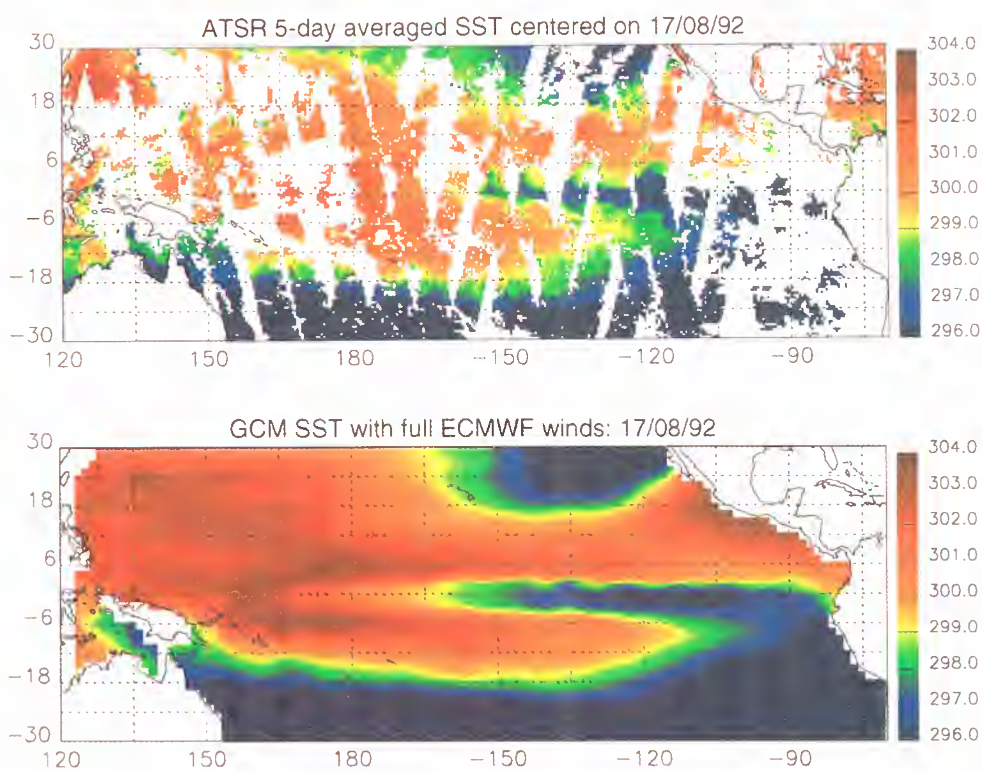

b

Figure 2.20 a,b. Comparing sea surface temperature observations from the ERS-1 ATSR with sea surface temperatures from a model of the tropical Pacific forced with observed daily windstress data, it has been found that the strongest 'instability waves' in the model sea surface temperatures are coherent with those in the ATSR data. It has been concluded that these waves are not pure internally-generated instabilities. Their phases and phase-speeds are at least partially determined by the winds, apparently via remotely-forced internal waves. The sub-surface evolution of the model suggests that the instability waves are phase-locked to equatorial Rossby waves, indicating that sea surface temperature fields may contain more information on subsurface wave activity than previously thought. Figures a and b show sea surface temperature across the Pacific estimated from the ERS-1 ATSR and from the ECMWF Global Circulation Model on around 26 July and 17 August 1992. Note that the model waves are not as well developed as the ATSR-observed waves for the months shown here, although the large-scale structure of the model sea surface temperature is well simulated. Courtesy of D Llewellyn-Jones, University of Leicester; M Allen, C Mutlow, Rutherford Appleton Laboratory, Didcot, UK.

2.5. Atmospheric aerosols

The ERS-1 ATSR was designed to measure sea surface temperatures by viewing the same area of the Earth's surface through two different atmospheric paths with a very short time separation. Modelling studies have shown that using these two views provides an indication of the presence of atmospheric aerosols. This is important for two reasons.

Firstly, aerosols cool the atmosphere and mitigate the effects of global warming. They achieve this, by reflecting sunlight, both directly because they are predominantly light in colour and indirectly through the formation of clouds. A second area in which aerosols are important is as a source of mineral input to the oceans. As a result of both these effects, an ability to derive estimates of aerosol concentrations at the global scale provides a valuable contribution to scientific understanding.

Secondly aerosols have a significant effect on the infrared measurements made by the instrument. If these are not accounted for, measurements of the sea surface temperatures may become inaccurate. Discrepancies of up to 2 K between retrieved temperatures and in situ measurements have been noted during serious volcanic dust episodes, although the normal aerosol errors are of the order of 0.2 to 0.3 K. In the past, this has made some satellite-derived sea surface temperatures unusable for meteorology or for climate research, and certainly of no value for the climate record. Direct information about atmospheric aerosols means that sea surface temperature retrievals from ERS-1 ATSR data are less prone to errors from aerosols than data from other satellite sources when data from both viewing paths are used.

The monitoring of aerosols is providing input to the following scientific activities:

- Monitoring the effects of aerosol clouds resulting from volcanic eruptions;
- Monitoring regular land aerosol emissions.

EFFECTS OF VOLCANIC ERUPTIONS

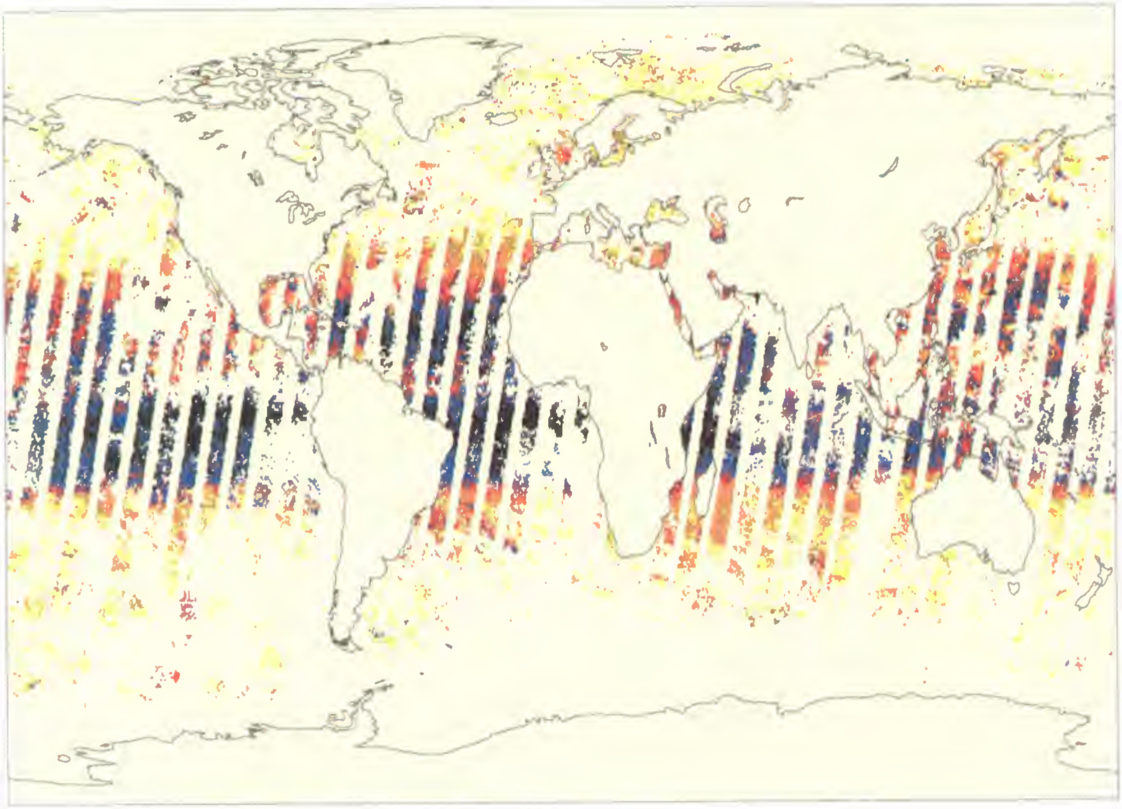

a

Figure 2.21 a,b,c. Analysis of the first two years of ATSR's global dataset shows with great clarity the evolution of the Mount Pinatubo aerosol cloud, which encircled the equator at the start of the ERS-1 mission and, during the next two years, gradually spread polewards and dissipated.

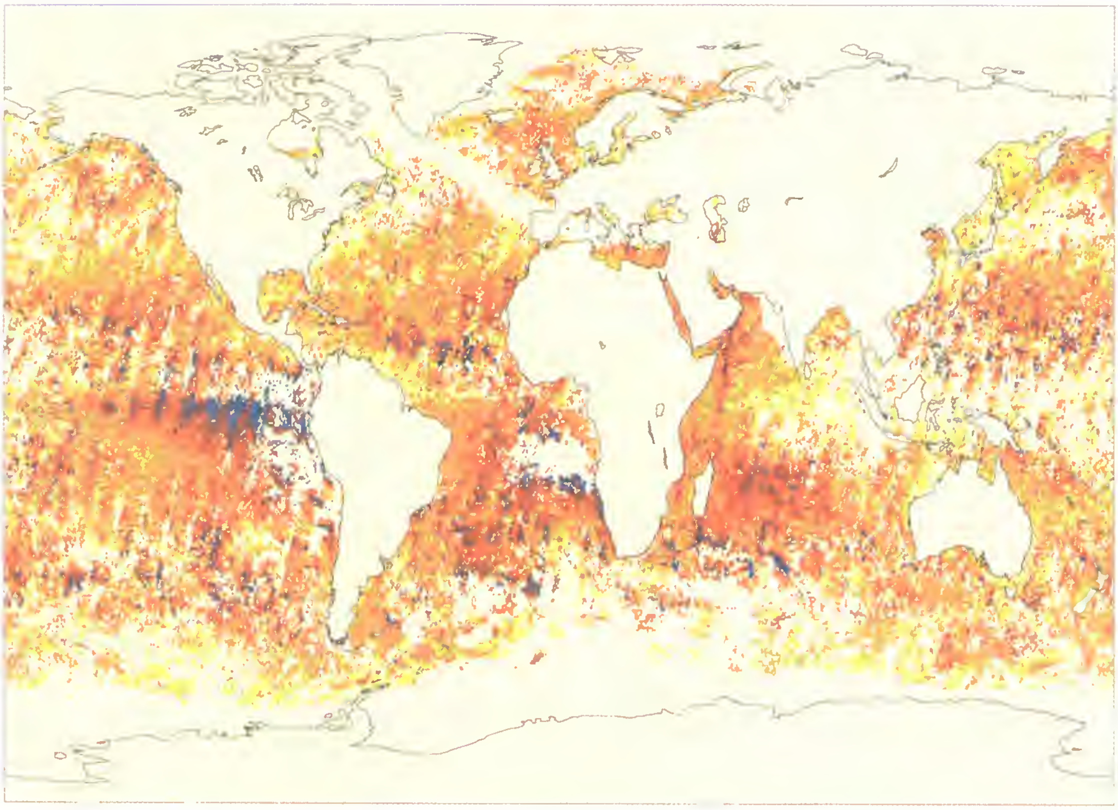

b

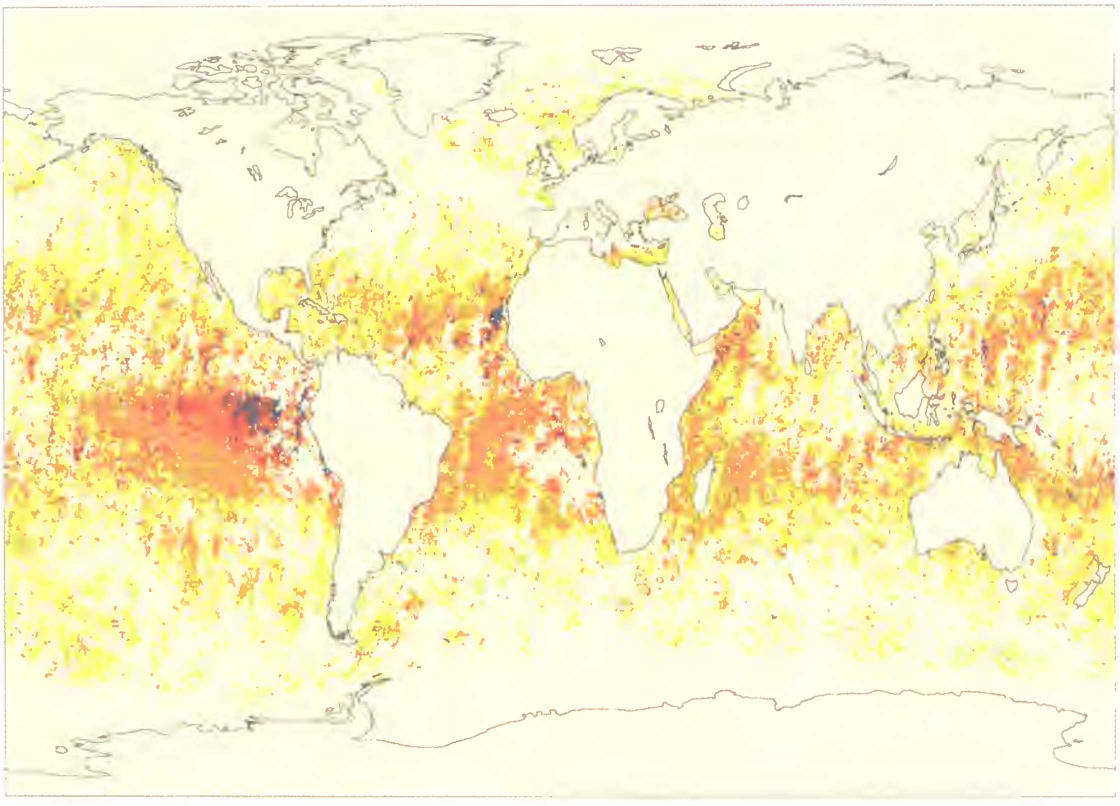

c

A preliminary analysis of these results showed that they are consistent with other observations of the motion of the stratospheric aerosol particles from the Pinatubo event. Figures a, b and c show global aerosol maps derived from ATSR data in August 1991, the month of ATSR's operation, when the aerosols were concentrated close to the equator, in October 1992 when the cloud had spread poleward and in October 1993 when the cloud had dissipated. The darker colours represent higher levels of aerosol concentrations. Courtesy C Mutlow, Rutherford Appleton Laboratory, Didcot; R Dundas, University of Leicester, UK.

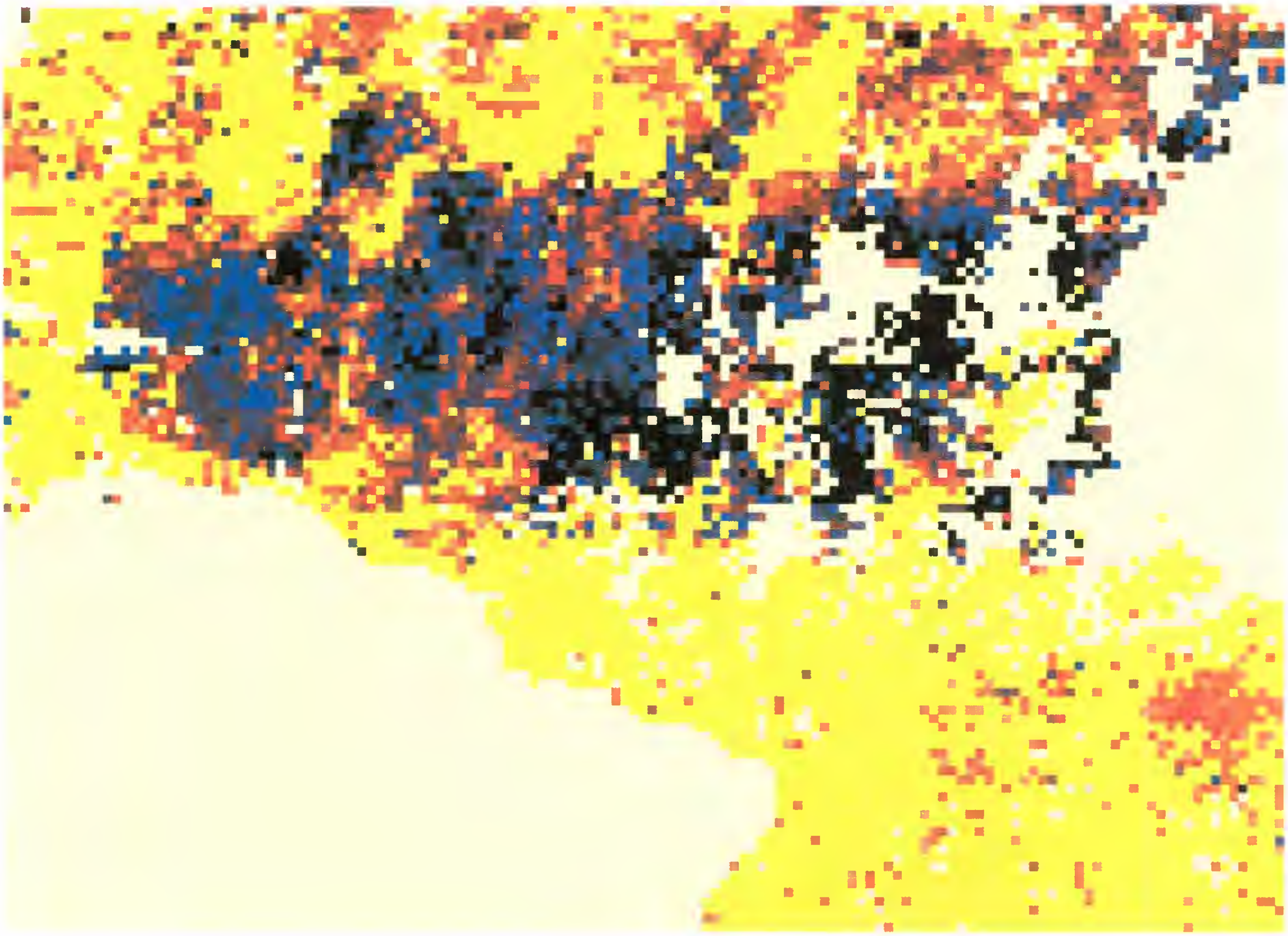

Figure 2.22. An outbreak of dust from the Sahara in July 1993 can be seen by using the difference between dual- and single-view sea surface temperatures from the ERS-1 ATSR. The darker colours indicate higher levels of dust. Such outbreaks are frequent, usually occurring at least once per year, and their overall impact on atmospheric radiative properties are not well characterised.

These data show that ATSR is also well-suited to monitor transient aerosol events in the troposphere as well the stratosphere. Current work is concerned with quantifying the radiative properties (and impact) of the aerosol clouds; with developing a correction for sea surface temperature retrievals in an aerosol-laden atmosphere; and with the examination of correlative data (on atmospheric aerosols) obtained from other sources. Courtesy of R Dundas, D Llewellyn-Jones, University of Leicester, Leicester; C Mutlow, A Zavody, Rutherford Appleton Laboratory, Didcot, UK.

3. REGIONAL OCEAN AND ATMOSPHERE

Regional features in the ocean and atmosphere are of interest for two reasons. Firstly they are a critical component of the climate response of the ocean. Secondly, in many coastal areas and regional seas there are economic and environmental pressures which require more detailed investigations than the global approach of the previous chapter.

In relation to climate processes, mesoscale dynamical features such as eddies and fronts at length scales of the order of 50 to 200 km, driven by transient, dynamical instabilities or related to seabed topography can influence larger-scale transport processes. Eddies also control the horizontal dispersion of chemicals such as nitrates which are essential for biological activity. Understanding the mechanisms by which such features operate and influence large-scale processes is the key to successful parameterisation of climate models. This in turn will lead to more reliable predictions. It is also now possible to implement real-time forecasting of the evolution of mesoscale activity, which is useful for the implementation of in situ ocean experiments.

The coastal zone includes the area extending from the landward margin affected by salt water to the outer edges of the continental shelf. The need for improved monitoring and modelling of the marine environment has increased dramatically in recent years along coastal boundaries and shelf regions where human activities are extensive and pollution has had a significant impact. The priority issues are the effects of changes in sea level, coastal ecosystems, regional wave patterns, shelf-ocean exchange processes and coastal discharge on the coastal environment. Changes in erosion and deposition along coastlines are also important.

In relation to these areas of scientific research, ERS-1 is contributing to the:

- Characterisation and measurement of small-scale atmospheric features which can be inferred from the ocean wave and cloud patterns;
- Understanding of ocean features such as mesoscale eddies and internal waves;
- Detection of changes in coastlines and shallow sea bathymetry;
- Provision of information for studying processes in regional seas.

3.1. Atmospheric features

Local variability of sea surface winds, especially close to the coast, can produce distinctive patterns in sea surface roughness which are more readily revealed by the ERS-1 microwave instrument than by conventional sensors.

ERS-1 SAR data are enabling scientists to characterise the patterns and lateral extent of atmospheric features in a way which was not previously possible. The ERS-1 SAR is more sensitive to changes in wind stress than the earlier SAR on Seasat because of its radar wavelength. In addition, the ERS-1 SAR can detect and measure wind patterns at a range of scales. These capabilities allow patterns to be measured under a wide range of conditions. This is leading to a more complete understanding of processes at the ocean/atmosphere interface.

At a larger scale, the ERS-1 ATSR instrument can be used to monitor wind patterns through the locations of clouds on its images. Particularly in polar regions, where the satellite covers the ground more frequently, movements of cloud from one image to the next can be used to give an indication of wind patterns. The high resolution of ATSR in both space and temperature allows studies of cloud structures and associated mechanisms. An example below is the examination of the structure of Hurricane Andrew. The ERS-1 scatterometer can be used to provide surface winds associated with such events.

The ERS-1 scatterometer allows regional scale atmospheric features to be identified on the basis of the patterns of surface roughness they generate. Examples of such features include tropical cyclones and monsoons.

Examples are given below of the use of ERS-1 instruments to identify a number of small scale atmospheric features, primarily over the ocean. These are:

- Tropical cyclones and monsoons;
- Storm structure;
- Katabatic winds and convective cells;
- Atmospheric gravity waves;
- Atmospheric boundary layer rolls.

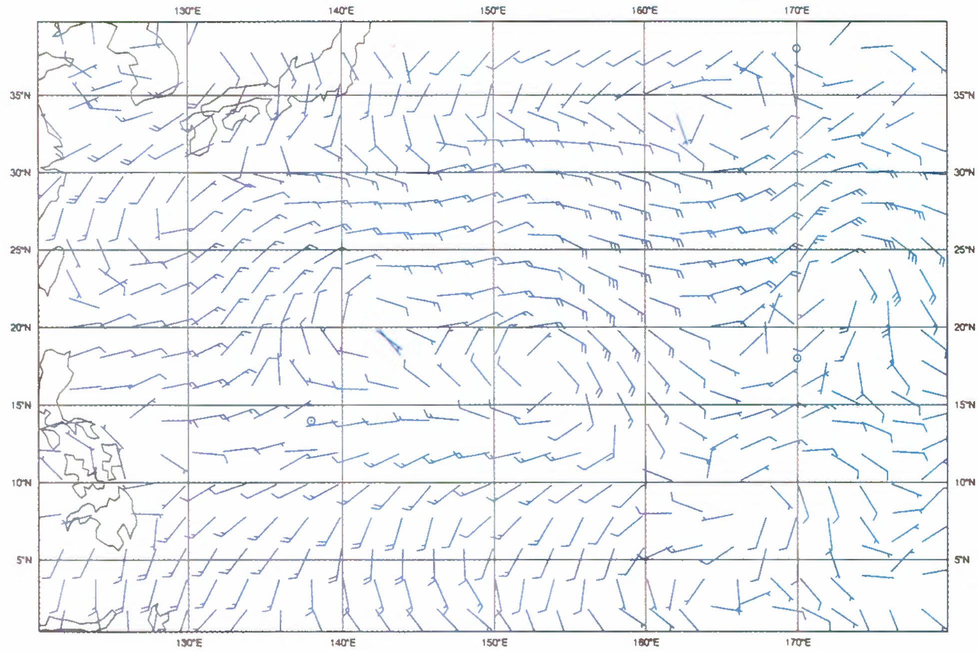

a

21 August 1993

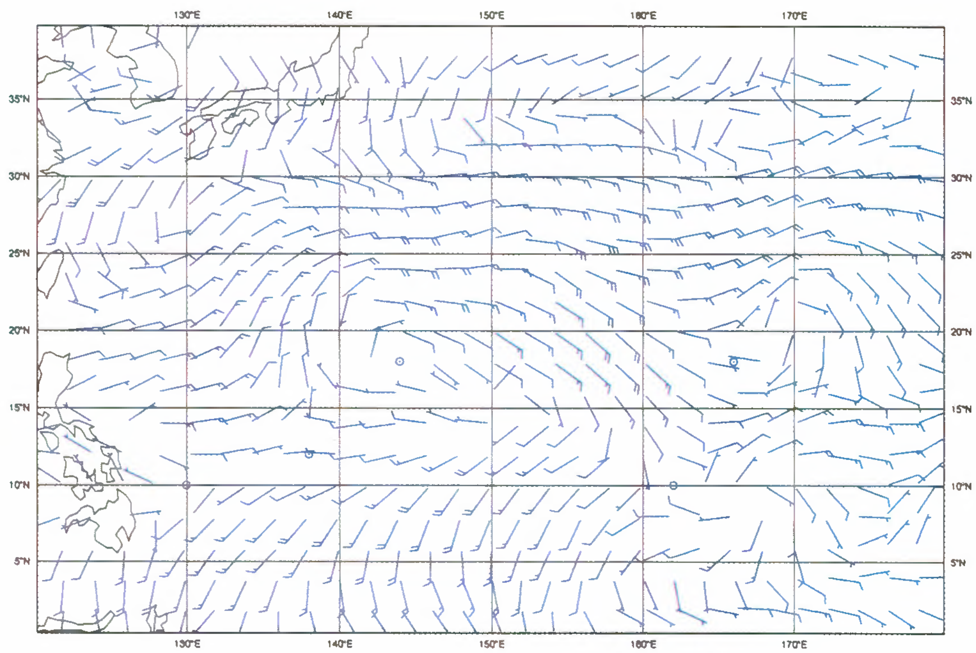

b

Figure 3.1 a,b,c. The main benefits of ERS-1 scatterometer data are to be realised in the observation of small-scale intense systems, such as the observation of otherwise unmeasurable polar lows, the accurate location of mid-latitude fronts and the measurement of the location and intensity of tropical cyclones. The scatterometer provides wind measurements of unprecedented density and accuracy on these systems. The unique capability of the scatterometer to provide measurements in areas of heavy cloud and rain is particularly valuable. The benefits of ERS-1 data for improving the quality of operational analyses of the surface wind field are readily demonstrated.

Figure a shows a wind field derived using ERS-1 scatterometer data while Figure b shows the same forecast without scatterometer data. For this particular area two tropical storms are present: '17W' located at 152°E, 17°N and 'Keoni' located at 173°E, 24°N. For the 17W case, without scatterometer data the storm is incorrectly located at 142°E, 18°N, and with lower winds (20 knots) than with scatterometer data (25 knots). For the Keoni case, without scatterometer data only a weak vortex appears (170°E, 22°N), with lower winds than with scatterometer data (up to 30 knots). The wind field associated with cyclone Keoni is shown in more detail in Figure c. Courtesy of C Gaffard, H Roquet, J Eyre, ECMWF, Reading, UK.

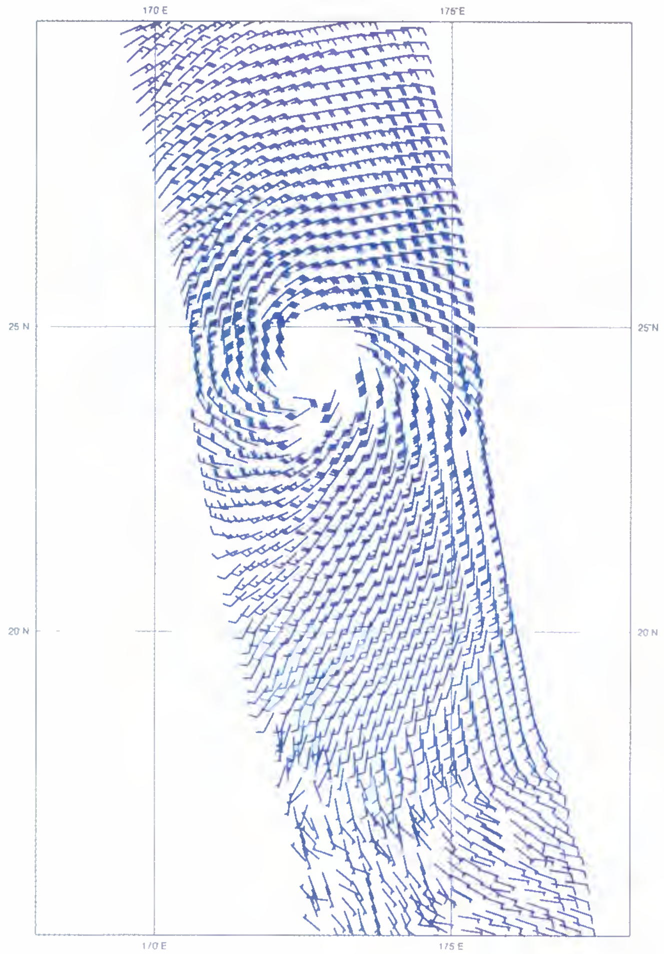

c

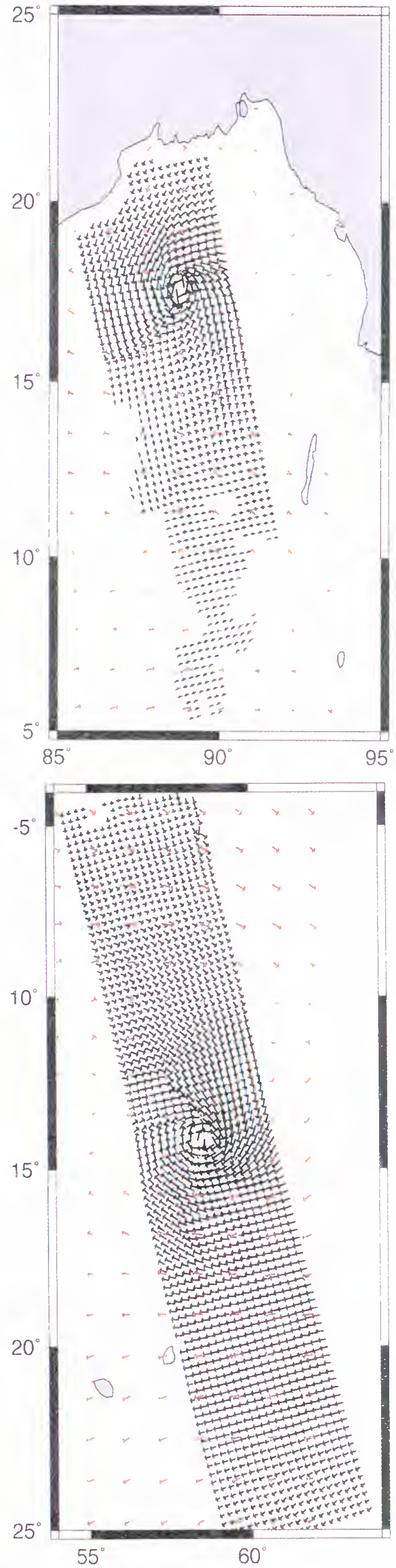

Figure 3.2. Surface wind vectors from the ERS-1 scatterometer provide comprehensive instantaneous views of the circulation patterns in tropical cyclones. The two examples in this Figure show more clearly than indicated by traditional observations that a region of surface convergence stretches out of the centre like a tail in the rear of the storm (with respect to its poleward movement). Differences in magnitude between the scatterometer winds and winds produced by the ECMWF also appear systematic. In the case of tropical cyclone Forrest (19.11.92, top), a total miss of the storm by the numerical model is probably due to the lack of observations. In other cases, such as tropical cyclone Colina (17.01.93, bottom), the ERS-1 scatterometer observations identify model deficiencies and may guide further research on forecasting these important phenomena.

Simultaneously with the scatterometer winds, the ERS-1 SAR obtains directional surface wave information in a small area within the scatterometer swath. The combination of the wind and wave data allows the study of the processes of air-sea interaction that are particularly intense and therefore of high interest in tropical cyclones. The choice of a low frequency, long wavelength for the ERS-1 scatterometer and SAR allows the signals to penetrate the heavy cloud of tropical cyclones.
Courtesy of Y Quilfen, Ifremer, Plouzane, France.

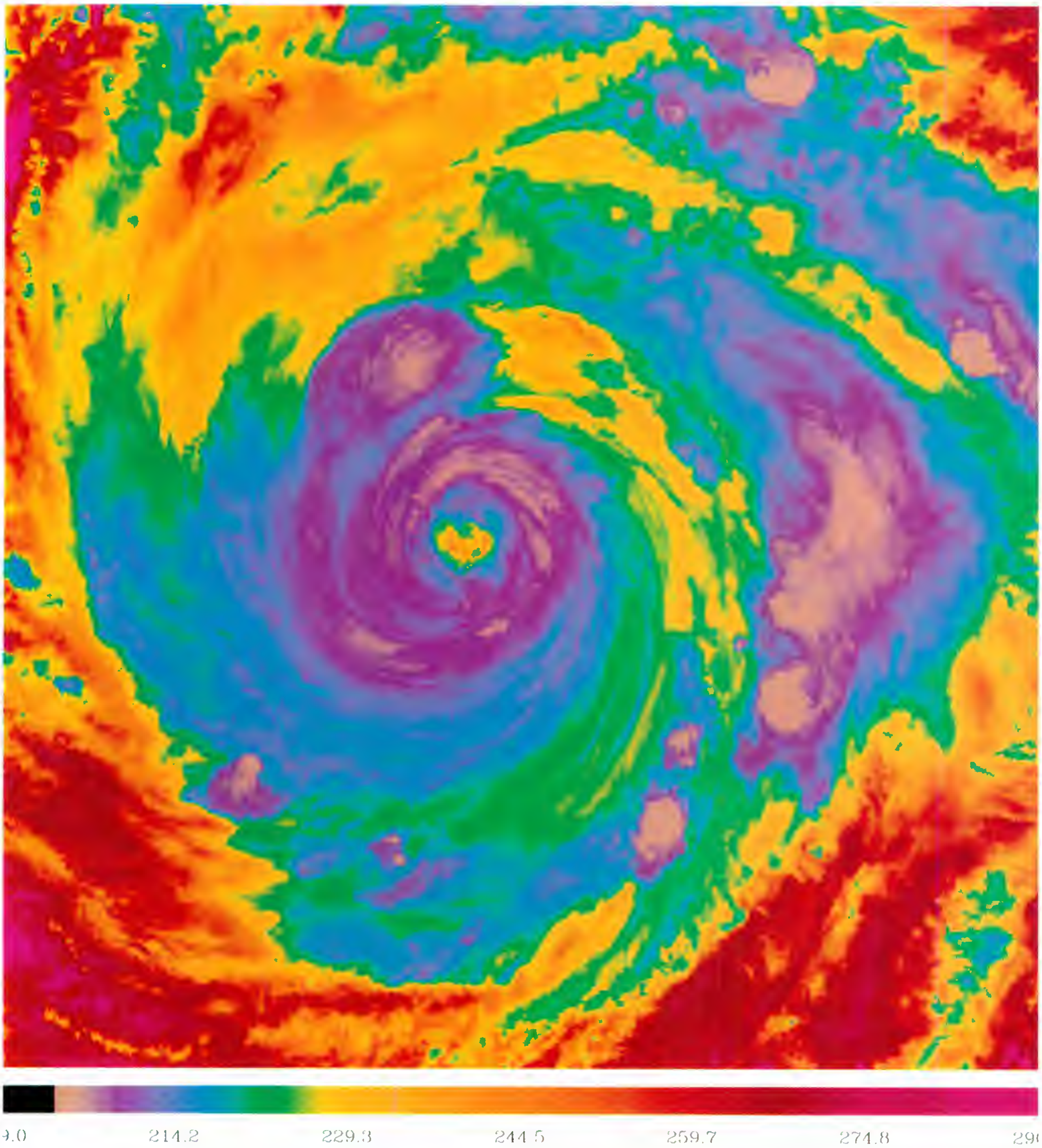

Figure 3.3. In the pre-dawn hours of 24 August 1992, Hurricane Andrew hit the south-east coast of Florida. The ERS-1 ATSR image shown here was acquired around at 11 am, by which time the eye of the hurricane had reached the Gulf of Mexico. Wind spirals in towards the storm centre in an anti-clockwise direction, as is characteristic of cyclonic flow in the northern hemisphere. Temperature decreases towards the central zone, falling to about – 70°C (shown in purple) only to rise by 30°C when the eye of the hurricane (shown in yellow/brown) is reached. This steep temperature gradient implies a strong downdraft at the eye. This and the small size of the eye (only 30 km in diameter) attest to the extreme intensity of Hurricane Andrew.

Satellite monitoring of tropical weather systems plays an important role not only in providing disaster warnings, but also in the study of the formation and development of severe storm systems, and their role in general circulation in the lower atmosphere. The ERS-1 ATSR instrument provides an ability to assess the cloud top temperatures at a higher spatial and thermal resolution than operational meteorological satellites. Recent work has also investigated additional information on cloud structures and cloud top heights. This can be obtained by deriving stereoscopic images from the two viewing paths of the ATSR instrument.
Courtesy of J Murray, Rutherford Appleton Laboratory, Didcot, UK.

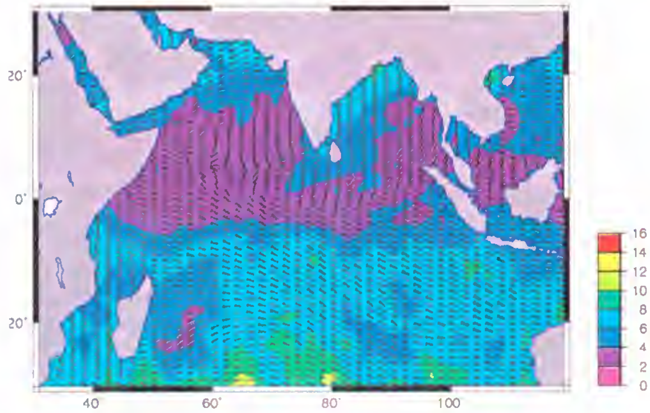

a) 10-16/5/1993

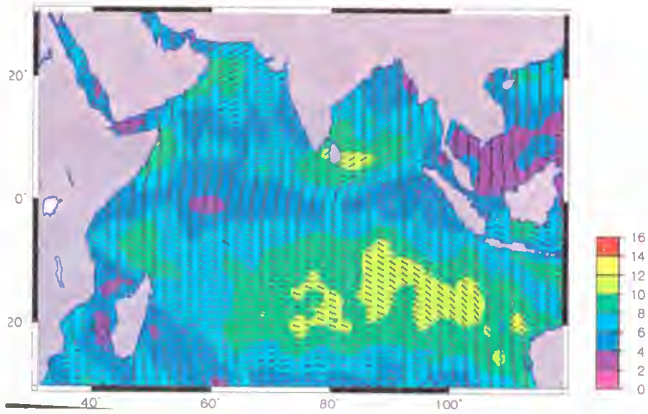

b) 24-30/5/1993

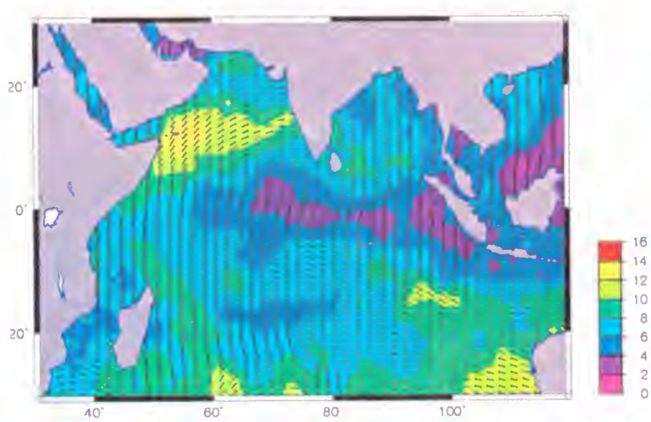

c) 7-13/6/1993

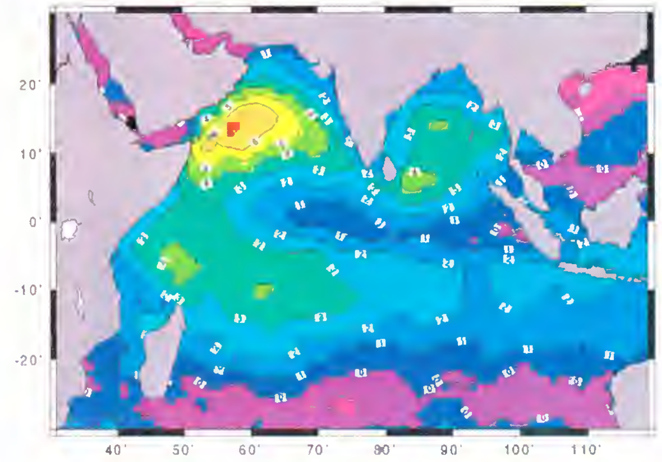

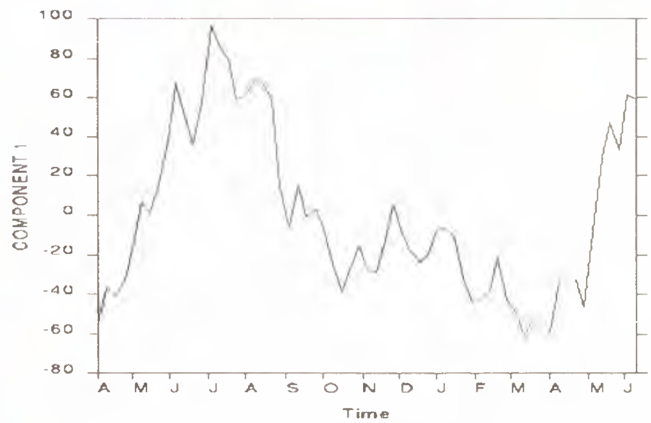

First principal component of the wind speed field.
Top: repartition of the variance. Bottom: time (1992/1993).

Figure 3.4 a,b,c. The global coverage of the ERS-1 scatterometer allows production of mean gridded wind fields with good temporal and spatial sampling in areas where conventional measurements are very scarce. Figure a shows mean wind fields during the time of the 1993 Indian monsoon onset at the end of May. The surface wind becomes southwesterly in the Indian Ocean along the African coast and blows towards Asia. A dramatic increase of wind speeds from 5 to 15 m/s off the coasts of Somalia and Arabia accompanies this turning of the wind.

The seasonal signal is characterised by a sharp increase of the wind speeds at the monsoon onset in May 1992 and 1993 and by a slow decrease during the rest of the year. Intensification of the wind speed near the Somali and Arabian coasts towards Asia is phase locked with the seasonal intensification of the southeast trades in the southern Indian Ocean.

The extension of the wind satellite archive over several years will allow investigation of the interannual variability of the wind field. The global coverage by ERS-1 scatterometer provides a unique opportunity to study the connections between oceans and especially the relationship between monsoon events in the Indian Ocean and El Niño events in the Pacific Ocean. Courtesy of Y Quilfen, Ifremer, Plouzane, France.

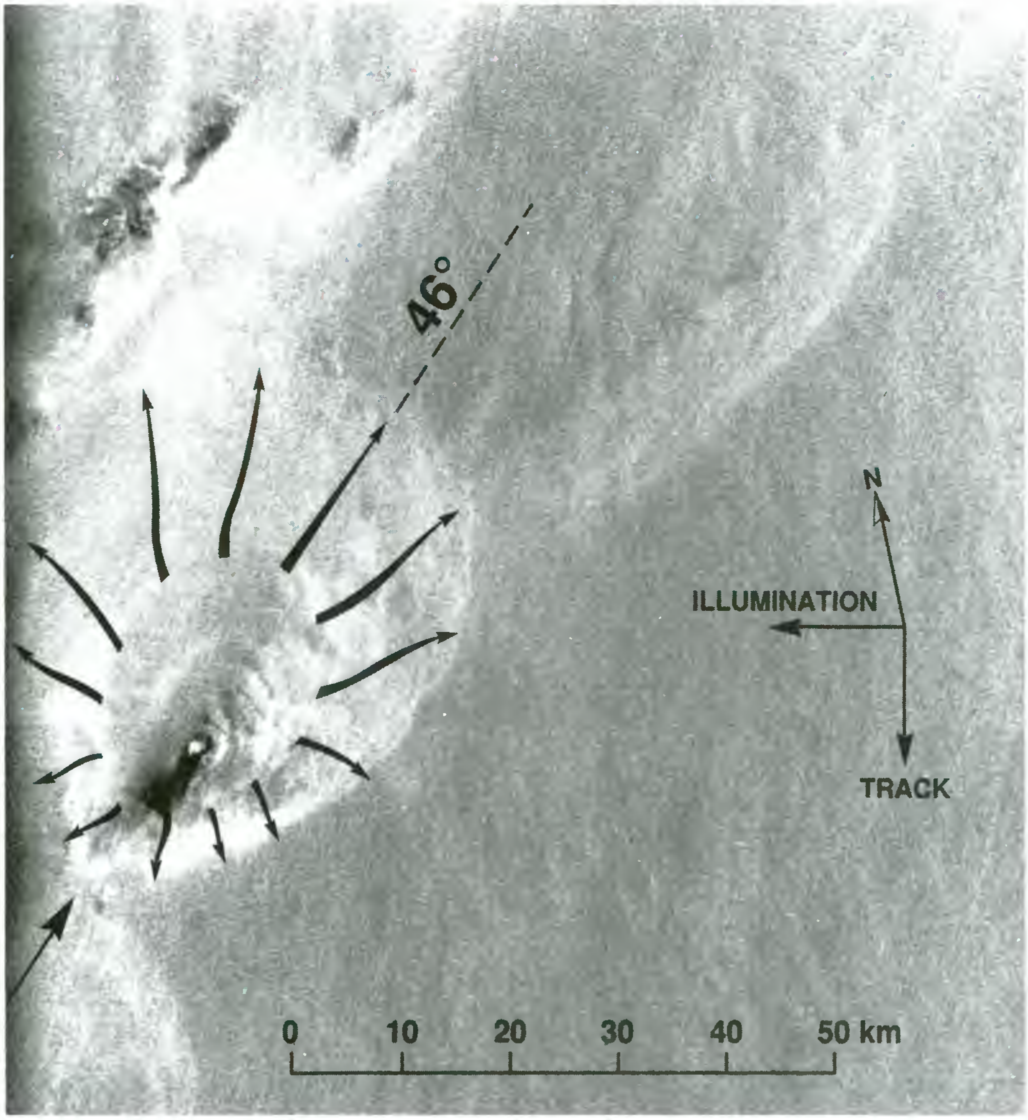

a

Figure 3.5 a,b. This ERS-1 SAR image was recorded at 15:36 UTC on 18 July 1992 off the Atlantic coast of the USA. The echoes are returned selectively from gravity waves of 10 cm length. The stronger the local wind, the larger the waves, and the brighter the echoes. The black, echo-free area near the SW end is due to the absence of waves, which have been damped by rain, a phenomenon known to sailors for hundreds of years. The bright spot at the NE end of this dark area is due to splash products of the rain. A downdraft accompanies the most intense rain as is shown schematically in Figure b. On impacting the surface the draft diverges to become horizontal winds which flow out in a manner shown by streamlines superimposed on Figure a and shown in Figure b. The tips of the streamlines correspond to the boundary of the outflow, i.e. the well-known gust front which accompanies most thunderstorms. When the streamlines are extrapolated back to their apparent origin they are found to emanate from the echo-free area near the SW end of the plume. The storm footprints reveal much of the nature and history of the storm evolution, some of which was not well known even over land where sophisticated observations were made. This helps to provide insights into the mechanisms of microbursts which are known to be responsible for fatal air crashes. Observations such as these also contribute to the global climatology of storms over seas which are important in driving the general circulation of the global atmosphere. Courtsey of D Atlas, NASA Goddard Space Flight Center, Greenbelt, USA.

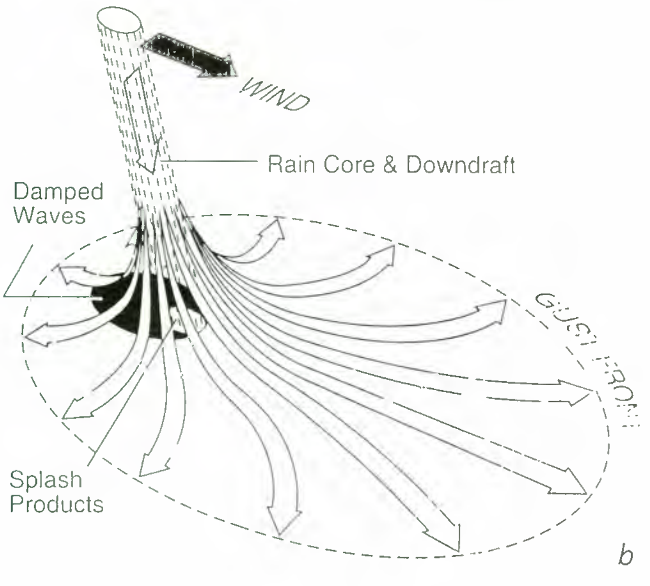

b

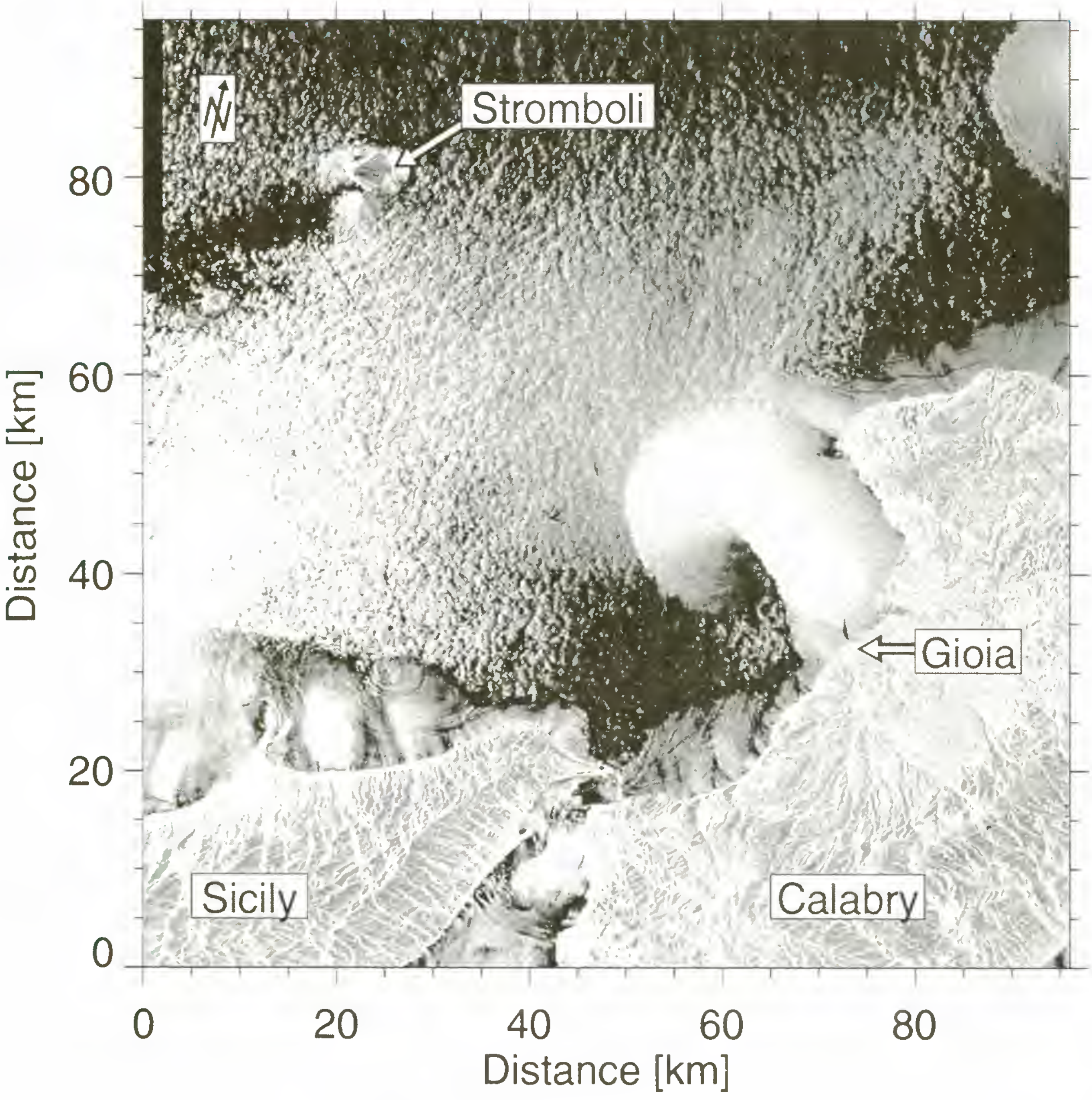

Figure 3.6. Katabatic winds are generated in the evening and night when air near the surface cools faster over land than over sea. As a result cold winds blow down sloping terrain and out over the adjacent sea surface. Sea surface evidence of katabatic wind fields has often been identified in SAR images for coastal regions in the Mediterranean Sea, especially those adjacent to mountainous areas. This Figure shows patterns arising from katabatic winds off the north coast of Sicily. The range of the katabatic wind onto the sea (typically 10-30 km) and the area of the 'katabatic tongue' can be inferred from ERS-1 SAR images. It is also possible to extract the distribution of sea surface wind velocities in the katabatic tongues from the SAR images by using the scatterometer model function.

Convective atmospheric cells are generated over the sea when the water temperature is higher than the air temperature and when the wind speed is low. It is believed that cellular features which are often visible on ERS-1 SAR images acquired over the Mediterranean Sea in the evening (during summer) are sea surface manifestations of atmospheric convective cells. An example of convective cells can also be found on this Figure. It is suggested that the granular features visible between Sicily and the island of Stromboli are surface manifestations of atmospheric convective cells. Courtesy of W Alpers, C Bruening, University of Hamburg, Germany.

Figure 3.7. ERS-1 SAR observations of long-wavelength wave phenomena associated with atmospheric processes over the ocean are common. Atmospheric gravity waves occur as quasi-periodic waves or as solitons. They are often generated behind mountain ranges in which case they are called lee waves. In the steady state, lee waves are stationary with respect to the terrain feature, but they propagate relative to the mean air flow above the Earth surface. Lee waves are often seen in visible remote sensing imagery where they manifest themselves as wave-like cloud patterns. However, they also can manifest themselves on the sea surface since they are associated with a varying surface stress which modulates the sea surface roughness.

Sea surface manifestations of atmospheric internal solitary waves have been delineated on ERS-1 SAR images. An example is given here. Simultaneous high-resolution wind measurements carried out from a meteorological mast on the island of Heligoland confirm this interpretation. The atmospheric internal solitary wave passed Heligoland 25 minutes before the ERS-1 SAR image was taken. Courtesy of W Alpers, C Bruening, University of Hamburg, Germany.

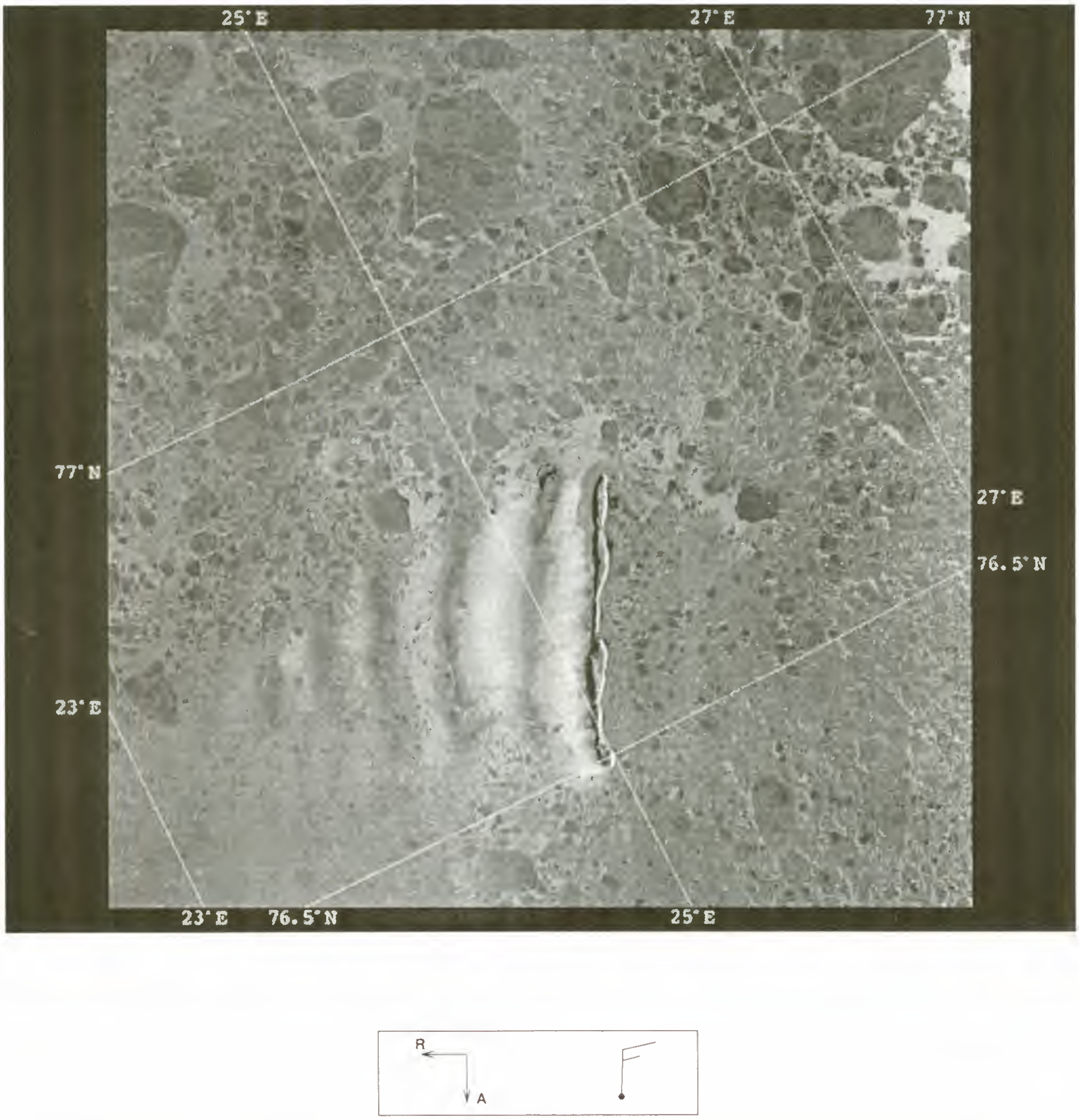

Figure 3.8. Atmospheric lee waves associated with the island of Hopen (southeast of Svalbard in the Barents Sea) are apparent in this ERS-1 SAR image recorded on 20 June 1993. Six well defined wave crests of 7.6 km wavelength oriented nearly parallel to the island can be observed. Two of the six crests are over open water. The ice in the upper portion of the image was comprised of large densely packed floes, while that in the lower portion was made up of smaller loosely packed floes. The open water around the smaller floes provides an imprint of the lee waves on the open water roughness, thus allowing the pattern to be imaged even over the ice-covered region. The amplitude and wavelength scale of these waves can be estimated allowing estimates of wind vector variations over kilometre scales. This is useful in near shore regions or in the marginal ice zone and could provide information on atmosphere boundary layer dynamics. Courtesy of P Vachon, Canada Centre for Remote Sensing, Ottawa, Canada; O Johannessen, Nansen Environmental and Remote Sensing Centre. Bergen, Norway; J Johannessen, ESA/ESTEC, Noordwijk, The Netherlands.

Atmospheric boundary layer rolls are helical circulation patterns in the atmospheric boundary layer which are superimposed on the mean wind field. They can be generated either by thermal instability when the layer is heated from below or cooled from above, or by dynamic instability when the wind velocity changes with height.

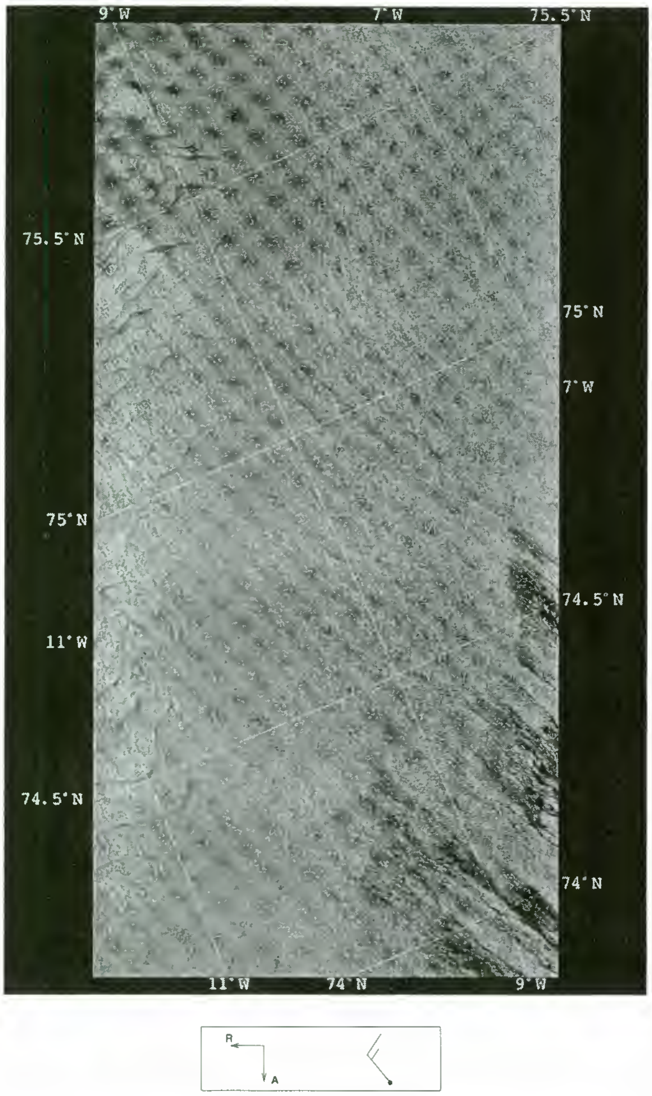

a

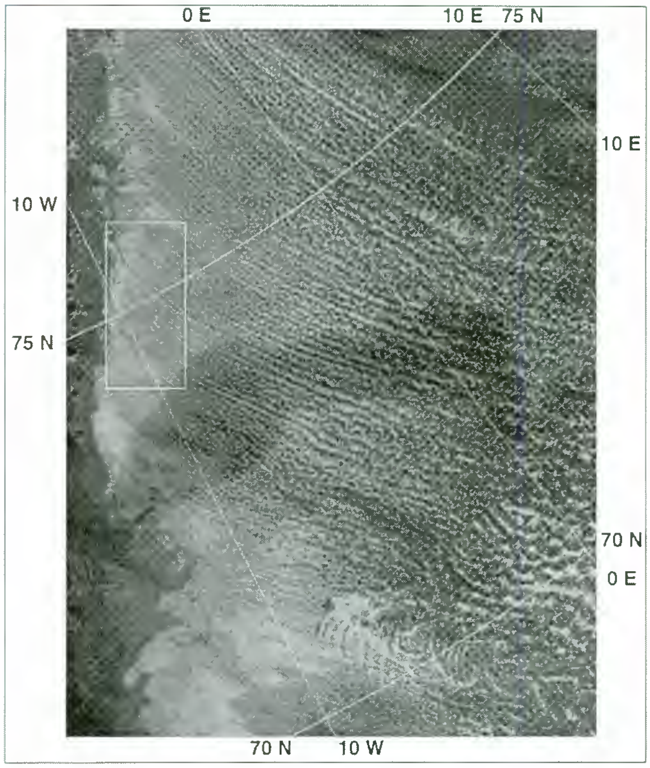

b

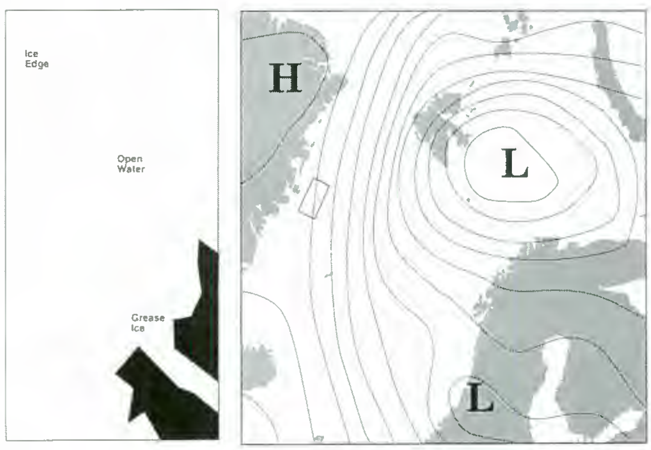

c

Figure 3.9 a,b,c. A good qualitative relationship between the boundary layer structure from cloud patterns in AVHRR (US optical sensor) images and the surface roughness from ERS-1 SAR has been found. In this example there is a cloud structure evolving downwind from the ice edge in the Greenland Sea. The cloud structures are associated with horizontal roll vortices in the atmosphere boundary layer. The ERS-1 SAR image (Fig. a) shows the corresponding surface roughness with a streak like pattern having an orientation aligned in the direction of the roll vortices. The mean streak spacing is 5 km, which is in agreement with the estimate from the AVHRR image (Fig. b). The short waves that produce this pattern are formed in response to the variations in the wind stress. Using a model with the SAR radar cross section values the mean wind speed was estimated to be 8.0 $\pm$ 2 m/s which compares well with the mean wind speed observed at Jan Mayen of 7.5 m/s. An interpreted weather map is shown in Figure c. This qualitative and quantitative information provided by ERS-1 SAR is additional to that from other data sources and is important for knowledge on surface wind fields and fluxes in the atmosphere boundary layer. Courtesy of J Johannessen, ESA/ESTEC, Noordwijk, The Netherlands; P Vachon, Canada Centre for Remote Sensing, Ottawa, Canada; O Johannessen, Nansen Environmental and Remote Sensing Centre, Bergen, Norway.

Figure 3.10. An unusual cloud formation around the South Sandwich Islands in the South Pacific was recorded from ERS-1 ATSR on 4 March 1992. It covers an area of 512 × 512 km. Most striking is the stable and regular pattern of crescent shaped clouds (shown in white) which are shed alternately from the east and west sides of the northernmost islands. Such a pattern is known as a Von Karman vortex sheet. Courtesy of D Llewellyn-Jones, University of Leicester, UK.

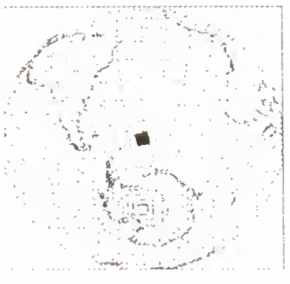

3.2. Ocean features

The modelling of global ocean circulation and transport requires a knowledge of processes which occur at smaller scales and which need to be studied regionally. For example, mesoscale variability of the ocean circulation at length scales between 50 and 1000 km has been identified in nearly all oceanic areas and may account for nearly half of the kinetic energy in the upper ocean. At even shorter scales, dynamical processes in stratified water can influence vertical mixing between the surface and lower layers and hence affect transport processes at much larger scales. There are several examples of how ERS-1 is contributing to the regional study of features such as:

- Eddies;
- Internal waves.

Surface slicks evident in SAR images can serve as tracers for delineating surface flow patterns associated with eddies in coastal waters and may be observed using ERS-1 SAR. Such slicks may be naturally occurring features associated with algae, or result from chemical pollution such as oil. Regional oceanic phenomena, particularly coastal current fronts become visible in SAR images from short-wave current interactions along shear and convergence zones, or from the spatial distribution of the slick material on the sea surface. However these relationships are far from being understood.

Mesoscale eddies in the Atlantic are dominant in the variation of ocean currents, dynamic topography and local temperature gradients. They occur mostly on scales of between 100 and 200 km. Moreover, at high latitudes, mesoscale eddies with scales of 30 to 50 km occur frequently. The scale of these phenomena is addressable with ERS-1 radar altimeter, ATSR and SAR data. The radar altimeter for example, has a high sampling rate making it well suited for mesoscale applications. Improvements in process understanding resulting from these observations has lead to an associated improvement in the parameterisation and validation of ocean models. This in turn will enhance weather and ocean forecasting as well as climate change studies.

Internal waves are undulations in the interface between layers of water of different density. They are caused by mechanisms such as the flow of water over sills, in the Strait of Gibraltar, or tidal currents meeting the coastal shelf. Their wide significance relates to the fact that internal waves can break at the ocean margins. This is an important cause of vertical mixing in the ocean and thus contributes to global water circulation.

Observation of the spatial structure and propagation characteristics of internal waves is possible only by using SAR. Internal waves create a surface roughness signature which is detected by SAR. ERS-1 has therefore made possible new scientific studies of internal waves and the data are also used in support of field observations and the validation of numerical models.

EDDIES — COASTAL

a

b

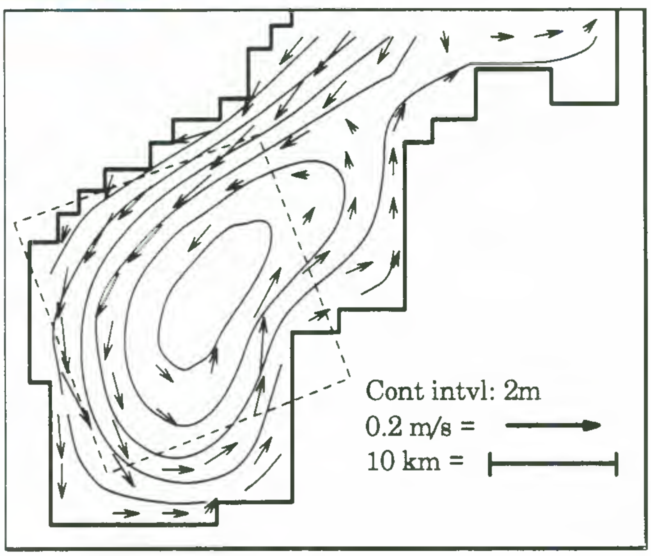

Figure 3.11 a,b. Figure a shows a cyclonic eddy in Frohavet obtained on 21 August 1991 from ERS-1 SAR. The image covers an area of 20 × 20 km. The bright point in the lower right is a ship and the larger bright areas along the left of the image are coastal islands. Figure b shows the upper circulation derived from a model. Arrows mark the flow direction and strength. The contour lines mark the departure from the initial upper layer thickness of 50 m at 5 m intervals. The area of the model is shown by the step-like boundary outlining the shallow water isobath (< 50 m) of Frohavet. The rotated square box represents the 20x20 km coverage of the ERS-1 SAR image. Courtesy of J Johannessen, ESA/ESTEC, Noordwijk, The Netherlands; L Röed, DNMI, Oslo, Norway; T Wahl, Norwegian Defence Research Agency, Kjeller, Norway.

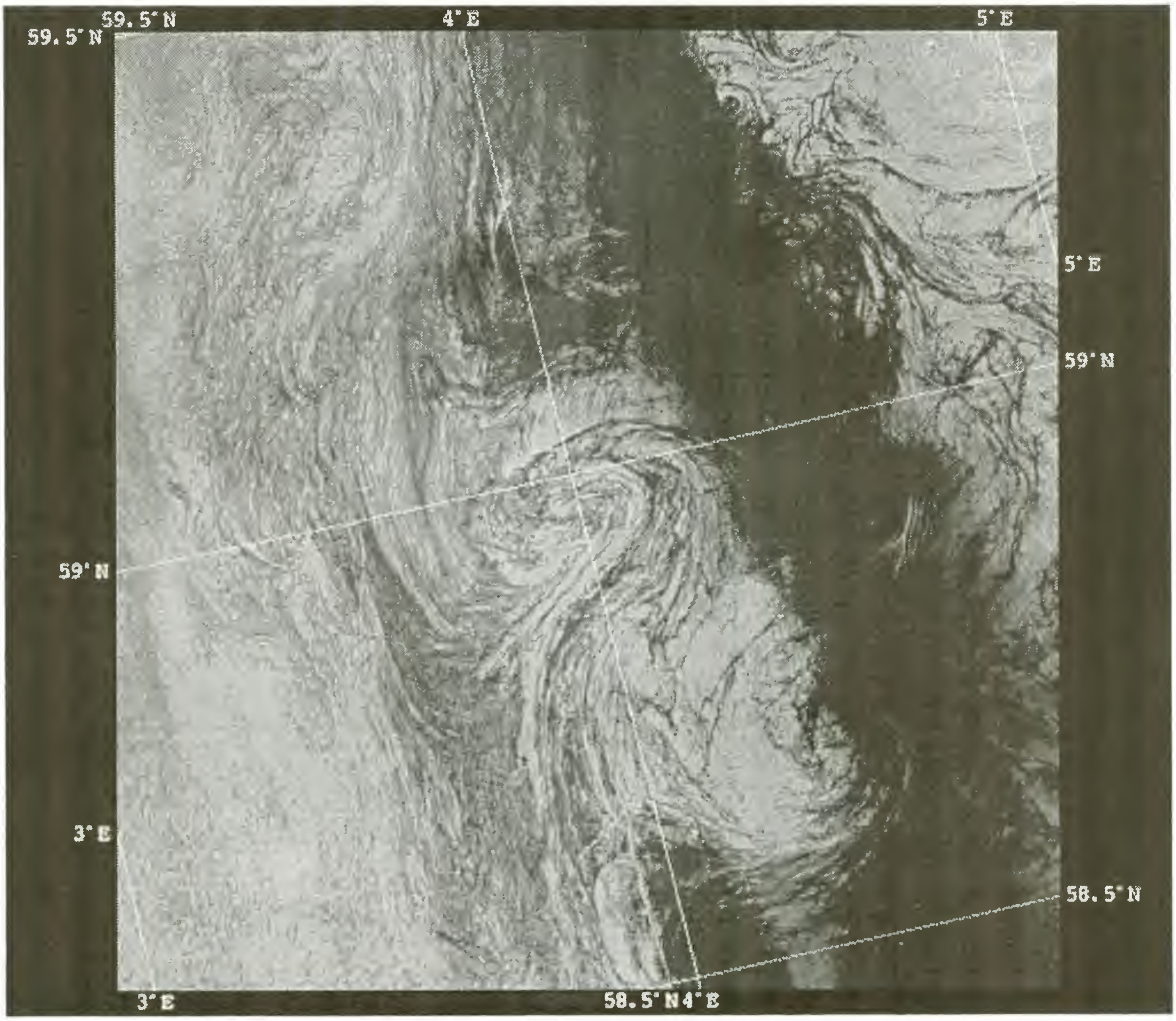

Figure 3.12. Understanding the circulation within the Norwegian Coastal Current is becoming more critical as concern about the environment grows. A major toxic algae bloom or a large oil spill due to a ship collision could have dramatic ecological and socio-economic impacts. ERS-1 SAR images, along with infrared images and ERS-1 radar altimeter data are being used to increase our understanding of these phenomena. They are combined with modelling tools where the model provides even higher temporal and spatial resolution. This Figure provides information on the local wind field variations, mesoscale circulation patterns and internal waves. In addition, slicks (natural film) at the sea surface can be seen as dark features. Although the coupling between slicks and ocean processes is not well understood, the surface expression is important for oceanography. The spiralling structure implies convergence towards the centre, providing information which is important for the validation of model results. Courtesy of J Johannessen. ESA/ESTEC, Noordwijk, The Netherlands.

Figure 3.13. Surface slicks have been identified off Vancouver Island on the west coast of Canada. At present, little is known about the seasonal or spatial distribution of these slicks, although the importance of organic matter in the sea surface micro-layer has long been recognised with benthitic plants and phytoplankton as common causes. Wind speeds need to be between 2 to 5 m/s to identify these slicks. At low wind speeds the surface is not rippled and the image appears black (see centre of Figure) and when the wind speed is too high, surface roughness dominates. In this Figure, which covers 100x100 km, the slicks show an eddy feature and are between 100 and 400 m wide and 5 to 20 km in length. Courtesy of J Gower, University of British Colombia, Sidney, Canada.

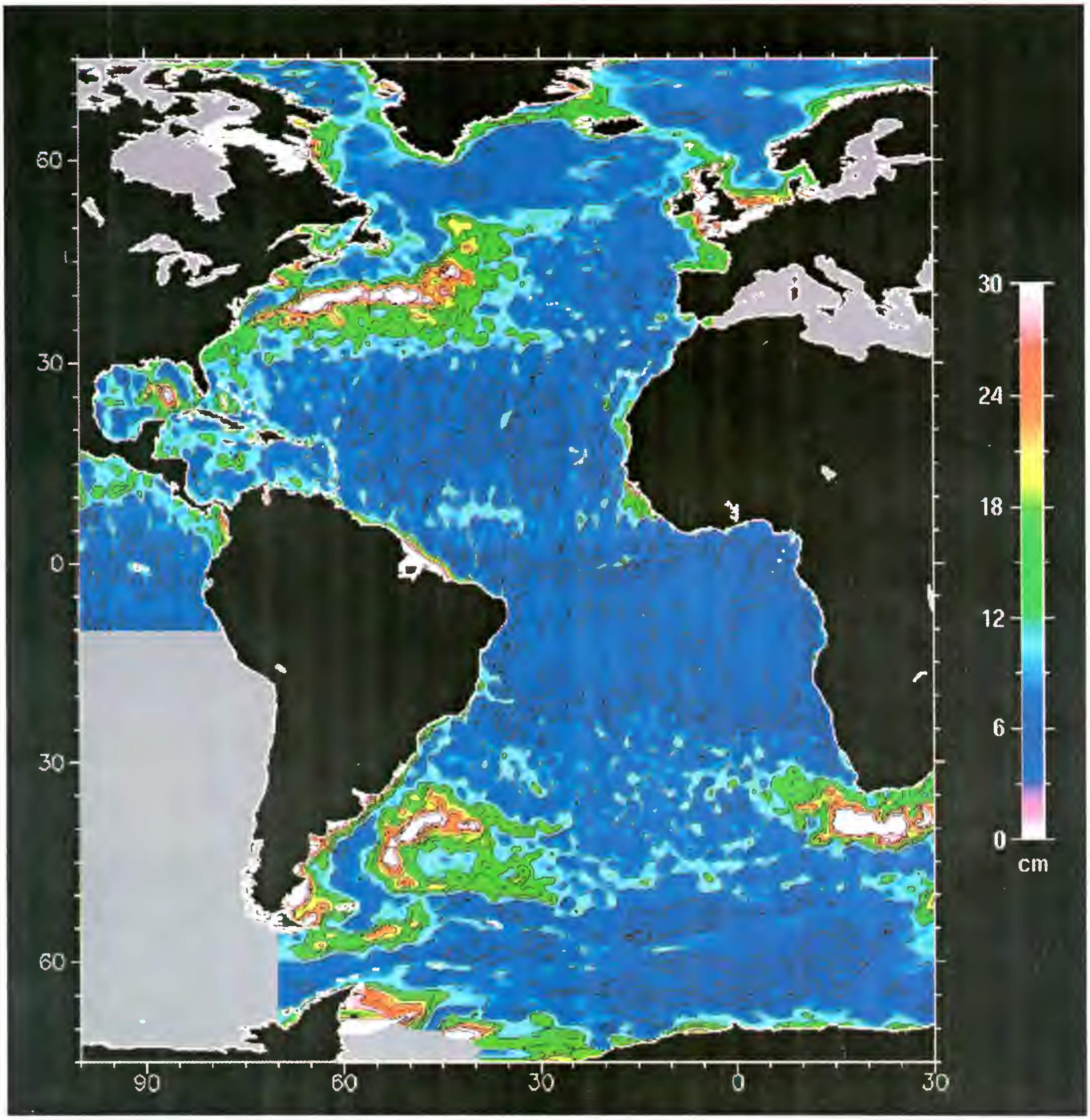

Figure 3.14. This Figure shows the sea surface variability in the Atlantic Ocean based on ERS-1 altimeter data from the multi-disciplinary phase (35-day repeat orbit), covering the period from April 1992 to April 1993. The variability has been computed as the root mean square of the differences from the mean sea surface and as such represents the energy related to ocean surface currents. Typical high-energy areas like the Gulf Stream, Agulhas Retroflection and Brazil-Falklands Confluence, display variability levels of over 25 cm. Most of this variability can be explained by meandering currents, the forming and motion of eddies, and moving fronts. In the North Atlantic, the Gulf Stream shows evidence of bifurcation in the Gulf Stream Extension and in a return current to the south forming the gyre around the Sargasso Sea. Courtesy of M Naeije, Delft University of Technology, The Netherlands.

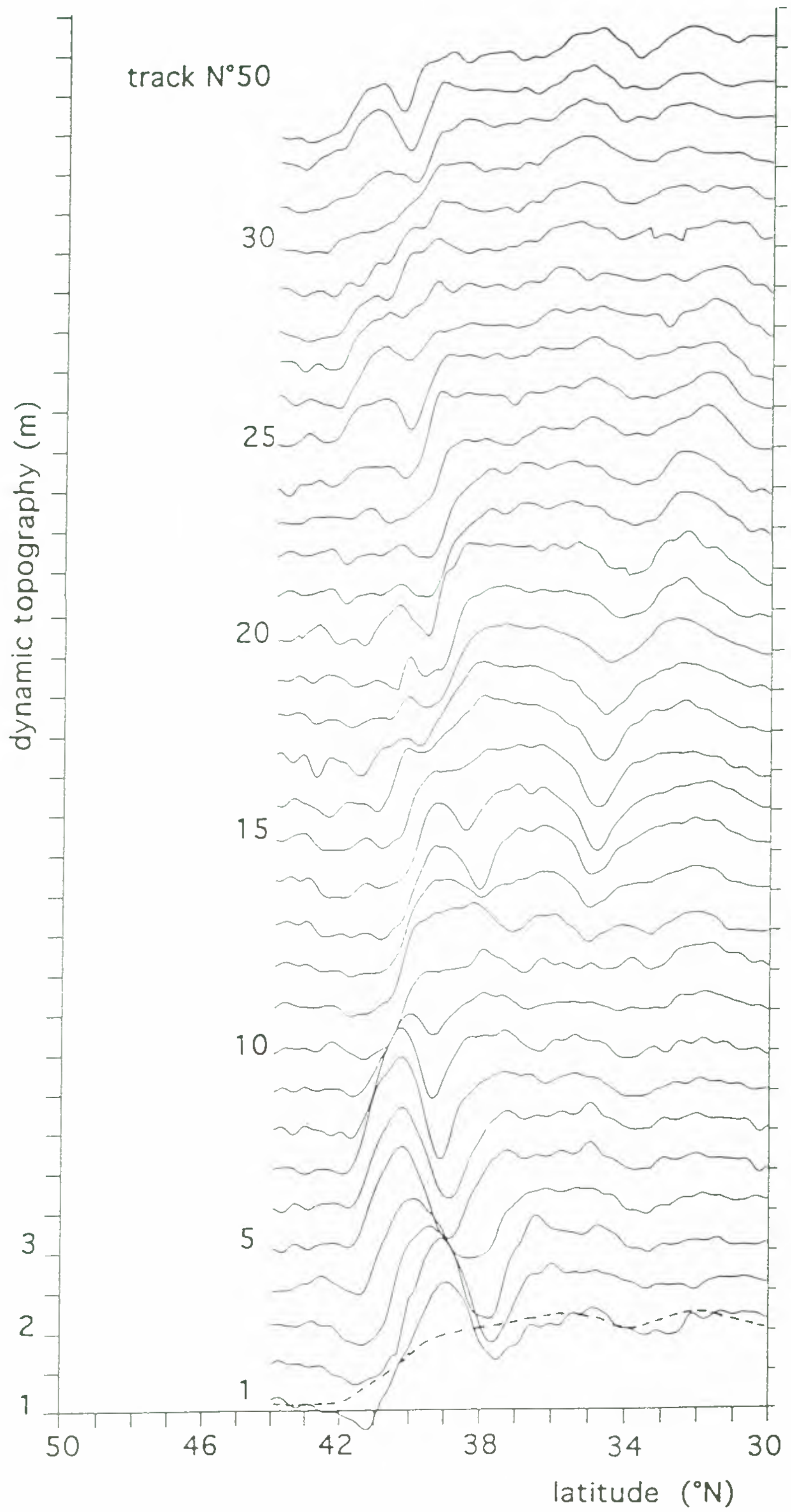

Figure 3.15. ERS-1 radar altimeter data are used extensively to monitor mesoscale features in many parts of the world's oceans. In particular, data from the three-day repeat period provides a unique sampling of high-frequency fluctuations of strong western boundary currents, which was not achievable using Geosat or Topex/Poseidon data. It was found that up to 15% of the sea level variance was due to evolutions on periods shorter than one month, while the surface transport of the Gulf Stream could vary by up to 50% during a meander event. Courtesy of J-F Minster, M-C Gerreno, CNES-CNRS/GRGS, Toulouse, France.

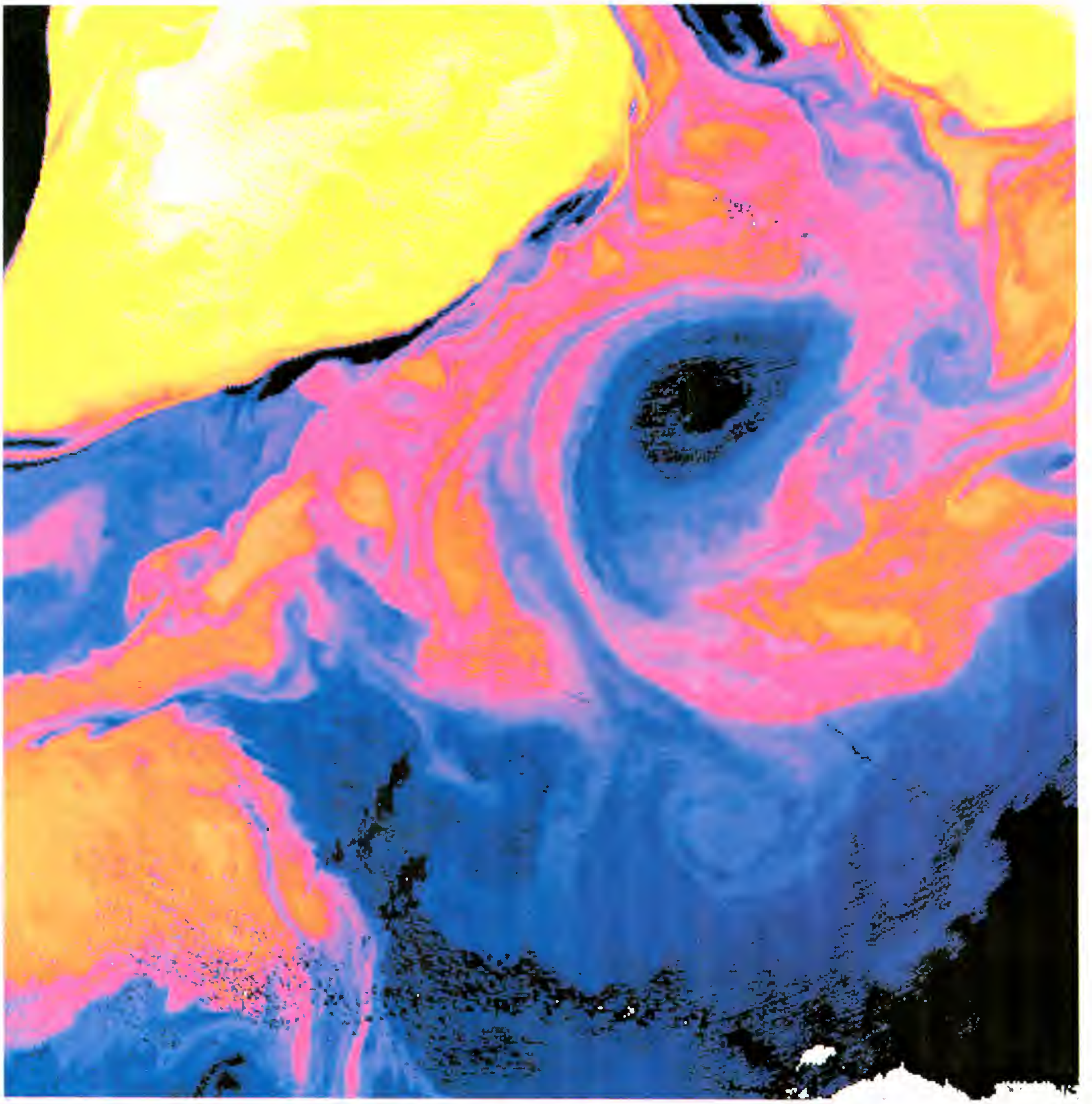

Figure 3.16. In the South Atlantic where the warm Brazil Current flowing from the northeast meets the cold Falkland Current flowing from the southwest, cyclonic cold eddies and anticyclonic warm eddies have been observed using ERS-1 ATSR data. The boundary between the two currents is made up of interleaving bands of warm and cold water and is not as homogenous as once thought. The dominant feature is a large cold core eddy some 150 km in diameter with long filaments of water entrained in the eddy's periphery. These filaments differ in temperature from their immediate surroundings by between 0.2 and 0.5°C. They are only 1 to 2 km wide, but extend as coherent entities for up to 200 km. They have apparently been drawn into patterns by the mesoscale geostrophic flow field. The temperature contrasts in this field are low. It is only because of the high sensitivity of the ERS-1 ATSR instrument that the structures can be seen. Images such as this will help physical oceanographers to understand more about the balance between advective and diffusive transport processes in the ocean. Courtesy of I Robinson; C Donlon, University of Southampton, UK.

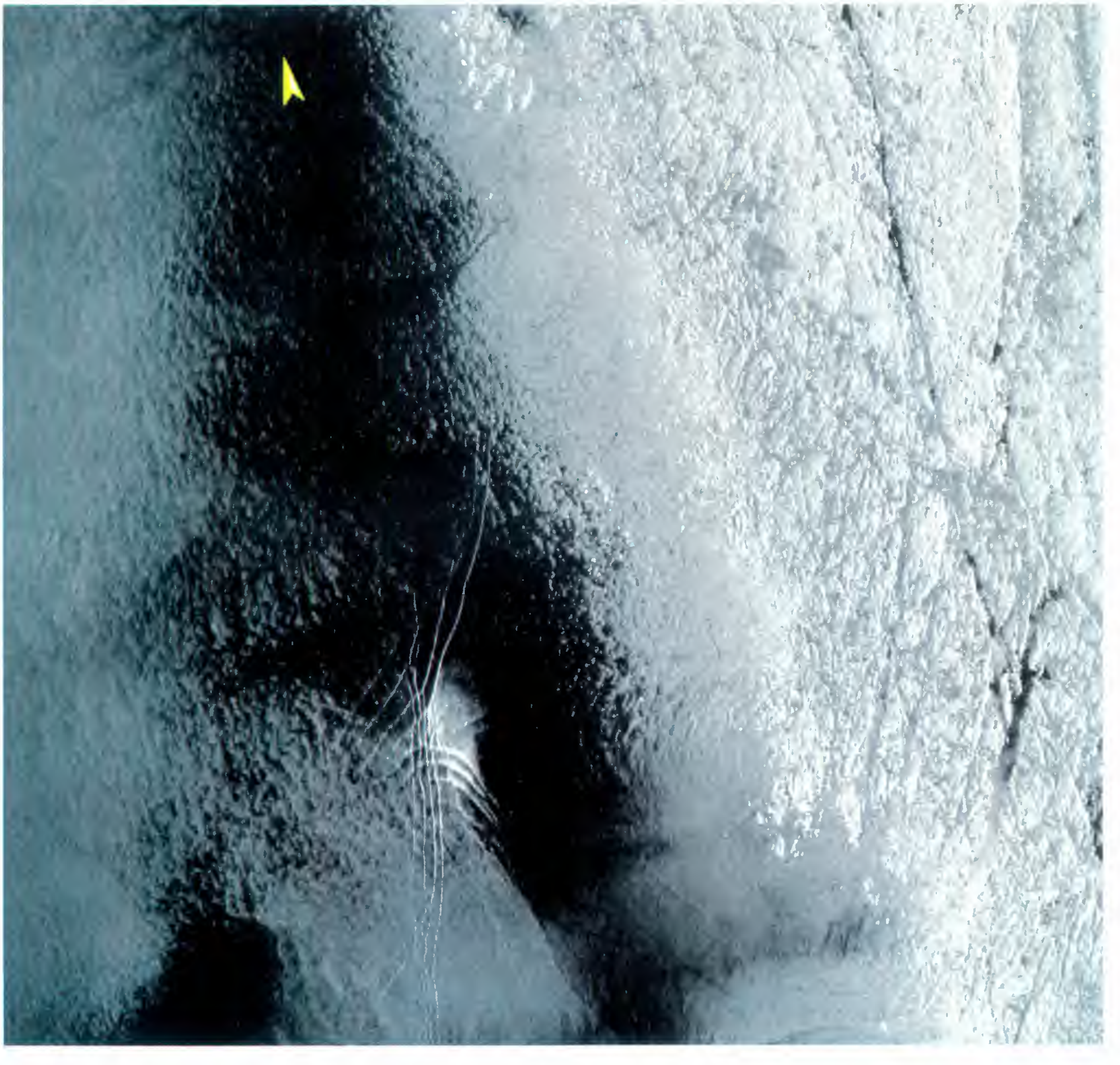

Figure 3.17. Wave propagation can occur on the horizontal boundary between different water masses (usually warm water overlying colder water). The spatial distribution and propagation characteristics of such ocean internal waves have been hitherto very difficult to define using in situ instrumentation. ERS-1 SAR data have shown that such internal waves occur frequently in coastal waters worldwide. The internal waves are usually generated by tidal flow over seafloor topographic features such as shelf breaks and sea mounts. Ideally one would like to use observations of internal waves generated at known places to deduce information about water stratification. This information is important for many sorts of acoustic sensing and communication systems, both military and civilian. This figure shows an example from the ERS-1 SAR recorded on 26 May 1993 in the Skagerak basin between Denmark, Norway and Sweden, where several trains of internal waves meet and interact in a linear way. Courtesy of T Wahl, Norwegian Defence Research Establishment, Kjeller, Norway.

Figure 3.18. Surface roughness patterns associated with an internal wave packet propagating eastwards can be delineated on this ERS-1 SAR image of the Strait of Gibraltar. These internal waves are generally thought to have been excited by tidal currents along the bathymetry of the strait. The internal wave pattern is crossed by a dark streak which is likely to be due to an oil spill released by a ship. Courtesy of W Alpers, C Bruening. University of Hamburg, Germany.

a

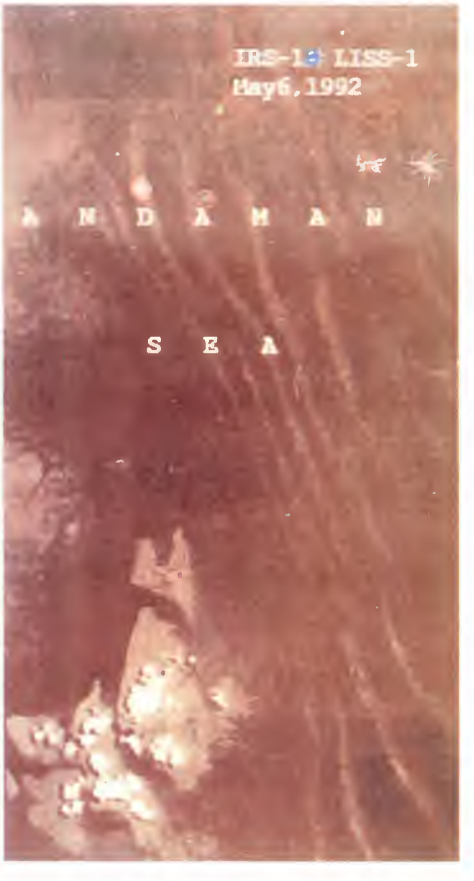

b

Figure 3.19 a,b. The phenomena related to the occurrence of internal waves in the ocean around India are being studied. Attempts are underway to model the interaction of large internal waves with shallow bottom topography using ERS-1 SAR data (Fig. a) and optical data from the IRS-1 LISS-1 (India) instrument (Fig. b). Considerably more detail can be observed in the ERS-1 SAR image than the IRS-1 LISS-1 image. Internal solitary waves identified in the ERS-1 SAR data have revealed unknown features of the topography over the shallow continental area of the Andaman Sea. Evidence of a second generation of internal waves has been found in the region north of the Outram islands. The internal waves have a length of 3 to 15 km and a crest length as large as 200 km. The inferred mechanism for these waves is the interaction of the semi-diurnal tide with the bottom topography under specific surface wind conditions. Courtesy of S Bhandari, Indian Space Research Organisation, Ahemedabad, India.

3.3. Coastal bathymetry and sediment movements

Coastal erosion and deposition are natural processes which have significant consequences for local communities and industries. It is important to understand how these processes work so that successful coastal protection schemes can be developed. This understanding can be incorporated into a modelling capability and used to predict the effects of different proposed developments.

Knowing the shape of the sea floor is vital for shipping, fisheries and off-shore activities. It is also needed for the calibration and validation of morphodynamic models which are being developed to forecast changes in shape linked with sediment transport, river deposition and coastal erosion. Traditional bathymetric surveys conducted by ship are time consuming and expensive. Assessments have shown that the efficiency of bathymetric surveys can be improved by combining traditional measurements and models with ERS-1 SAR data. SAR images of the water surface can be used to estimate the shape of the sea bed in shallow waters for the following reasons:

1. Interactions between tidal flows and the sea floor cause modulations in the surface current velocity;
2. The modulations lead to local variations in the spectrum of wind-generated waves or the surface roughness;
3. This shows up as intensity variations in radar images.

ERS-1 SAR is improving our knowledge of the coastal zone by providing higher spatial resolution data than previous satellite radar sensors. Many coastal and estuarine features can be observed in detail and detection of changes in coastlines is also possible. However, there is an important complementary role with other data in providing sufficiently frequent coverage.

The three main areas of research to which ERS-1 data, especially SAR, are contributing include:

- Tidal features;
- Erosion and sediment transport;
- Topographic mapping of tidal flats which requires repeat datasets at specific times of the tides.

ERS-1 SAR data are providing new information of value to industry and also to coastal oceanographers.

TIDAL FEATURES

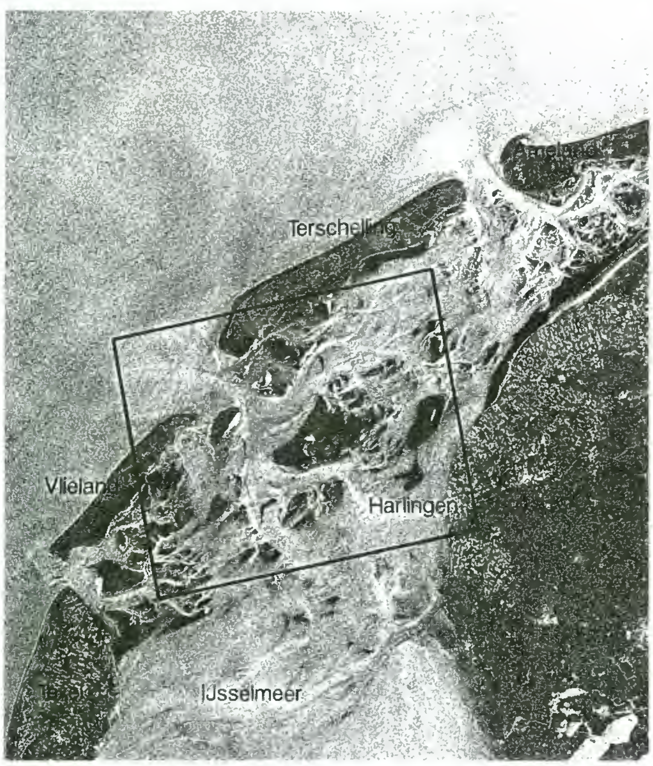

a

Figure 3.20 a,b,c. Topographic maps of the tidal flats in the Wadden Sea, The Netherlands have been produced. These are used to monitor sedimentary and erosional processes in the tidal flat areas and evaluate the shifts in the tidal channels. These maps can be rapidly updated as the topography changes. Figure a shows an ERS-1 SAR image recorded on 9 August 1992 at 1 hour 19 minutes before low tide. This provides a base for land-water boundary delineation. Figure b shows the land water boundary integrated with the water surface model 'Wadden' of the Rijkswaterstaat, to derive height values along the water line.

Figure c is a colour composite of images acquired during different tidal stages.

Red: 9 August 1992 (as Fig. a)
Blue: 7 September 1991 during outgoing high tide for ebb tidal delta mapping
Green: 20 August 1991 during outgoing low tide for flow patterns in the tidal channels

Courtesy of B Koopmans, International Institute for Aerospace Survey and Earth Sciences, Enschede, The Netherlands.

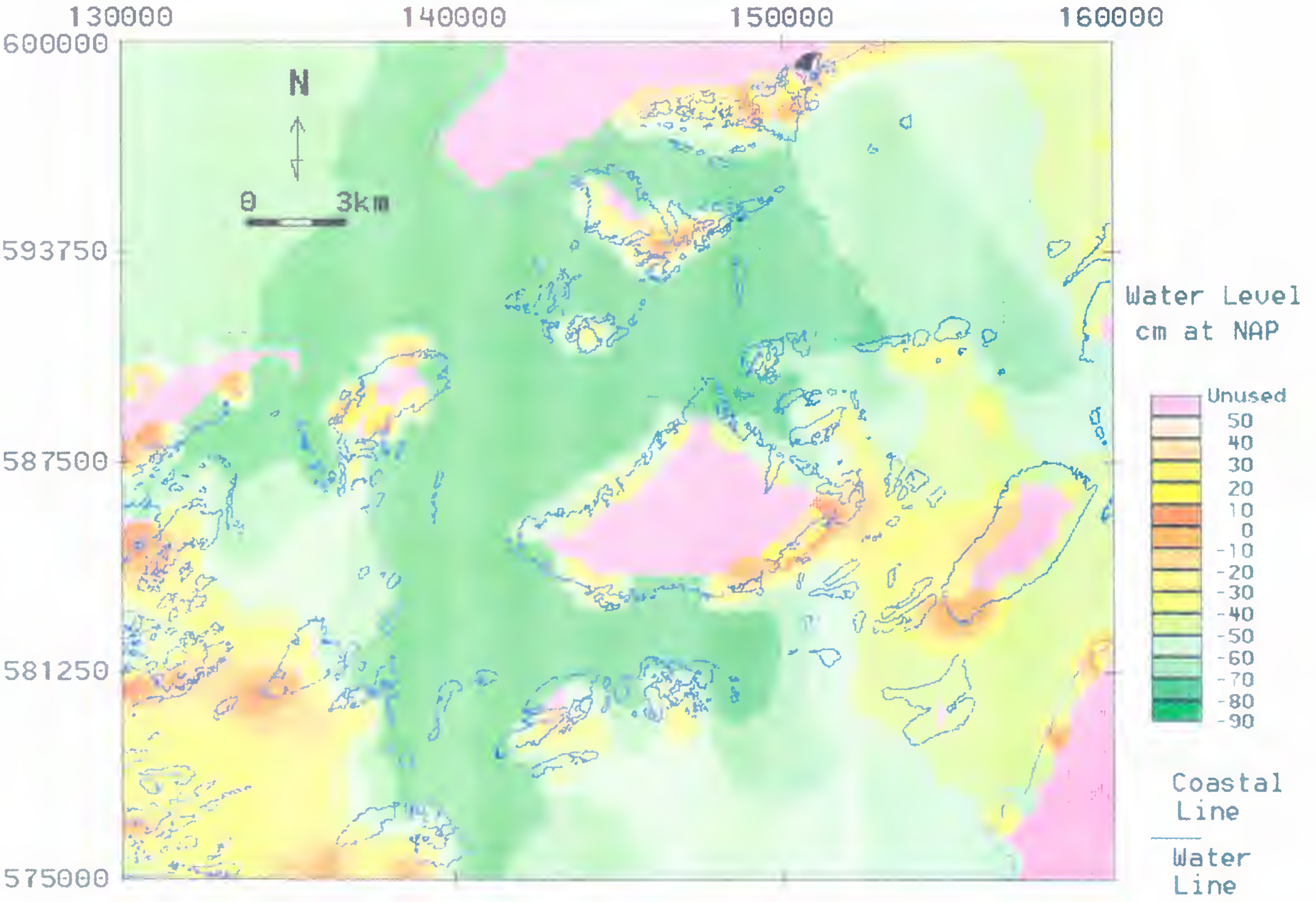
130000
140000
150000
160000
600000
593750
587500
581250
575000
N
0
3km
Water Level
cm at NAP
Unused
50
40
30
20
10
0
-10
-20
-30
-40
-50
-60
-70
-80
-90
Coastal Line
Water Line

b

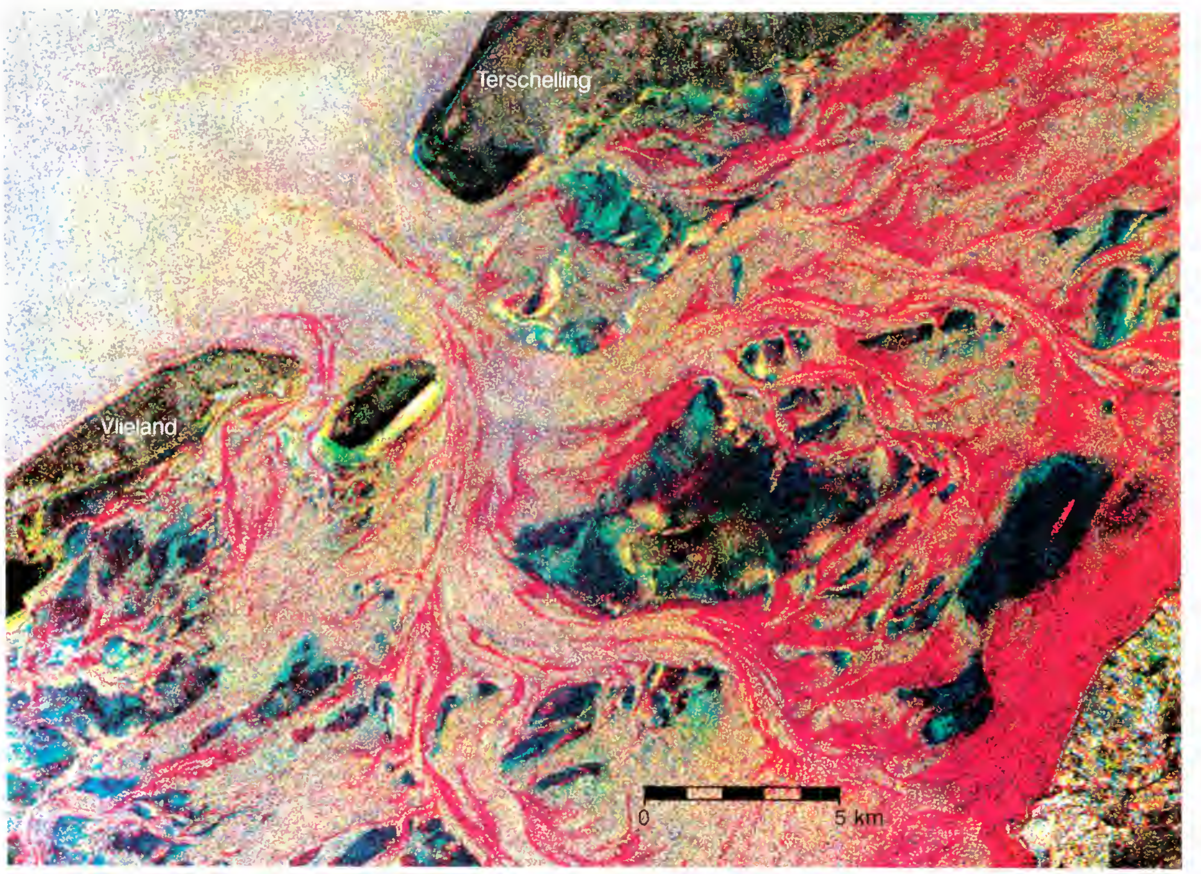
Terschelling
Vlieland
0
5 km

c

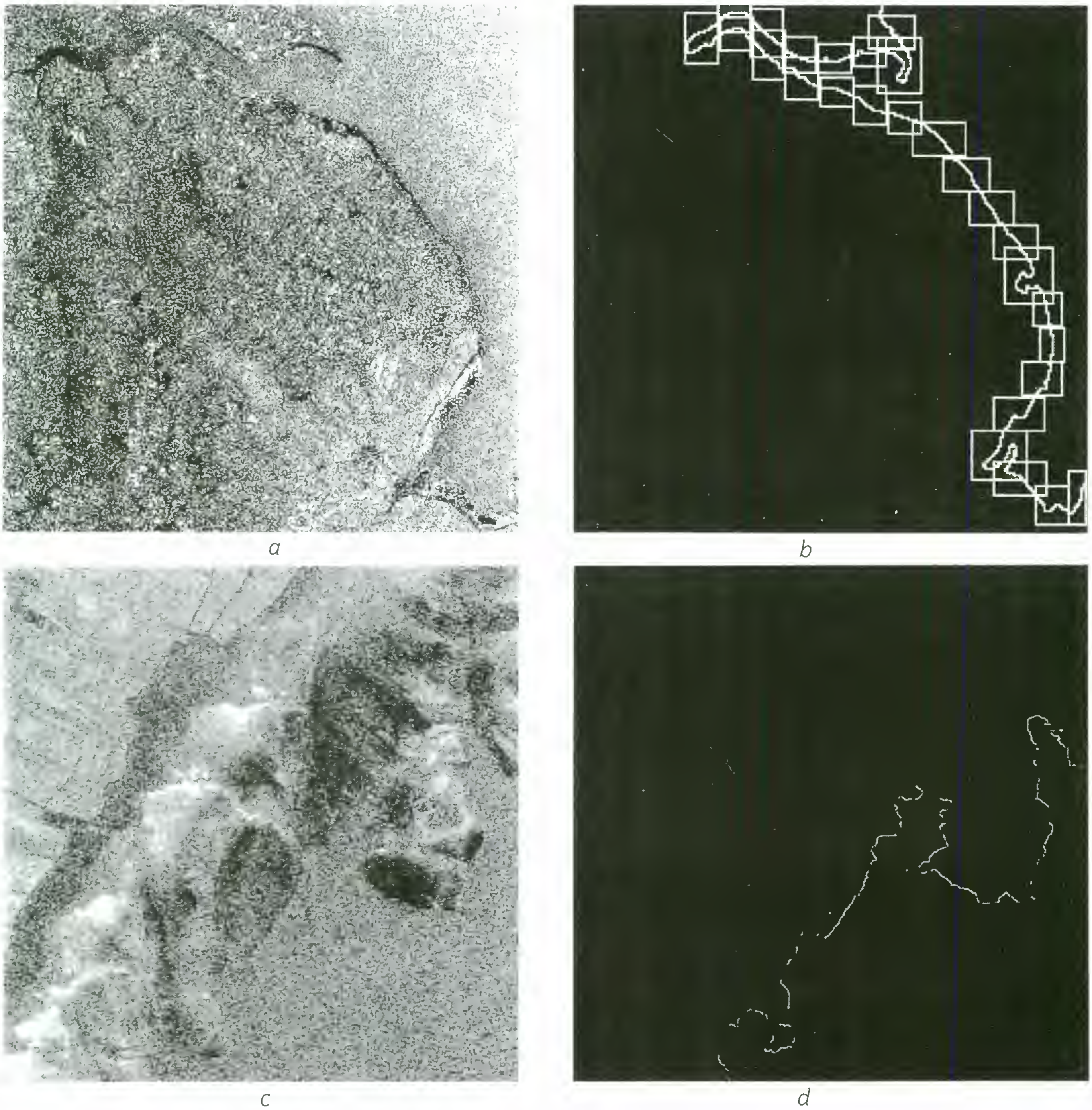

Figure 3.21 a,b,c,d. An inter-tidal digital elevation model for the area between the Wash and Humber (UK) is being developed. It will provide an integrated holistic view of how coastal ecosystems work, and how they are likely to respond to future environmental changes. A digital elevation model will lead to the production of improved tide surge models and also make it possible to detect changes caused by sediment mass transfer within the inter-tidal zone. The data are being incorporated into a hydrodynamic model which simulates the tides for six-month periods. Figure a is an ERS-1 SAR scene of the Humber-Wash area; Figure b is a set of rectangles generated along the land-sea boundary; Figure c shows a small part of this area in more detail and Figure d the land-sea boundary derived from this. The determination of this land-sea boundary is an essential input into the model. Courtesy of D Mason, NUTIS University of Reading, UK.

a

b

Figure 3.22 a,b,c. The coast of French Guyana is low, swampy and fringed by extensive mangrove forests. The entire coast is strongly affected by the load dispersal system associated with the Amazon River, which has its mouth some 500 km to the east. Each year, the Amazon pours around one billion tonnes of sediment into the ocean. The suspended load reaching the French Guyana coast is estimated at 10% of this total. This results in significant changes to the coastline which have been demonstrated with multi-temporal ERS-1 SAR images acquired on 3 May 1992 (Fig. a) and 14 November 1993 (Fig. b) with predicted tidal levels of 0.65 m and 0.80 m respectively. The mud bank located to the west of Cayenne (black area on the image) underwent extension towards the ocean and a 3 km displacement to the west. The difference of 0.15 m in the predicted water level existing between the two images suggests that the thickness and volumes of annual deposits could have a minimum of 0.10 m and 100 000 m³ respectively.

c

Figure 3.22 c is a photograph of Kaw Island, southeast of Cayenne in the process of silting up. Smooth, soft emerging silt zones appear black on the images. Courtesy of J-P Rudant, UPMC, Paris, France.

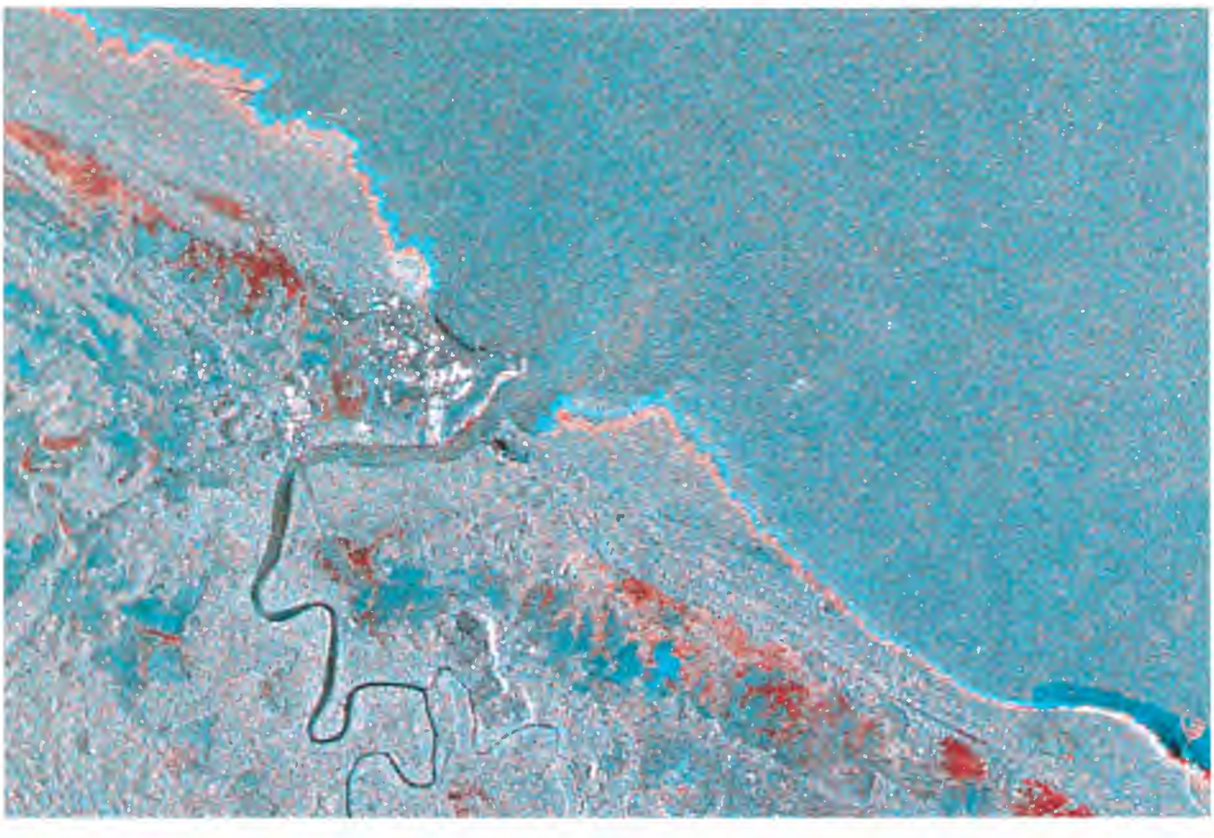

a

Figure 3.23 a,b,c. Along the coast of French Guyana, erosion also occurs. This can be observed in Figure a which lies to the west of the deposition area (shown in Fig. 3.22 a,b). The image recorded on 3 May 1992 is shown as blue and that from 14 November 1993 as red. The light contour along the coast shows the eroded section of the coastline. In several places a significant evolution of the coastline over 100-m width can be observed between these two dates. Figure b shows the effects of coastal erosion in close up. The coastal features have been mapped showing the main areas of erosion (Fig. c, after M-T Prost). Courtesy of J-P Rudant, UPMC, Paris, France.

b

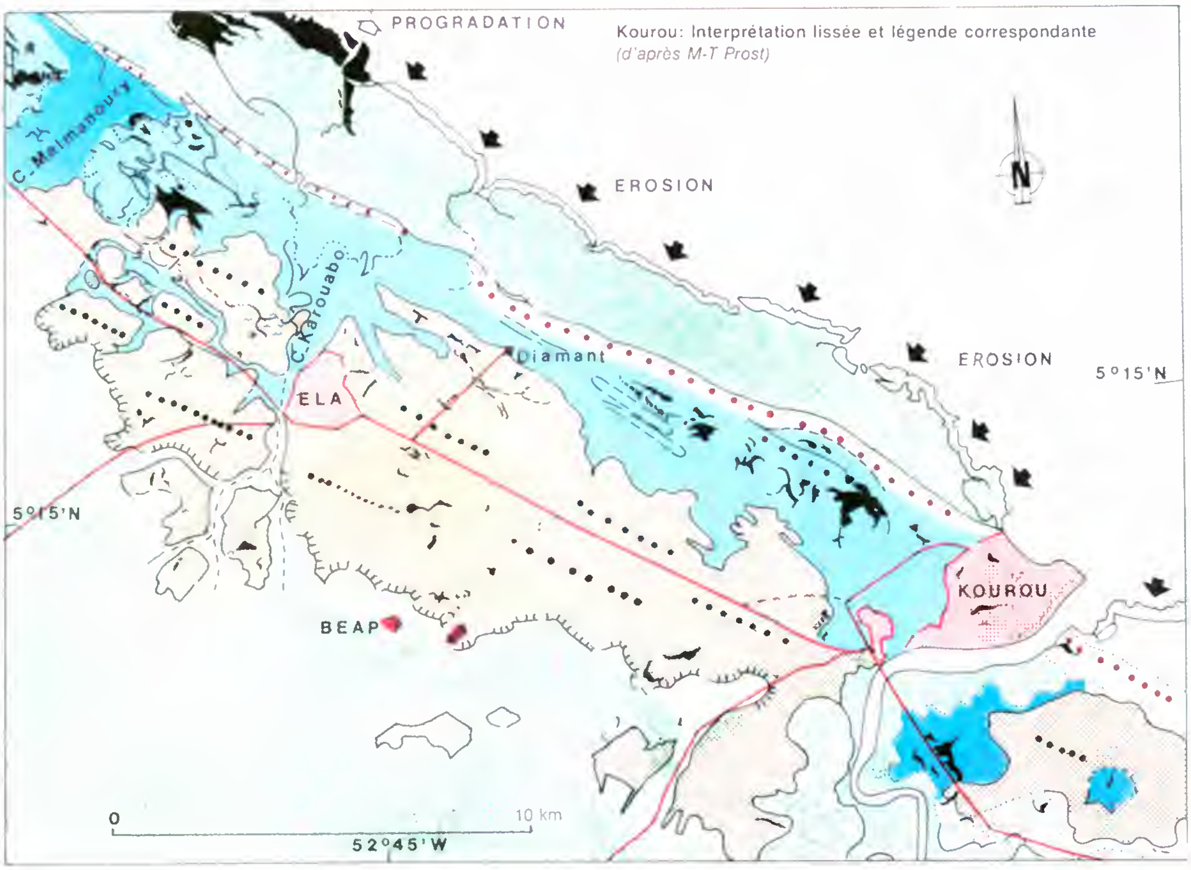

c

Progradation coast	Swamps	Sandy ridges
Erosional coast	Forest on basement	Savanna
Intertidal mud. Dead mangrove	Tidal creek	Contact forest savanna
Waterfront mangrove	Building	Fresh water swamps Free water
Adult mangrove	Progradation	Shrubby area
Dead mangrove	Erosion	Turbid water
Fluvial mangrove	Offshore bars	Road

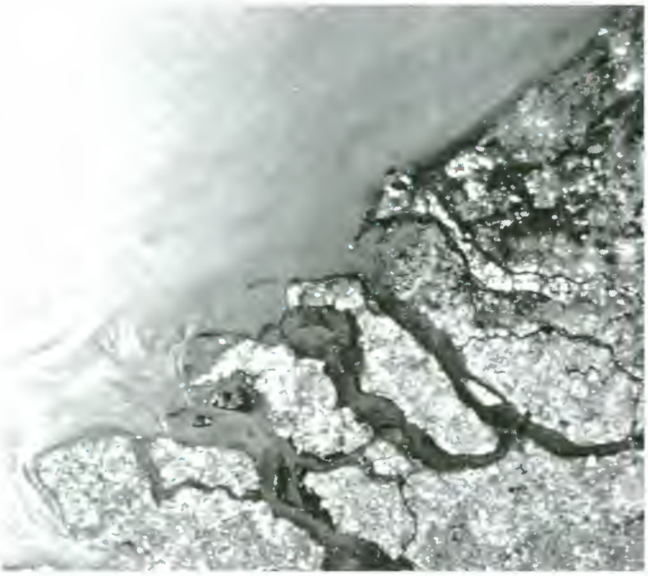

Figure 3.24. Sea bed topography has been mapped off the coast of The Netherlands. This is an area dominated by sand waves of 2-6 m which have a crest to crest distance of 500 m and are located at an average depth of 20 m. As an example, this ERS-1 SAR image shows the southwestern part of the Netherlands, recorded on 5 March 1992. In the lower left part, complicated structures of sand banks and ebb-deltas are visible near the coast. Further offshore, in the middle left part, three large sand banks parallel to the coastline can be seen. Above the centre of the image, the shipping channel to the harbour of Rotterdam can be discerned as a faint line almost perpendicular to the coast. Courtesy of J Vogelzang, Rijkswaterstaat, Rijswijk, The Netherlands.

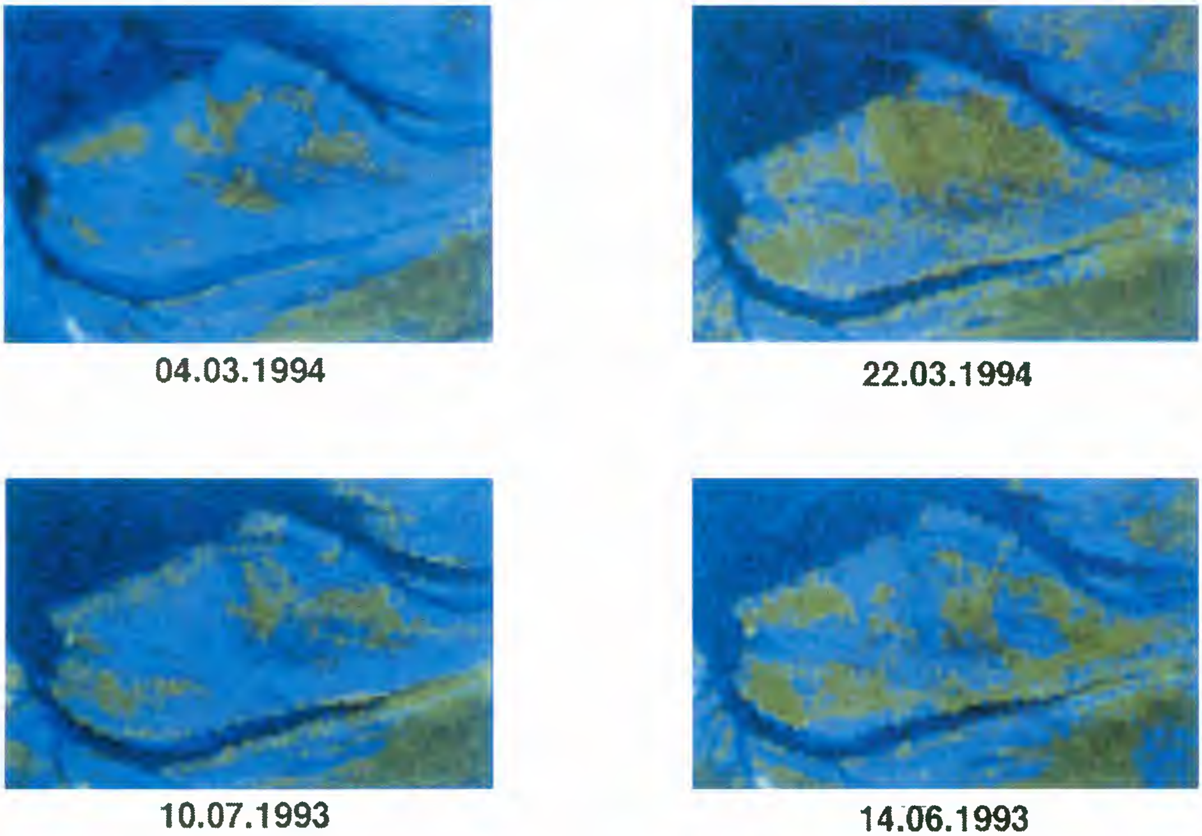

Figure 3.25. This Figure shows a time series of combined optical (Landsat TM optical sensor) and ERS-1 SAR data collected over one year in the back barrier tidal flat area of Spiekeroog in the Wadden Sea. Information on currents and morphological changes is shown. Sediment distribution, which is a very stable parameter in the coastal ecosystem of Spiekeroog, can be derived from a multispectral satellite or airborne classification. Additional information from ERS-1 SAR data allows current conditions together with ripple formation to be studied at a larger scale. The linear features on the images (dark blue) correspond to the deepest channel areas with the highest flow velocity (80 cm/s) during incoming and outgoing tides. Courtesy of O Kramer, GeoScan, Hildesheim, Germany.

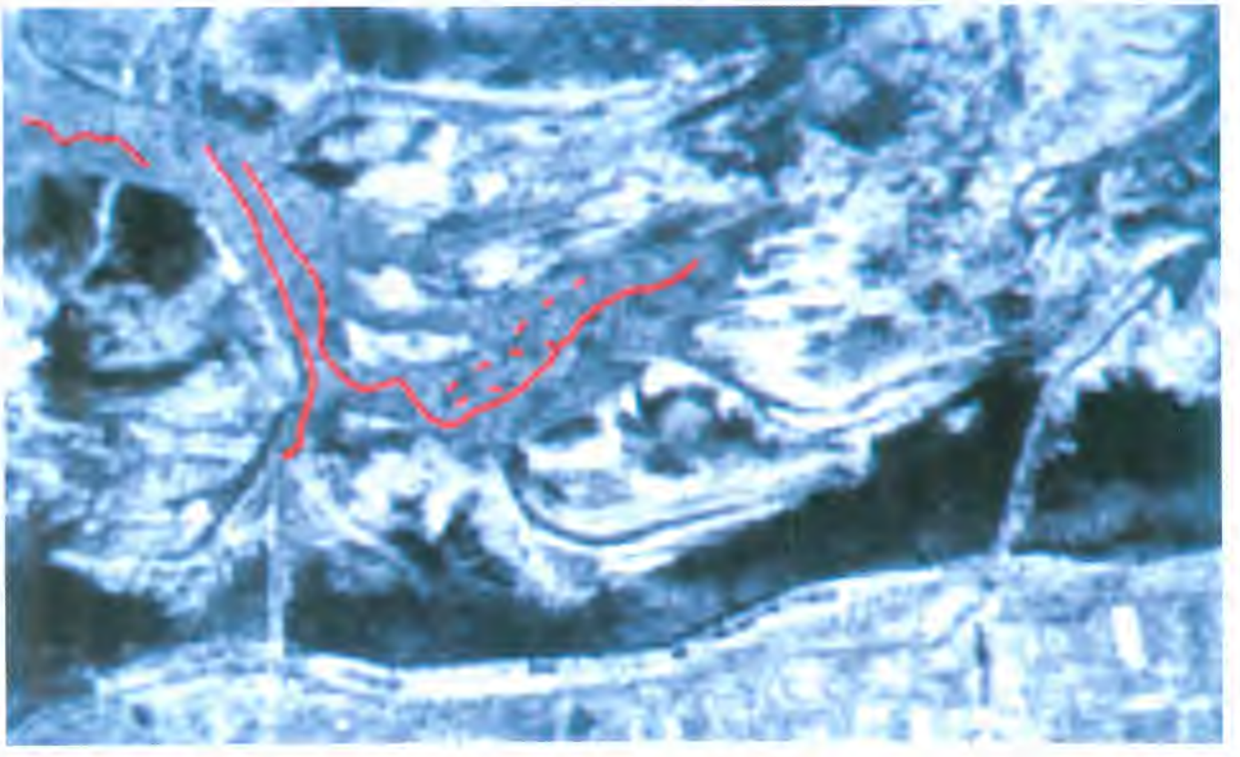

a

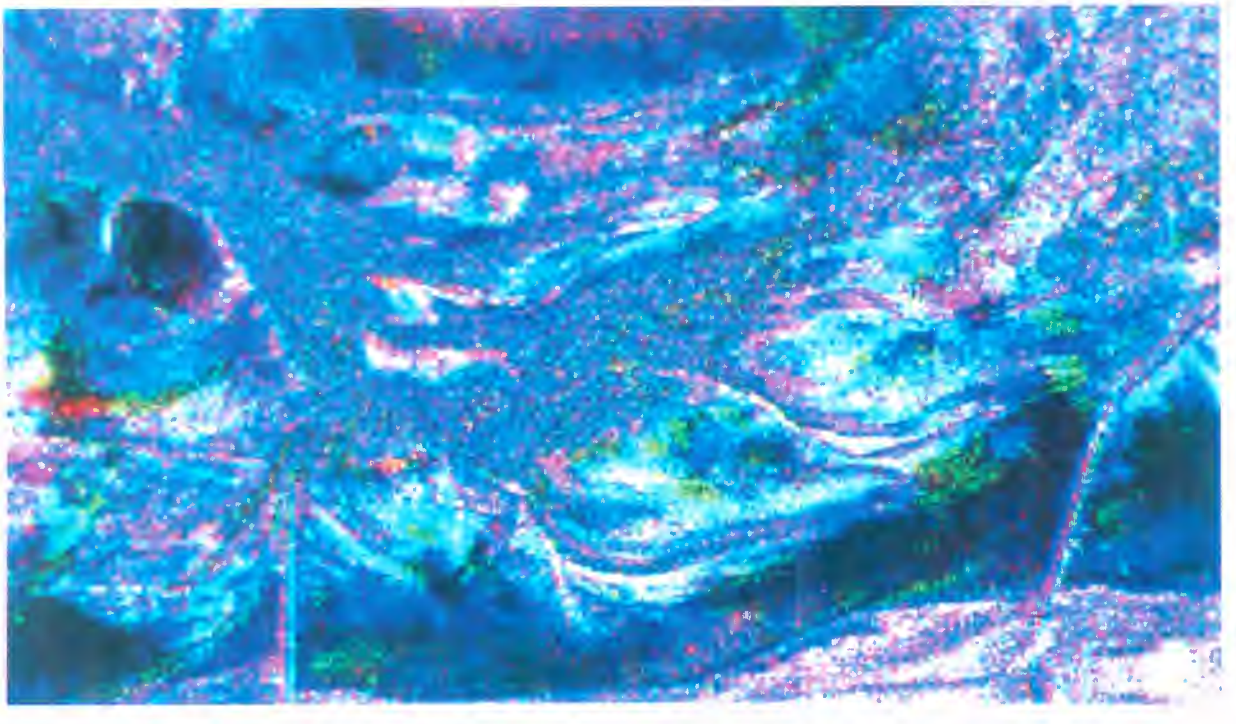

b

Figure 3.26 a,b. Linear current features have been derived from an ERS-1 SAR image (Fig. a). Permanent current features are emphasised in median images and are coloured in red. Changing current features of different median images will indicate a certain change within the channel bottom. Because of the large number of ERS-1 images available during the ebb tide, simple multitemporal red/green/blue overlays can be produced.

Figure b shows a multitemporal ERS-1 image in this form, 22 March 1994 (red), 4 March 1994 (green) and 10 July 1993 (blue). These overlays show highly dynamic areas (changing ripple marks) in different colours ranging from blue to yellow, while homogeneous areas with a mostly constant surface roughness appear in dark grey or black. These areas are mainly covered with organic layers (diatom) in winter months. This is caused by the high fertiliser input of the intensive agriculture along the coastline. Channel shifting as morphological change can be detected. After heavy storms the weather and daytime independence of ERS-1 SAR provides a large-scale overview of the affected area, for the first time. Courtesy of O Kramer, GeoScan, Hildesheim, Germany.

3.4. Processes in regional seas

The relatively dense spatial and temporal sampling of ERS-1 data enables them to contribute to regional oceanographic studies. Regional oceanographers need to understand more about the physical, biogeochemical and ecological processes which control the marine environment. Given the many ways in which industrial societies interact with their regional seas, there is a requirement to be able to construct models to forecast variables such as waves and sea level, which can describe the circulation, and which predict the dispersion of material discharged into them. To be effective, such models require regular and repeated observations of a variety of ocean parameters. Long-term programmes for developing these models for European seas are being supported by the European Union.

ERS-1 is providing some of the measurements required. The role of satellite data is to complement other observation methods by offering a better sampling capability. The weather independent nature of the microwave sensors is particularly important for the northern European seas which are often cloud covered.

ERS-1, through the SAR (image and wave mode) and the ATSR, is contributing to the understanding of processes in regional seas. Examples considered below are:

- The Mediterranean Sea;
- The English Channel.

THE MEDITERRANEAN SEA

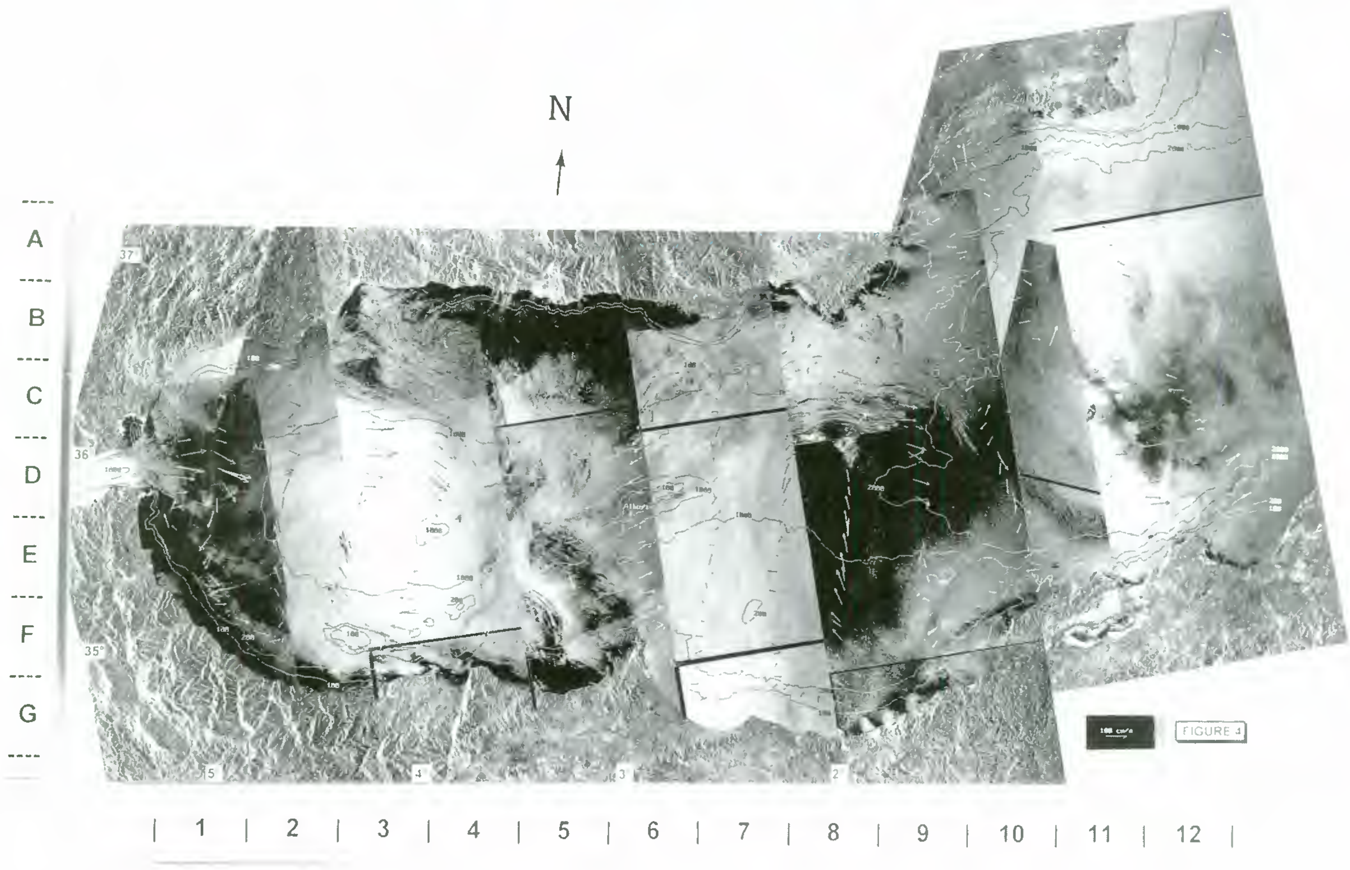

Figure 3.27. In the Alboran Sea the Atlantic water, flowing inward through the Strait of Gibraltar, encounters the denser Mediterranean surface waters, and sharp gradients occur due to the geostrophic adjustment. The inflowing jet forms a wavy pattern with two big anticyclonic gyres that usually occupy the whole Alboran basin. Intense mesoscale phenomena are present, and small cyclonic eddies develop along the border of the big gyres. The corresponding surface shear lines can be observed, under certain atmospheric conditions, in ERS-1 SAR images. An oceanographic cruise of the Spanish R/V Garca del Cid in September-October 1992 covered the whole Alboran Sea with high horizontal resolution in situ sampling. This Figure shows a mosaic of ERS-1 SAR scenes recorded during the cruise period and velocity vectors recorded on board by an acoustic Doppler current profiler. It is possible to distinguish in the images the shape of the two big gyres as well as some small cyclonic eddies. The current vectors have a general agreement with this structure and demonstrate the capability of ERS-1 SAR to detect mesoscale motion in the Mediterranean. Courtesy of J Font, Institut de Cinces del Mar CSIC, Barcelona, Spain.

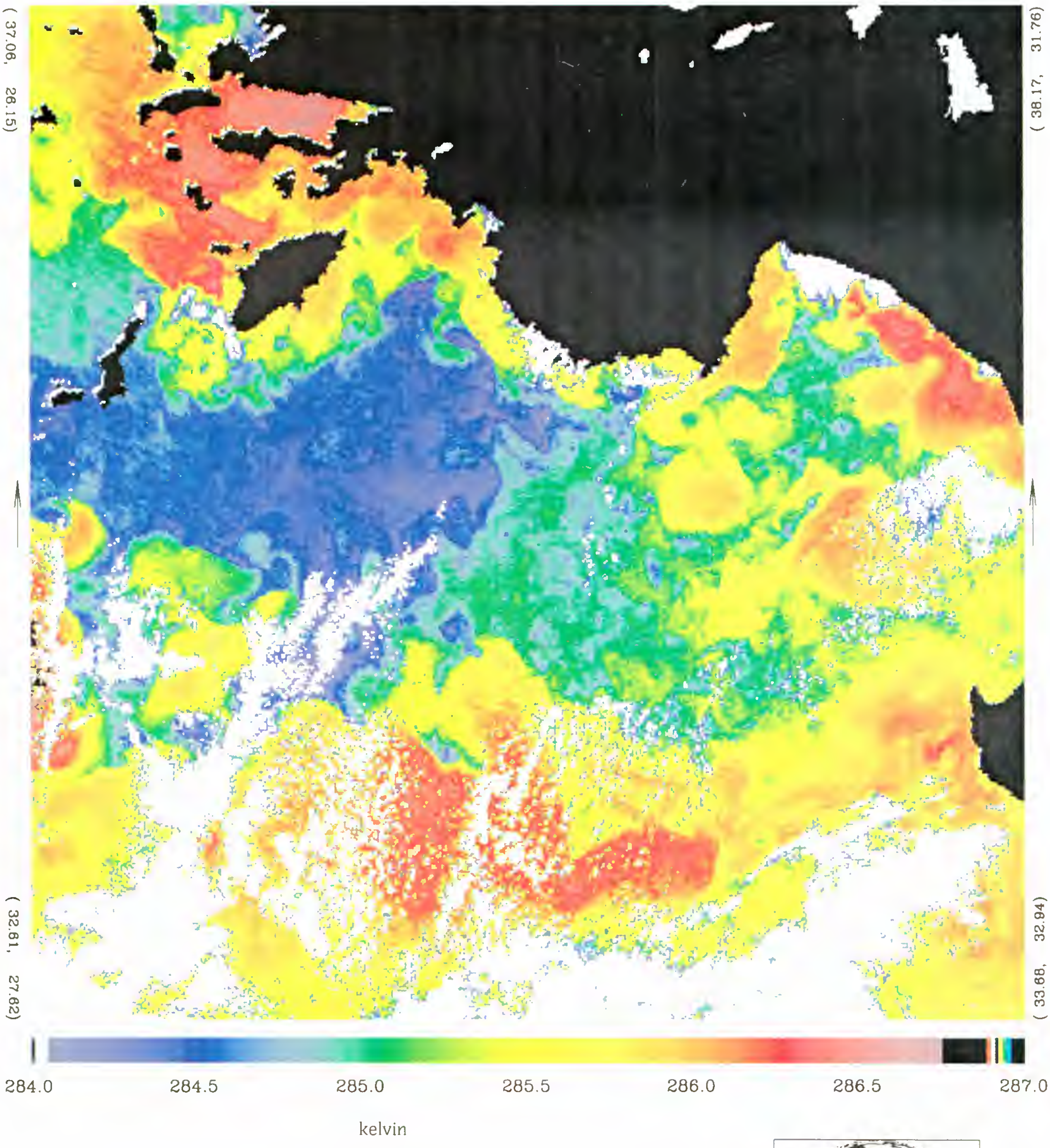

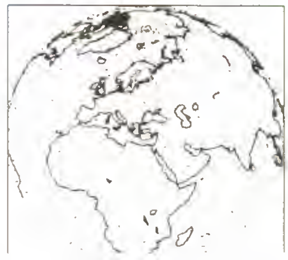

Figure 3.28. This ERS-1 ATSR image of the eastern Mediterranean was recorded in the winter of 1993. The coast of Turkey can be seen at the top with part of Cyprus to the right and the large island of Rhodes in the top left. The area of blue water is cold and shows a semi-permanent cyclonic gyre known as the Rhodes gyre. This gyre is associated with a deep pit in the sea floor going down to over 4 km. The gyre is a region of 'water formation' where surface waters can sink to deeper levels when they are cooled in winter. The small eddies and vortices surrounding the gyre may indicate 'baroclinic instability' associated with this

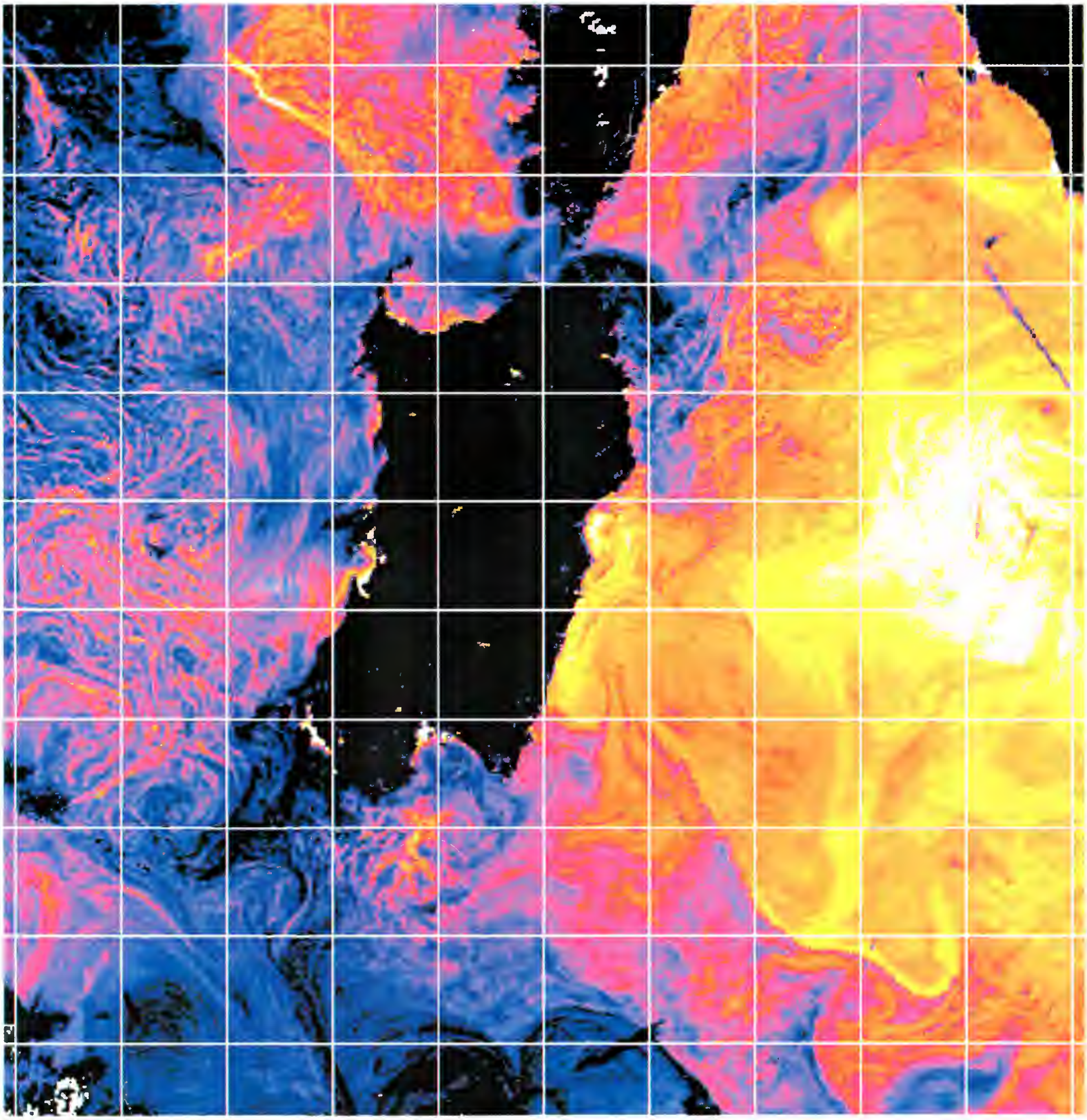

Figure 3.29. This ERS-1 ATSR image shows the sea surface temperature around Corsica and Sardinia. The dominant features west of Corsica are banded linear structures, a few tenths of a degree in amplitude and 2-4 km wide. These patterns appear to be the result of deformation by the mesoscale eddy structures typical of this part of the sea, and the resolution of the ATSR is able to demonstrate that the structures are coherent over lengths of 50-100 km. The cause of this temperature anomaly is uncertain but it is thought that the phenomenon is a surface effect coupled to the underlying motion as the patterns are similar to those of sun glitter taken by the Space Shuttle. Courtesy of I Robinson, C Donlon, University of Southampton; D Llewellyn-Jones, University of Leicester; C Mutlow, Rutherford Appleton Laboratory, Didcot, UK.

Figure 3.30. ERS-1 SAR image of the Isle of Wight (2 July 1993). In the coastal embayments narrow slicks can be seen which appear to be aligned with the local tidal circulation. In other coastal areas the slicks may relate to old ship wakes. Further offshore some larger slicks are apparent, probably patches of surface film discharged from ships. These show clearly the shear associated with the strong tidal streams which flow along the English Channel. The shear has distorted the slick into a corrugated shape. From this evidence the length scale of the instantaneous tidal current shear can be estimated, something that would be difficult to detect by any other means. Courtesy of I Robinson, University of Southampton, UK.

4. SEA ICE

Sea ice covers about 13% of the oceans in the northern hemisphere and 10% in the southern hemisphere. It thus plays an important role in the Earth's climatic and biological systems. The hostility of the sea ice environment coupled with physical inaccessibility, frequent cloud cover and long periods of polar darkness have prevented comprehensive study prior to the advent of remote sensing spacecraft. ERS-1 has provided a range of precision measurement capabilities which allow these areas to be studied in detail. The results of the studies are a growing understanding of the dynamics of sea ice and the associated ocean and ocean/atmosphere fluxes.

Changes in the patterns of sea ice occur as a result of freezing and thawing, and the movement of ice. During the formation of sea ice, important convective processes are established which trap brine and atmospheric gases in the deep ocean for 50 to 100 years. Measuring and thus understanding these processes is important for the development of ocean and climate models.

The movement of ice across the ocean surface represents a substantial transfer of both heat and fresh water. Knowledge of this movement is used for modelling ocean dynamic processes.

It is clear that the scientific requirement is for both global monitoring of sea ice and also for detailed studies which lead to greater process understanding. ERS-1 contributes to both of these requirements. Data are being used to:

- Monitor global and regional sea ice extent, type and concentration;
- Derive detailed information on sea ice movements;
- Understand and begin to quantify energy fluxes.

Each of the ERS-1 instruments is able to measure a different characteristic of the ice cover, allowing a comprehensive understanding to be achieved.

The techniques required to measure sea ice data for environmental science are also being applied to the production of sea ice maps used for monthly or weekly meteorological forecasting and in ship navigation. ERS-1 data have allowed the development of techniques and methods which are already paving the way for operational support to shipping and offshore operations.

4.1. Sea ice extent, type & concentration

ERS-1 has contributed significantly to mapping the extent, type and concentration of sea ice. The all-weather capability of the SAR and radar altimeter, coupled with their ability to record data at extreme latitudes up to 82°N and 82°S, provide reliable coverage of many sea ice regions for the first time. The area in the centre of the Arctic Ocean is not covered because of the orbit configuration.

The 30-m resolution of the ERS-1 SAR permits detailed mapping of ice coverage, revealing the processes of build up and change that occur rapidly throughout the seasons. This also makes it feasible to detect and track the movement of large icebergs and ice islands that have broken away from ice shelves. In areas where SAR data are unavailable, the ATSR instrument can be used to provide a very good image of the ice edge when clouds are not present. The 1-km resolution provides a very useful intermediate stage. At a coarser scale still, the radar altimeter is also being used to determine the ice edge precisely at low sea ice concentrations.

The distinction between ice types, such as first-year and multiyear ice, provides vital information on the processes of ice formation, migration and melting. In addition, the determination of ice type is necessary for ship routing and ice breaker support. With ERS-1 SAR it is possible during winter conditions to distinguish ice types using the image texture and the strength of the reflected signal. This was not routinely possible before ERS-1.

In addition to providing wave information for input to ice modelling, ERS-1 SAR has been shown to observe the propagation and attenuation of waves through the ice. This has immense potential significance. Not only can the mechanics of the wave motions be introduced to the ice process models but the attenuation of the waves is being used to estimate the ice thickness. This research is at an early stage and it is premature to suggest how accurately ice thicknesses could be measured by this process. However, the potential to measure sea ice thickness in large and remote areas is of great importance to mapping ice volumes and volume changes.

Examples are shown below of the contributions of ERS-1 data to:

- Monitoring sea ice extent;
- Detecting sea ice type;
- Evaluating iceberg characteristics;
- Estimating sea ice thickness.

MONITORING SEA ICE EXTENT

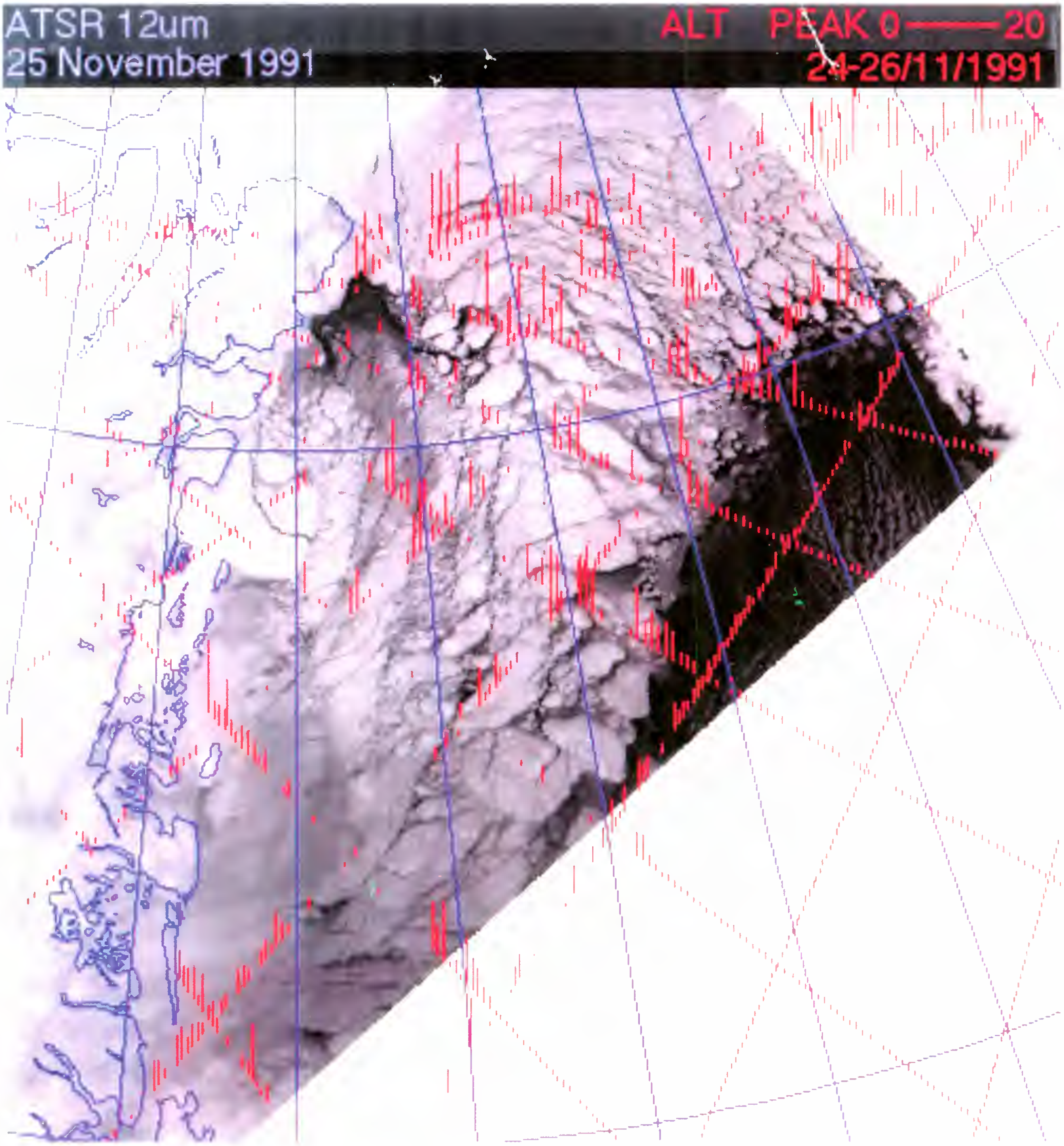

Figure 4.1. The sensors on ERS-1 all detect different facets of sea ice. This Figure shows the way in which two of the instruments, the radar altimeter and the ATSR, detect sea ice.

The ATSR image forms a base over which the altimeter measurements are overlaid. Areas of open water are black, ice is white and the coastline of East Greenland has been overlaid as a purple line. The transition from fast ice to open water can be seen. Each of the red lines constitutes a response to a radar altimeter pulse. The response is high over ice, and low over the ocean. A network of radar altimeter tracks can thus be used to construct a map of the ice edge for the whole of the Arctic and Antarctic sea ice. Courtesy of S Laxon, Mullard Space Science Laboratory, University College London, UK.

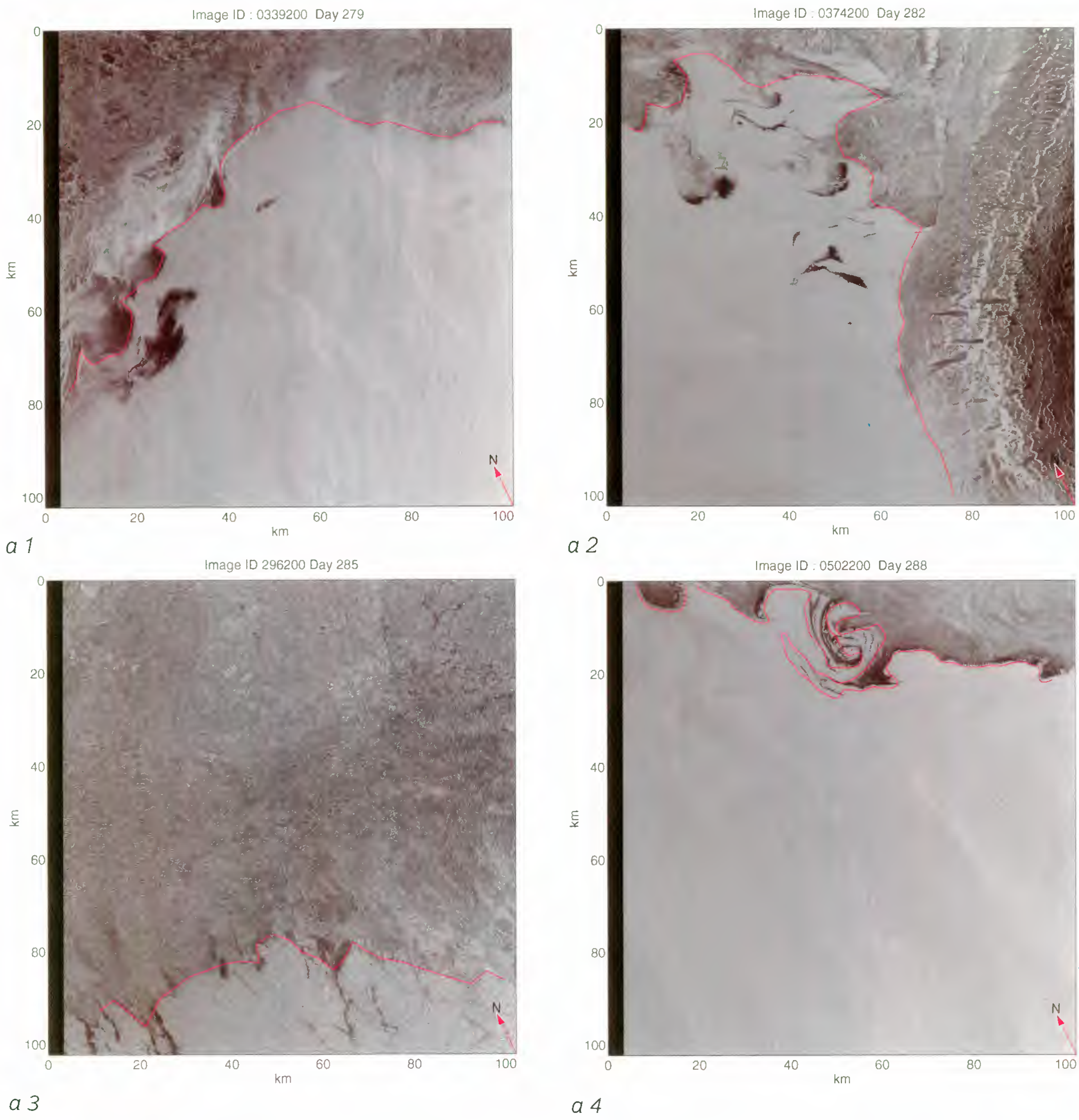

Figure 4.2 a,b. Ocean ice interaction processes in the marginal ice zone by wind waves and mesoscale features contribute to the break up of ice floes and to other processes that modify the ice cover and ice edge. In the Chukchi Sea, a sequence of five ERS-1 SAR images from 6 October (Julian day no. 279) to 18 October (Julian day no. 291) 1991 with a 3-day interval have been studied for ice edge advance/retreat (Fig. a). The locations of the ice edge are shown in Figure b. The ice edge movement of 100 km in three days matches well with the wind data recorded at the time. Observed eddies at the ice edge (15 October) and waves in the ocean and ice provide information about the processes in the marginal ice zone and can be used in coupled ice-ocean interaction models. Courtesy of A Liu, NASA Goddard Space Flight Center, Greenbelt, USA.

Figure 4.3 (see opposite page). *ERS-1 SAR data were used as part of a large study in the Barents Sea in March 1992. They were used with in situ measurements, aerial photographs and video records to obtain information on different ice types such as multiyear, first-year, refrozen leads, pancake ice, grease ice and icebergs. This Figure, recorded on 5 March, covers an area 100x100 km and shows:* a. *open water;* b. *grease ice;* c. *pancake ice;* d. *uniform field of 2-3 m thick broken up first-year ice;* e. *consolidated first-year ice in the interior of the ice pack;* f. *multiyear floes.*

This acquisition of data from a range of different ice types will play an important role in monitoring ice for scientific and operational applications. Courtesy of S Sandven, O Johannessen, Nansen Environmental and Remote Sensing Center, Bergen, Norway; W Campbell, US Geological Survey, Tacoma; R Shuchmann, ERIM, Ann Arbor, USA.

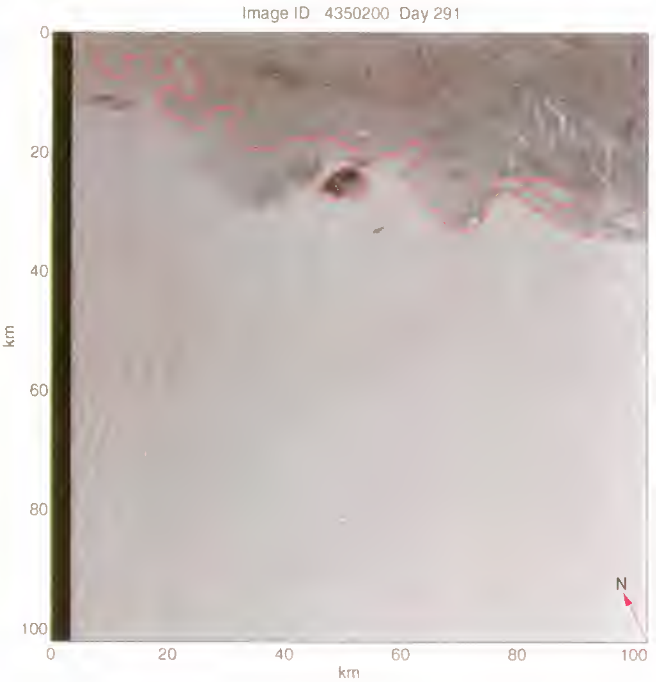

a 5

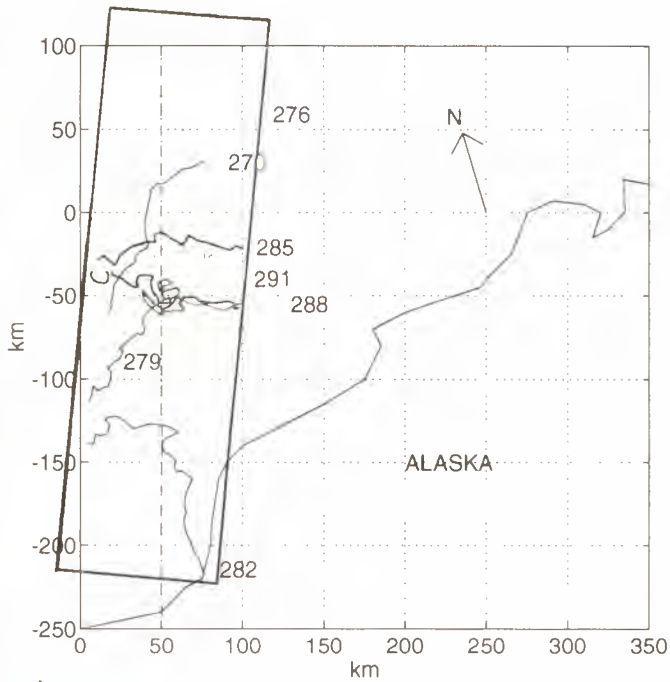

b

DETECTING SEA ICE TYPE

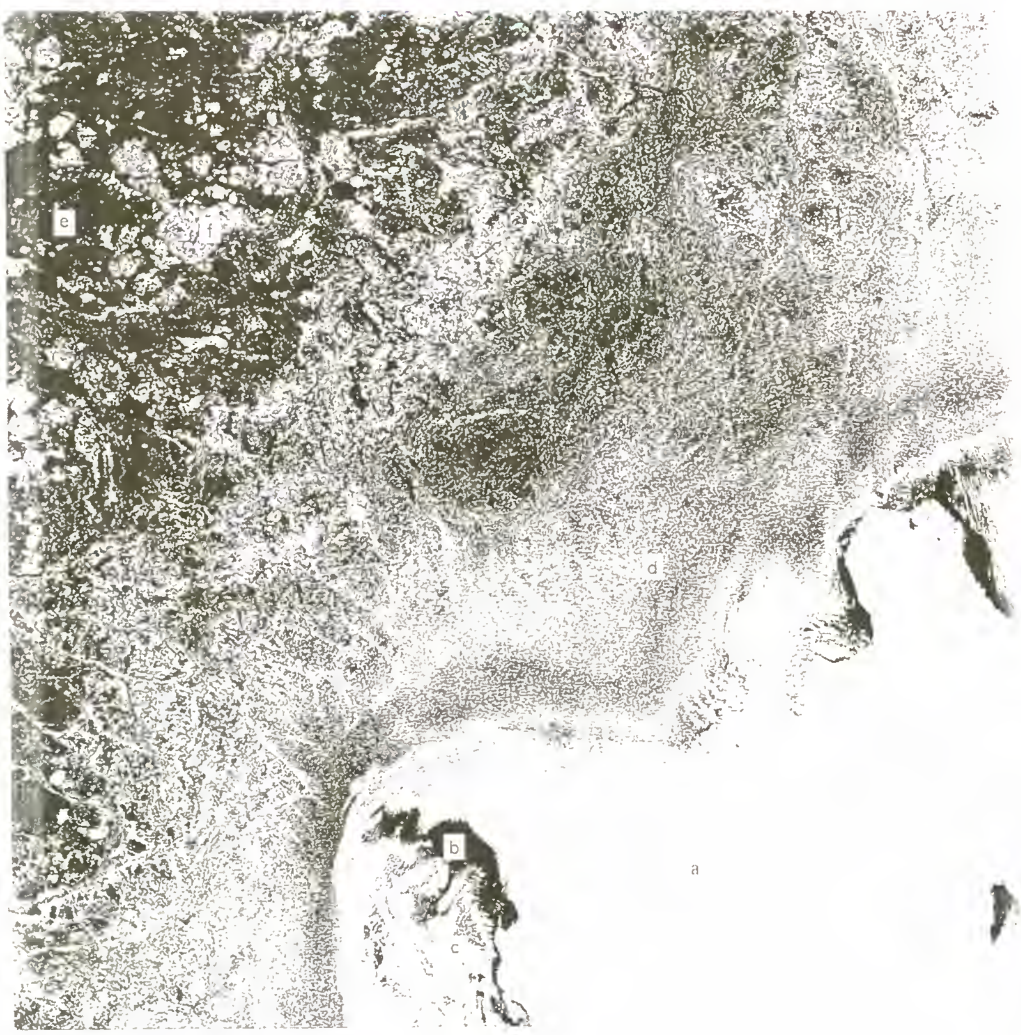

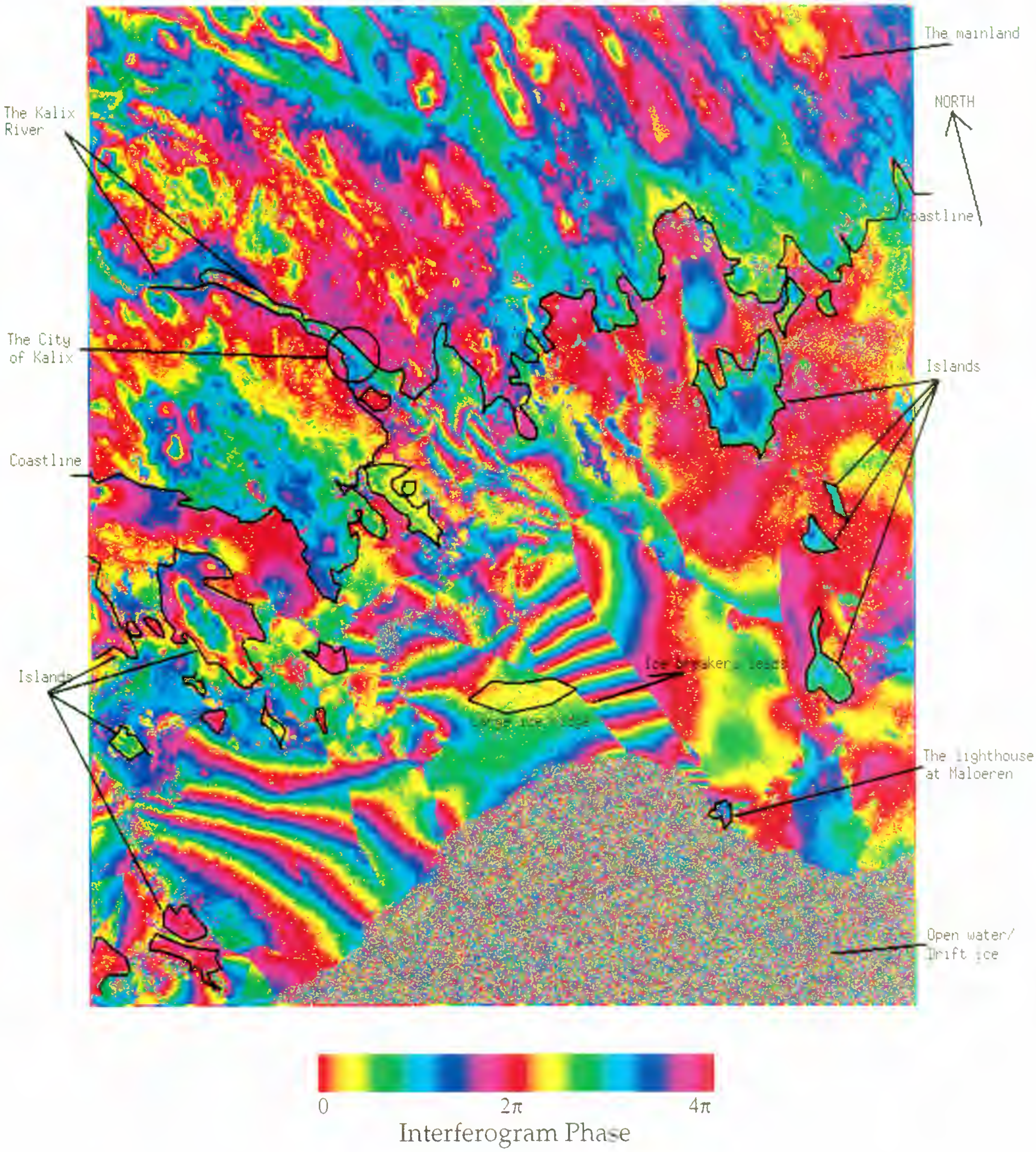

Figure 4.4. New developments in interferometry applied to shore-fast ice may reveal important features, as yet unknown. This figure was computed from two ERS-1 SAR images obtained on 27 March and 30 March 1992 and covers an area of 50x50 km over the archipelago south of the city of Kalix on the Swedish east coast. The drift ice is moving south. An area in the centre of the scene is divided by two icebreaker leads which are very easily identified in the interferogram. These leads have divided the ice and the narrow area between them has moved in a different way to the ice around. The most southern part of this narrow ice floe between the leads has moved approximately 17 cm relative to the northern part. Since the ice floe is around 16 km long, these measurements in cm- and mm-scales over such large distances are probably unique. The achievements of the first few years of regular ERS-1 data point to the substantial progress which can be made during the remainder of the ERS programme.
Courtesy of J Hagberg, L Ulander, J Askne, Chalmers University of Technology, Gothenberg, Sweden.

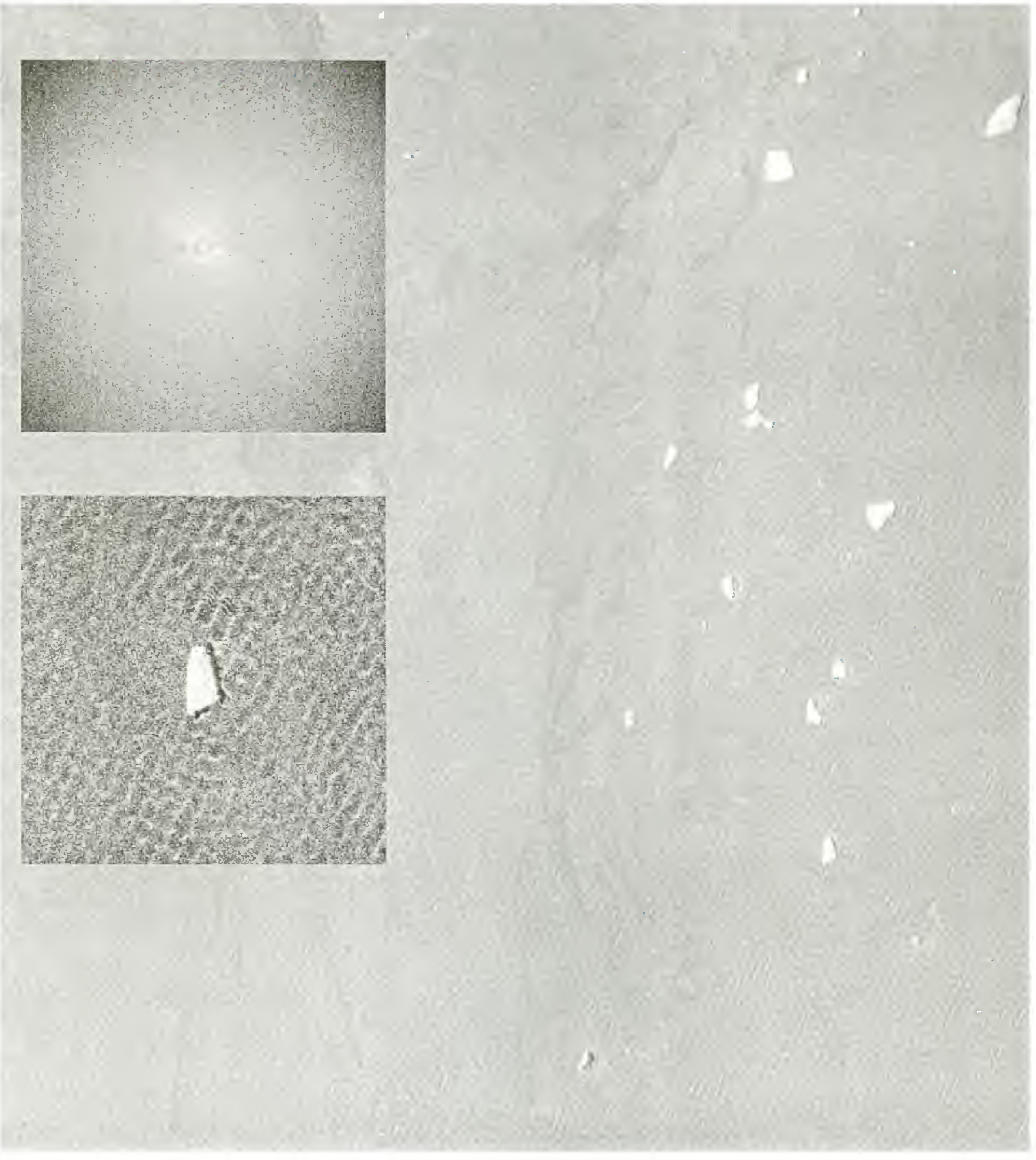

Figure 4.5. This ERS-1 SAR image, recorded on 15 July 1993 off the west coast of Antarctica, shows a 310-m swell coming in from the northwest causing diffraction patterns at the table icebergs. Two subscenes showing the circular wave pattern around an iceberg and corresponding power spectrum are included. This wave pattern could be used to determine the submerged geometry of the iceberg. Courtesy of S Lehner, DLR, Oberpfaffenhofen; S Hasselmann, Max Plank Institute for Meteorology, Hamburg, Germany.

Figure 4.6. This ERS-1 SAR image was recorded on 23 January 1992 near the southeast coast of Greenland, to the west of Iceland. The lower left corner shows open water while three types of ice can be distinguished closer to the coast. A 20-30 km wide dark strip corresponds to grease ice, then a broad area of about 70 km of pancake ice is followed by a compression ridge and an area of larger floes. A 500-m swell system is seen travelling up to 100 km into the ice, disappearing in the grease ice zone. The waves were created by a storm system passing along the south east coast of Greenland and over Iceland on 23 January with wind speeds reaching up to 25 m/sec. A series of subscenes (r 1-7) were analysed and estimates of the ice thickness at different locations were made. Courtesy of S Lehner, DLR, Oberpfaffenhofen; S Hasselmann, Max Plank Institute for Meteorology, Hamburg, Germany.

4.2. Sea ice movement

The repeat characteristics of ERS-1 and its range of instrument capabilities give it the ability to monitor the movement of sea ice effectively. The scatterometer provides visibility of sea ice drift on a large scale. At a more regional level, the main contributions come from the ERS-1 SAR. Pattern recognition techniques are being used to identify individual features within the ice and to track these from one image to the next. In this way, not only can the bulk migration of the ice be mapped, but divergence or convergence of the ice floes can also be determined.

Divergence is of particular significance as the diverging ice generates areas of open water. These provide areas for rapid heat transfer from the ocean to the atmosphere and rapid ice production.

In addition to the heat fluxes associated with ice drift, the measurement of ice movement and its melt water is of major importance to the modelling of ice generation mechanisms and to the understanding of biological processes within the ocean. The quantities of fresh water transport involved are substantial and represent significant influences on a global scale. For example, the ice flow through the Fram Strait represents a large proportion of the total discharge of ice from the Arctic Ocean.

The techniques for detecting ice motion can be applied in most of the areas world-wide where sea ice drift occurs. Examples are given below from:

- The Arctic Ocean;
- Oceans off Antarctica.

SEA ICE MOTION IN THE ARCTIC

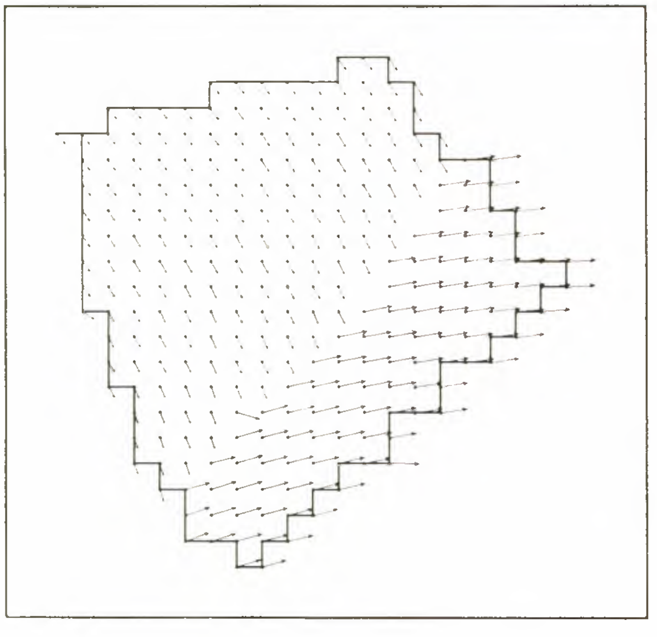

a

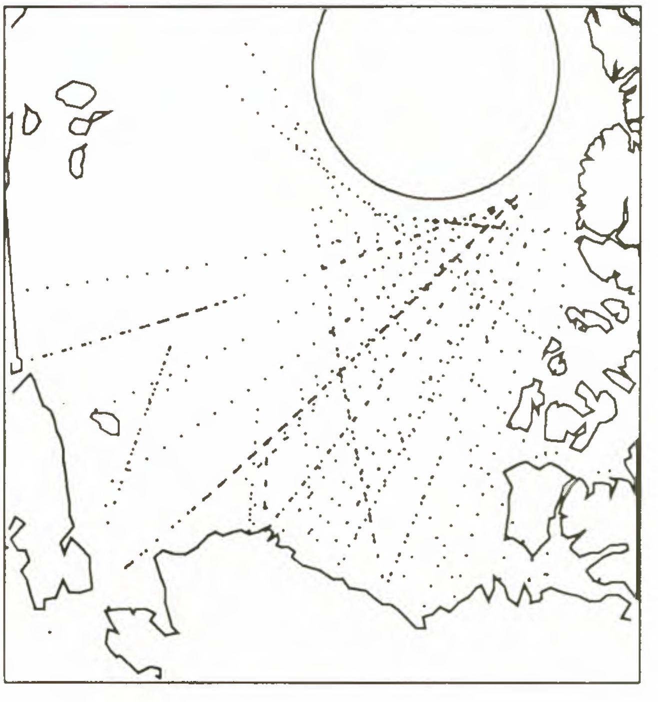

b

Figure 4.7 a,b. Sequential pairs of ERS-1 SAR images have been used to track a regular 5-km array of grid points in the Arctic resulting in a field of ice displacements that contains on average more than 200 vectors. All pixels were also classified into one of four ice types so that leads could be identified. The opening, closing and deformation of the leads were measured providing information on the processes involved. Figure a shows a typical ice motion product from this work. In this example, there is slow ice movement in a south-easterly direction in the upper left of the image, and an easterly movement towards the right of the image. The discontinuity in the ice motion field running diagonally across the scene can be seen. In Figure b each dot is the centre location of one ice motion product. The circle is 85° N latitude, the approximate northern limit of satellite coverage. Courtesy of H Stern, D Rothrock, University of Washington, Seattle; R Kwok, JPL, Pasadena, USA.

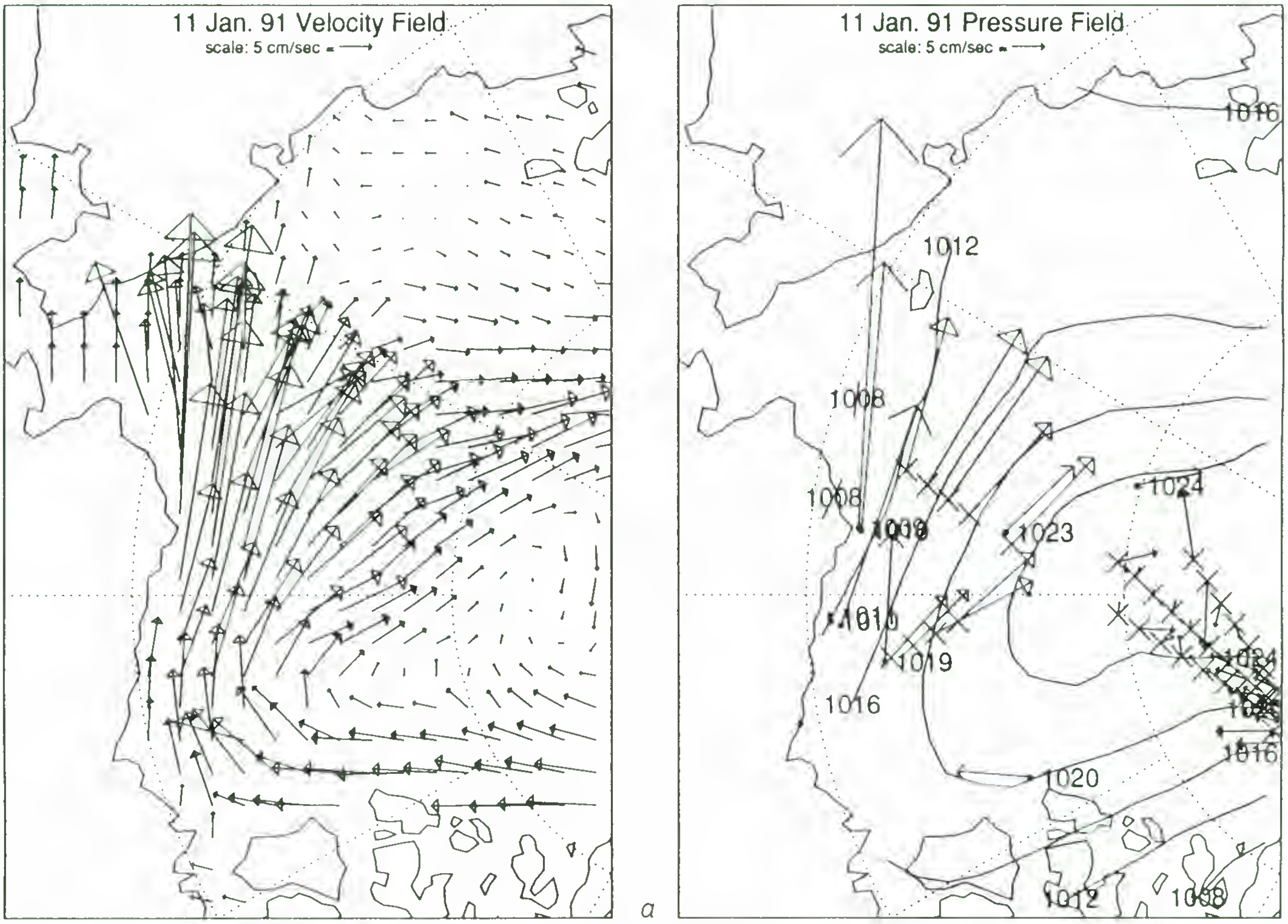
11 Jan. 91 Velocity Field
scale: 5 cm/sec
11 Jan. 91 Pressure Field
scale: 5 cm/sec
1016
1012
1008
1008
1023
1024
1019
1016
1020
1016
1012
1008

a

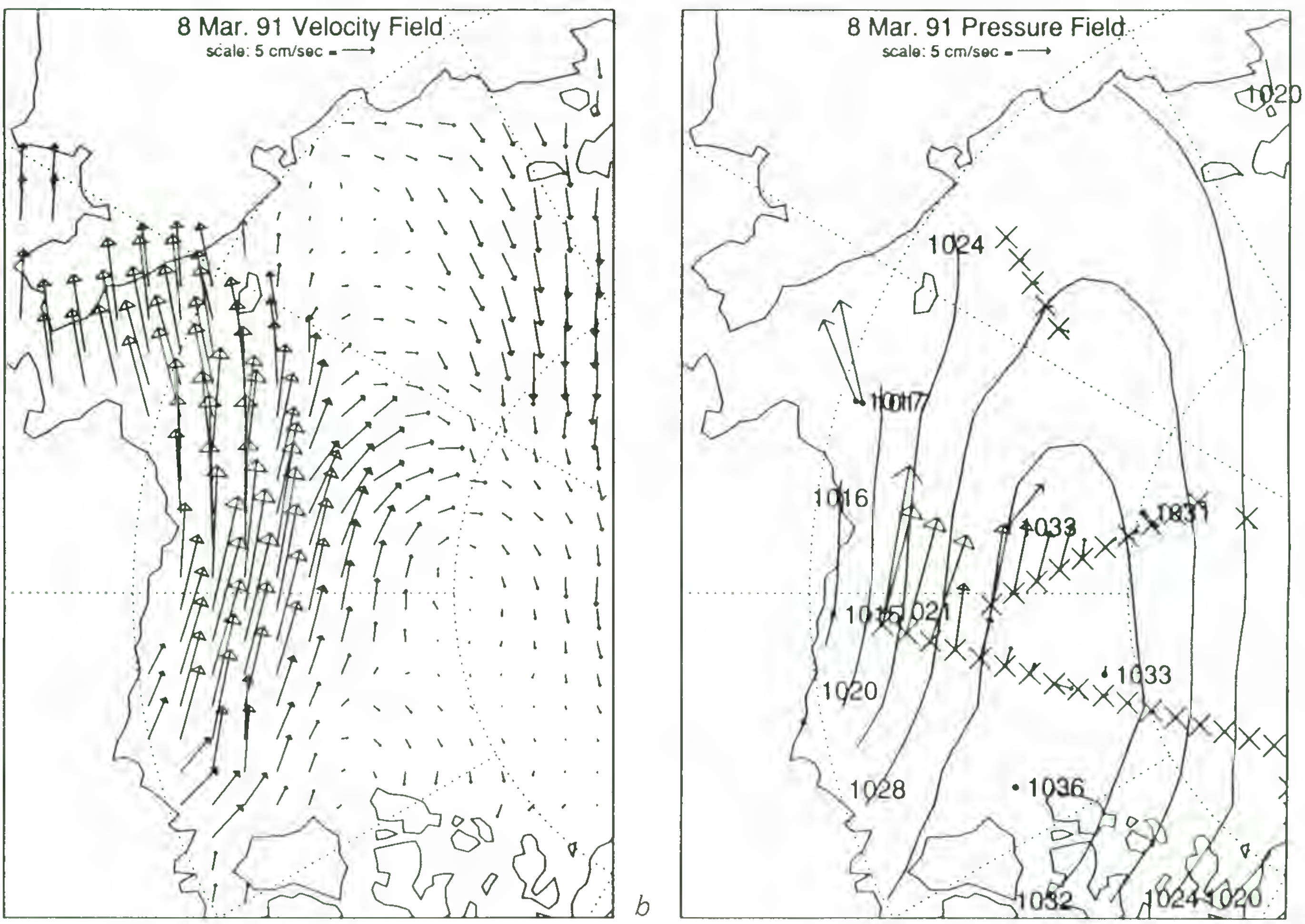
8 Mar. 91 Velocity Field
scale: 5 cm/sec
8 Mar. 91 Pressure Field
scale: 5 cm/sec
1020
1024
1016
1033
1033
1020
1028
1036
1032
1024
1020

b

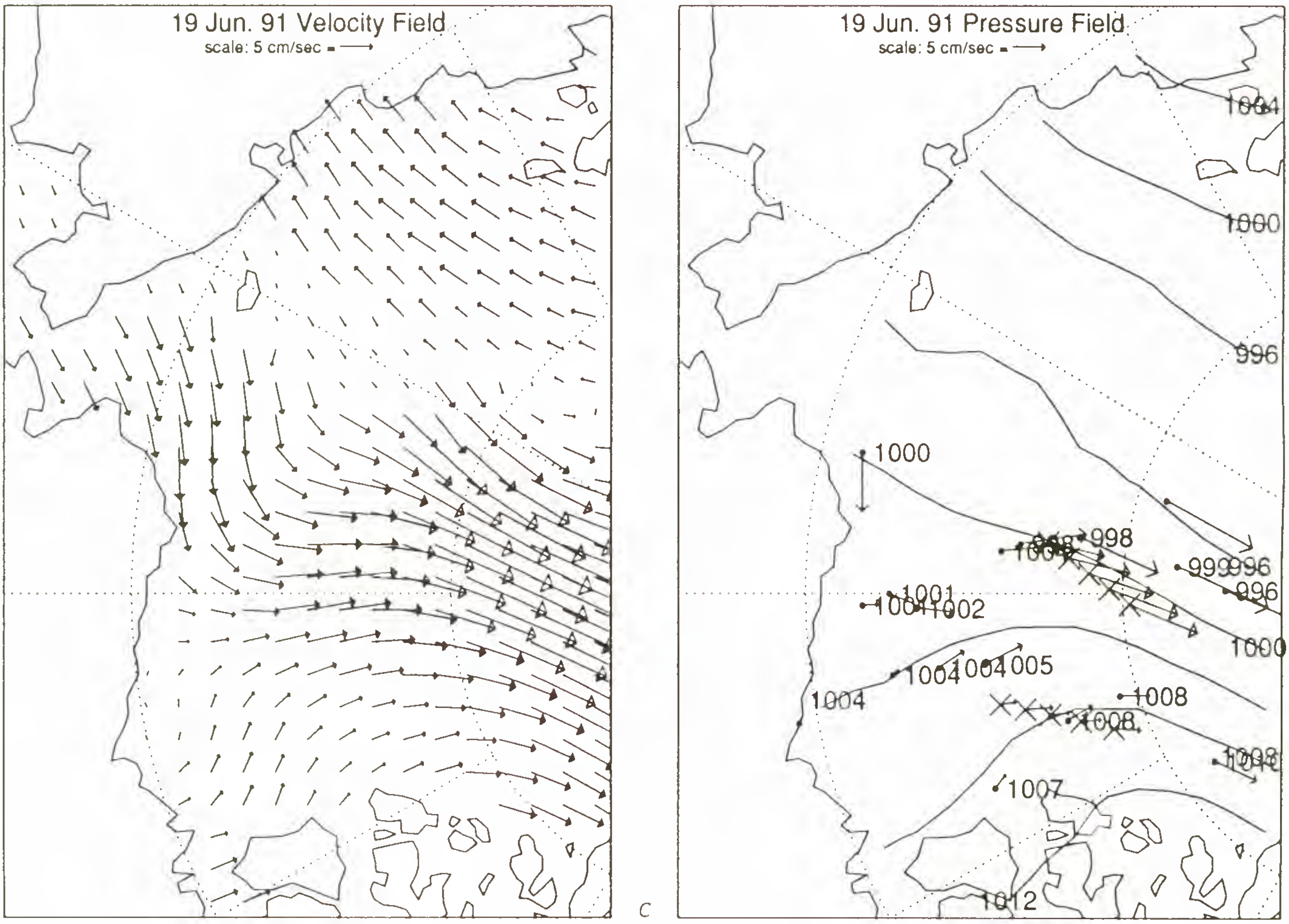

Figure 4.8 a,b,c. This time series shows ice motion information derived during the winter of 1991 in the Beaufort Sea. On the right are ice motion vectors obtained from the analysis of sequences of ERS-1 SAR images. Also shown are smoothed ice motion data and surface pressures from drifting buoys (positions indicated by black dots). On the left are modelled ice motion vectors. These vectors are obtained by using the SAR data and the surface pressures to initiate and force a model of air-sea-ice interaction for the Arctic. This procedure allows accurate ice motion estimates to be made in areas where no data are available. These ice motions are scientifically valuable in providing fresh water fluxes and data on ice opening and closing. The seasonal and regional variations of the relationship between surface winds (generated from surface pressures) can be at least partially accounted for in this algorithm. Courtesy of R Kwok, JPL, Pasadena; R Colony, University of Washington, Seattle, USA.

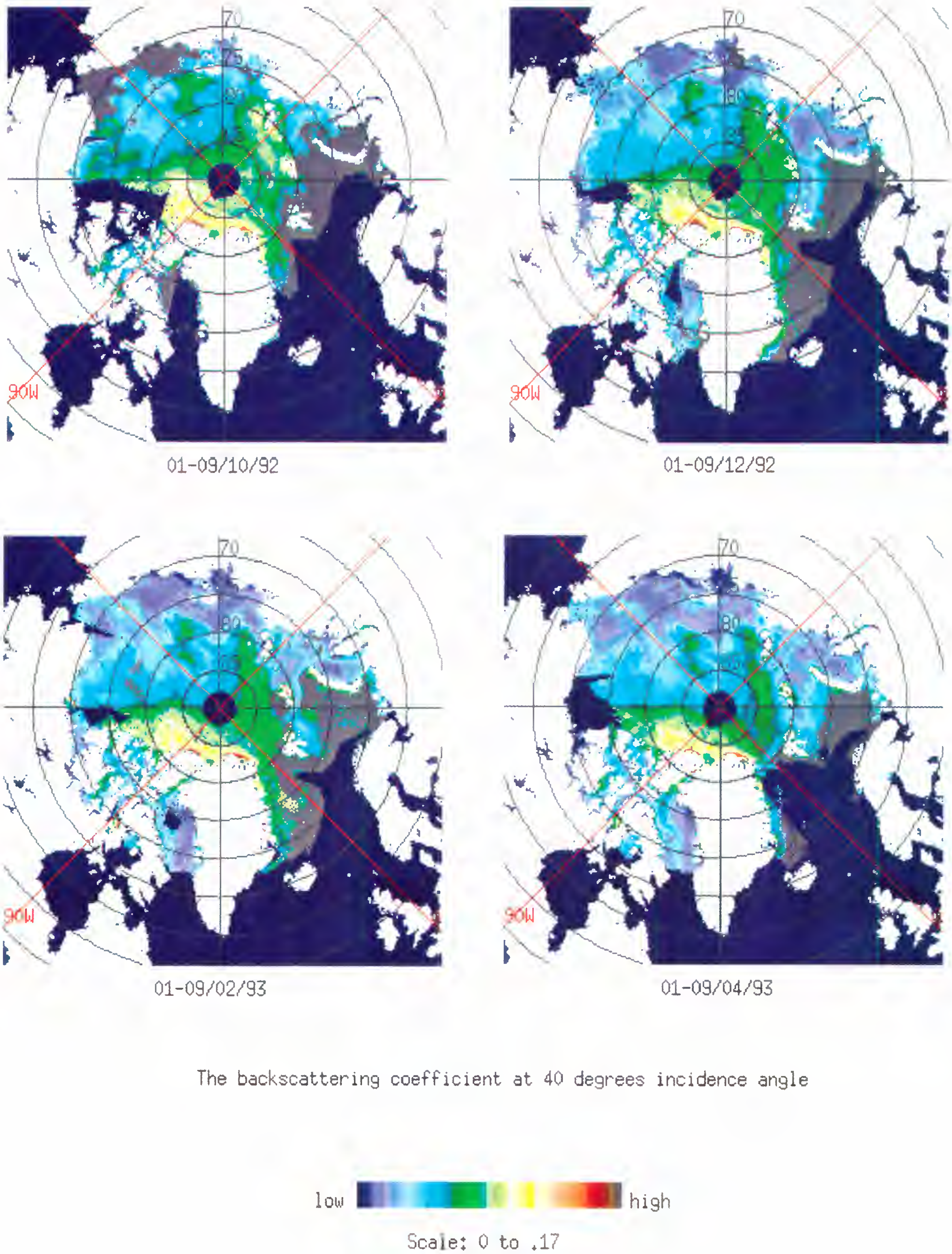

Figure 4.9. Studies of large-scale sea ice phenomena have been carried out using ERS-1 scatterometer data. The pattern of the backscatter coefficient over the Arctic Ocean was compared in the winters 1991, 1992 and 1993. This figure shows the change in backscatter at two-month intervals over the winter of 1992-93, open water areas are in brown, non observed regions in dark blue, while the multiyear ice gives a high backscatter and is shown in reds and yellows with the first-year ice shown in blues and purples. The northward drift of large areas of multiyear ice from the New Siberia Islands (at about 75°N, 140°E) shown in green can be observed. It has been demonstrated that with a spatial resolution of 50 km, studies of the ice movement over the Arctic Ocean can be made and potentially can be included as components of climate studies. Courtesy of A Cavanie, Ifremer, Plouzane, France.

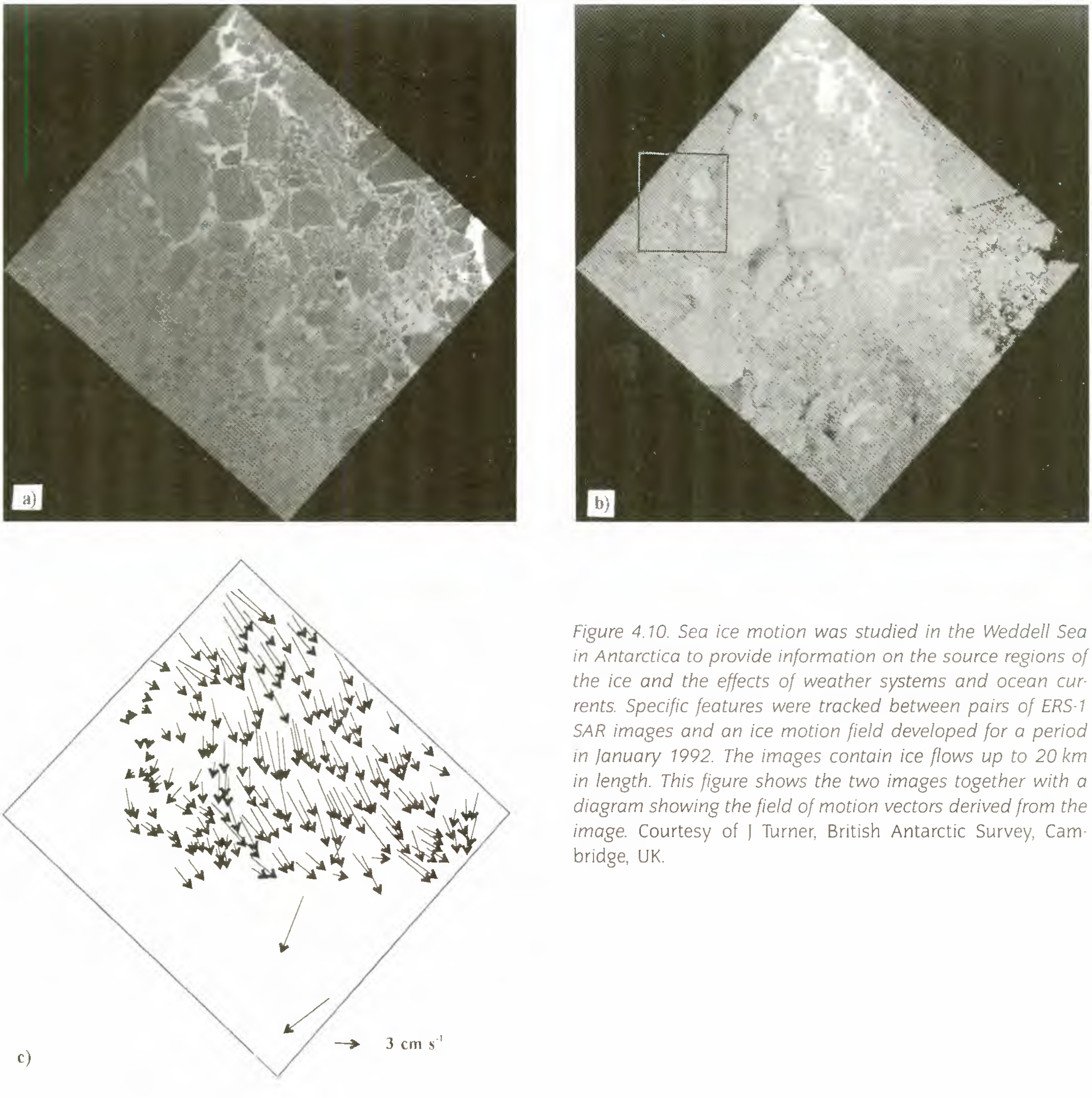

Figure 4.10. Sea ice motion was studied in the Weddell Sea in Antarctica to provide information on the source regions of the ice and the effects of weather systems and ocean currents. Specific features were tracked between pairs of ERS-1 SAR images and an ice motion field developed for a period in January 1992. The images contain ice flows up to 20 km in length. This figure shows the two images together with a diagram showing the field of motion vectors derived from the image. Courtesy of J Turner, British Antarctic Survey, Cambridge, UK.

4.3. Energy fluxes

Sea ice controls a number of energy fluxes of significance to climate modelling. Sea ice limits air-sea interaction and insulates the atmosphere from the ocean. Movement of large icebergs also represents a significant transfer of cold, fresh water. In addition to the areas which it controls, sea ice patterns have also been used to provide evidence of convective processes within the ocean.

Areas of open water within the sea ice, in particular leads, could not be reliably observed from space prior to the availability of the all-weather, day or night high resolution imagery of ERS-1 SAR. This has allowed better estimates of energy transfer to the atmosphere within such ice frequented waters. Ice drift also represents a substantial component of the horizontal heat fluxes within the oceans.

Deep water convection is a process which is important for energy transfers within the ocean and for maintaining the thermohaline circulation, but which is difficult to detect from satellite. Such convective processes do provide some surface evidence, particularly when sea ice is present at the surface. In such cases, the pattern adopted by the sea ice can be observed with ERS-1 SAR data and used to indicate the presence of convection below the surface.

As well as overall monitoring, it is also possible to study specific features within sea ice. An example of such a feature is the polynya. Polynyas are areas of low sea ice concentration in an ice canopy or along a coast bounded by ice out in the ocean. They are sites of intense air sea-ice interactions. The vast amount of salt produced makes polynyas important sources of cold, highly saline water which helps maintain the water mass structure of the polar oceans. ERS-1 SAR observations have been used to determine the cause and size of polynyas. Even under severe weather conditions with dense cloud cover, advection of ice into the polynya can be studied.

Examples are provided of the use of ERS-1 data in:
- Detecting open water areas within the sea ice;
- Measuring ice flux;
- Observing convection processes at the ice edge;
- Detailed studies of polynyas.

DETECTION OF OPEN WATER AREAS WITHIN SEA ICE

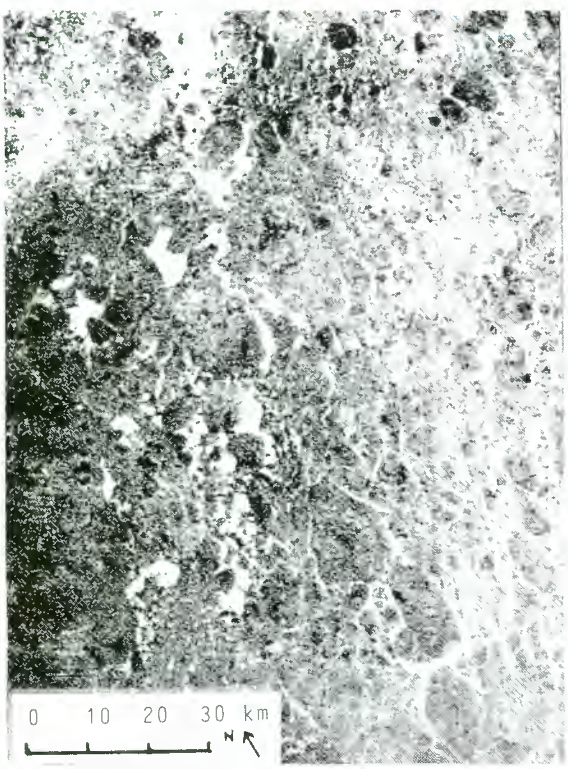

a

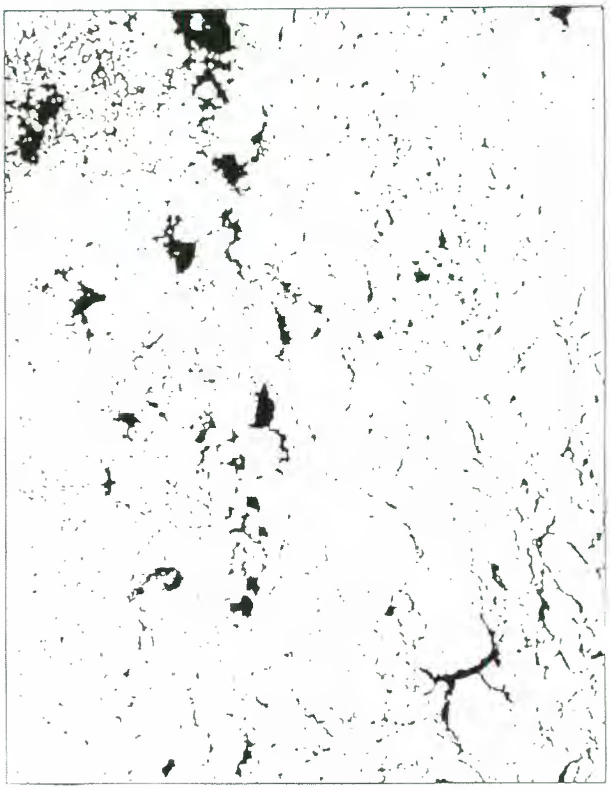

b

Figure 4.11 a,b. An area of sea ice off the coast of Antarctica was imaged by the ERS-1 SAR. Figure a shows the SAR image in which the dark areas represent first-year sea ice while the bright areas are open water regions. Figure b shows the areas of open water (in black) which have been detected. The proportion of the area covered by open water can be determined by relating the black pixels to the overall area. Courtesy of R Roth, University of Hannover, Germany.

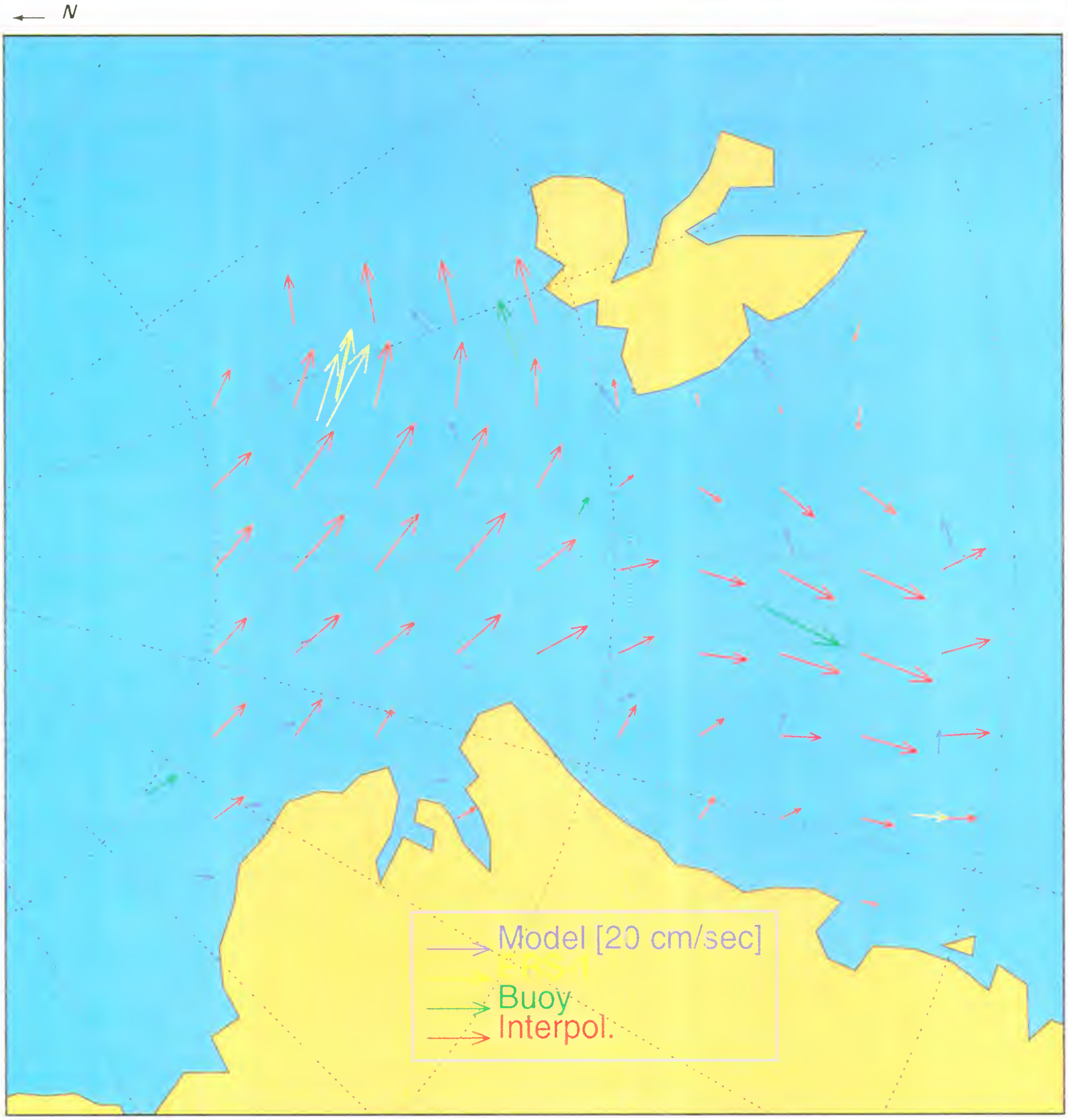

Figure 4.12. The Fram Strait is the most important area of southward ice transport from the Arctic, accounting for over 90% of the ice flux and around 25% of the total heat exchange between the Arctic seas and the global ocean. The ice budget of the Greenland Sea area is also thought to play a role in the North Atlantic deep water formation and thereby influences global ocean circulation.

Sequential images from the ERS-1 SAR are used to determine ice velocities. These ice velocities are used in conjunction with other information to construct fields of ice motion for the Fram Strait area. If these fields are combined with measurements of ice thickness which may be obtained from the sea bed by means of upward looking sonar, the total volume of ice passing through this area can be determined. The multiyear mission of ERS-1 allows the study of interannual variability of ice fluxes and has the potential to help detect climate change signals in the longer term. This figure shows an interpolated field of ice motion (red) for 3 April 1993 which was constructed from three separate sources: a simple wind drift model (blue), ERS-1 SAR images (yellow) and ice velocities from drifting buoys. Courtesy of A Schweiger, University of Washington, Seattle, USA.

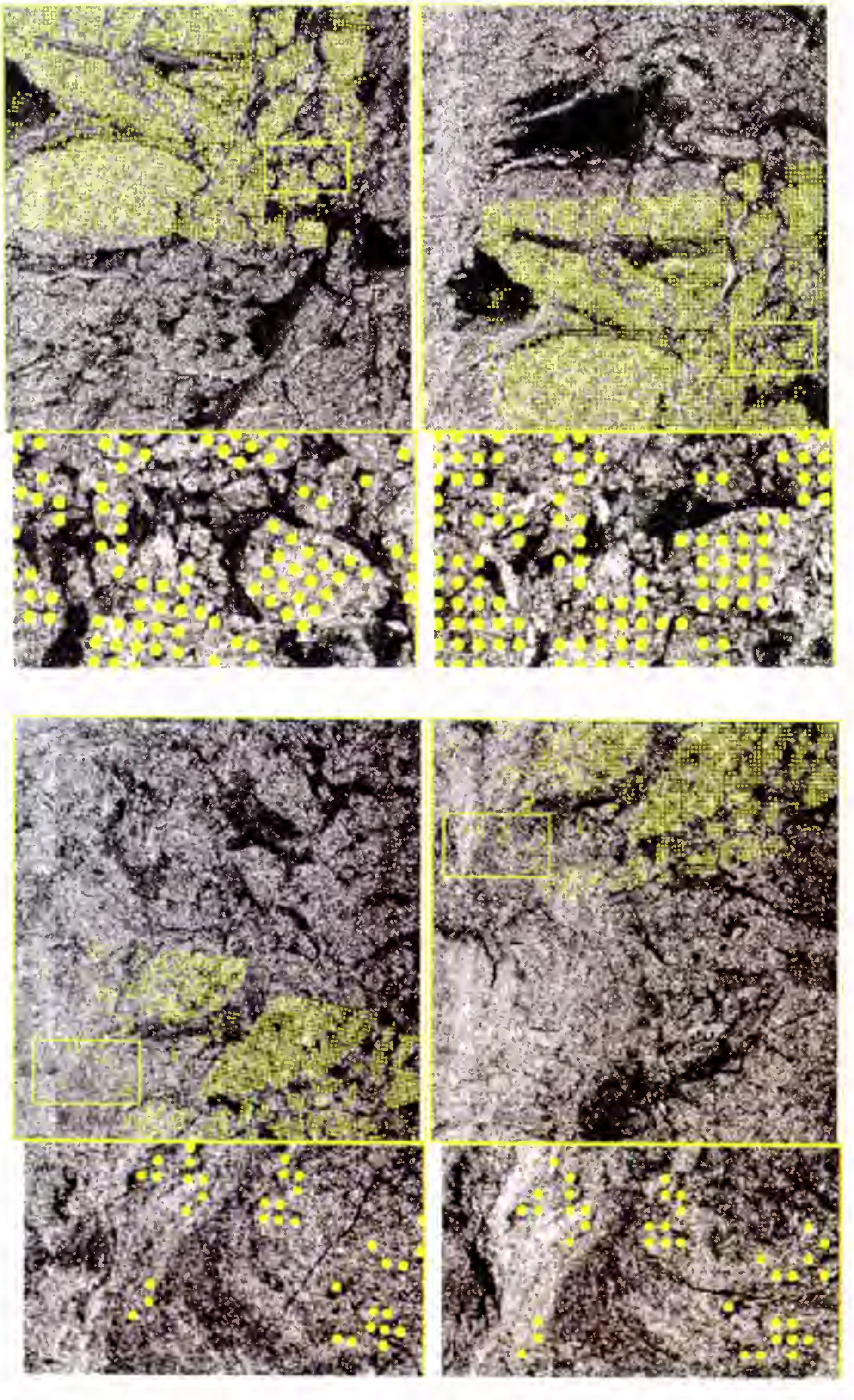

a

b

Figure 4.13 a,b. A method of tracking ice using multitemporal ERS-1 SAR imagery through the Fram Strait is shown in this Figure. The dots in Figure a illustrate positions for successful ice displacement sampling. Figure b is an example where ice monitoring is more difficult. The top images are more detailed examples of small parts of the lower images. This is seen as a more accurate method of monitoring ice drift than through the use of drifting buoys. The temporal variation in the aerial ice flux through the Fram Strait was measured from the ERS-1 SAR images during the spring of 1994. The total ice flux was calculated (January: 144 000 km²; February: 69 000 km²; March: 134 000 km²).

This large range indicates that a considerable variation occurs in the rate of ice production and heat loss from the divergent areas upstream in the Arctic Ocean during the freezing season. Courtesy of R Korsnes, Norsk Polarinstitut, Oslo, Norway.

OBSERVATION OF CONVECTIVE PLUMES

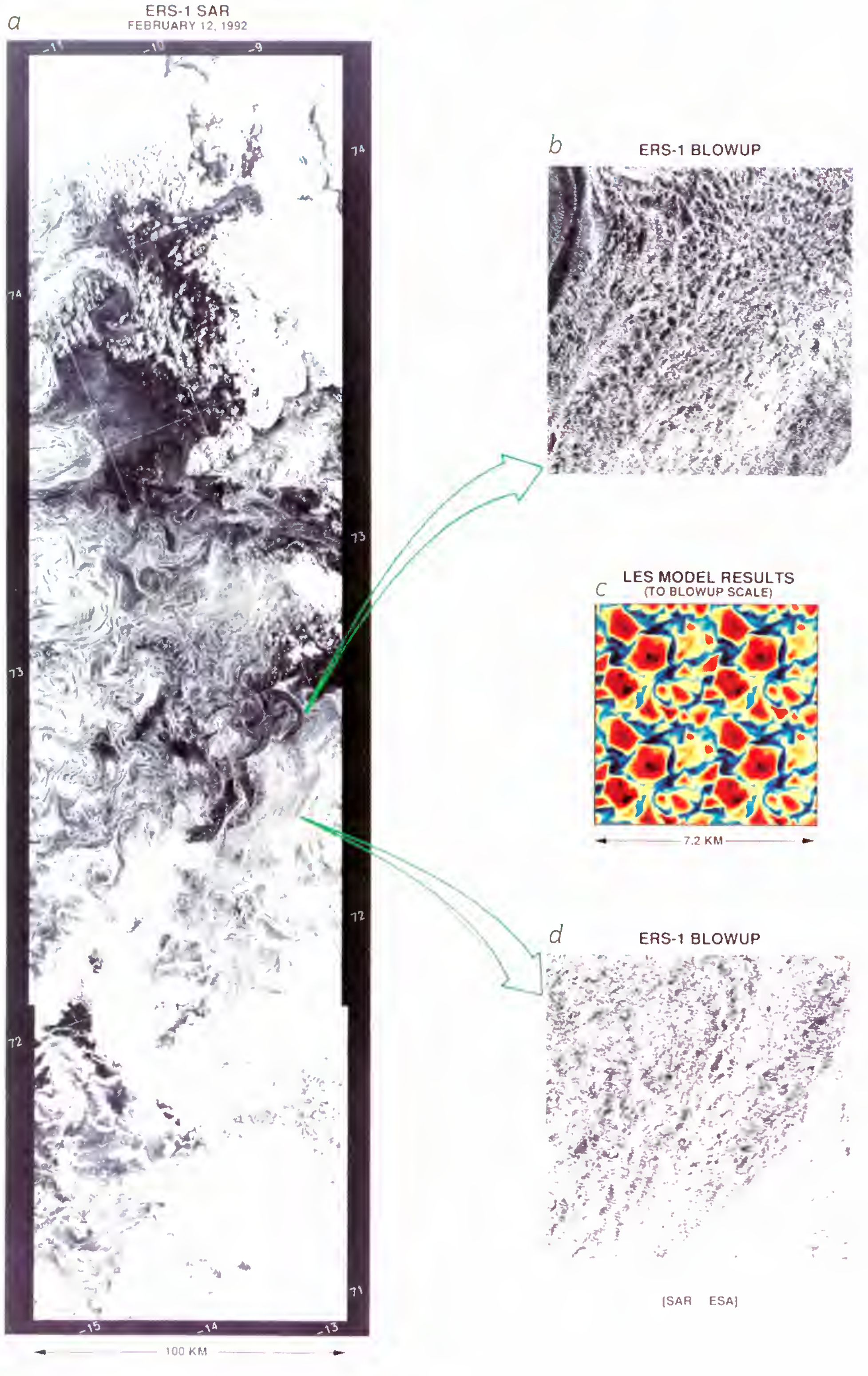

Figure 4.14 a,b,c. Deep ocean water formation mostly occurs in very limited areas of deep water convection. In the past, these areas have been very difficult to find and study using in situ techniques and have been little studied using satellite techniques.

This Figure shows plumes in the Greenland Sea as modelled and observed in ERS-1 SAR images. The SAR data in Figure a are at a nominal swath width of 100 km and at a reduced resolution of about 100 m; in the blowups of Figures b and d the resolution is 30 m. The model result covers an area of 3.6 x 3.6 km and four identical regions are grouped in Figure c. One can see how the formation predicted by the model has been detected in the SAR image, although the scale observed is different from that modelled. Courtesy of F Carsey, JPL, Pasadena, USA.

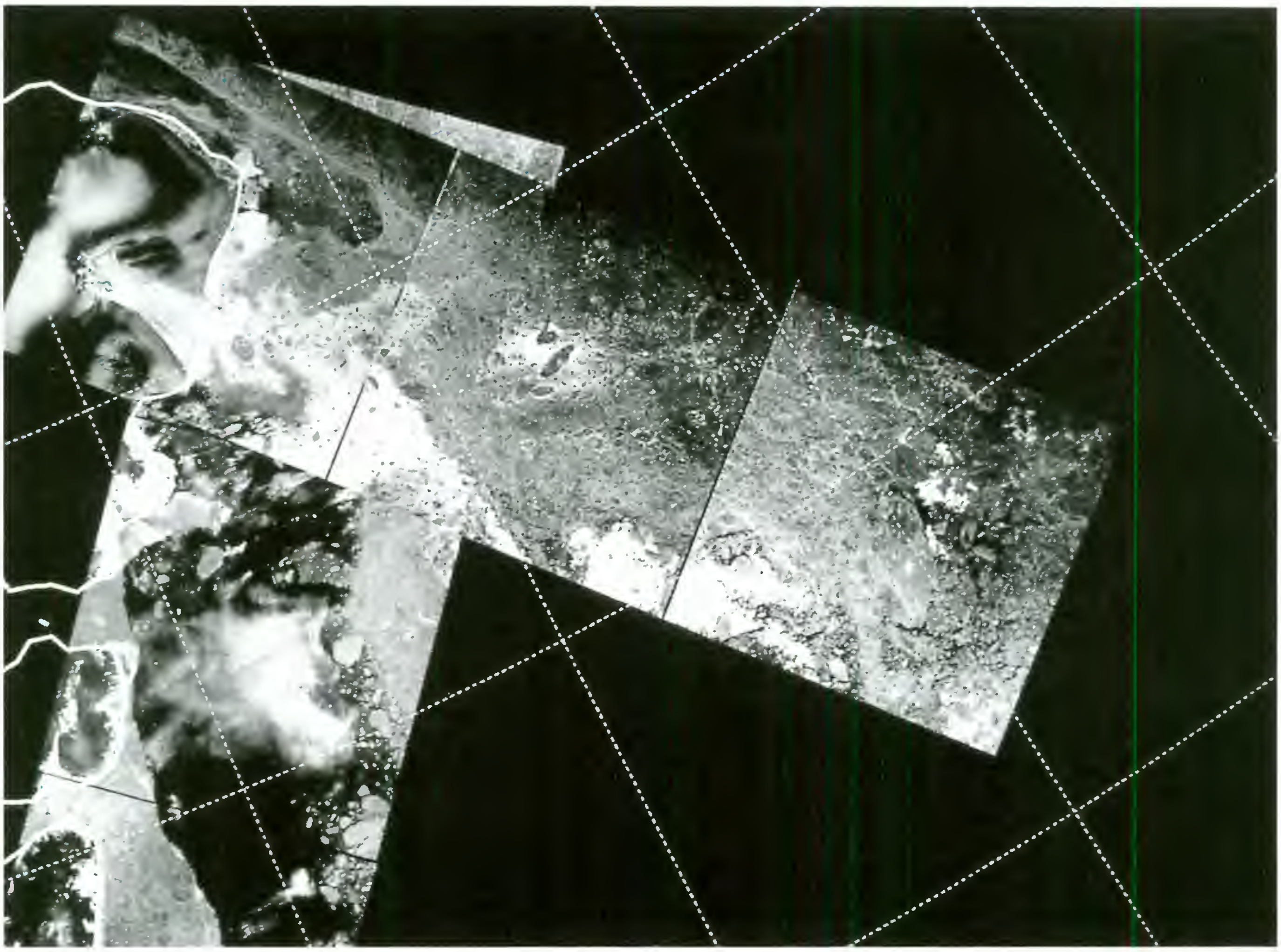

Figure 4.15. The mechanism of the initial formation of the Northeast Water Polynya is not known but it may be possible to understand it from data acquired in winter and early spring. It has been found that the polynya increases from its initial size and is maintained during summer by solar radiation. It may cover a large area (40 000 km²), with large variations from year to year, which have so far proved unpredictable. From ERS-1 observations it is also concluded that the existence and the size of this polynya is due to the protection offered by two barriers of shorefast ice, north and south of the polynya. Thus, even under severe weather conditions (often associated with dense cloud cover) advection of ice into the polynya can be studied with ERS-1 SAR.

This Figure is an ERS-1 SAR image mosaic of the area recorded on 24 July 1992. The mosaic consists of three SAR scenes in ascending and descending passes acquired at a time interval of about 8 hours under different wind conditions. This advection of old ice into the polynya area might have a bearing on the life of the polynya, and on its formation and maximum size the following summer. Other ERS-1 SAR observations have confirmed the anticyclonic circulation of the ocean in the area and determined the velocity of the surface water using floes as tracers. Courtesy of P Gudmandsen, Technical University of Denmark, Copenhagen, Denmark.

5. GLACIOLOGY AND SNOW

Glaciological and snow processes are fundamental to environmental change studies. Temporal changes in the total volume and distribution of ice contained within the major polar ice sheets are good indicators of climate trends. In addition, temperate glaciers and seasonal snow cover are highly sensitive to climate change. They can also have a significant impact on economic activities within Alpine areas.

Polar and high-altitude areas present remote and harsh environments where it is difficult to measure key parameters. Researchers have thus relied heavily on three-dimensional modelling. Consequently, present estimates of ice sheet mass balance, glacier and snow extent show considerable uncertainties. For example, it is not known if the ice sheets of Antarctica and Greenland are growing or shrinking. New and highly accurate observations from ERS-1 are being used for model verification and for determining seasonal and annual changes, based on repeat measurements.

Ice sheet research was one of the main targets for the ERS-1 programme. In comparison with other satellites and field data, ERS-1 provides significant advances, particularly for polar ice sheet monitoring. A key factor is the improved extent and frequency of coverage of the polar region in relation to previous satellites. Improved microwave sensor technology has also provided major steps forward in measurement capability, for example:

- The ERS-1 altimeter has been designed with a specific mode for mapping ice sheet topography and investigating volume changes;
- Radar interferometric techniques and multitemporal sequences of radar images offer a completely new dimension for studies of ice dynamics enabling flow velocity fields to be derived;
- The ERS-1 SAR and scatterometer have great sensitivity to the physical properties of polar ice, snow and temperate glaciers. SAR offers the possibility to monitor the areal extent of snow and the temporal dynamics during the melt period. This capability of regular repeat observations has not previously been provided by satellite remote sensing.

5.1. Polar ice sheet mass balance

The ice sheets of Antarctica and Greenland are the principal stores of fresh water. Changes in the size of these sheets have been reflected by mean sea level changes over the Pleistocene period (approximately 2 million to 10 000 years ago). Yet, of the possible sources for the present sea level rise of 1.6 mm per year, the contribution of the Antarctic ice sheet is the least certain. Knowledge of its mass balance is currently constrained by observations to an equivalent uncertainty of 1.1 mm per year.

As a result of changes in the climate, ocean currents near the edge of the Antarctic continental shelf may change, allowing comparatively warm water to circulate beneath the ice shelves. This would substantially increase the rate of melting and may be sufficient for the ice shelves to disintegrate. Resulting changes to ice dynamics at the edge of the main Antarctic continental ice sheet may increase the rate of flow from the interior regions towards the coast, thereby reducing the total mass of ice over the Antarctic Continent. This process could lead to an increase in sea level worldwide as well as changes in the salinity and temperature of the surrounding oceans.

Three-dimensional dynamic and thermodynamic models have been developed to help understand the past and present behaviour of ice sheets in relation to climatic parameters and to extrapolate to the future. Major model improvements are needed to account for feedback mechanisms between ice sheets, oceanic and atmospheric circulation. Improvements in the quality and coverage of data in space and time, based on satellite and field measurements, are needed for the advancement of models and for the development of an improved understanding of the response and sensitivity of ice sheets to climate change.

ERS-1 has contributed to the monitoring of ice sheet mass balance in two ways:

- The ERS-1 SAR, scatterometer and ATSR have all been used to monitor the margins of ice sheets and the condition of the ice;
- The ERS-1 radar altimeter has been used to measure the elevation of the Greenland ice sheet and much of the Antarctic ice sheet to new levels of accuracy.

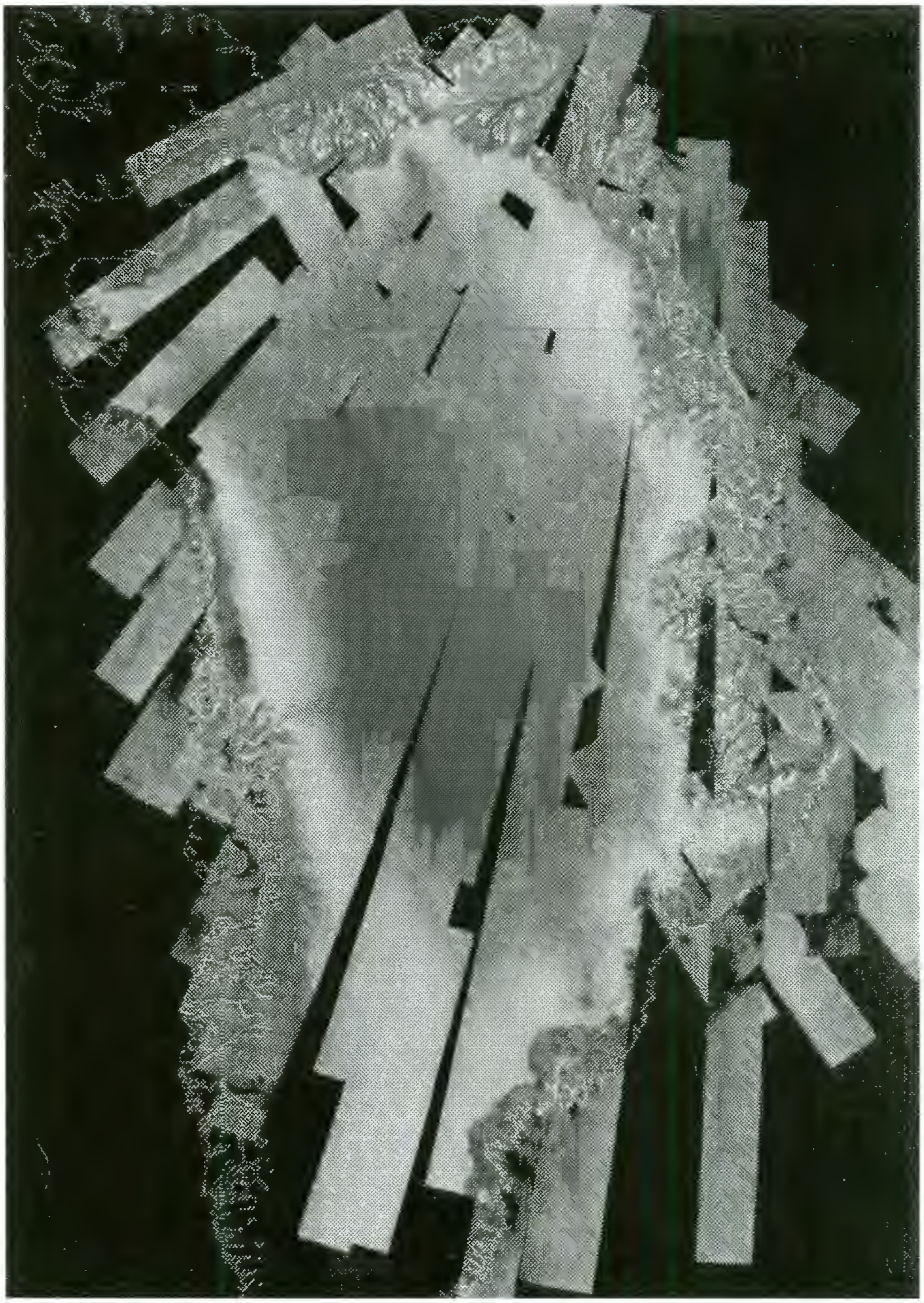

Figure 5.1. This ERS-1 SAR mosaic of the Greenland ice sheet illustrates the difference in the snow pack of the high interior (low backscatter) which does not melt (the accumulation zone) and the high backscatter region surrounding it where melt water produced at the surface percolates into the snowpack and freezes. Darker areas around the ice are regions of net ablation. Repeat measurements allow monitoring of changes in the patterns of melt. Courtesy of R Bindschlader, M Fahnstock, NASA Goddard Space Flight Center, Greenbelt; R Kwok, JPL, Pasadena; K Jezek, Byrd Polar Research Center, Ohio, USA. (Published in *Science*, 3 Dec. 1993, vol. 262, p. 1532).

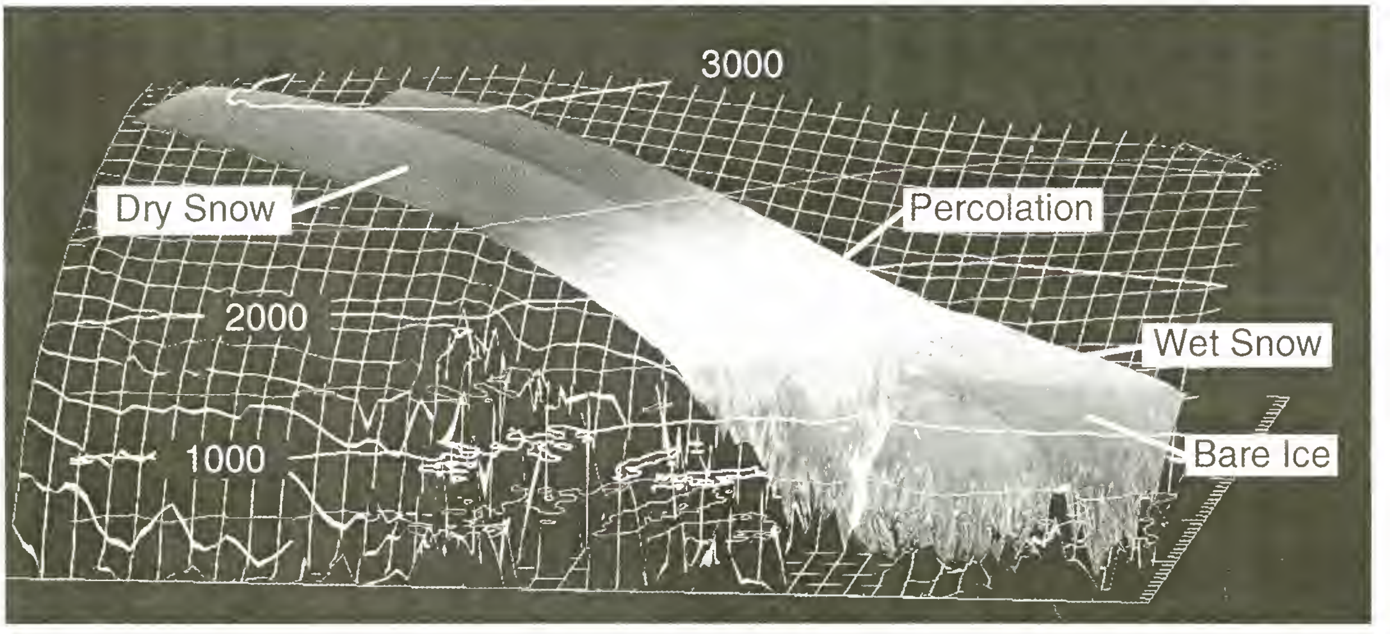

Figure 5.2. The structure of the snow pack varies across polar ice sheets and shows the balance between accumulation and melt at different elevations. The transitions from the bare ice zone to the wet ice zone and the percolation zone are clearly shown in this Figure. The wet snow zone shows an unusually high level of backscatter as the melted snow had refrozen at the time this winter scene was recorded. This Figure was produced by draping a mosaic of 18 ERS-1 SAR images recorded in the winter of 1992 over a digital elevation model of the western Greenland ice sheet. The vertical exaggeration is 100:1, the contour interval 500 m and the grid spacing 25 km. The view is looking eastward towards the west coast between 67°N and 74°N. Changes in the level of these zones are sensitive indicators of temperature and any significant displacement could be the first reliable indicator of climate change. Courtesy of R Bindschlader, M Fahnstock, NASA Goddard Space Flight Center, Greenbelt; R Kwok, JPL, Pasadena; K Jezek, Byrd Polar Research Center, Ohio, USA. (Published in *Science*, 3 Dec. 1993, vol. 262, p. 1531).

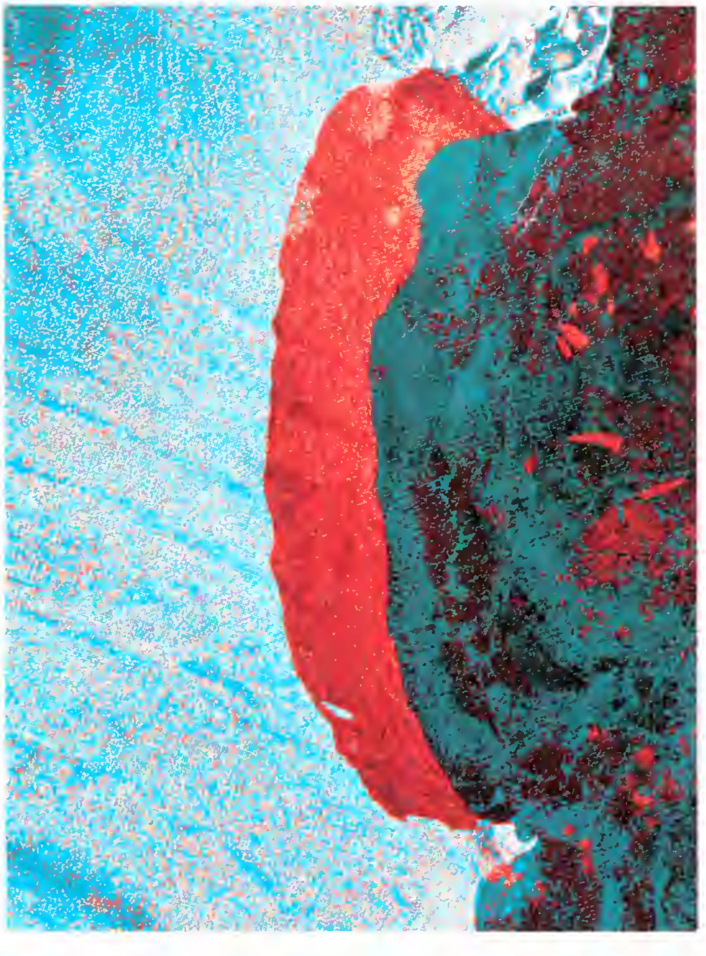

Figure 5.3. Co-registered ERS-1 SAR images of the northern part of the Larsen Ice Shelf, Antarctic Peninsula, show the ice extent for 2 July 1992 (red) and 26 August 1993 (blue). The size of the image is 33 × 45 km. Between the two dates the ice shelf boundary between Sorbral Peninsula (top) and Lindenberg Island (bottom) retreated by about 6 km. The loss in ice-covered area within one year (which appears as a bright red colour down the centre of the image) corresponded to about 15% of the total area of this part of the ice shelf. In this way, the ERS-1 SAR was used to measure the accelerated retreat of the small ice shelves at the northern part of the Antarctic Peninsula. Courtesy of H Rott, University of Innsbruck, Austria.

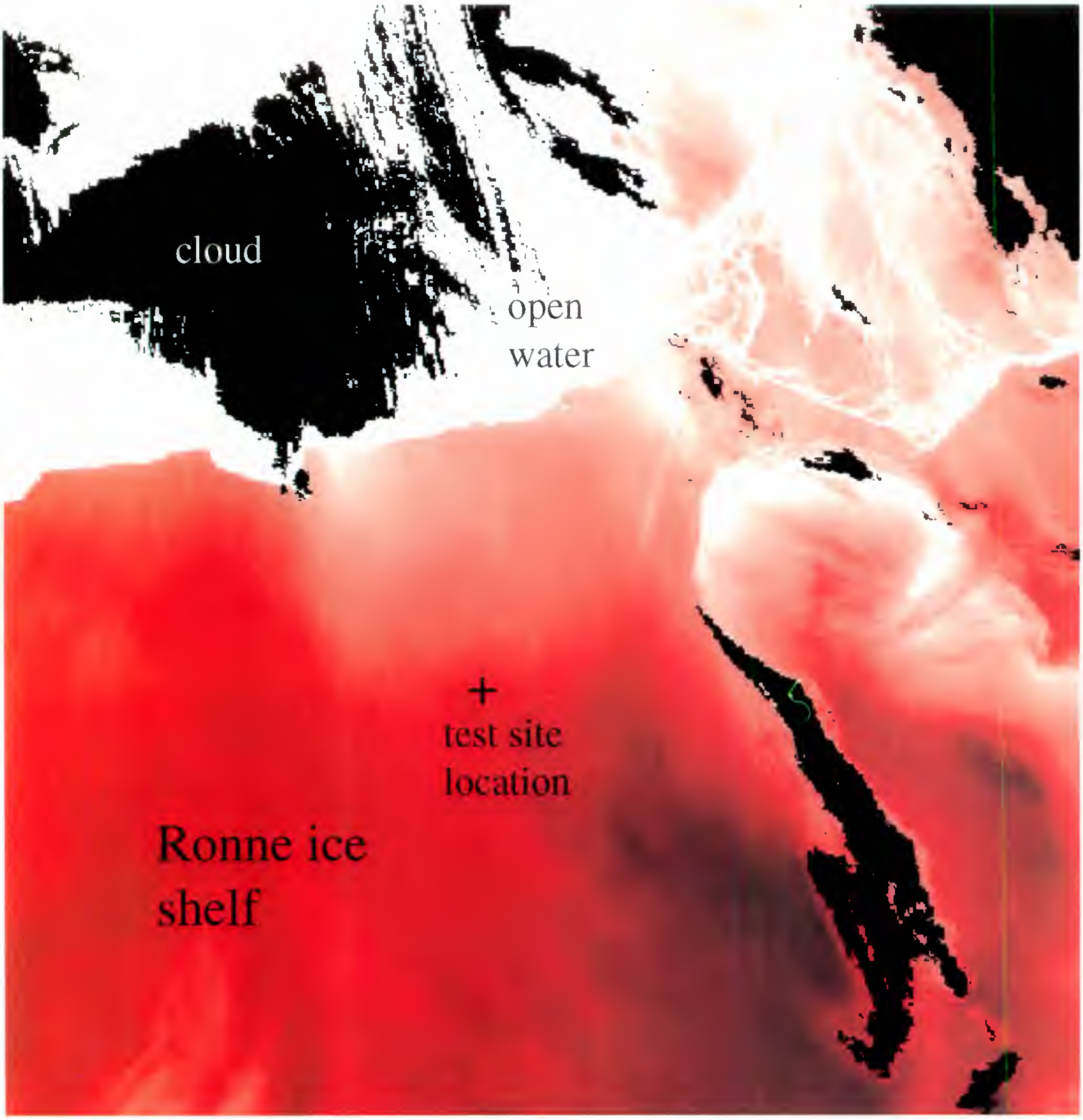

Figure 5.4. This thermal infrared image of the Ronne ice shelf, Antarctica, was acquired at the same time as ground measurements of the surface temperature. Hotter areas are brighter. The location of the test site is indicated by a cross. The validation campaign has demonstrated the ability of the ERS-1 ATSR to derive accurate surface temperatures over snow-covered areas and in particular the great ice sheets of Antarctica and Greenland, where in situ measurements are extremely scarce. Routine monitoring of temperature over the ice sheets will provide valuable input into global climate models that are currently poorly constrained in the polar regions. The data will also be useful for determining the climatology of the ice sheets, and in the long term, identifying temporal trends in temperature due to climate change. Courtesy of J Bamber, Mullard Space Science Laboratory, University College London, UK.

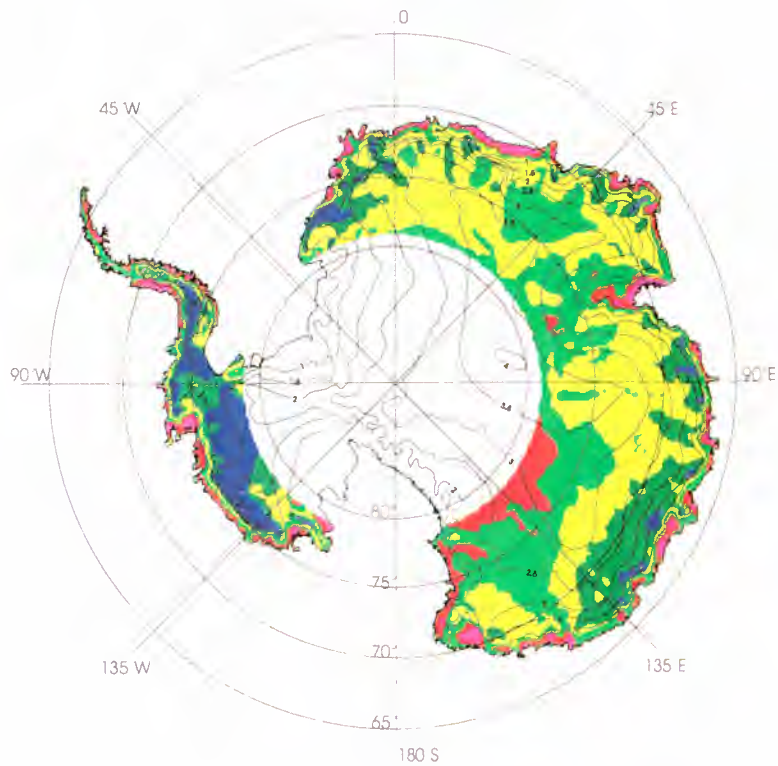

a

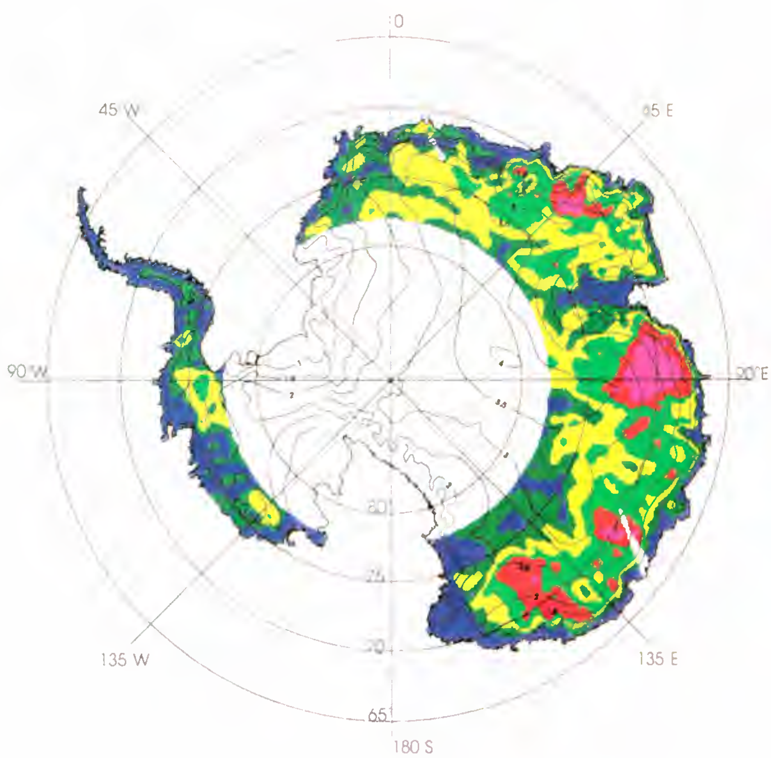

b

Figure 5.5 a,b. Information on the physical properties of snow and ice in Antarctica and Greenland can be obtained from ERS-1 scatterometer measurements. This information is of interest for supporting mass balance studies and for evaluating altimeter measurements.

Figure a represents mean backscattering coefficients at an incidence angle of 35° from ERS-1 scatterometer data recorded over Antarctica in April 1993. The highest backscattering coefficients are observed for refrozen firn along the coast (magenta, $\sigma^0 > -4$ dB). Comparatively high values are also found on the high central plateau where the accumulation rates are low and the snow pack shows pronounced layering (red, σ^0 -7 to -4 dB and light green, σ^0 -10 to -7 dB). Backscatter is low in areas of dry snow and high accumulation (blue, $\sigma^0 < -16$ dB). The area of no scatterometer data south of 78.5°S is due to the orbital configuration of the satellite and look direction of the sensor.

Figure b shows the factor of azimuthal asymmetry of the backscattering coefficient based on ERS-1 scatterometer data. The pattern of responses can be explained by the varying orientation of the reflecting interfaces at the surface and the top few metres of the snow pack. These effects are related to sastrugi (snow dunes) formed by strong winds. High values of asymmetry (shown in magenta and red) are found over the regions with strong katabatic winds along the slope of the East Antarctic Plateau. In these regions the azimuth direction of minimum backscattering corresponds to the dominating wind direction. Courtesy of H Rott, University of Innsbruck, Austria.

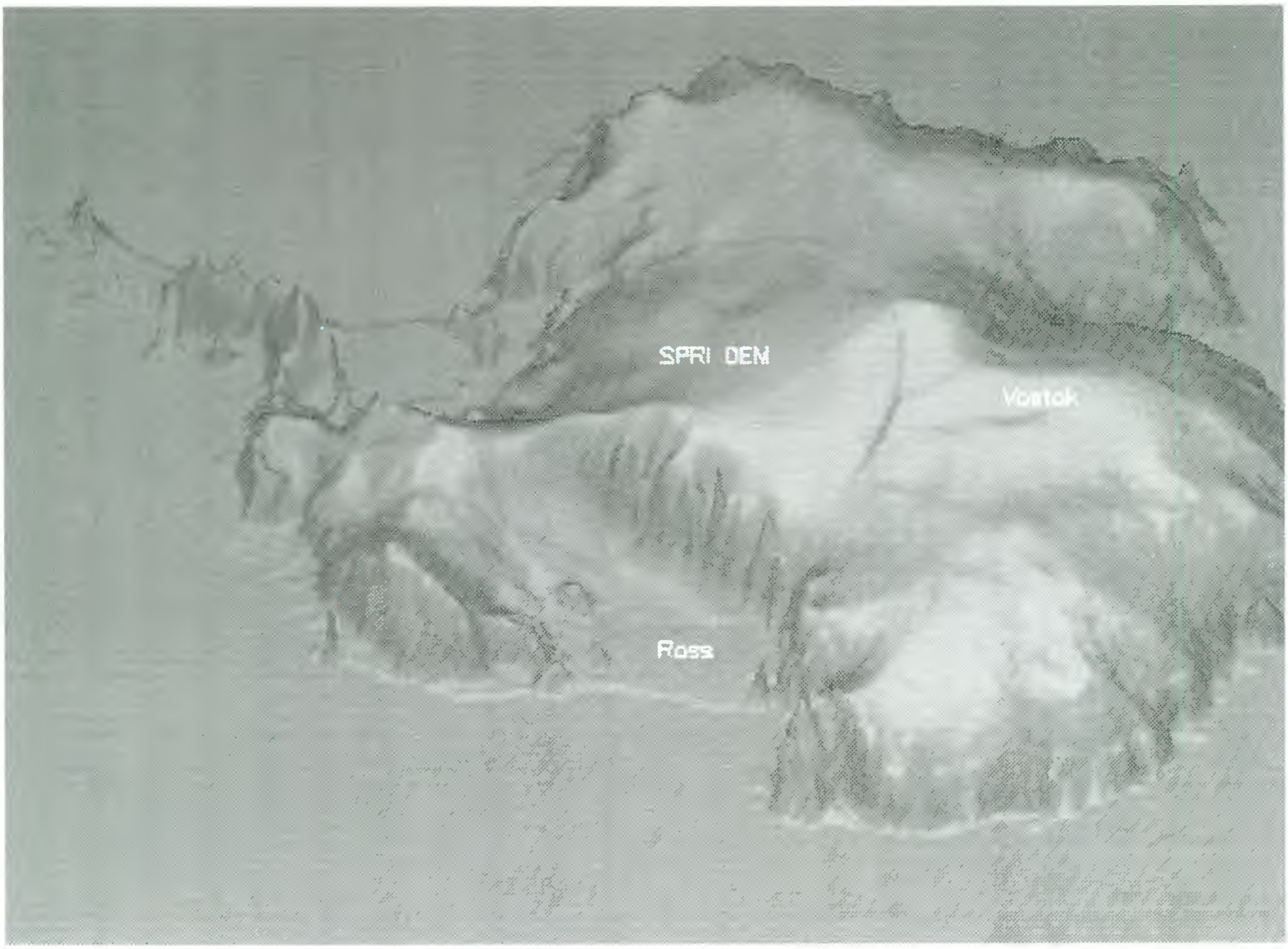

Figure 5.6. A digital elevation model with grid spacing of 20 km has been produced for the Antarctic ice sheet, based on 1 000 000 height estimates from the ERS-1 radar altimeter. Comparisons with levelling surveys indicate that the mean error is in the order of a few metres for the interior of the ice sheet. This compares with previously available data which had estimated errors of 50 m. The area in the centre of the map is based on a digital elevation model produced by the Scott Polar Research Institute. This is because the ERS-1 orbit only passes as low as 82°S and so no measurements are available between this latitude and the South Pole. Courtesy of J Bamber, Mullard Space Science Laboratory, University College London, UK.

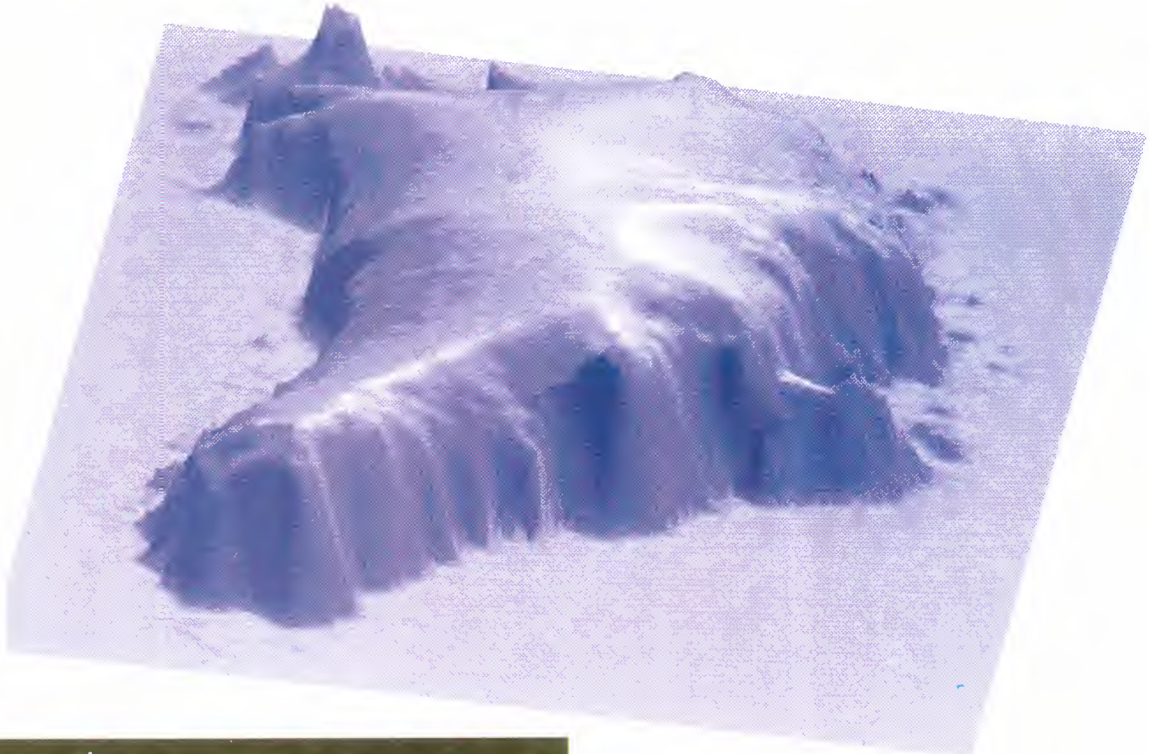

a

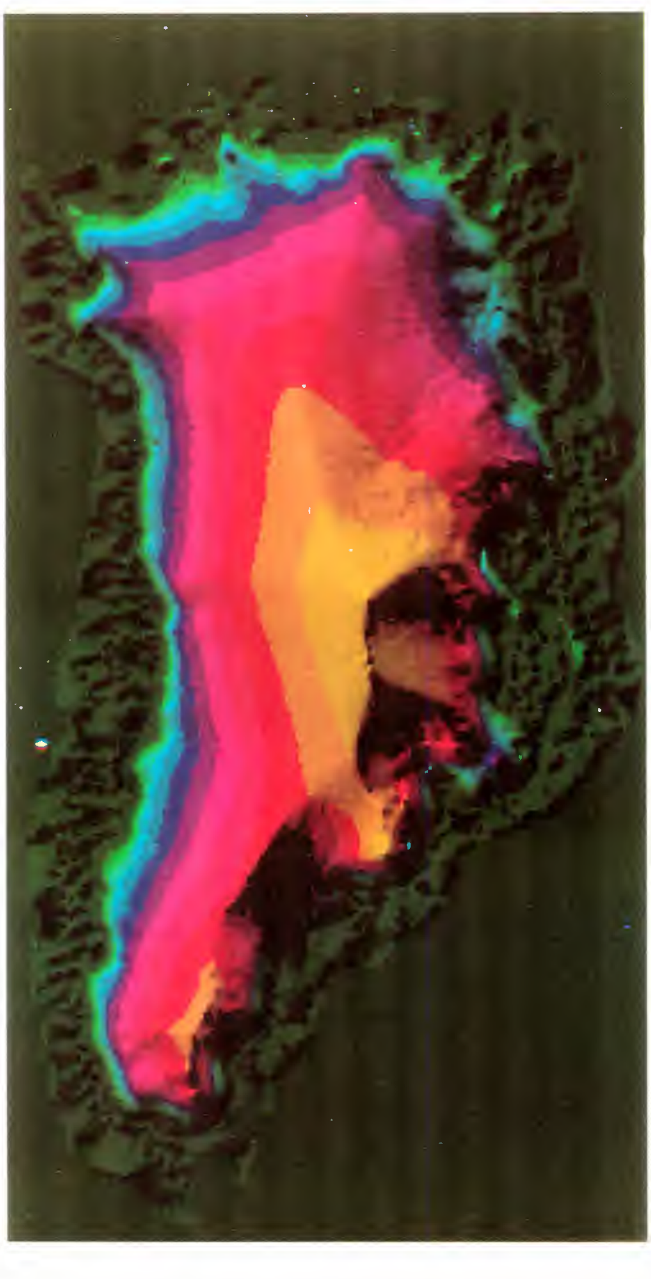

b

Figure 5.7 a,b. In addition to the ice topography map of Antarctica (Fig. 5.6), a topographic map of the Greenland ice sheet has been developed, using the ERS-1 radar altimeter. This map is shown both as a perspective view (Fig. a) and as a contour map (Fig. b). These datasets now form a reliable foundation for scientific applications which require data for mass balance investigations and for modelling ice dynamics. Such applications include the correction of SAR imagery, the recalculation of drainage basin area and modelling studies. The improved topographic accuracy of these data has shown that previously identified drainage basin boundaries could be in error by as much as 100 km. The establishment of this new level of precision in topographic mapping has also provided for the first time a reference map from which future changes can now be identified with confidence. Courtesy of J Bamber, Mullard Space Science Laboratory, University College London, UK.

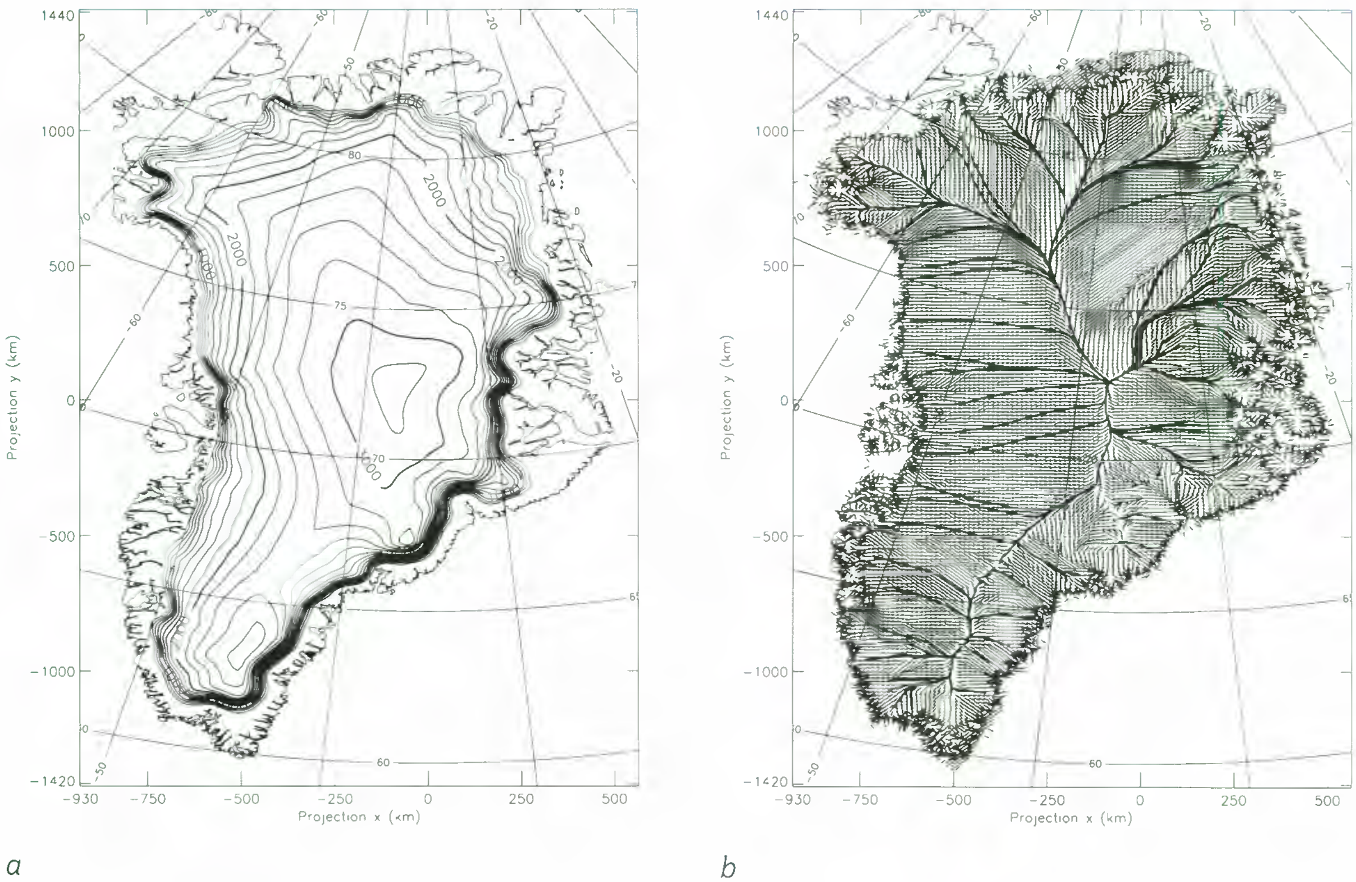

Figure 5.8 a,b. Figure a shows a height map of the complete Greenland ice sheet derived from ERS-1 radar altimeter data. Contours are shown at 200 m intervals from 400 m. This result is the first topographic map of the whole ice sheet derived entirely from satellite radar altimeter data. The gridded heights are the most accurate mapping of the centre of the ice sheet. More accurate results are expected from the inclusion of data from the ERS-1 altimeter's purpose-built ice mode, and data from the geodetic phase of the mission.

Figure b shows surface slope directions (as vector arrows) derived from the height map in Figure a. Due to the nature of ice sheet dynamics, the surface slope directions on this scale also show the directions of flow of the ice through the ice sheet. Overlaid on the surface slope directions (as bold lines) are derived ice sheet drainage basin boundaries. Each drainage basin represents an enclosed region of ice flow leading to an ice outlet. This result is the first look at the drainage basins of the entire ice sheet derived from a single topographic source. Understanding the ice sheet drainage allows better modelling of the ice sheet, either in its current state, or in response to previous or future climate changes. Courtesy of J Morley, Mullard Space Science Laboratory, University College London, UK.

5.2. Ice sheet dynamics

An important objective of glaciological work in Antarctica and Greenland is to understand the motion and deformation of ice and to relate these processes to changes in mass balance and ice volume. Of particular importance are the flow dynamics of ice streams draining the inland ice towards the coast, the dynamics and stability of ice shelves, and the position of the grounding line. Information on ice dynamics is needed to model the processes which relate the external forcing such as accumulation, ablation and temperature to changes of ice volume. For example, one of the threats from global warming is that, instead of a gradual melting of ice, there could be a rapid collapse of parts of a major ice sheet, with consequent sea level rise. Particular concerns regarding stability have been expressed for the West Antarctic Ice Sheet, because large parts of the ice sheet are grounded several hundred metres below sea level, and if the ice volume decreases, parts of the ice sheet would begin to float reducing its stability. Accurate models of ice dynamics are also required to date deep ice cores which provide a unique source of information on climate history.

A technique which has helped the development of ice sheet dynamics monitoring is interferometry using ERS-1 SAR data. By comparing the phase information from images of the same area at different times, very small changes in the relative positions of the surface can be identified. This can be achieved without the need for large specific features to be identified and so relative movements across the whole area can be monitored.

SAR interferometry is very well suited to the monitoring of ice sheets because the small motions over time are difficult to identify by any other means. In addition, the use of this technique means that variations of ice sheet motion over much smaller time periods than previously possible can be made. This allows a much better understanding of the mechanisms governing the movements of ice sheets.

MONITORING ICE SHEET MOVEMENTS

a

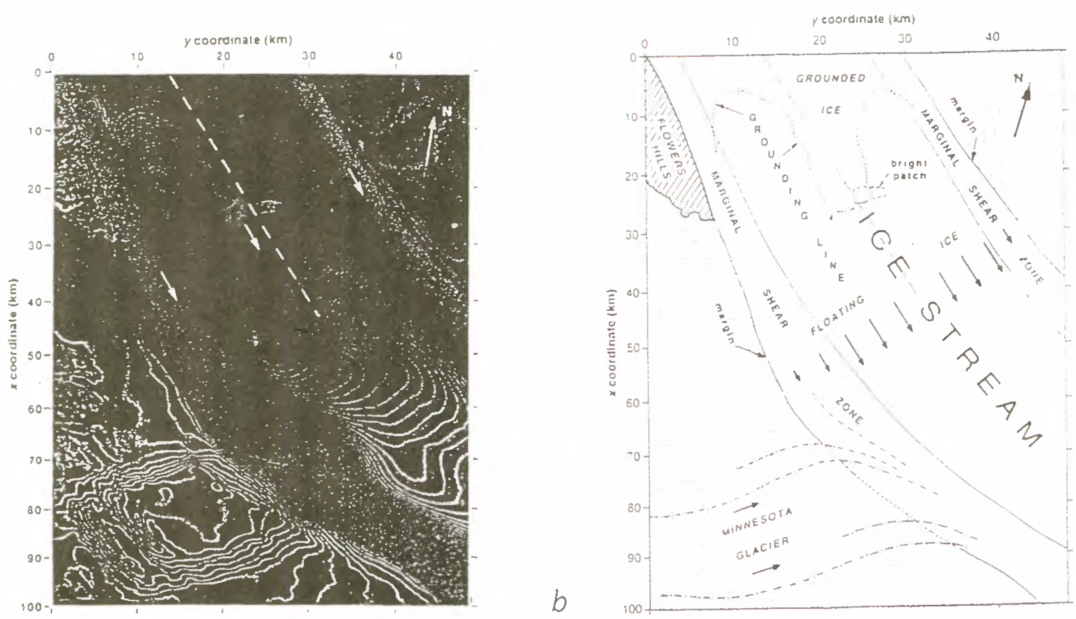

b

Figure 5.9 a,b. ERS-1 SAR data and interferometric techniques have been used to measure the motion of the Rutford ice stream precisely and to locate the line beyond which the ice sheet is floating. The Rutford Ice Stream is 40 km wide, 150 km long and 2 km thick. It flows from the West Antarctic Ice Sheet into the Ronne Ice Shelf. This radar interferogram shows a portion of the Rutford Ice Sheet. Ice flow is indicated schematically by arrows.

A transformation from blue through yellow and red to blue again represents a 2.8-cm movement towards the spacecraft. Superimposed on the interferogram is the SAR image. The location map shows the features in the interferogram. The ice stream is the unpatterned area in the middle, flowing as indicated by arrows. The division between the grounded ice and floating ice is shown by a dotted line. Without satellite measurements, the velocity of these ice streams can only be determined by laborious and costly in-situ surveys. Prior to ERS-1 the technique of comparing optical images taken on different dates could produce velocity measurements with accuracies of about 0.5% for imagery collected about one year apart at locations where temporally stable surface features could be identified. With SAR interferometry the ice stream velocity can be measured quickly (within a few days) to accuracies corresponding to 0.1%. This allows changes in flow over much smaller timescales to be assessed. Courtesy of R Goldstein, JPL, Pasadena; H Engelhardt, B Kamb, California Institute of Technology, Pasadena, USA; R Frolich, British Antarctic Survey, Cambridge, UK. (Published in *Science*, 3 Dec. 1993, vol. 262, pp. 1525-1530).

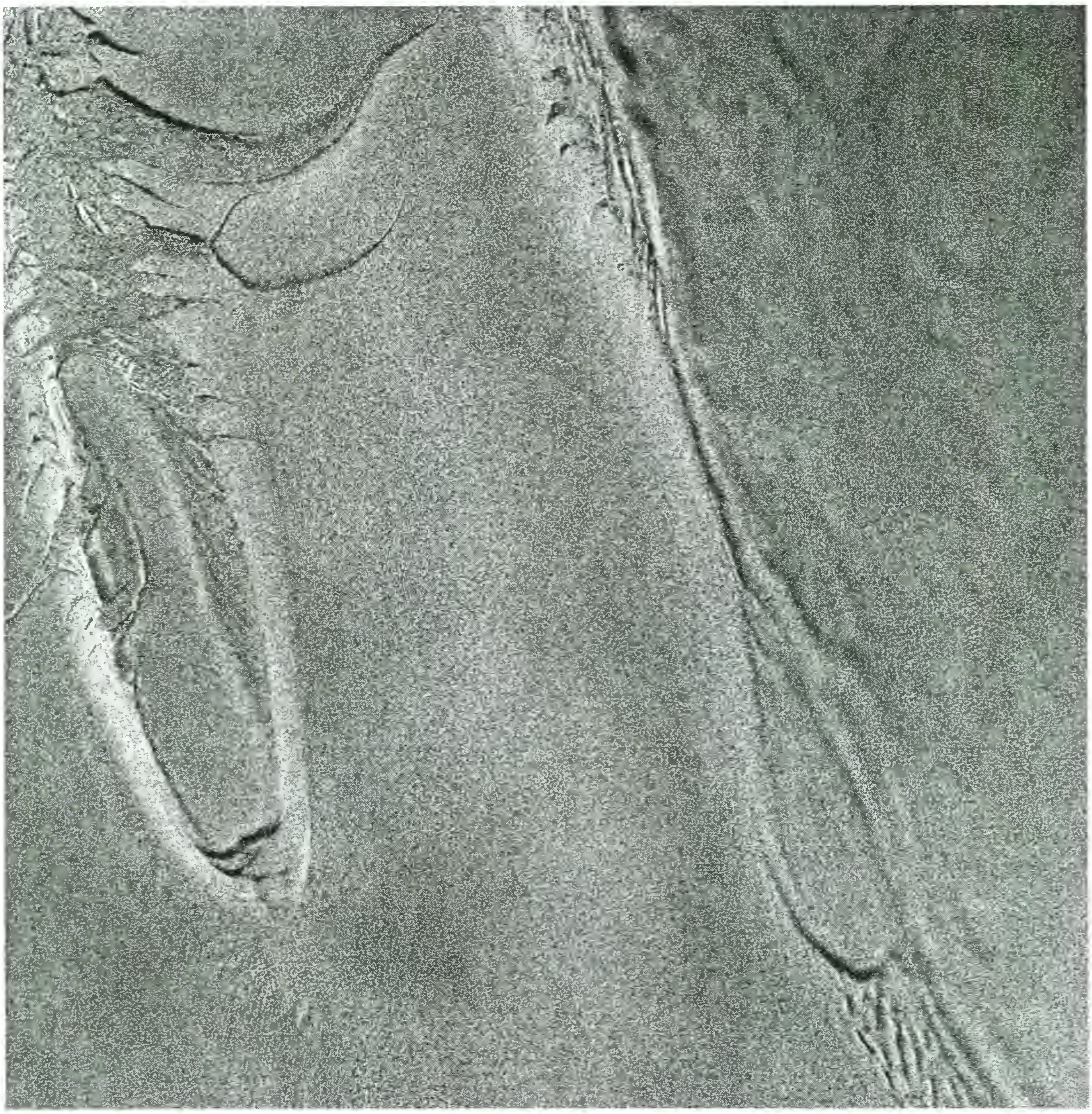

a

Figure 5.10 a,b,c. SAR interferometry has been used to detect ice motion in the area around the Hemmen Ice Rise on the Filchner-Ronne Ice Shelf. Figure a is a ERS-1 SAR image showing the Ice Rise to the left and Berkner Island on the right. Images from 26 and 29 January 1992 were used to identify stable areas through interferometry. Figure b is the interferogram, and the fringes are generated predominantly by dynamic effects: the rise and fall of the ocean tide; and the seaward movement (towards the top of the image) of the ice. Figure c shows the difference between two interferometric images derived from data in January 1992 reducing some of the unknown parameters from Figure b. From this a total tidal difference of 1 m has been estimated. The fringes around the southern tip of the Ice Rise show the boundary between grounded and floating ice.

Very strong horizontal velocity gradients resulting from the contrast between almost stationary grounded ice and the rapid seaward movement of the ice shelf are clearly identifiable in the fringe pattern. Tidal flexure can be distinguished from the horizontal velocity between the grounded ice rise and the fully floating ice shelf. Courtesy of P Hartl, H Thiel, X Wu, University of Stuttgart; J Sievers, Institut für Angewandte Geodasie, Frankfurt, Germany; C Doake, British Antarctic Survey, Cambridge, UK.

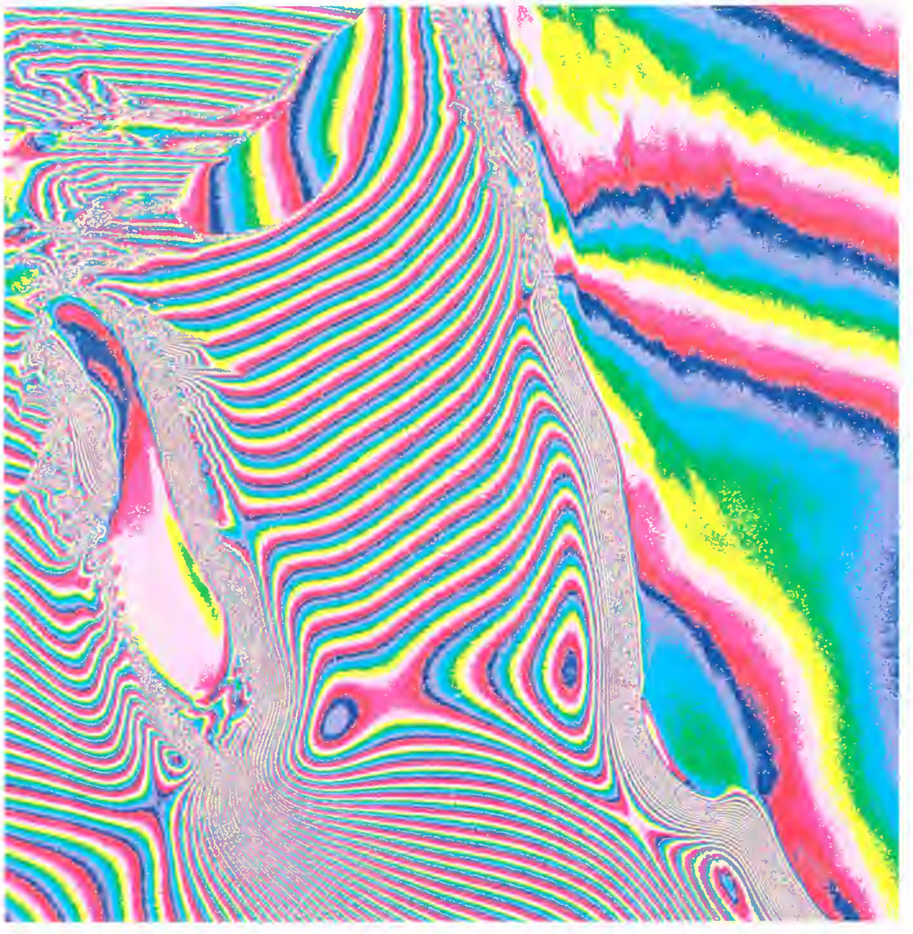
b

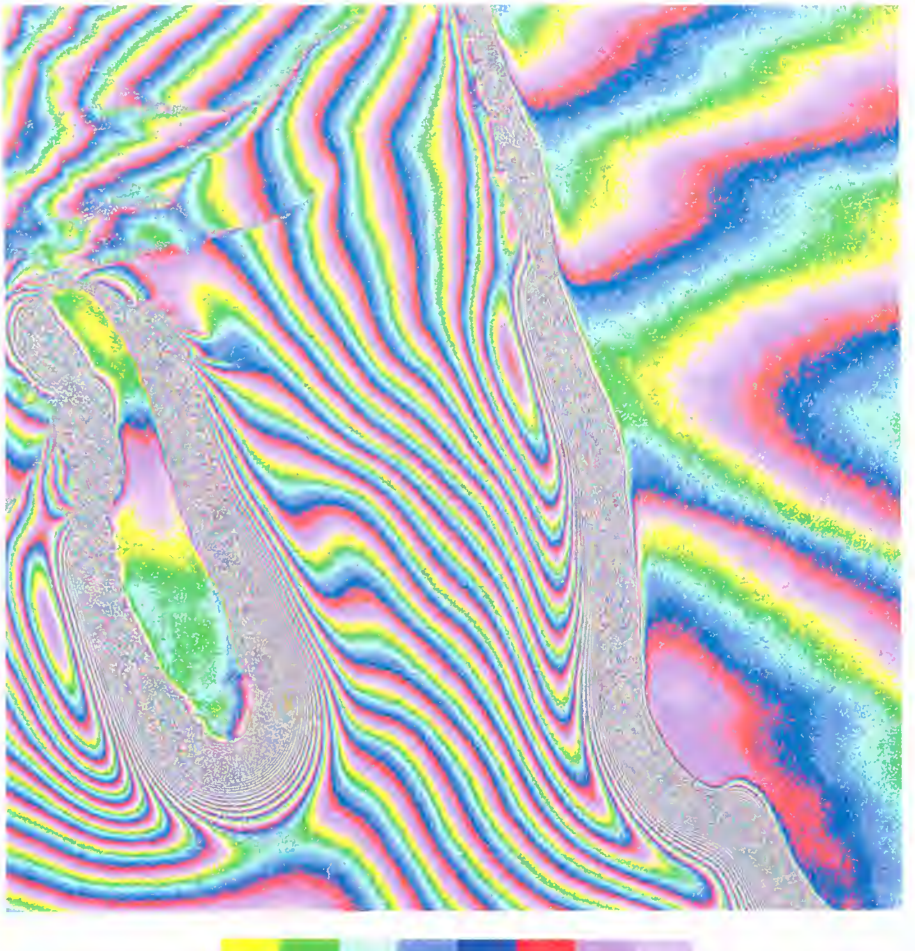
c

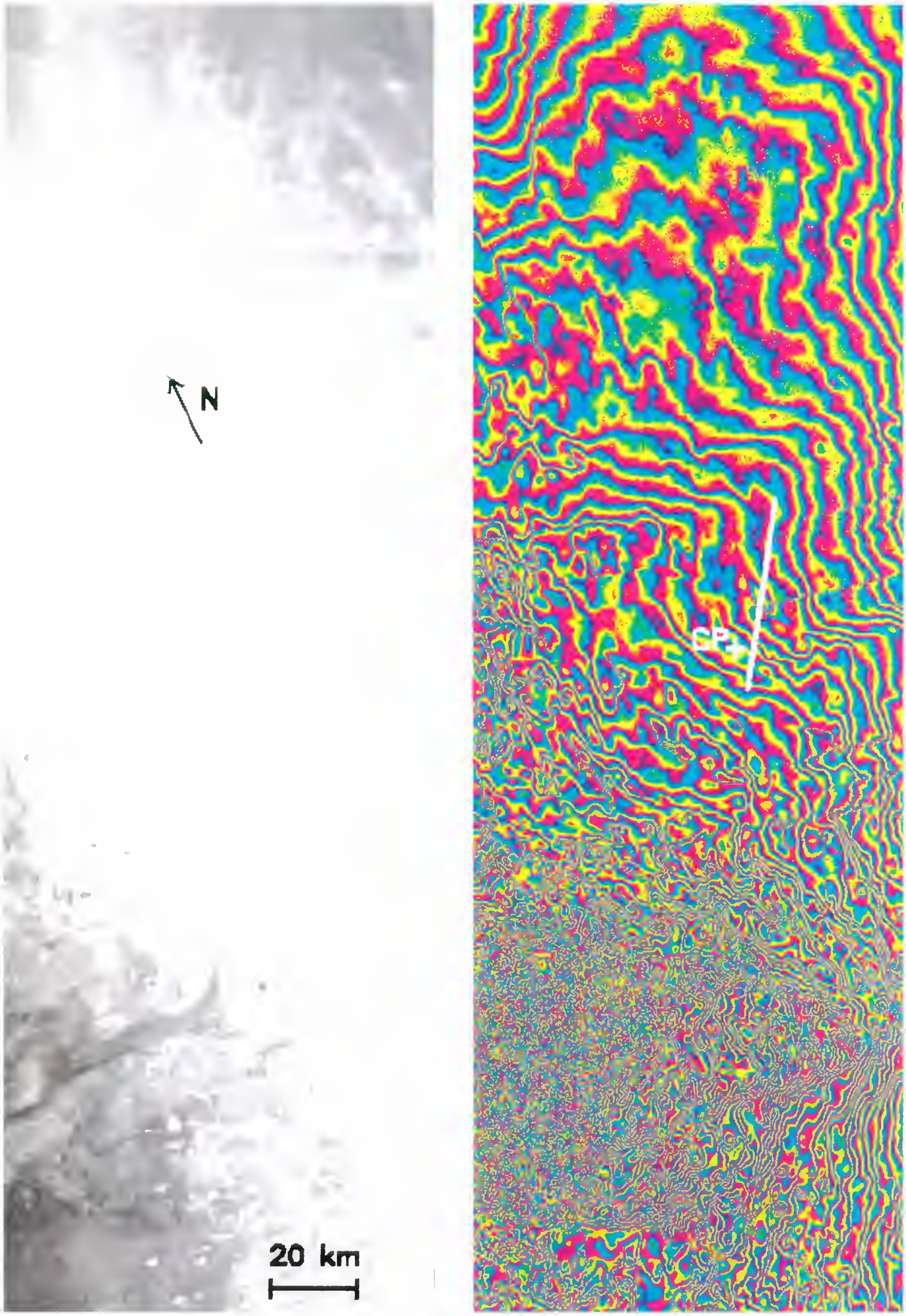

Figure 5.11. Ice flow can be studied in regions where there are no apparent ice features. The example shown is from the western flank of the Greenland ice sheet and shows that interferometrically derived estimates can be obtained across all regions of an ice sheet. The fringes are caused by surface displacement. One fringe is a horizontal displacement of about 2.8 cm. Rapid variations in the fringe patterns in the lower left part of the image derived from ERS-1 SAR data recorded during November 1991 correspond to the outflow of the Jacobshaven Glacier. Smoother phase gradients correspond to more uniform flow in the ice sheet interior. Courtesy of K Jezek, Byrd Polar Research Center, Ohio, USA.

5.3. Temperate glaciers and small ice sheets

Temperate glaciers and small ice sheets are sensitive indicators of regional climate change as they respond to changes in climate over a timescale of decades. During the past century, most of the world's valley and mountain glaciers have been receding. Water contributed by glacier melt in response to climate change represents an important component of the hydrological cycle in mountainous areas and high latitudes.

Evidence on the extent of glaciers during the Pleistocene and Holocene is available from the shape and construction of landforms, and during the last millennium historical documents provide further evidence. To learn from these data about past climatic change and to extrapolate to the future, it is necessary to establish relations between mass balance and dynamics of glaciers and atmospheric parameters. To understand and model these interaction processes, it is necessary to monitor the glacier's dynamic response to external forcing. Remote sensing techniques are able to contribute significantly to this task.

ERS-1 SAR enables mapping of frontal variations of glaciers with unprecedented temporal resolution. This is of particular interest for surging glaciers. The first complete documentation of frontal changes during a glacier surge has been carried out for a glacier in Alaska by means of ERS-1.

It should also be noted that some areas currently depend for their water supply on glacial melt water, snowmelt alone being insufficient. As the temperate glaciers continue to recede, there is a danger that this source of supply may begin to diminish. The scientific studies thus have direct relevance to the lives of those living in regions adjacent to glacier covered mountains.

ERS-1 has contributed to this area of glaciology in two ways:

- Measuring the temporal dynamics of ablation and accumulation areas;
- Identifying temporal changes in small ice sheets.

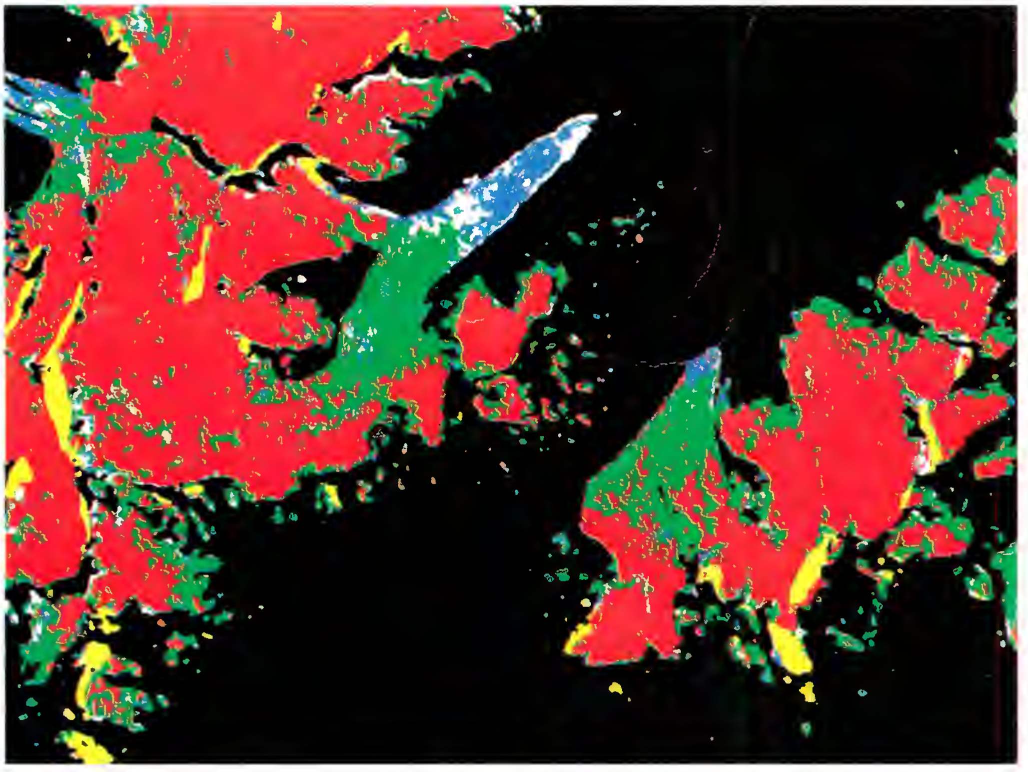

a

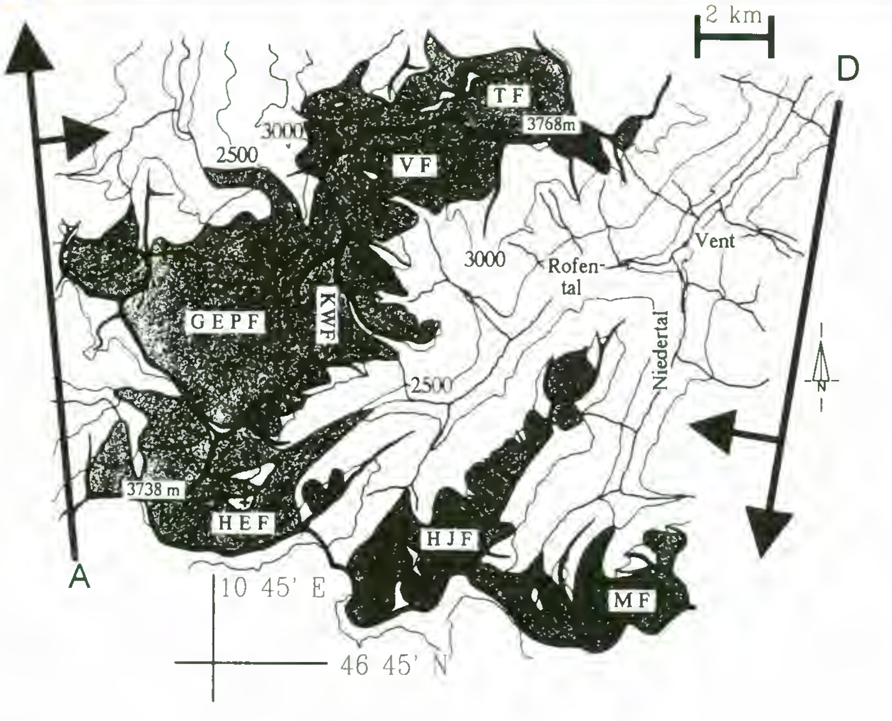

b

Figure 5.12 a,b. The rate at which snow is removed from glaciers by melting and the resultant snowline retreat is of significant interest. Such information is used for studies of runoff due to glacier melt and for mass balance estimations. ERS-1 SAR enables the temporal dynamics of ablation and accumulation areas on glaciers to be monitored.

Figure a shows the extent of snow and ice areas on glaciers of the Ötztaler Alpen in Austria derived from ERS-1 SAR images of 1 June, 6 July and 14 September 1992. In order to resolve the loss of information due to fore-shortening and layover ERS-1 SAR images from two different viewing angles were used based on ascending and descending orbits for the same day. Snow depletion on glaciers between 1 June and 6 July is shown as blue, snow depletion between 6 July and 14 September as green, the firn area on 14 September as red and the yellow indicates layover or areas with no data. The sketch map (Fig. b) shows the location of the glaciers. Courtesy of H Rott, University of Innsbruck, Austria.

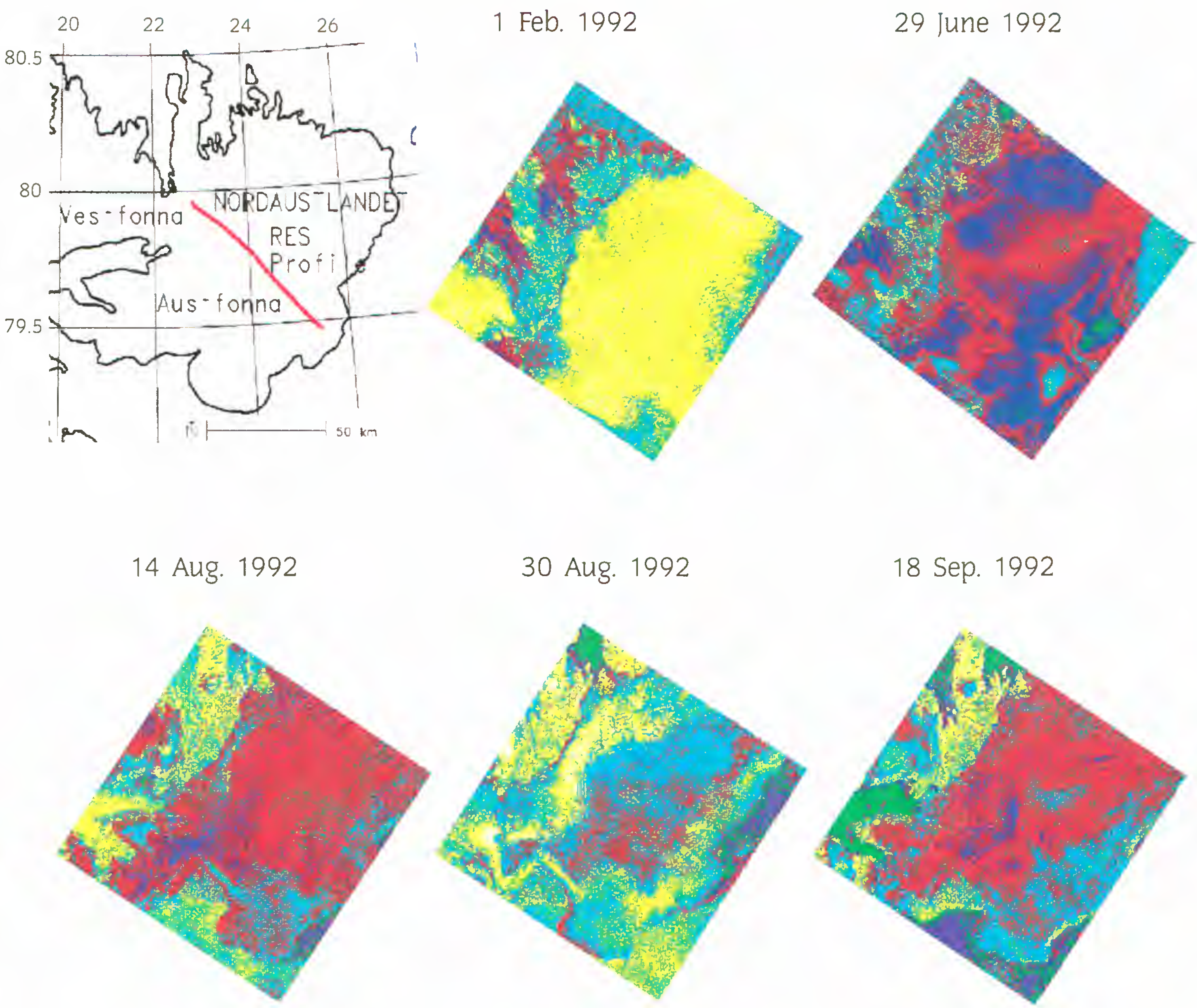

Figure 5.13. ERS-1 SAR data have been used to map the climatologically important surface zones on the ice caps of Nordaustlandet in the Svalbard archipelago north of Norway. The boundary between bare ice and melting snow at the end of the summer melt season and its altitude are believed to be particularly sensitive to global climatic changes.

This Figure shows a time series of 5 ERS-1 SAR images covering 30 weeks from 1 February to 18 September 1992. These are shown at the same scale and orientation as the map of Nordaustlandet. The images illustrate the annual cycle of changes in the Nordaustlandet ice cap. The colour code moves from yellow (low backscatter) through cyan, red, blue, green, purple to black (high backscatter). Dynamic changes in the ice caps can be observed as the snow compacts and ice is exposed. The position of the snow line (seen in the 30 August image between the cyan and yellow regions) can be mapped to an accuracy of a few kilometres, and its elevation to an accuracy of about 50 m. Validation data have been recorded along the profile indicated by the red line. This technique should substantially improve our ability to monitor this parameter, and hence to estimate variations in mass balance, since the data are unaffected by cloud cover and precipitation. Courtesy of W Rees, J Dowdeswell, A Diament, Scott Polar Research Institute, Cambridge, UK.

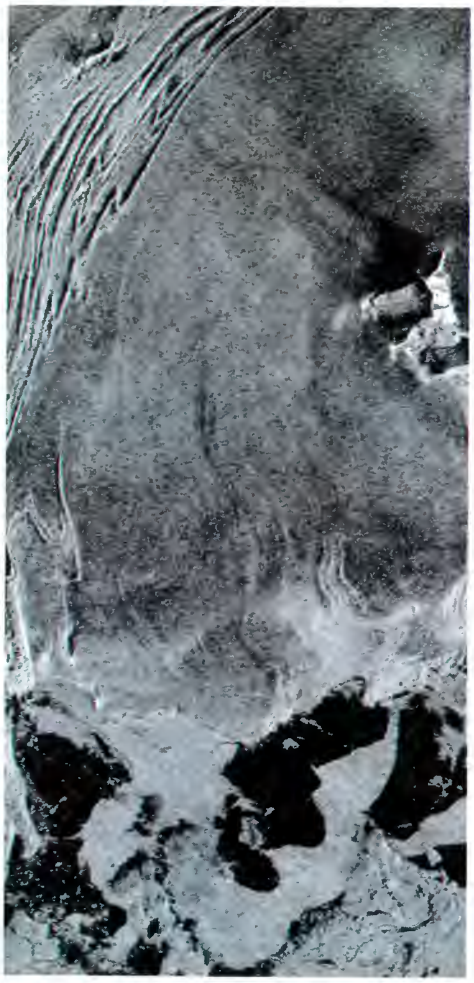

a

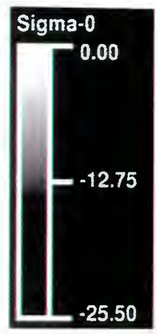

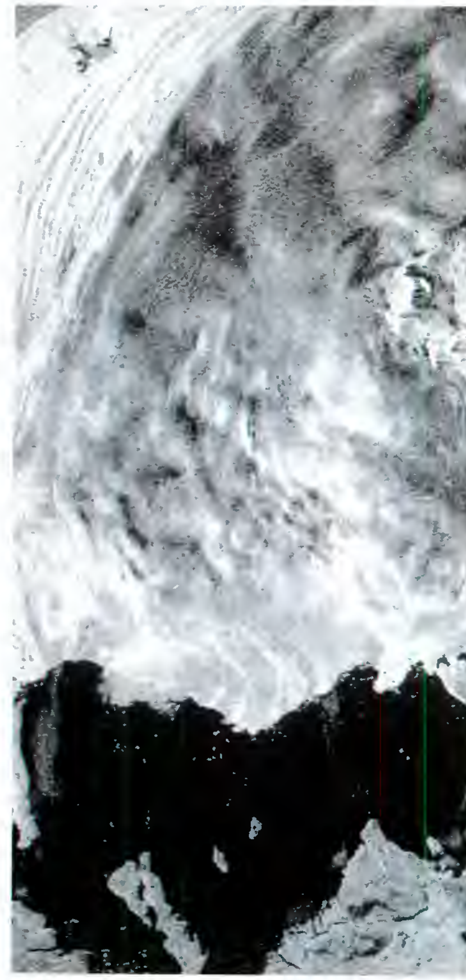

b

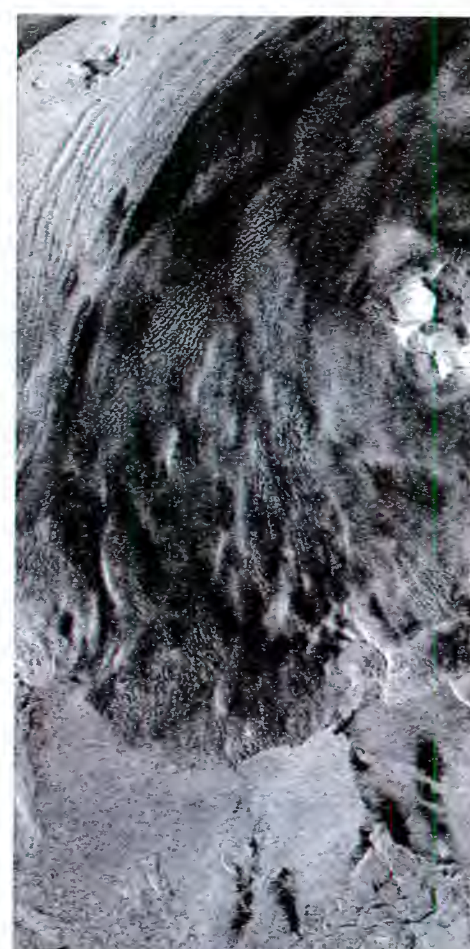

c

Figure 5.14 a,b,c. A set of ERS-1 SAR images are being used to construct a time lapse film showing the onset and propagation of a surge in the lower Bering Glacier. Three of the images used are shown here. The image recorded on 22 November 1992 (Fig. a) was acquired well before the surge began. The surface of the glacier is smooth. Subsequent ERS-1 SAR acquisitions (not shown here) indicate the surge onset occurred between late March and late April 1993. Figure b recorded on 9 August 1993 shows the propagating surge front about one month before it reached the terminus. The surge front is the somewhat diffuse boundary between the area of 'hummocky ice' in the centre of the scene, and the smooth ice closer to the black water of Vitus Lake. The glacier surface is now undulating which is characteristic of the fast flowing ice. Many crevasse fields are visible. The image recorded on 18 October 1993 (Fig. c) was acquired about one month after the surge front reached the terminus. The terminus has advanced visibly. Vitus Lake is now completely covered by icebergs and floating brash, resulting from the transition to chaotic calving caused by the arrival of the surge front at the terminus. The crevasse fields have evolved and expanded. Courtesy of J Roush, C Lingle, R Guritz, University of Alaska, Fairbanks, USA.

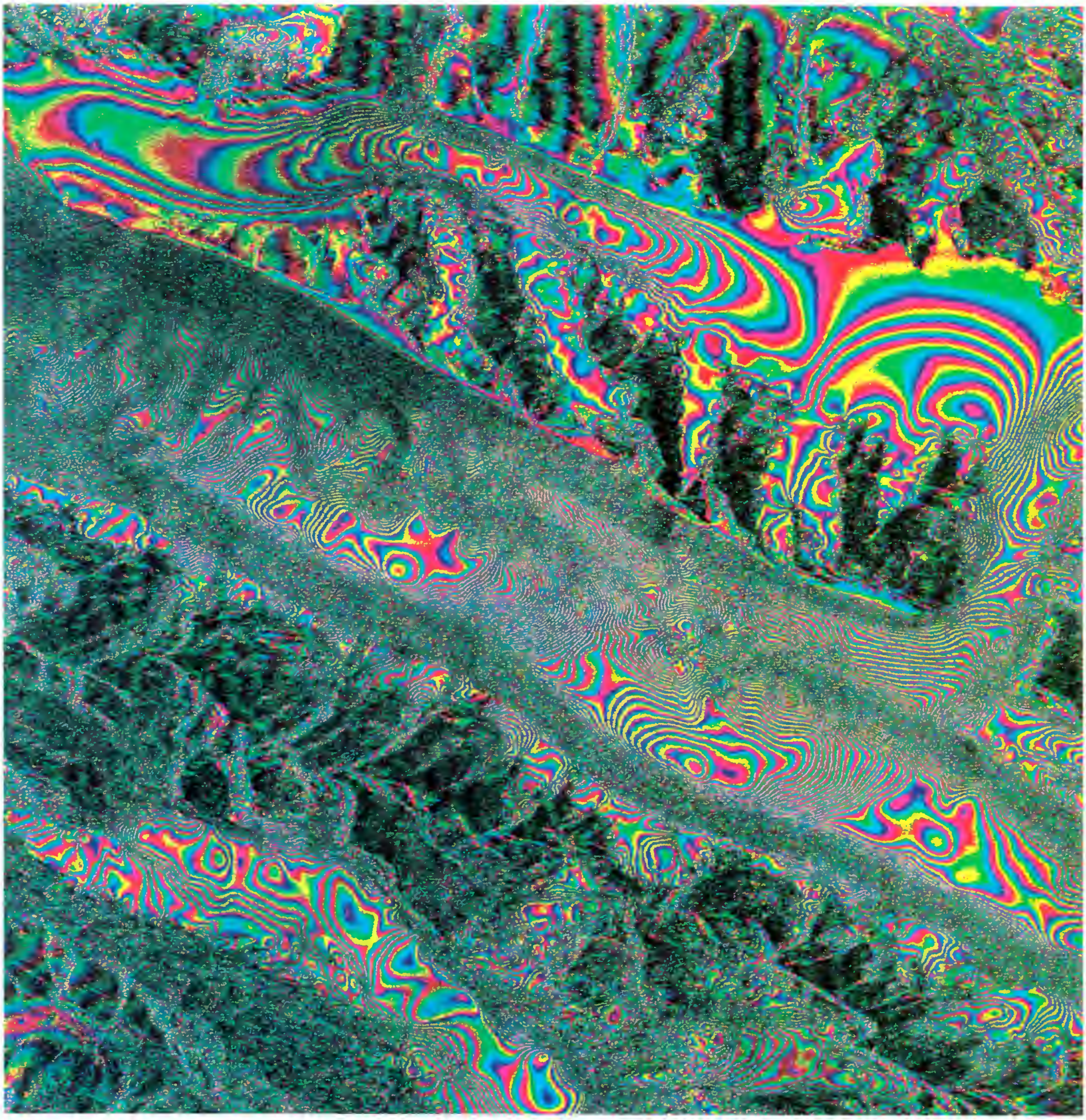

Figure 5.15. This interferogram of Bagley Icefield, Alaska, was derived from ERS-1 SAR images acquired on 7 and 10 February 1994 during the surge of the Bering Glacier (see Fig. 5.14). Bagley Icefield is the main source field for the Bering Glacier. It is the broad linear feature extending from lower right to upper left with a width of about 10 km. The direction of flow is from right to left. (North is to the upper right corner). The Bering Glacier which descends south-west towards the coast is 'out of view' to the left. By comparing this interferogram with one acquired prior to the onset of the glacier surge, it has been shown that the surge propagated up-glacier into the accumulation area as well as down-glacier to the terminus. The surface velocity was calculated from the interferogram and found to be similar to that measured independently using the Global Positioning System during a visit to the area in late July 1994. Courtesy of D Fatland, C Lingle, University of Alaska, Fairbanks, USA.

5.4. Snow cover

Seasonal snow cover responds rapidly to changes in the air temperature and is thus a good indicator of local climatic conditions. Snow is also a vital water resource in many regions of the world and measuring its water content and predicting the expected run-off rate can provide major inputs for hydrology, the management of water resources and hydro-electric power schemes.

The presence of snow on the ground has a significant influence on the radiative balance of the Earth surface and on the heat exchange between the surface and the atmosphere. The positive feedback mechanism between snow extent and atmospheric temperature (increased snow extent leads to reduced temperature which causes a further increase of the snow areas) tends to amplify climatic anomalies. Representation of the snow cover in present climate models is not satisfactory, because the models do not yet account for the feedback mechanisms between the global snow cover and the atmosphere.

Existing passive microwave satellite instruments are sensitive to dry snow, but not to wet snow and have a spatial resolution in the order of tens of kilometres. Dry snow is almost transparent to the ERS-1 SAR, but melting snow causes a reduction in the backscatter coefficient and can thus be clearly identified. A method has been developed for automatic mapping of melting snow, based on multitemporal ERS-1 SAR imagery. The method has been successfully applied even in steep mountain areas. SAR-derived snow cover maps are an excellent basis for climatological studies of snow cover depletion and for hydrological research at regional scales.

SNOW COVER STUDIES

a

b

c

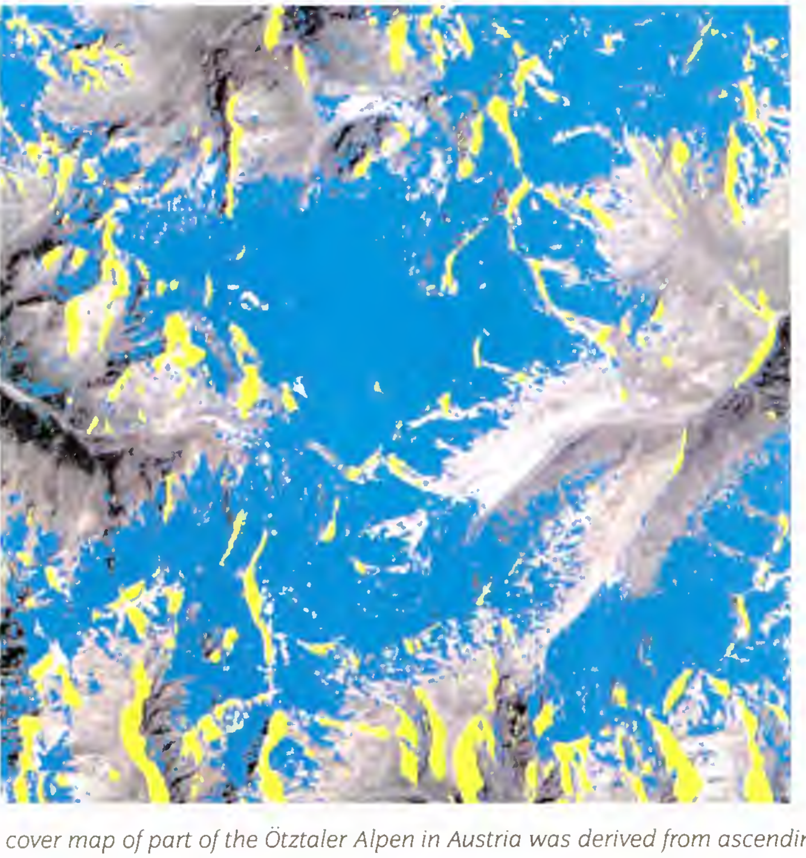

Figure 5.16 a,b,c. This snow cover map of part of the Ötztaler Alpen in Austria was derived from ascending (Fig. a) and descending (Fig. b) passes of ERS-1 SAR on 6 July 1992 (Fig. c). The different viewing angles arise because the satellite passes the area in both a northerly and southerly direction and the ERS-1 SAR views to the right of the satellite, thus giving two opposite views of the same area. The area shown (15 × 15 km) contains altitudes from 2000 to 3700 m above sea level and is partly covered by glaciers. The snow cover is in blue, areas with no information (due to very high slope angles) in yellow and the snow-free areas are shown in various shades of grey.

In the ice-free areas patchy snow cover was observed above 2900 m. The main parts of the glaciers were covered by snow. Glacier ice was exposed on the lowest parts of the tongues of the large glaciers, as evident on the elongated tongue of Hintereisferner at the centre of the image. This example demonstrates the great potential of ERS-1 SAR for snow mapping during the melt period as well as for mapping the snowline on glaciers. Courtesy of H Rott, University of Innsbruck, Austria.

6. LAND

ERS-1 was originally intended to focus on ocean and ice applications. However, land surface observations are being used in a diverse range of scientific applications. The main characteristics being mapped are:

- Global vegetation and crops;
- Forestry;
- Hydrology;
- Surface geology and geomorphology;
- Cartography.

Global vegetation, crop and forest cover plays a major role in the climate system as well as being of economic significance. Many vegetation types are highly sensitive to changes in their local climatic conditions and ERS-1 scatterometer and SAR data are being investigated as reliable and regular sources of information on vegetation, at global and more regional scales respectively.

There are important applications in the hydrological sciences. ERS-1 SAR data have produced valuable information on the extent of major flood events. It is also possible to monitor near surface soil moisture levels under certain conditions using the SAR. These hydrological capabilities allow spatial verification of distributed hydrological models, something which has hitherto been constrained by a lack of observations.

The study of geology provides information on the history of the Earth. ERS-1 SAR can contribute to the more accurate determination of surface landforms, and can also detect very small relative movements using interferometry.

The main benefits of the ERS-1 SAR and scatterometer are all-weather image acquisition, accurate data calibration and a sensitivity to surface roughness and moisture conditions. The timing of data acquisition and multi-temporal imaging are important in the context of many scientific studies of the land surface. In contrast with optical imaging, where it is more difficult to correct for atmospheric effects, ERS-1 provides stable calibrated measurements of the land surface, enabling accurate comparison of measurements in time and space.

Interpretation of ERS-1 data over the land surface is new and complex. Research continues to highlight new areas of potential. However, although the science base has to be extended and developed further, the results for land applications generally have a direct economic impact or an impact on the quality of life.

6.1. Global vegetation and crops

ERS-1 is enabling the status of vegetation to be monitored globally without constraints imposed by cloud cover. As a result, data from ERS-1 is contributing to research developments in areas from climatology to agricultural research. Changes in the volume of vegetative material, or biomass, are being used to identify trends in regional climate.

A number of scientific investigations have demonstrated the ability of ERS-1 sensors to distinguish different crop types. This provides a basis for monitoring crop growth and crop area. In addition to policy implementation, such monitoring can also allow variations in productivity to be identified and related to possible causes.

Agricultural monitoring requires reliable and frequent imaging of crop area and conditions through the crop growing season. All-weather data acquisition by the ERS-1 SAR satisfies a basic requirement for reliably timed and frequent imaging which cannot be guaranteed by optical systems because of the cloud cover problems. In addition ERS-1 scatterometer data are now also being used to monitor drought and crop development over large areas. This is of particular value as in most areas of the world, the main growing period coincides with the cloudy season. This will provide benefits to the humid tropics and many temperate parts of the world.

Although research is still at an early stage, some preliminary results are given below for:

- The generation of global vegetation maps;
- Crop monitoring and area estimation.

There is still much work needed to establish the fundamental relationships between radar backscatter and agricultural features, and how these data can be used.

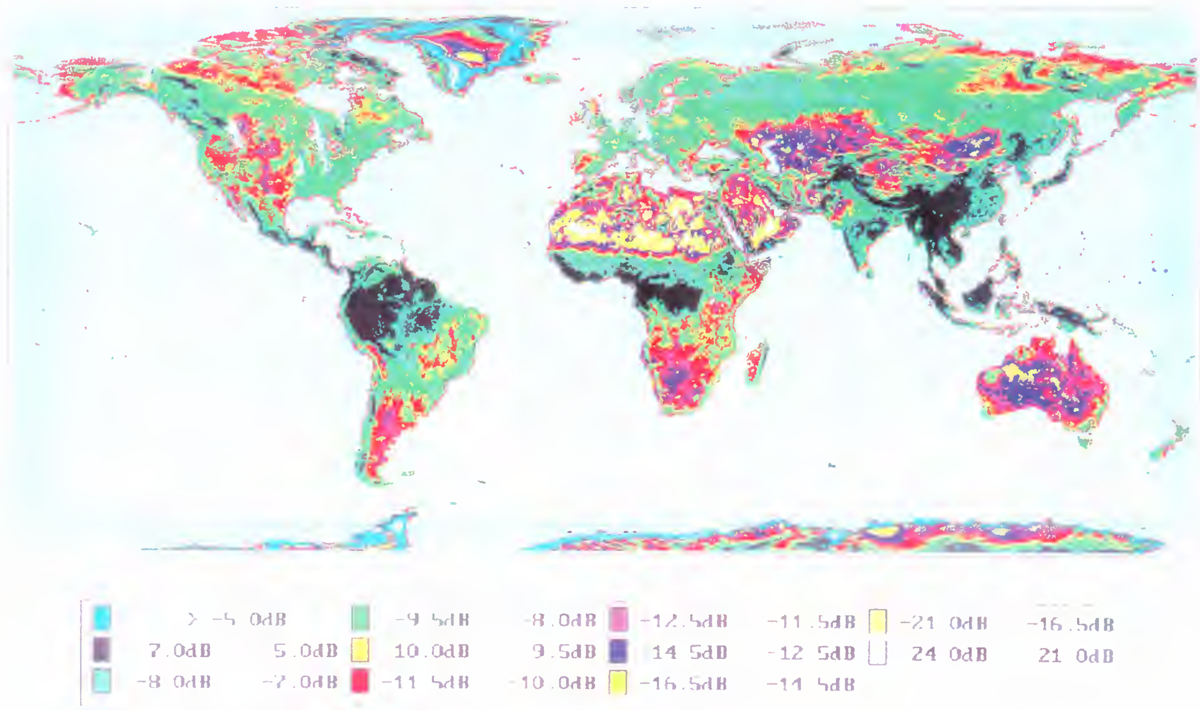

a

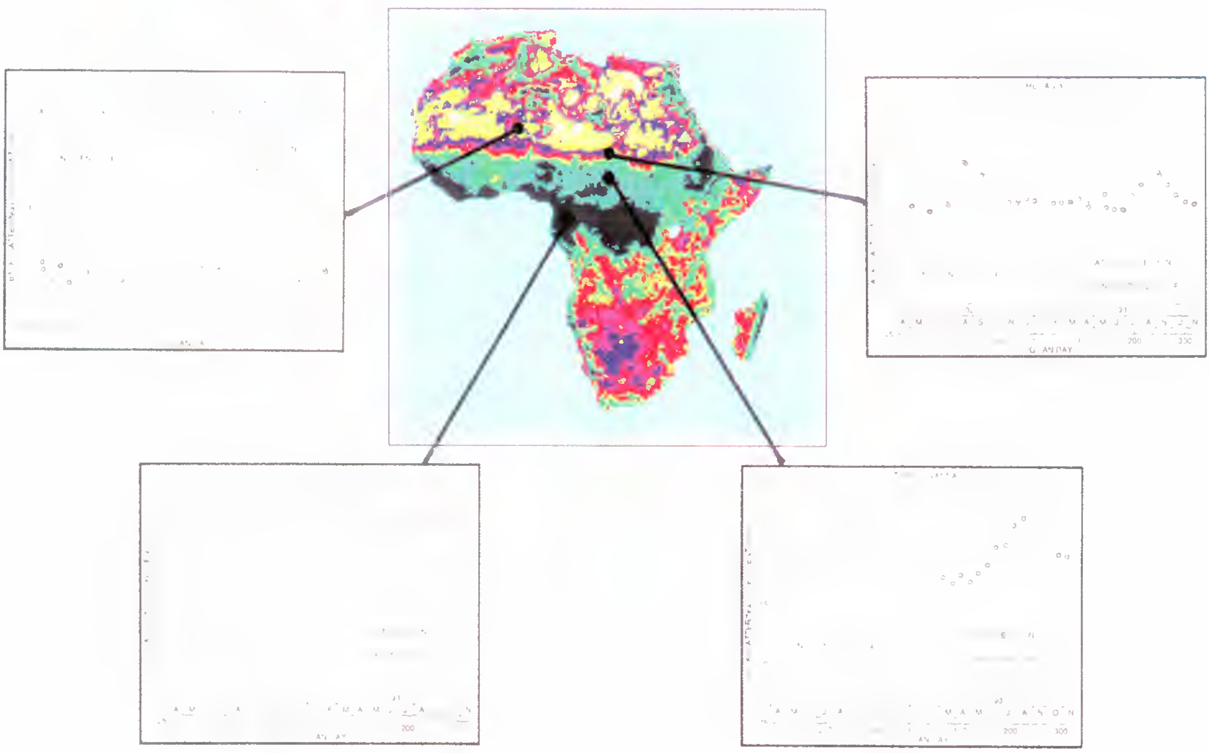

b

Figure 6.1 a,b. Global databases are being produced from ERS-1 scatterometer data with information on vegetation type, standing biomass and active vegetation. These can be used in models of the vegetation cycle, water exchanges and net primary production. The main vegetation types and morphological units (tropical rain forests in the intertropical belt, savannah, deserts, mountain ranges, tundra) can be identified from the map derived from data collected in August 1993 (Fig. a). More detail can be observed in the close up of Africa (Fig. b) where the tropical forests of the Congo basin and Guinean forests (coloured in black), sparse forests and tree savannahs (in green), Sahel (in magenta), and deserts (Sahara and Kalahari) can be easily discriminated.

Within the Sahara, strong variations in tone can be observed which depict the topography. The temporal variations in backscatter through the period from April 1992 to November 1993 are shown for four of the major vegetation types. For example the vegetation growth period in the Sahelian savannah is clearly discernible and from this the length of the rainy season can be monitored accurately. Courtesy of E Mougin, P Frison, CESR, Toulouse; Y Kerr, LERTS/CESBIO, Toulouse, France.

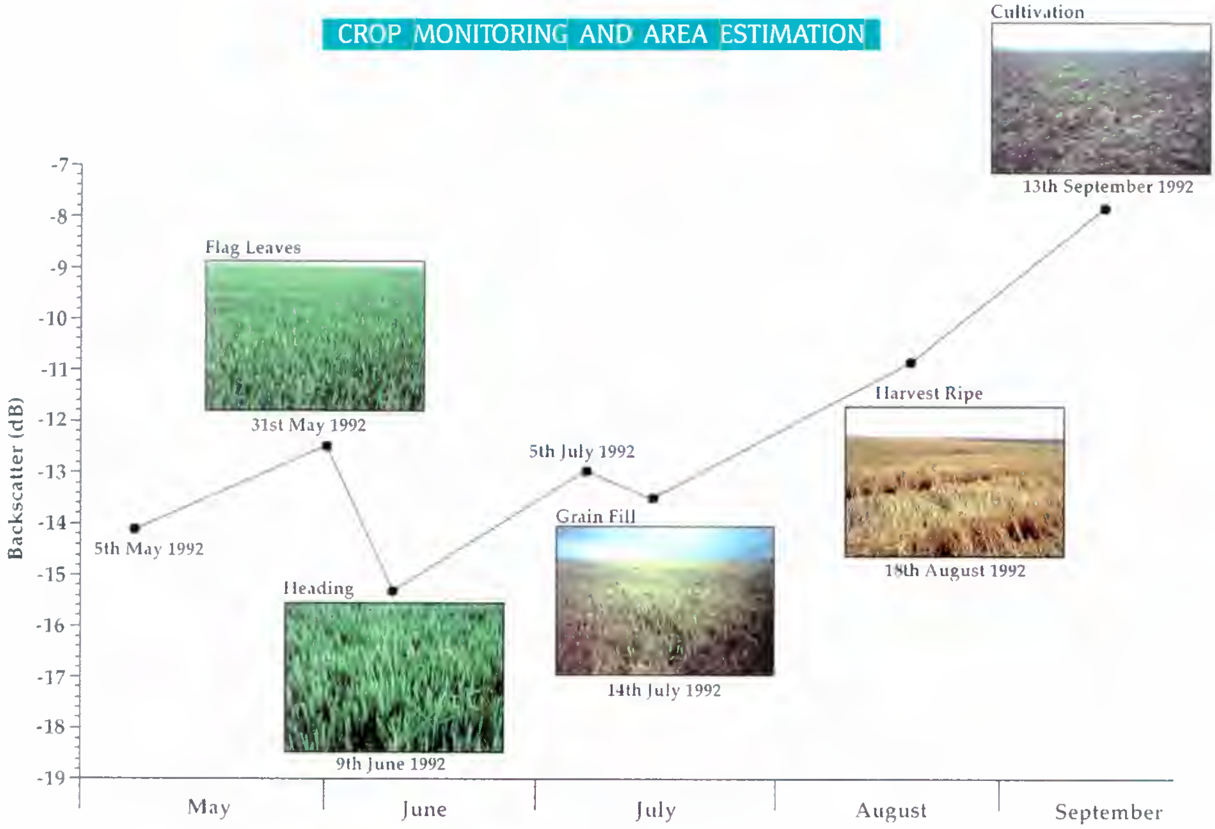

Figure 6.2. The temporal behaviour of agricultural crops over two crop growing seasons has been analysed in eastern England. This has demonstrated the potential of multi-date ERS-1 SAR data for crop discrimination and mapping. The key to successful crop discrimination is the careful selection of a temporal series of SAR images to exploit the fact that crops have different growth cycles throughout which their appearance on radar images follows a particular temporal sequence. In the early part of the year, crop canopies are well established, while bare soil conditions exist in fields where other crops are in the process of being sown. Later in the growing season, differences in the timing of harvest for particular crops may also result in large contrasts in the backscatter between differently cropped fields. Analysis of the temporal changes in crop backscatter has shown that many crops are characterised by unique temporal profiles, and this can be exploited for classification purposes. This Figure shows the change in the appearance of a wheat crop through the crop season and the associated changes in ERS-1 SAR backscatter. Courtesy of M Wooding, Remote Sensing Applications Consultants, Alton, UK.

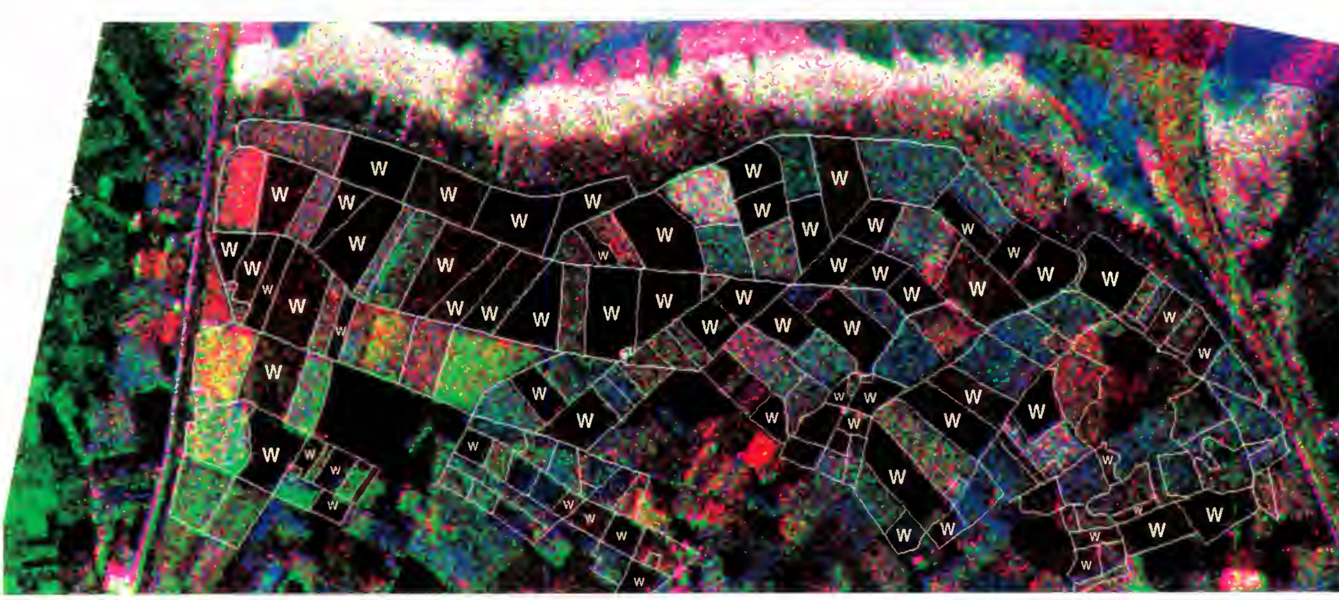

Figure 6.3. The area of wheat grown in a study area around the Wash in eastern England has been mapped using a multi-temporal ERS-1 SAR colour composite. The three dates used were 25 May (red), 13 June (green), and 29 June 1993 (blue). This Figure shows field boundaries with the location of winter wheat fields (W). Winter wheat appears very dark on the image in contrast with the brighter blue and green colours associated with other crops such as sugar beet and potatoes. The area planted under wheat can be estimated from this. Courtesy of M Wooding, Remote Sensing Applications Consultants, Alton, UK.

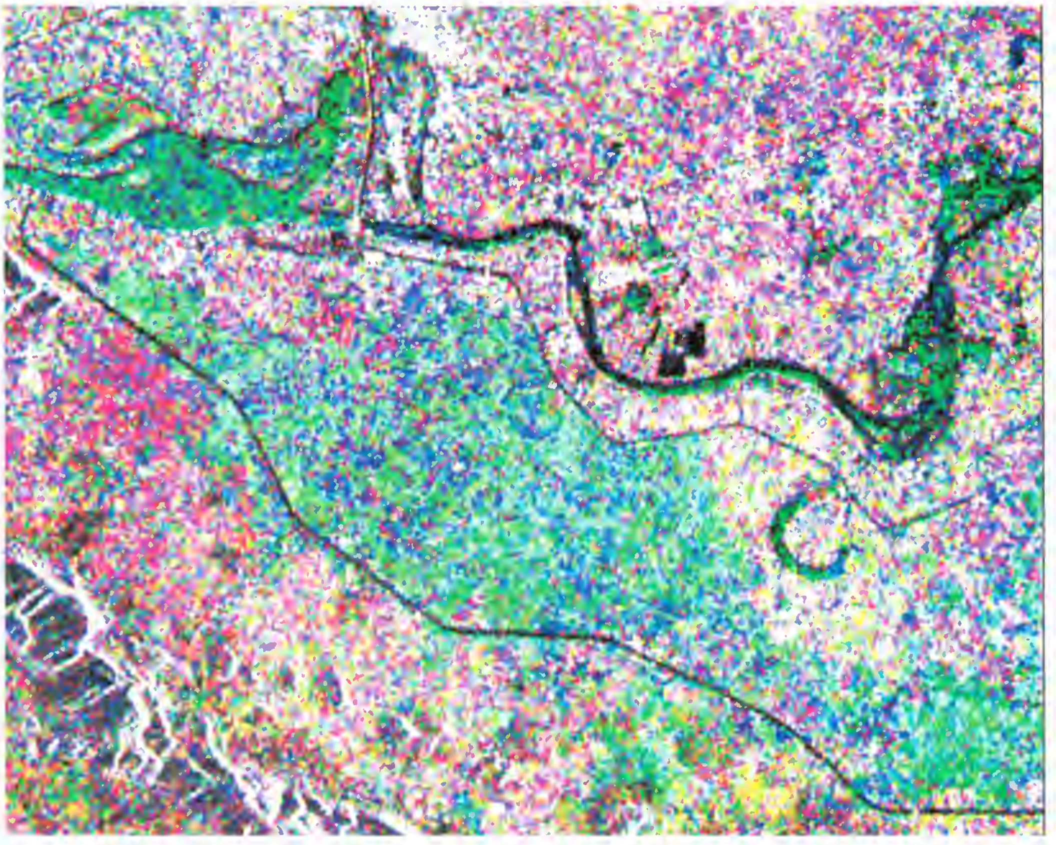

a

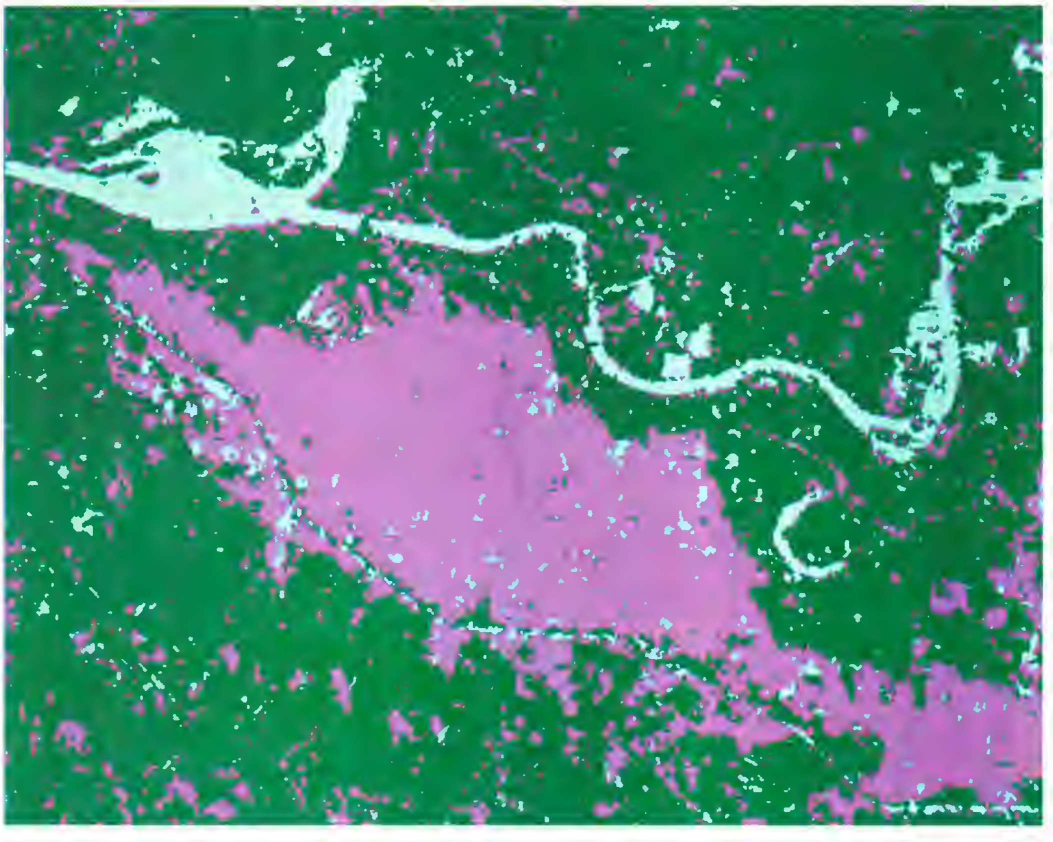

b

Figure 6.4 a,b. Rice crops are being monitored with ERS-1 SAR data in Thailand making use of the plant's characteristic growing pattern. During the planting and early growth stage rice fields are flooded. Later during the maturity phase water is drained from the fields and plants become dry and turn yellow. After harvest the soil remains bare. The full cycle from planting to harvest lasts between 120-180 days depending on the crop variety. Figure a shows a multitemporal ERS-1 SAR image recorded on 6 June (red), 29 October (green) and 3 December 1993 (blue), from the province of Kanchanaburi, western Thailand. The rice fields appear in green/blue colours and are reasonably well separated from other land use classes (sugar cane, maize, bush-fallow, shrubs, water, urban areas). A rice map has been produced from this and is shown in Figure b. The rice is shown in magenta, the water in blue and other land use classes are displayed as dark green. Courtesy of J Aschbacher, Joint Research Centre, Ispra, Italy.

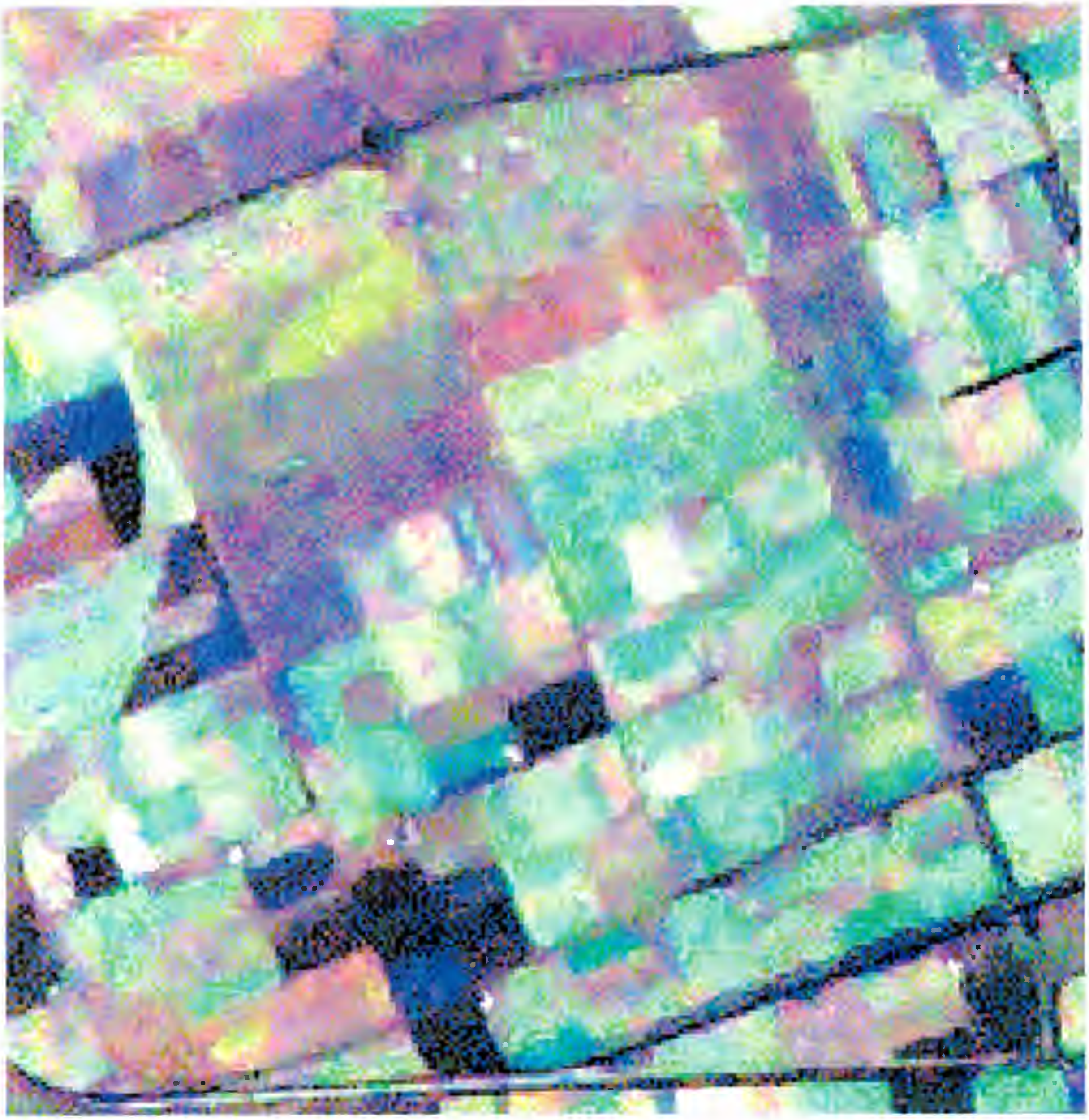

a

Figure 6.5 a,b. Figure a shows multitemporal ERS-1 SAR imagery acquired during the autumn: 19 October (red), 18 November (green) and 6 December 1991 (blue). These have been incorporated in a land-use assessment and monitoring scheme for agricultural areas. Transitions in soil roughness which are measured by the ERS-1 SAR are used to delineate land preparation activities which relate to cropping practices in the next growing season. The classified autumn imagery (Fig. b) is used to identify various future crop types by their typical tilths in the autumn, such as grass, winter wheat, sugar beet and potato. This approach can lead to a significant improvement of early season crop areal estimates, especially when used in combination with classification results from the preceding growing season, a priori information on meteorological conditions and crop rotation practices, and additional SAR and optical remote sensing data from the spring season. Courtesy of G Lemoine, J Bakker, Synoptics, Wageningen; H van Leeuwen, Wageningen Agricultural University, The Netherlands.

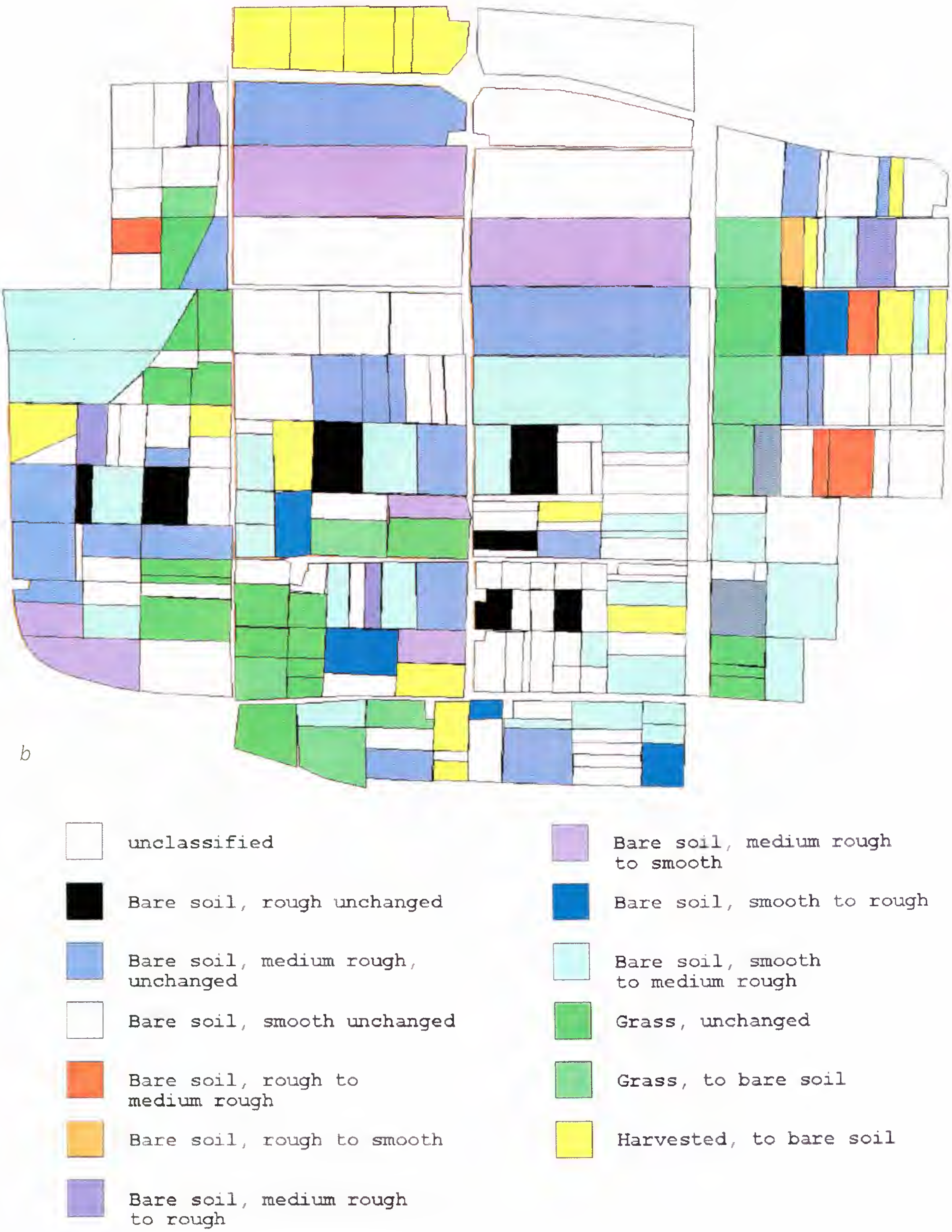
unclassified
Bare soil, rough unchanged
Bare soil, medium rough, unchanged
Bare soil, smooth unchanged
Bare soil, rough to medium rough
Bare soil, rough to smooth
Bare soil, medium rough to rough
Bare soil, medium rough to smooth
Bare soil, smooth to rough
Bare soil, smooth to medium rough
Grass, unchanged
Grass, to bare soil
Harvested, to bare soil

b

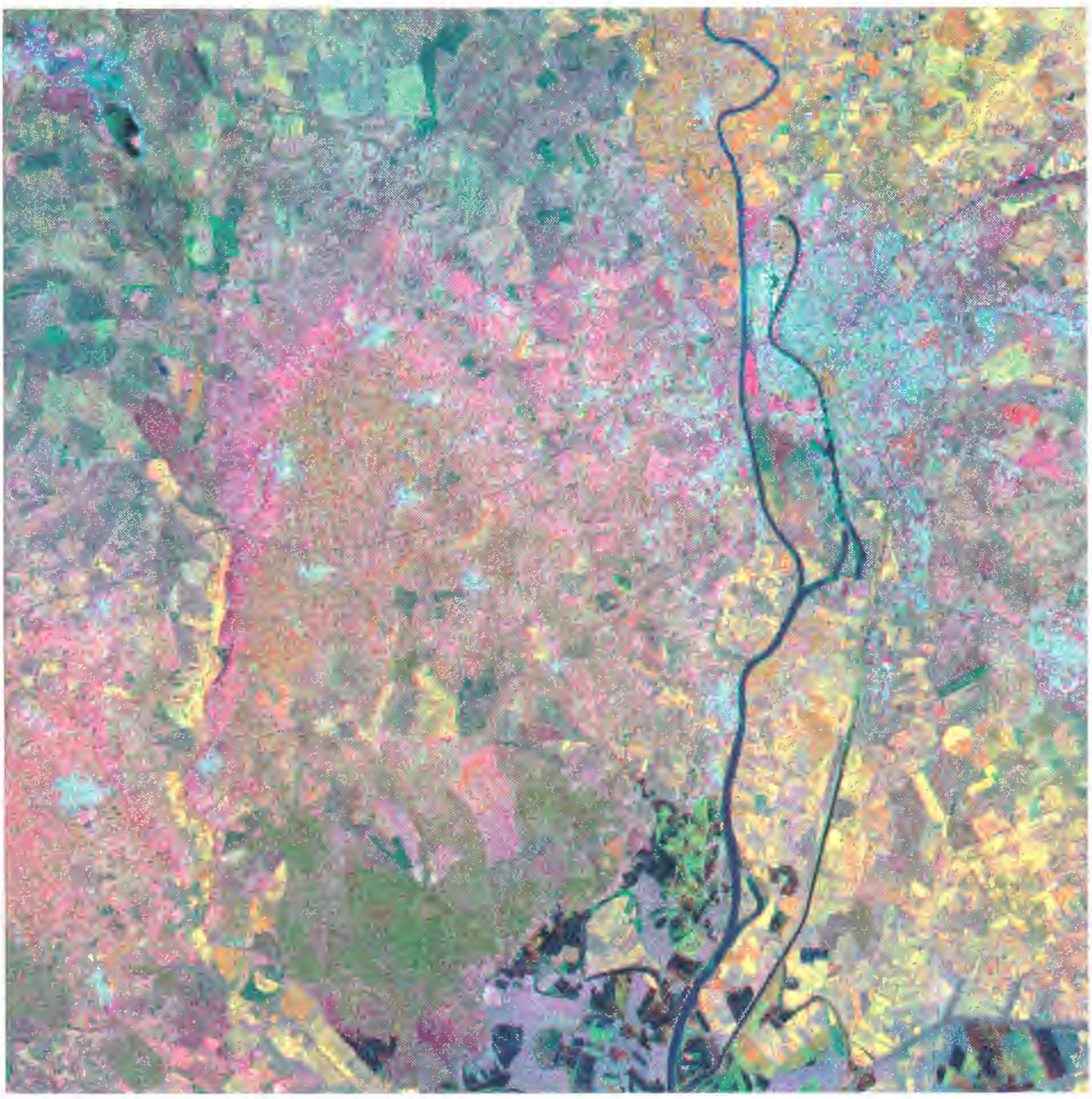

Figure 6.6. Optical satellite data are being used to estimate crop production using sample areas distributed across Europe. However, cloud cover problems mean that data are seldom available early in the growing season and there are often gaps within the optical dataset later in the season. ERS-1 SAR data can be used to help overcome this problem and also to provide information which supplements that available from the optical images. This Figure shows a test site in Seville, Spain. It is a composite of ERS-1 SAR and Spot HRV (French optical sensor) data for 1 July 1992 and aims to develop the synergy between the two datasets. Courtesy of J Harms, Scot Conseil, Ramonville, France.

6.2. Forestry

Tropical forests are today in the forefront of environmental considerations because of their important role in the global carbon cycle. A number of research programmes are in progress to evaluate the potential role of SAR data in monitoring deforestation. It is the capability of radar to obtain images through cloud cover which makes it such an attractive tool for monitoring tropical forests.

In higher latitudes, changes in forest management are leading to new patterns of deforestation and re-growth and there is an increase in the number of forest fires and diseased trees. Thus not only is the overall level of forest cover important, but also the distribution of this cover.

In the tundra, the ERS-1 scatterometer can give very accurate dates for the freeze and thaw periods, and when used with passive microwave sensors, it enables permafrost areas to be delineated. This capability is closely linked to the monitoring of the boreal forests.

There are thus two overlapping areas of research in forestry to which ERS-1 data can contribute:

- Monitoring forest change;
- Assessing the role of forests in the carbon cycle.

MONITORING FOREST CHANGE

Figure 6.7. This ERS-1 SAR image of the area to the northwest of Rio Branco in the State of Acre, Brazil shows forest clearance for cattle ranching in an area of primary rain forest. The rain forest is bright, clearings are generally dark, but differences from one pasture to another can be related to differing amounts of weed and bush growth, with the more overgrown pastures appearing brighter on the images. Courtesy of M Wooding, Remote Sensing Applications Consultants, Alton, UK.

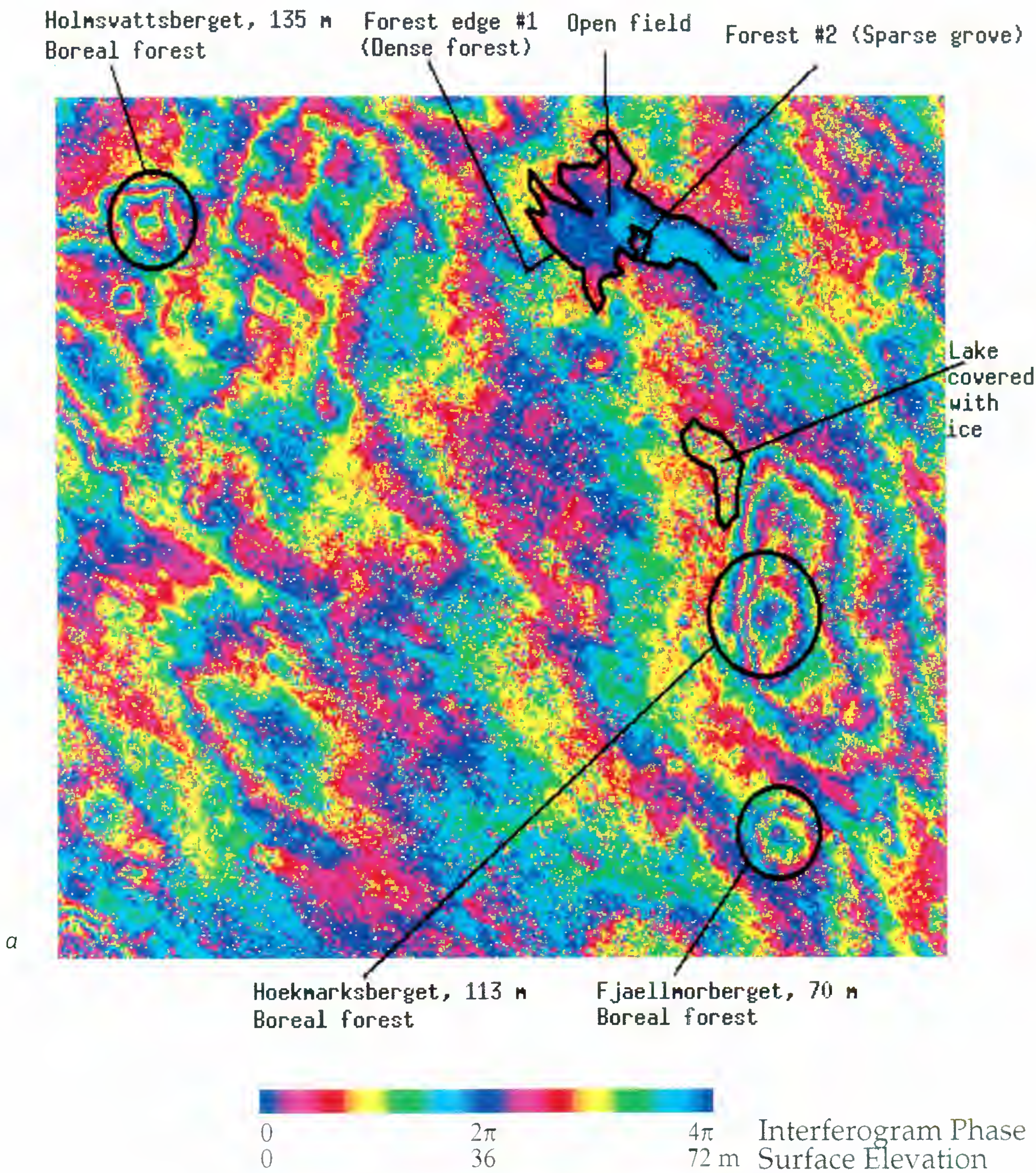

Figure 6.8 a,b. Interferograms have been successfully produced based on repeat track ERS-1 SAR images over the boreal forests in northern Sweden. In some cases it has been possible to map digital elevation models or slope maps of forested areas. This method may also be used to map clear cuts and to measure the effective tree height in combination with another digital elevation model. Bole volume or forest biomass might also be possible to determine since the interferogram tree height is mainly determined by the height and density of the trees. Seven ERS-1 SAR images acquired during February and March 1992 were used to produce the interferogram in Figure a. This test site of 8×8 km at Hökmark in northern Sweden (Fig. b shows the location and land type of the study) is mainly covered by boreal forests but there are open fields, bogs, ice-covered lakes and some small areas of birch. Tree height estimated from the interferogram has been compared with tree heights measured on the ground in two areas. In forest No. 1 the estimated height was 14.9 ± 1.6 m compared to 15.9 m on the ground, and in forest No. 2 the estimated height was 4.6 ± 1.6 m compared to 9.9 m measured on the ground. This is an entirely unexpected area of ERS-1 science that is only now beginning to be explored. Courtesy of J Hagberg, L Ulander, J Askne, Chalmers University of Technology, Gothenberg, Sweden.

b

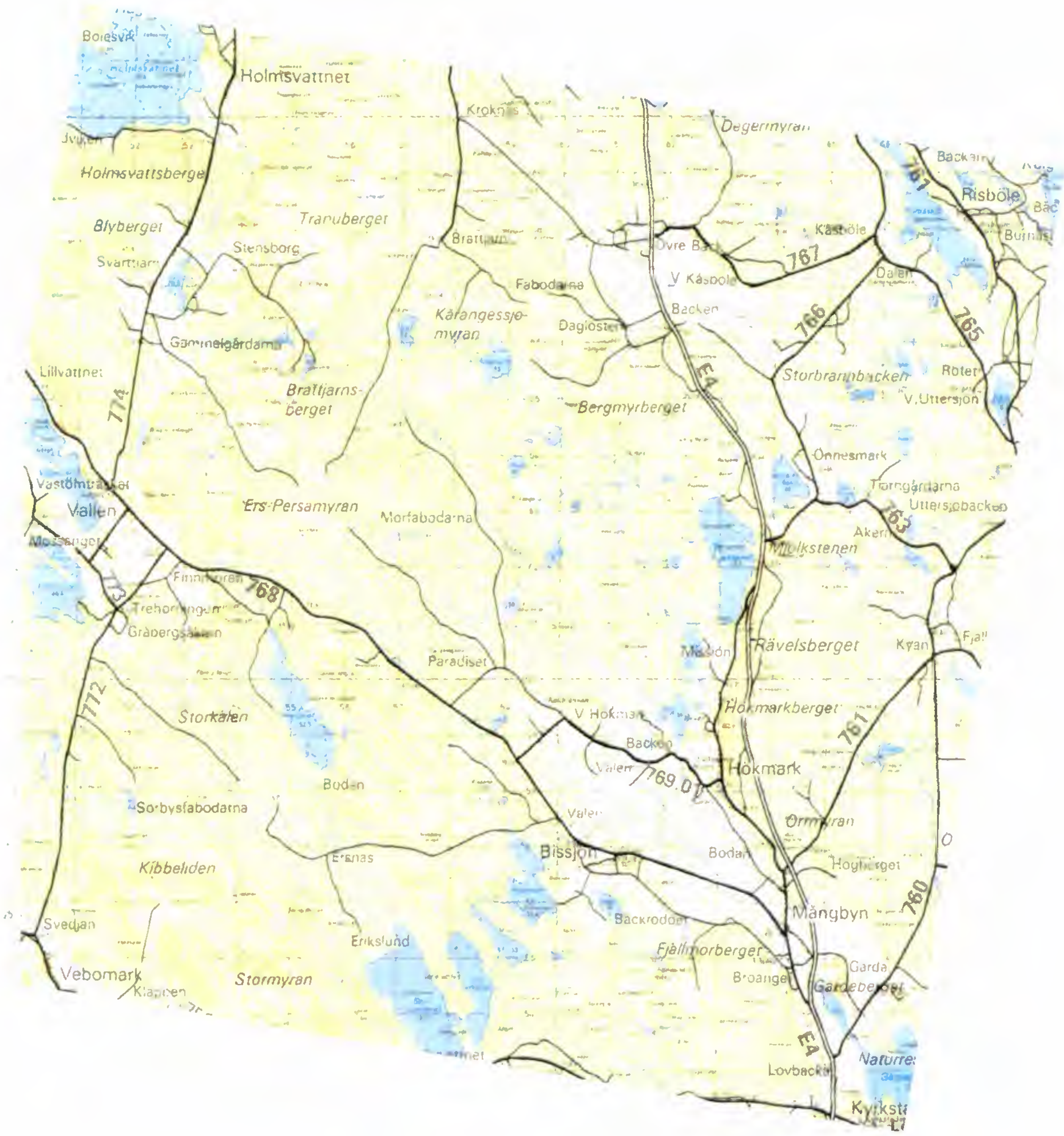

Holmsvattnet
Holmsvattsberget
Blyberget
Tranuberget
Stensborg
Brattarn
Fabodarna
Kårangessjö-
myran
Dagloster
Gammelgårdarna
Lillvattnet
Brattjärns-
berget
Bergmyrberget
Degermyran
Risböle
Kåsböle
Övre Bäck
V Kåsböle
Backen
Dalen
Storbrännbacken
V. Uttersjön
Önnesmark
Torngårdarna
Uttersjöbacken
Åkern
Mjölkstenen
Västomträsket
Vallen
Ers-Persamyran
Morfabodarna
Finnmyren
Trehörningen
Gråbergsåsen
Paradiset
Rävelsberget
Hökmarkberget
V Hökmark
Backen
Hökmark
Storkälen
Boden
Sörbysfabodarna
Kibbeliden
Ormmyran
Bissjön
Ersnäs
Boden
Högberget
Mångbyn
Backrödder
Svedjan
Eriksiund
Fjällmorberger
Broänget
Gårda
Vebomark
Klappen
Stormyran
Lövbacka
Kyrksta
Naturres
Kyan
774
772
768
767
766
765
763
761
760
769.01
E4

Figure 6.9. Many areas in the Amazon basin experience a rapid change in land use and, consequently, in land cover, as settlers move in. To plan and guide the development of the area towards a sustainable land use, planners and decision makers need up-to-date information on the rapidly changing land cover. ERS-1 SAR images have been studied for their use and were shown to provide relevant information for these areas where alternatives, because of the poor accessibility of the terrain and the persistent cloud cover, are hardly practical. This Figure shows a 50x70 km section of a multitemporal composite ERS-1 image. The observation dates are 26 May (blue), 4 August (green) and 22 December 1992 (red). It shows the town of San Jose del Guaviare at the southern bank of the river Guaviare, flood plain forests along the river, the Llanos savannah (dark tones) dissected by gallery forests north of the river, other savannahs (in several colours) and rock outcrops south of the river and patterns of deforestation in the Amazon forest extending (mainly) towards the south and east. Courtesy of D Hoekman, Wageningen Agricultural University; W Bijker, International Institute for Aerospace Survey and Earth Sciences, Enschede, The Netherlands.

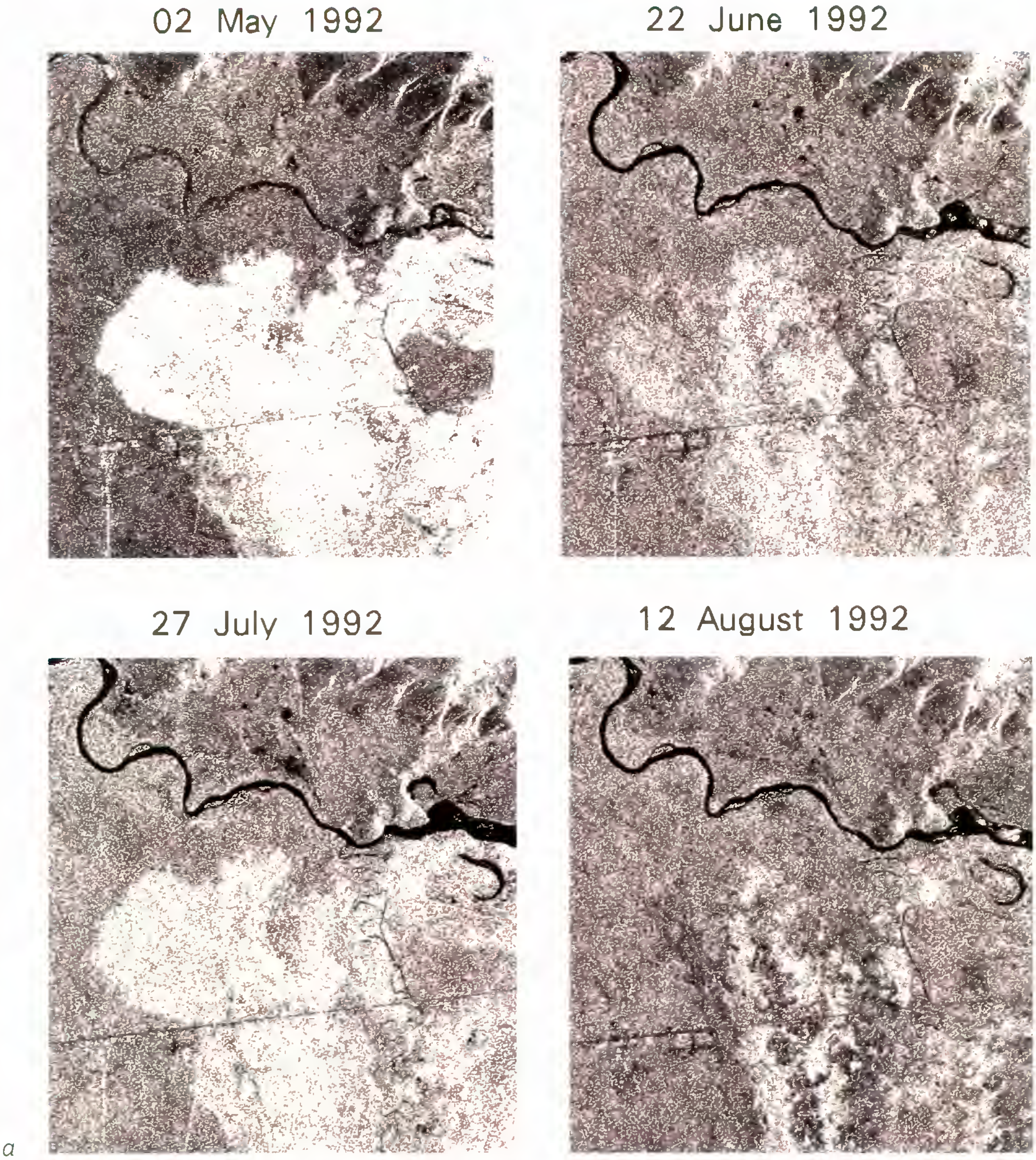

Figure 6.10 a,b. A forest fire began on 1 July 1990 near the Tok community in Alaska. This fire eventually covered 41 000 ha and was not finally extinguished until October. ERS-1 SAR data were used to assess the variability within the fire affected region. Figure a shows four images taken two years after the fire. The fire scar areas are brighter than the surrounding unburned forest as the fire resulted in the melting of the permafrost. Variations within the fire scar are caused by variations in the intensity of the fire, while variations between the images are caused by seasonal changes in the soil moisture. This information is useful in determining the amount of biomass consumed during a fire, the amount of carbon released into the atmosphere, and assessing the ecological evolution that is likely to follow the fire. The photographs of the study area (Fig. b: see next page) show the differences within burned areas. Courtesy of E Kasischke, Duke University, Durham; L Bourgez-Chavez, ERIM University of Michigan, Ann Arbor, USA.

b

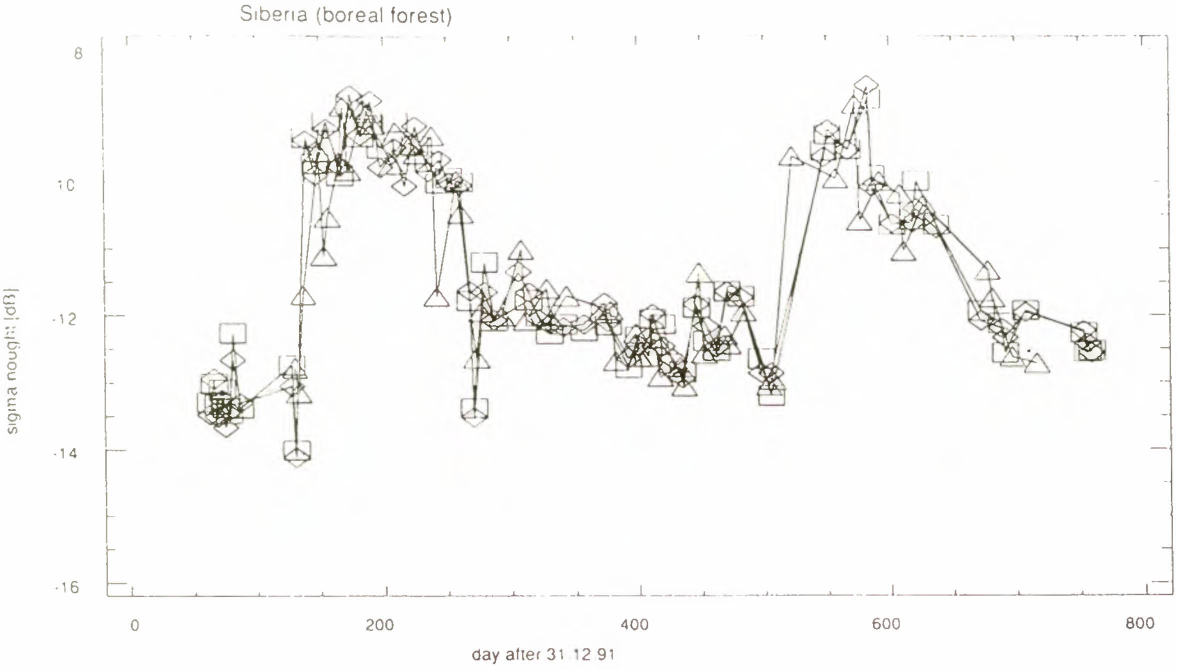

Figure 6.11. This temporal variation in backscatter has been measured with the ERS-1 scatterometer over a boreal forest in Siberia during 1992 and 1993. Three different periods can be seen. The time period is shown as days after 31 December 1991. The winter/spring period when the soil is frozen and covered with dry snow starts in December (day 350) and ends with very low values in June when the snow melts and becomes wet (days 165 and 520). Summer starts in early July once the snow has disappeared and the frozen soil starts thawing. This leads to a very high water content since water from thawing cannot percolate, giving way to a 'marshy' surface (days 190 and 550). Summer lasts only until the end of August (days 250 and 610). Autumn lasts until November during which time the soil dries and freezes (days 300 and 660). This permits monitoring of the vegetative period and of the freeze thaw cycles in areas of the world which were rarely accessible with optical systems due to cloud cover and poor solar illumination. The work is still at an early stage as this is an area of science that has developed only since the launch of ERS-1. Courtesy of C Matzler, A Wiesmann, University of Bern, Switzerland.

6.3. Hydrology

The ERS-1 SAR and scatterometer are sensitive to the moisture levels of the soil surface, and can also be used to detect the extent of open water surfaces.

An operational role for ERS-1 SAR in support of flood monitoring irrespective of cloud cover is emerging. It should also be stressed that the data are making valuable scientific contributions to the understanding of braiding patterns in large channels, such as in Bangladesh, and the modelling of flood inundation. Visualising the progress of floods using ERS-1 SAR imagery during the 3-day repeat phase helps to indicate how future floods might behave and to understand the processes leading to river bank erosion.

At a more regional scale, there is increasing potential for improving our understanding of catchment hydrology. Spatially distributed models of river catchments which aim to simulate the full physical processes in order to forecast are still largely in the research phase. Soil moisture and vegetation cover data from satellites can be used in such models both to specify the static parameters and to initialise the variables. Uncertainties remain regarding the representativeness of data at different scales. It is hoped that research will eventually lead to more routine initialisation of such models and possibly to routine operation. As part of this scientific development process, surface water and soil moisture data from ERS-1 SAR can be used to validate the spatial outputs of models.

For longer range weather forecasts, vegetation growth monitoring, net primary production and carbon dioxide flux assessment, climate monitoring and process studies, it is crucial to have access to information related to the surface/atmosphere interface. This information describes the status of surface characteristics such as temperature, net radiation, soil moisture, vegetation amount and status and surface water.

ERS-1 data are playing a role in three areas of hydrological research which are reported below:

- Use of surface water measurements to develop and test hydrologic models;
- Development of our understanding of wetland ecosystems;
- Estimation of surface fluxes from soil moisture measurements and vegetation status.

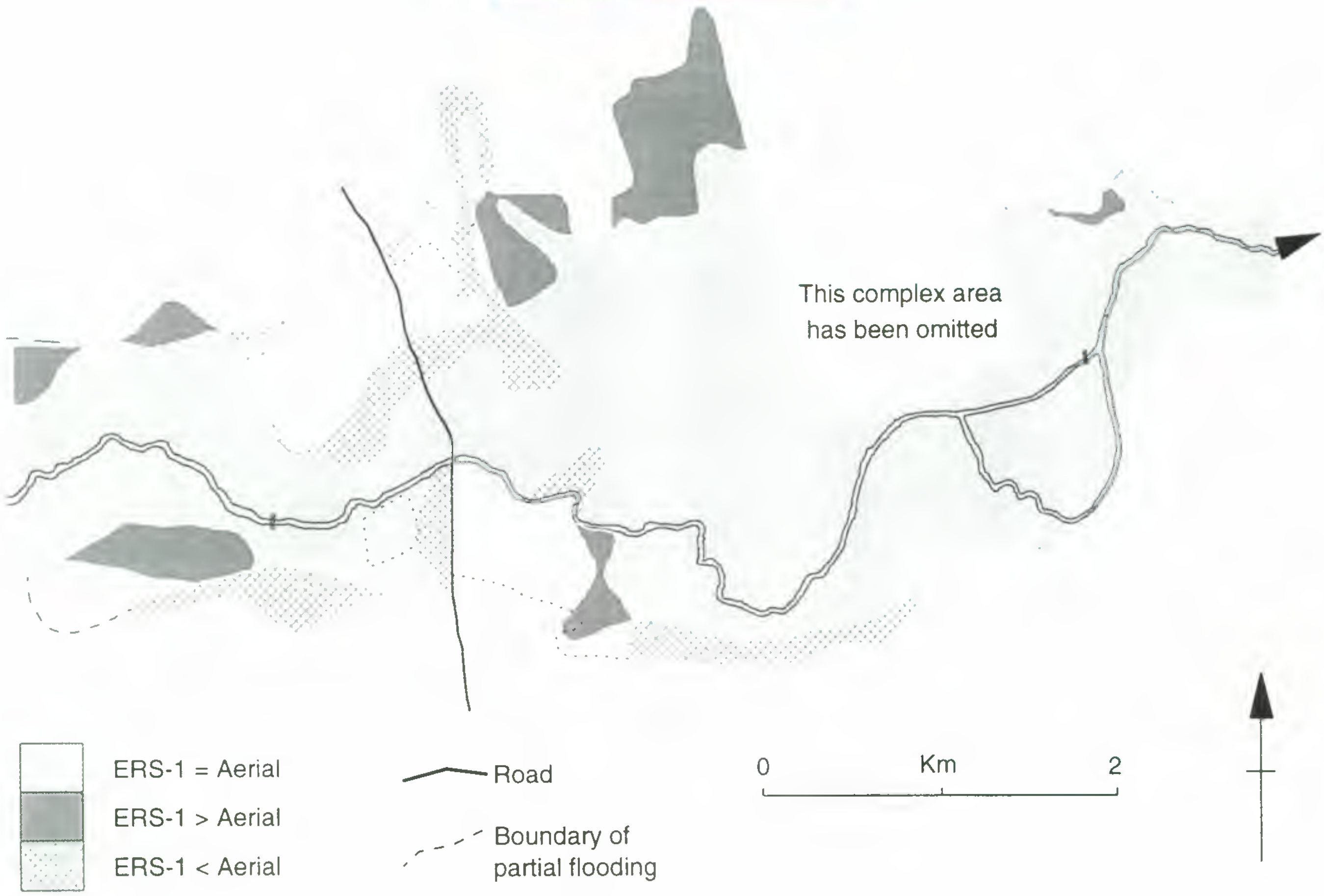

Figure 6.12. The extent of floodwater distribution along 400 km of the mainstream Thames and its tributaries in December 1992 was mapped during a period of overcast and low cloud and rainfall when data were not available from any other source. A time series of images allowed flood water to be separated from permanent water bodies. These results are hydrologically significant as they enable flooding within an entire river system to be observed in a single overview, thus allowing key areas controlling river flow to be pinpointed. This Figure compares the maps of flooded land produced from the ERS-1 data and from aerial photographs obtained from a light aircraft within two hours of the ERS-1 overpass, for an area to the west of Oxford. The main differences between the two data sources were found where flood water was very shallow and emerging vegetation was present. Courtesy of K Blyth, Institute of Hydrology, Wallingford, UK.

Figure 6.13. The 1993 pre-Christmas flooding of the Rhine, the Rhône, the Danube and smaller rivers in Europe was the worst for over 60 years. SAR images taken by ERS-1 provided an overview of the devastated areas. This Figure shows the area between the Petit Rhône and the Rhône and the extent of the flooded area on 15 January 1994, shortly after a broken dam had lead to the flood. Such information can also be used to measure volumetric soil moisture to determine whether the soil can still absorb water or whether it is saturated, so that the resulting run-off could cause flooding. Courtesy of ESA.

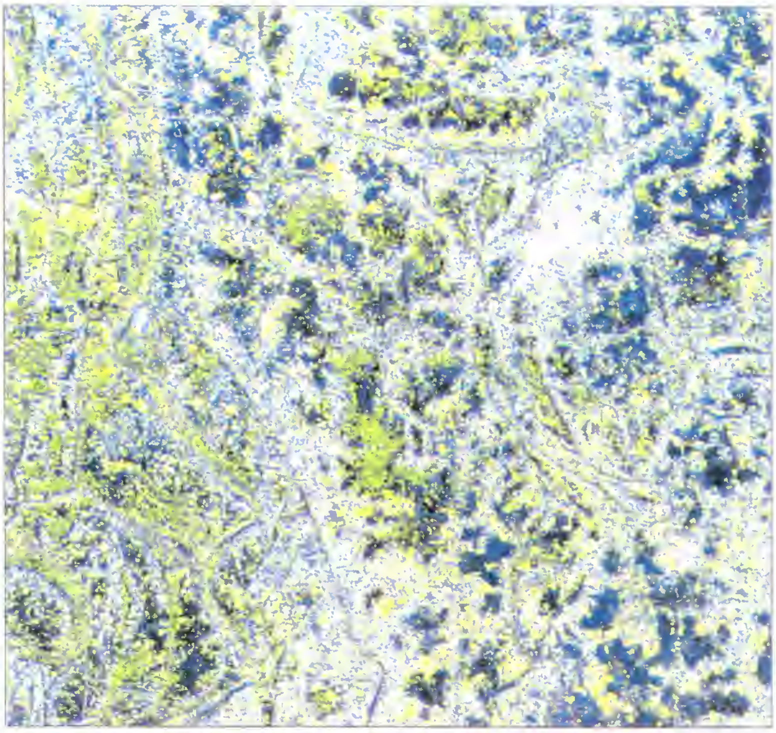

a

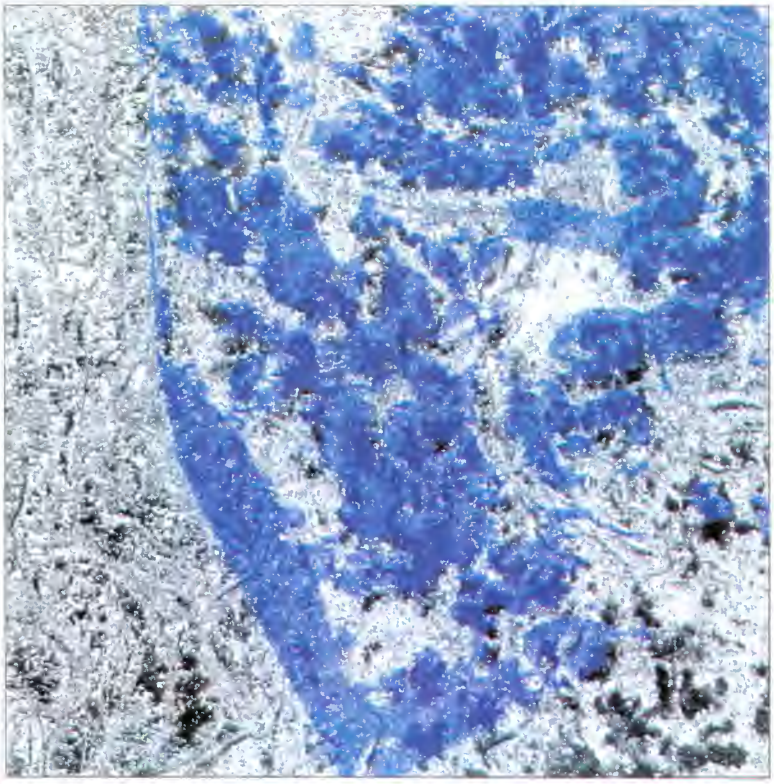

b

Figure 6.14 a,b. ERS-1 SAR imagery has been used as part of a programme to develop new techniques to support project planning and environmental monitoring in Bangladesh. ERS-1 SAR data are being used because optical data are rarely available due to high levels of cloud cover.

Figure a shows actual flooding of the area on 24 July 1993 (in blue) and additional areas flooded on 28 August 1993 (in yellow). A hydrological model was used to predict areas which would be flooded to a depth of 30 cm or more on 24 July 1993. Figure b shows these predictions. At the time the flood model was made, it was at an early stage of development and further studies were underway to increase understanding of the local hydrological system.

ERS-1 SAR data are particularly valuable in helping to validate hydrological models in the early stages of this type of investigation. The SAR data have also been used to monitor the braiding of the channel. Using the validations provided by the SAR data, the predictive capability of the model can be improved. Courtesy of T Chidley, ISPAN Flood Action Plan – GIS Component 19; Flood Plan Coordination Organisation, Bangladesh.

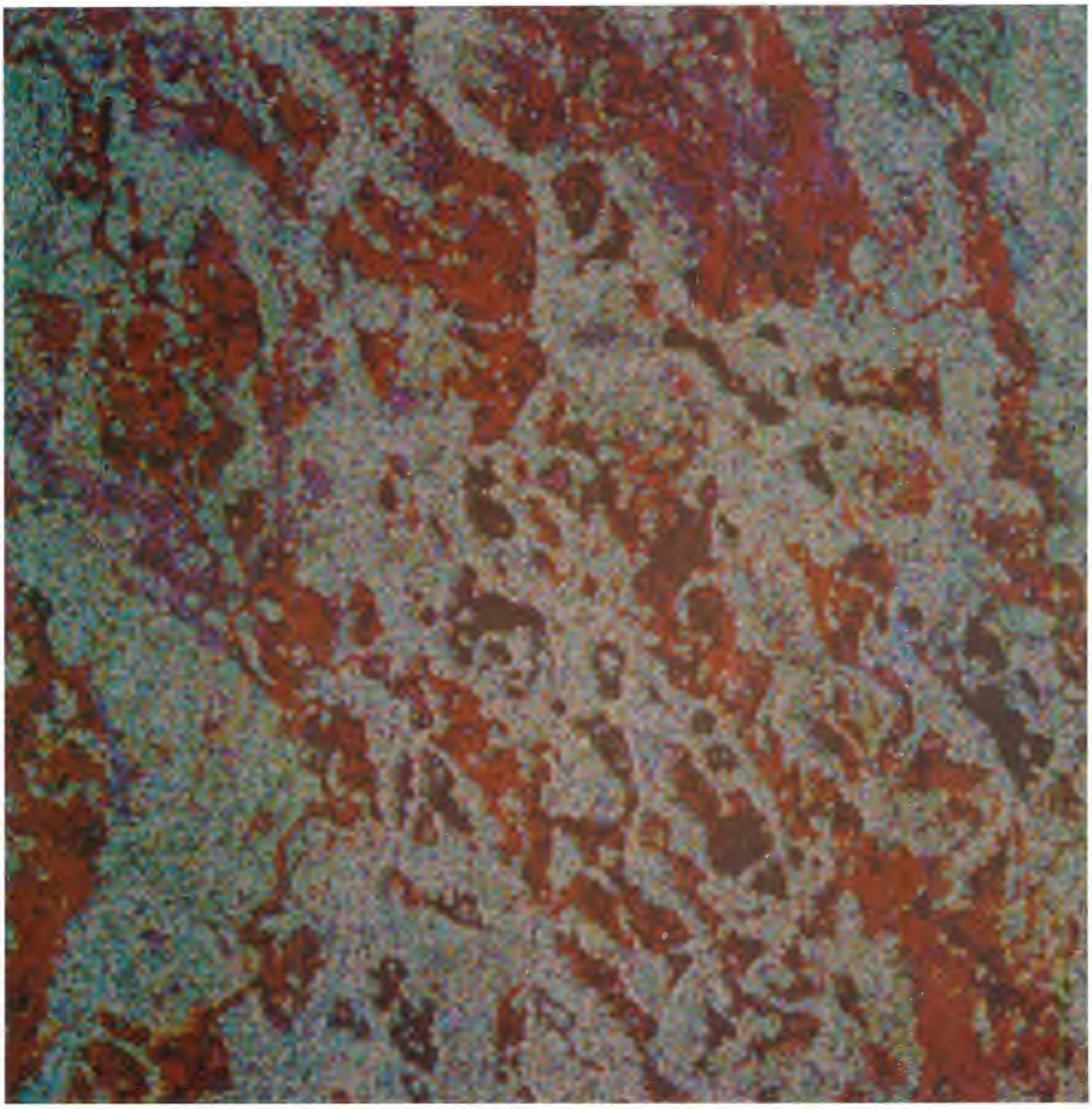

Figure 6.15. The dynamics of flooding in the Pantanal (Brazil), one of the largest wetland areas in the world is being studied with ERS-1 SAR data. It is an immense alluvial plain covering 139 000 km² and was formed during the Holocene. There is extensive seasonal flooding by the Rio Paraguai and its tributaries. It is a complex mosaic of shallow lakes, periodically inundated grasslands and islands and corridors of forests. Changes in the spatial pattern of land cover were measured from the dry season through to the flooding peak. This Figure has been computed from three ERS-1 SAR images of the Nhecolândia region within the Brazilian Pantanal, on 12 December 1992, 20 February 1993 and 1 May 1993, which span the transition from a dry landscape with sharp boundaries between grassland and forest to an inundated wetland with emergent aquatic plants. Red shows areas of emergent aquatic vegetation, the black clusters in the centre of the image are saline lakes and white areas are forested corridors. This information will be valuable in understanding the ecology of the area and in developing management schemes.
Courtesy of G Henebry, University of Kansas, Manhattan, USA; H Kux, INPE, São Paulo, Brazil.

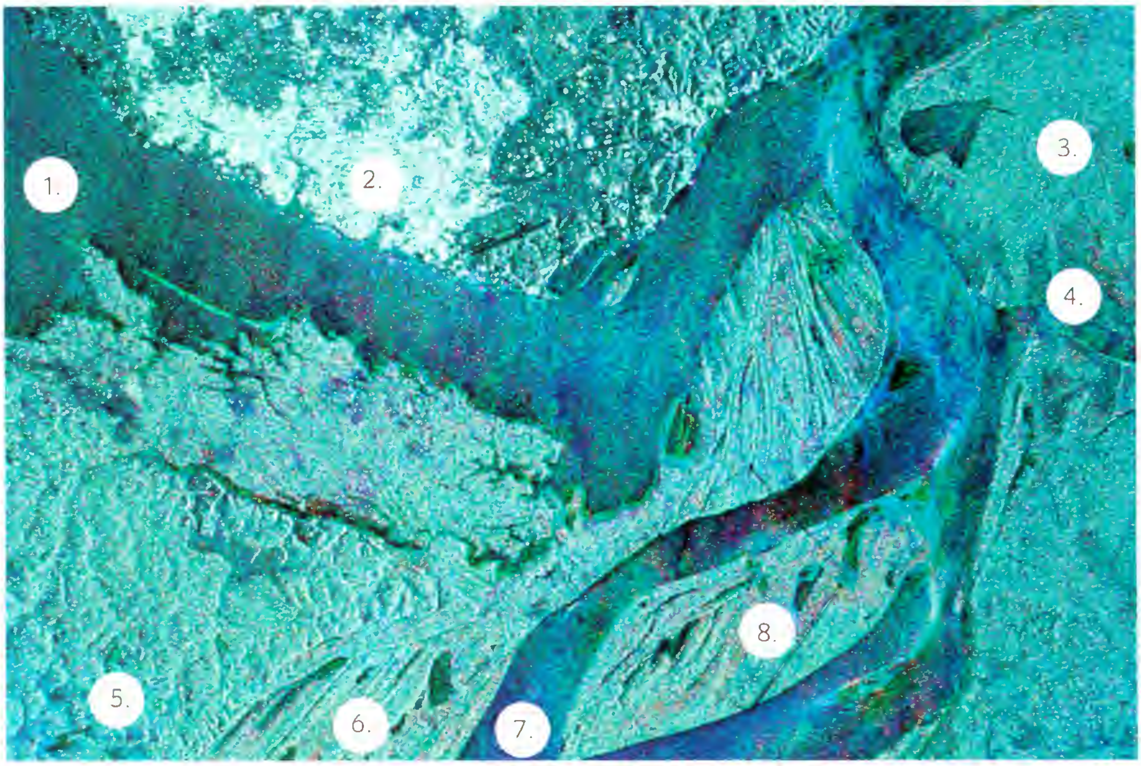

a

b

1. Rio Negro
2. Manáus City
3. Forest: bright grey
4. Terrestrial non-flooded grassland (dark grey)
5. Dissected, non-floodable upland terrain
6. Flood plains
7. Amazon river
8. Floating aquatic grasses (red)

Rectangle indicates the area shown in Figure b

Figure 6.16 a,b. Global budget calculations indicate that tropical wetlands make a substantial contribution to methane levels in the troposphere. The ERS-1 SAR allows the mapping of land cover and inundation over large areas, independent of cloud cover. This provides a unique opportunity to analyse the spatial and temporal variations in areas where cloud cover is persistent.

Figure a shows an area located at the confluence of the Rio Negro and the Amazon river. The image is produced by combining ERS-1 SAR images of the same location from three different dates. Red areas indicate the existence of floating aquatic grasses in May (high water season) while these areas are covered by terrestrial grasses in November and December (low water season). Figure b is an air photo of Marchantaria Island (bottom centre of Fig. a) during the high water season showing in close up the large expanse of floating aquatic grasses which appear red in Figure a. The results obtained in this region demonstrate that ERS-1 SAR data can enhance our knowledge of the spatial and temporal behaviour of tropical wetlands as source areas of greenhouse gases. Courtesy of C Corves, University of Edinburgh, UK.

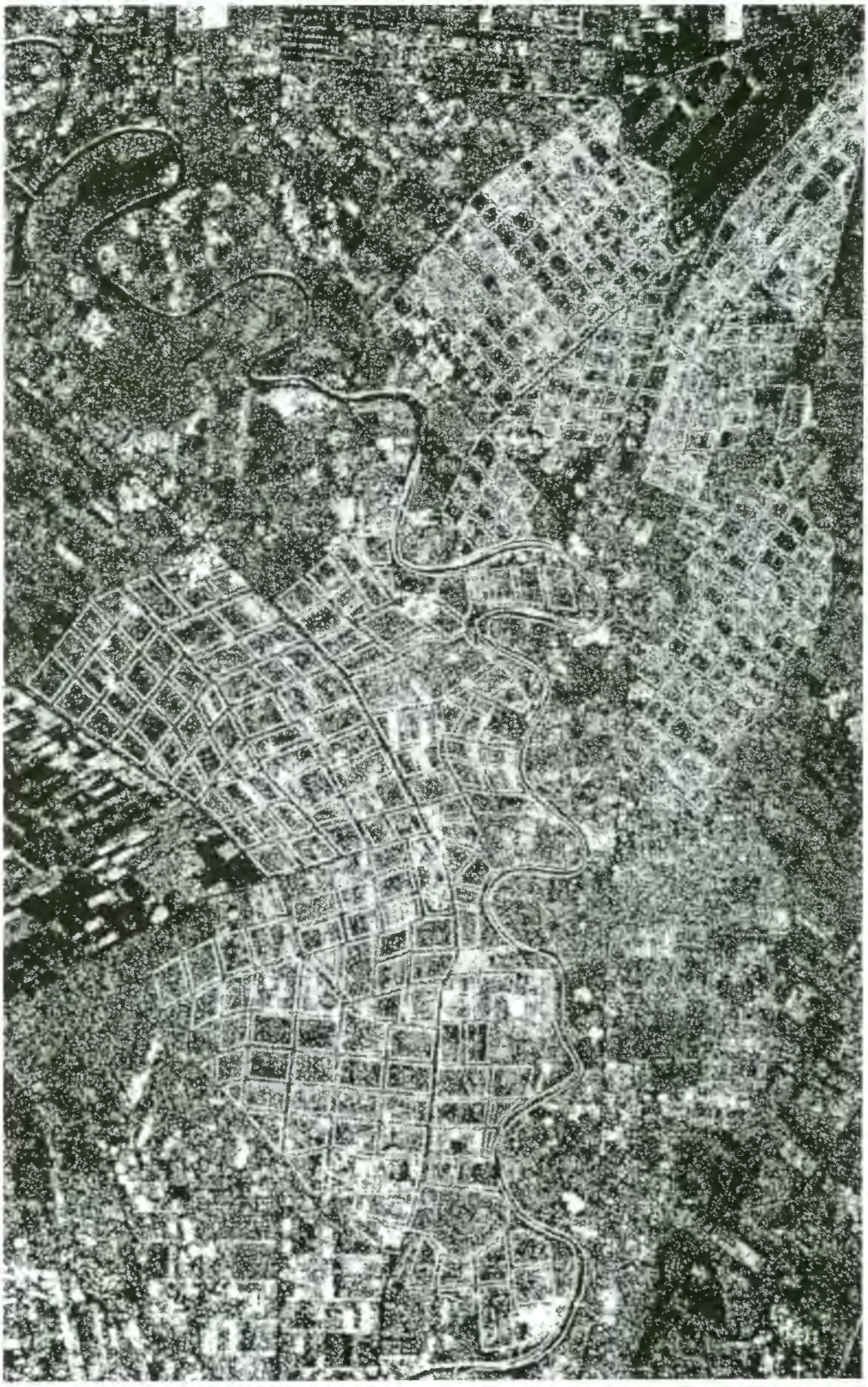

- *dark : non irrigated fields.*
- *very bright : fields being irrigated.*
- *diffuse bright : fields already irrigated.*
- *very dark : flooded rice fields.*

Figure 6.17. The use of ERS-1 data for soil moisture retrieval in an irrigated farming area of a semi-arid region in Morocco was assessed. Data were collected in July 1992 and April and May 1993 over bare fields and sugar cane and sun flower fields. A map of the state of irrigation in the field was produced from ERS-1 SAR data. This included fields being irrigated, fields already irrigated, flooded rice fields and non irrigated fields. This was one of a series of studies that found that soil moisture could be retrieved if vegetation cover is sparse and roughness parameters lie within a well defined range. Courtesy of T Le Toan, CESR, Toulouse, France.

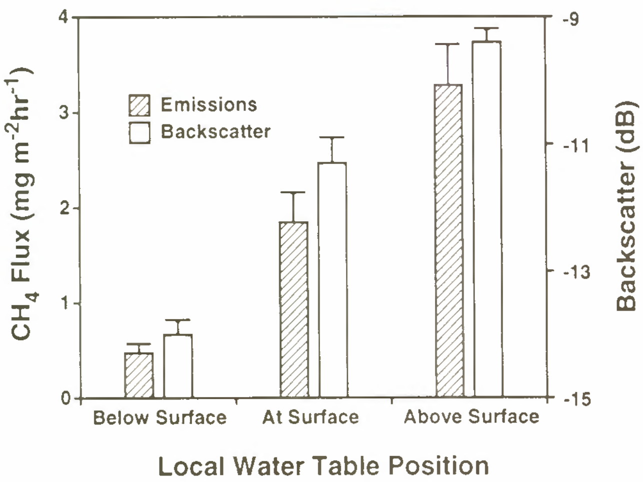

Figure 6.18. Arctic and boreal ecosystems are believed to contribute between 4 and 16% of the annual atmospheric methane burden, but uncertainties in the spatial and seasonal extent of methane source and sink areas remains one of the greatest unknowns in the global methane budget. ERS-1 SAR data have proven to be useful in delineating levels of inundation, a key indicator of the anaerobic conditions in the substrate necessary for methane production. ERS-1 SAR data were acquired over Barrow, Alaska, a non-forested tundra area, on 18 August 1991 to differentiate water table levels. As shown in this Figure, methane emissions and ERS-1 SAR backscatter were positively related to water table position and rates of methane emission were greatest for inundated sites, decreasing dramatically for comparable sites where the water table is either at or below the surface. This will enable the seasonal and interannual extent and periodicity of inundation to be quantified. Courtesy of L Morrissey, G Livingston, NASA Ames Research Center, Moffett Field; S Durdan, JPL, Pasadena, USA.

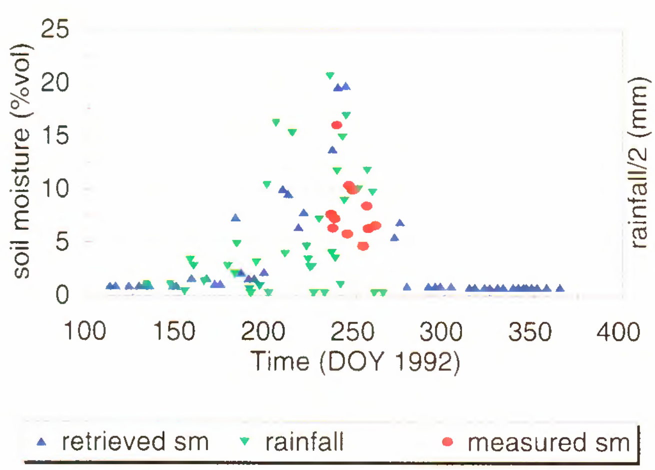

a

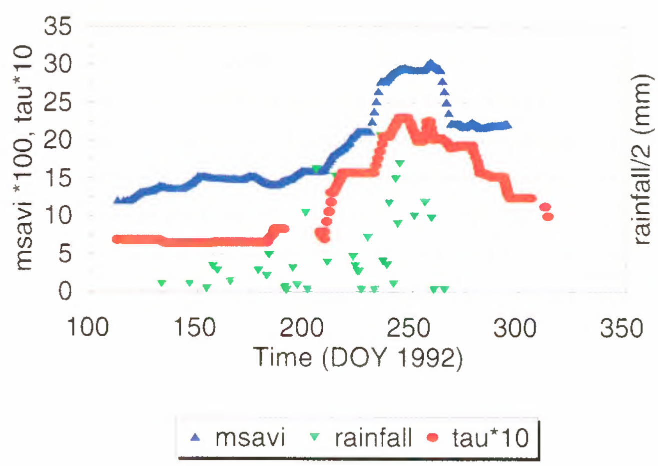

b

Figure 6.19 a,b. ERS-1 scatterometer data allow surface parameters to be retrieved at global scales for inclusion in flux models. Figure a shows retrieved soil moisture (sm) values from the Sahel which have been plotted with rainfall amounts and measured soil moisture. The temporal evolution of soil moisture is quite discernible with an increase after the onset of the rainy season, and a subsequent decrease which is linked to the drying out of the soil. Some ground measurements were performed and are plotted on the graph. These measurements are very local and the scatter indicates the spatial heterogeneity of the surface. However they are fully compatible with the more spatially integrated estimates derived from the scatterometer data.

Figure b depicts the temporal evolution of vegetation. The blue curve represents a vegetation index derived from NOAA AVHRR (USA optical sensor) datasets (msavi). The red points give the canopy opacity as retrieved from the scatterometer (τ.10). The similarity of the two curves shows that biomass can be more efficiently monitored with the scatterometer since no compositing and atmospheric corrections are required. Moreover the canopy opacity is linked to the vegetation-integrated water content rather than to the green vegetation fractional cover. This is a more representative way to quantify vegetation in flux estimates. Courtesy of Y Kerr, R Magagi, LERTS/CESBIO, Toulouse, France.

6.4. Surface geology and geomorphology

The underlying basis for geological study is the mapping of general lithology, rock boundaries, fractures and folds. The geology of large regions of the world is poorly mapped. These are often remote areas covered with thick forest and persistent cloud cover.

SAR imagery have been used for the mapping of rock units and fracture patterns even when the soil, sand and forest cover would otherwise make this impossible. One of the main challenges is the mapping and monitoring of geological hazards, such as landslides.

ERS-1 SAR images are proving to be an effective and reliable tool for the identification and subsequent mapping of geomorphological units. The capabilities of SAR data are particularly appropriate in flat arid regions where the resolution and penetration depth of the radar allows the location of subtle sandy accumulations and superficial characteristics. This information is not available from aerial photographs and traditional satellite imagery.

MAPPING GEOLOGY

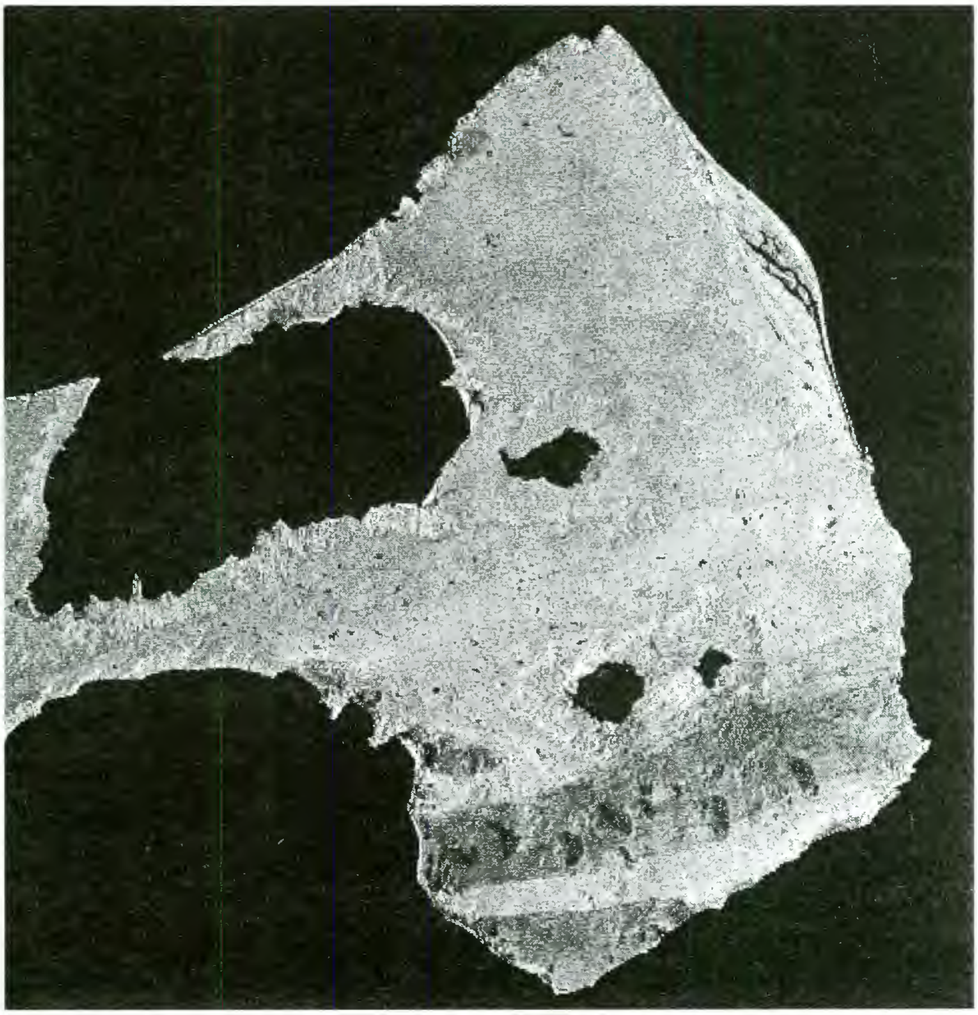

a

Figure 6.20 a,b. The Patagonian and Tierra del Fuego coastal environments are poorly mapped due the near continual cloud cover. ERS-1 SAR with its ability to penetrate clouds and its capability to locate subtle sandy accumulations and superficial characteristics is of great value in mapping these flat arid regions. Figure a shows the ERS-1 SAR image recorded on 9 July 1992 of the Peninsula Valdés on the central Patagonian coast. Four geoforms were identified and are shown in Figure b. These are:

1. *Plateaux, constituted by Patagonicos, marine tertiary outcrops, erosion fronts, small closed saline basins and gullies;*
2. *Coastal environments, these vary from sand beaches to active and inactive cliffs;*
3. *Dunes and aeolian mantles consisting of active colonial dunes and associated erosion tongues, longitudinal dunes, interdune areas with aeolian mantles, fixed dunes together with old aeolian mantles, blowouts or wind scoured basins;*
4. *Tectonic depressions inside which glacis and lacunar geoforms have developed.*

Courtesy of D Gagliardini, CONICET/CAERCEM, Buenos Aires, Argentina.

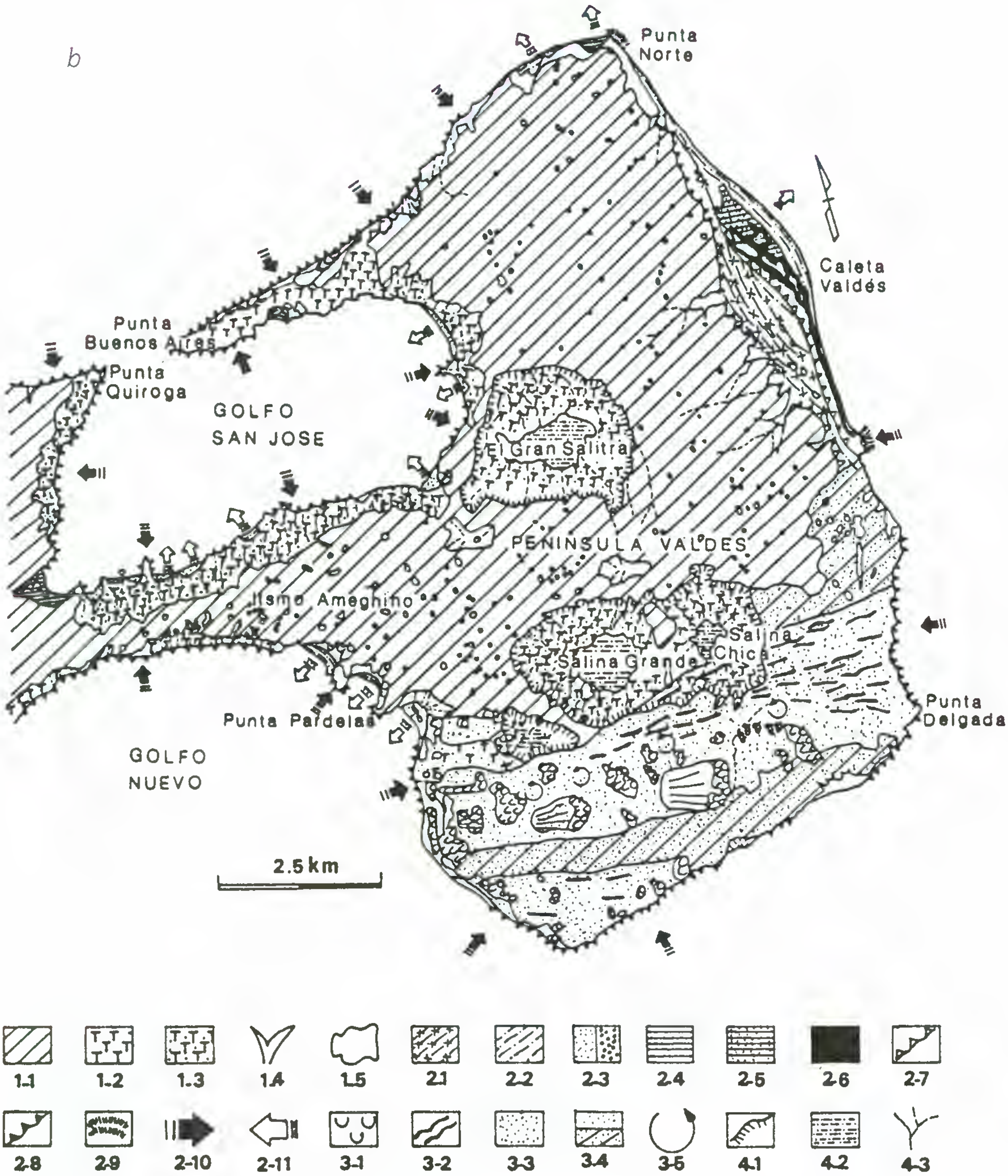

Plateaus:
1.1 Structural plains.
1.2 Marine tertiary outcrops.
1.3 Erosion fronts.
1.4 Gullies.
1.5 Small closed saline basins.

Coastal environment:
2.1 Pleistocene beach ridges.
2.2 Holocene beach ridges.
2.3 Gravelly and sandy beaches.
2.4 Tidal plain not functional.
2.5 Tidal plain functional.
2.6 Lagoon.
2.7 Inactive cliffs.
2.8 Active cliffs.
2.9 Abrasion platform.
2.10 Marine erosion.
2.11 Marine accretion.

Dunes and aeolian mantles environment:
3.1 Barchanoid dunes.
3.2 Longitudinal dunes.
3.3 Interdune areas together with aeolian mantles.
3.4 Fixed dunes together with old aeolian mantles.
3.5 Deflation.

Tectonic depressions:
4.1 Erosion fronts.
4.2 Salines.
4.3 Temporary channel.

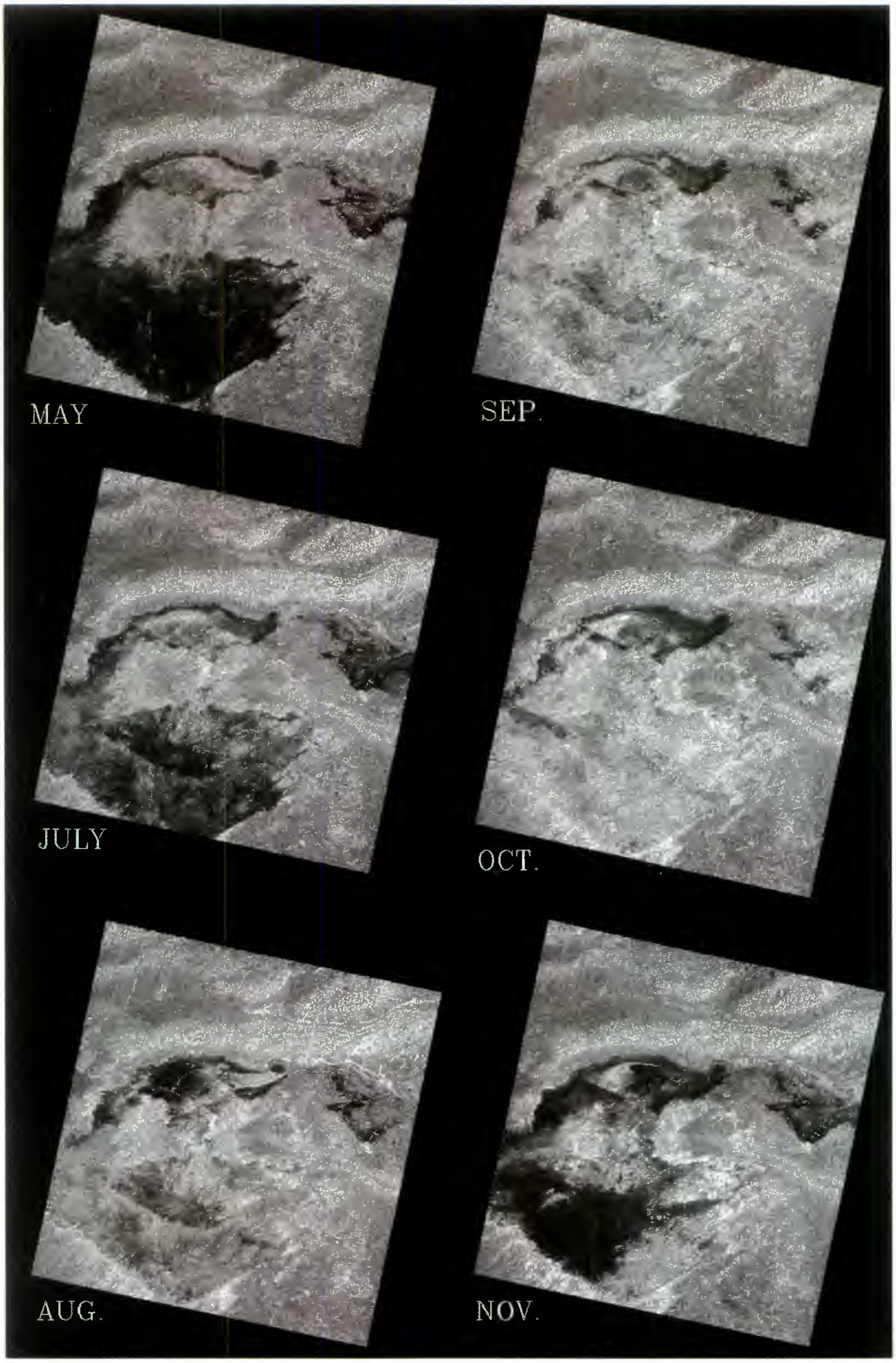

Figure 6.21. Evaporative sedimentation has been monitored in the Chott el Djerd, a playa in central Tunisia. Two major aquifers discharge water into the Chott el Djerd from areas hundreds of kilometres to the south. Evaporation of these waters controls the sedimentary processes of the playa. The sequence of six ERS-1 SAR images shown here were recorded at 35-day intervals in 1992 on 29 May, 3 July, 7 August, 11 September, 16 October and 20 November. The playa is identifiable as the areas of predominantly low backscatter in the May and November scenes. During the summer months increasing evaporative crystallisation of gypsum and particularly halite crystals roughen the surface and increase the overall level of backscatter. In addition there are more localised sedimentary events on the playa that can also be detected as marked changes in backscatter month to month. Courtesy of G Wadge, NUTIS University of Reading, UK.

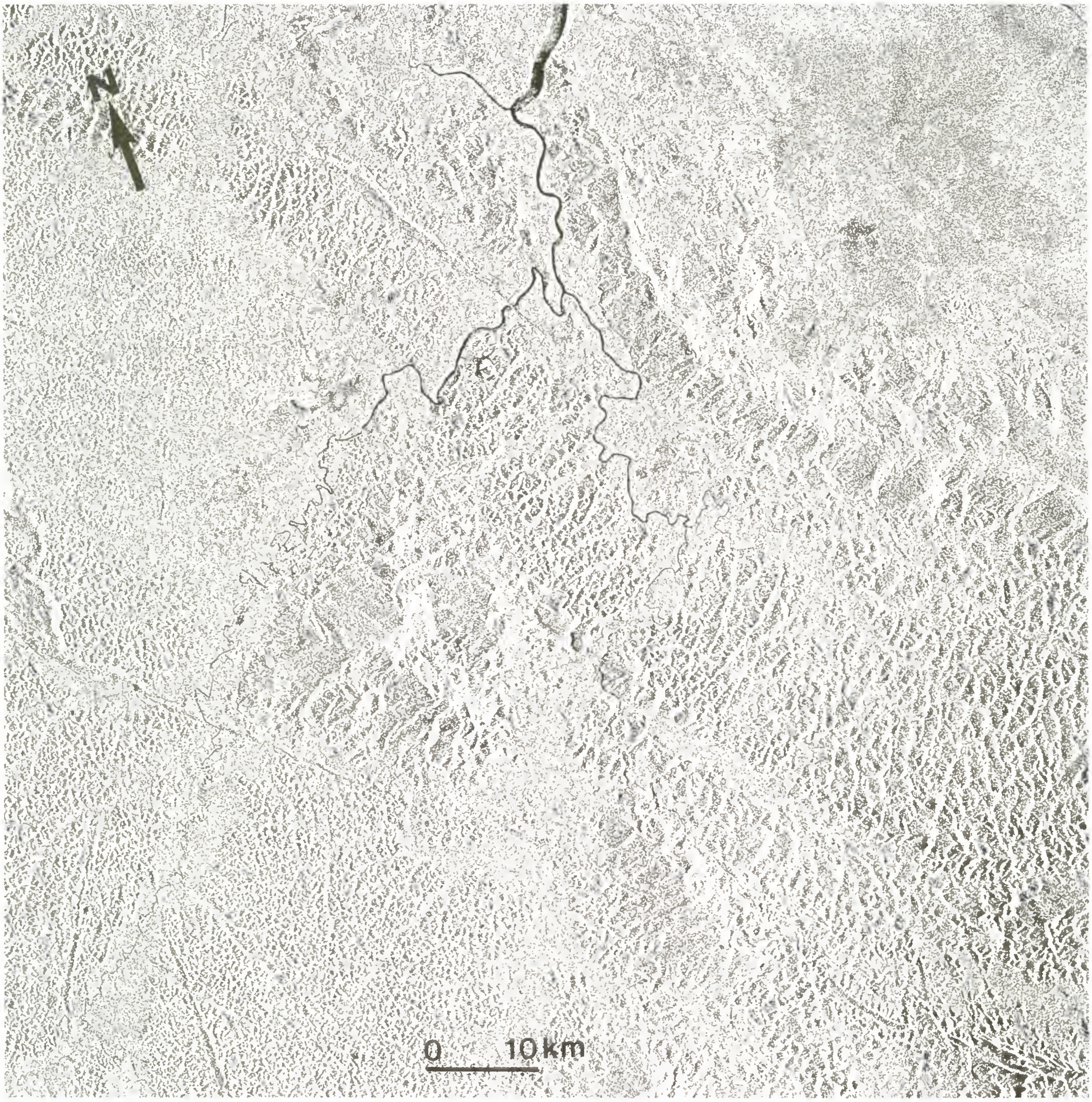

Figure 6.22. ERS-1 SAR data are particularly useful for geological mapping in areas covered by rainforest such as French Guyana. In addition to abundant vegetation, mapping of basement rock types is further complicated by weathering in an equatorial climate and the extent of laterisation phenomena. This Figure shows an ERS-1 SAR image over the Kaw region of French Guyana that was recorded on the 25 November 1992. Detailed geological structures can be observed beneath the rain forest. The northern sector of the image is a gold prospecting area. A morphostructural map and a lineament map were made. These were combined with local geology maps and gold anomalies found by geochemical exploration for the French Mineral Inventory. Courtesy of J-P Deroin, French Geological Survey BRGM, Orleans, France.

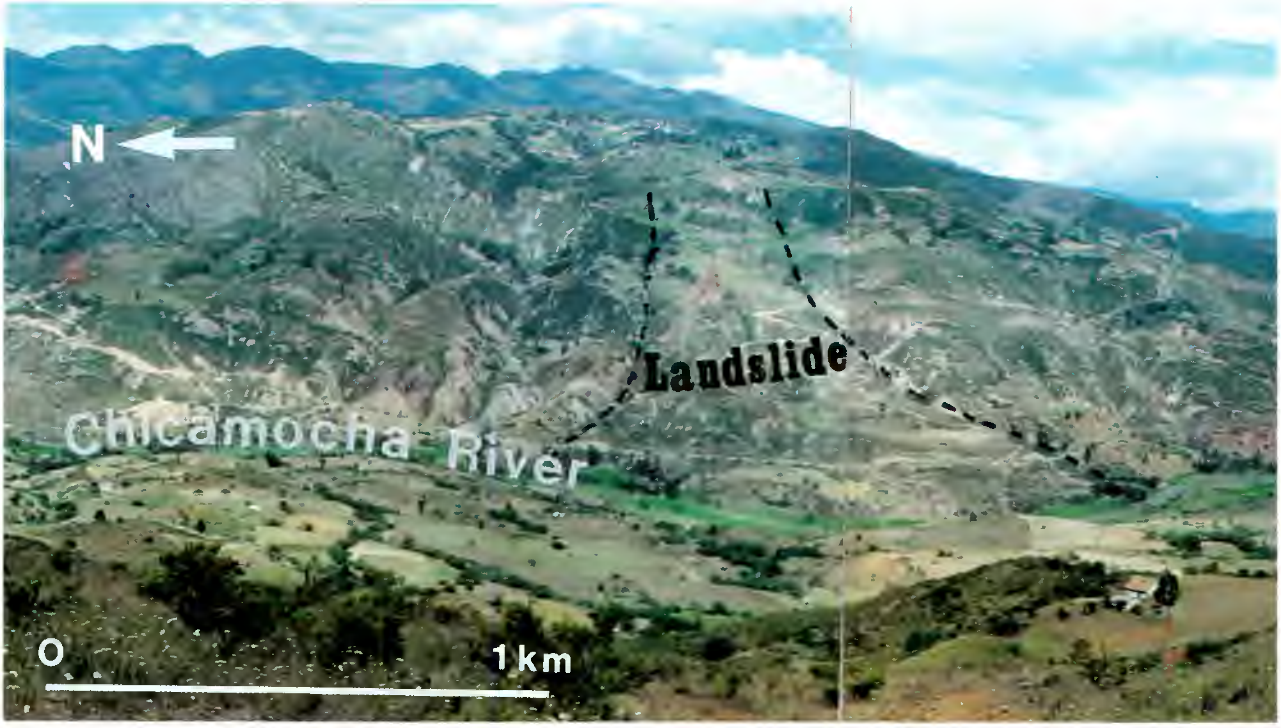

a

b

Figure 6.23 a,b. Until recently, the inventory and study of landslides has been based on interpretations of aerial photography, but this is restricted to small areas. In mountainous areas, where many landslides occur, persistent cloud cover often restricts the use of optical satellite data and techniques are being developed in the use of ERS-1 SAR data. Figure a shows a large landslide in the Colombian Andes which can be identified in an ERS-1 SAR image of approximately the same area (Fig. b). The landslide area shows geomorphological characteristics that are different from the surrounding stable area. Courtesy of C Vargas, J Chorowicz, University Pierre and Marie Curie, Paris, France.

6.5. Cartography

Many areas of the world are poorly mapped due to the difficulties of access into a region for ground surveying and the lack of cloud-free optical remotely sensed data. Examples of such regions are areas of S-E Asia and South America. There is a need for basic topographic and thematic maps for these areas, both for economic reasons, and also to support scientific investigations. As in many areas of the world, there is also a need to update the thematic information regularly.

The creation of digital elevation models through air photo interpretation is one approach for mapping difficult areas, but this is often costly and inefficient. The Spot optical satellite system provides an alternative approach, but it is often difficult to obtain two cloud-free images sufficiently close together for stereo viewing. ERS-1 SAR data are one source of information from which both the topography and much of the thematic information can be derived.

Two main types of mapping techniques are supported by ERS-1 data:

- Digital elevation modelling to produce topographic maps;
- Data fusion and mosaicing to produce thematic maps.

Topographic mapping requires pairs of images from which information can be obtained either through stereoscopic or interferometric techniques. Data fusion and mosaicing allow additional information to be obtained as compared with the use of single images. In particular, hazard mapping involves both building up data bases to assess the risks of potential hazards and the measurement and monitoring of events after they have happened.

DIGITAL ELEVATION MODELLING

	Case 1			Case 2			Case 3		
	E	N	H	E	N	H	E	N	H
Minimum (m)	− 48	− 91	− 116	− 85	− 64	− 103	− 65	− 44	− 78
Maximum (m)	+ 137	+ 93	+ 8	+ 72	+ 45	+ 28	+ 67	+ 44	+ 24
Mean (m)	+ 51	+ 6	− 42	+ 4	− 7	− 51	+ 1	− 6	− 31
Std. Dev. (m)	70	35	52	37	23	64	39	24	44

Figure 6.24. SAR stereoscopic intersection is a convenient way to obtain spatial elevation information about the surface of the land. This Table illustrates the accuracy achieved from test images around northwest Marseilles in southern France where the topography and land use are very variable. The accuracy in plan (E, N) and height (H) at 38 check points with no ground control points is given for three cases which use different radargrammetric and image combinations. This is possible because of the very good orbit information which is provided with ERS-1. The results improve by up to 60% if two ground control points are used. The best result comes with case 3 which uses an opposite side pair from a roll-tilt mode image and a PRI image (the standard ERS-1 SAR image for applications work). Case 1 combines a same side roll-tilt mode image with a PRI type ERS-1 SAR image and case 2 is two opposite side ERS-1 SAR PRI images. These results indicate that the geometry of ERS-1 stereoscopic SAR can produce very high accuracy height information and if the stereo matching can be improved, good quality digital elevation models can be produced. Courtesy of I Dowman, University College London, UK.

a

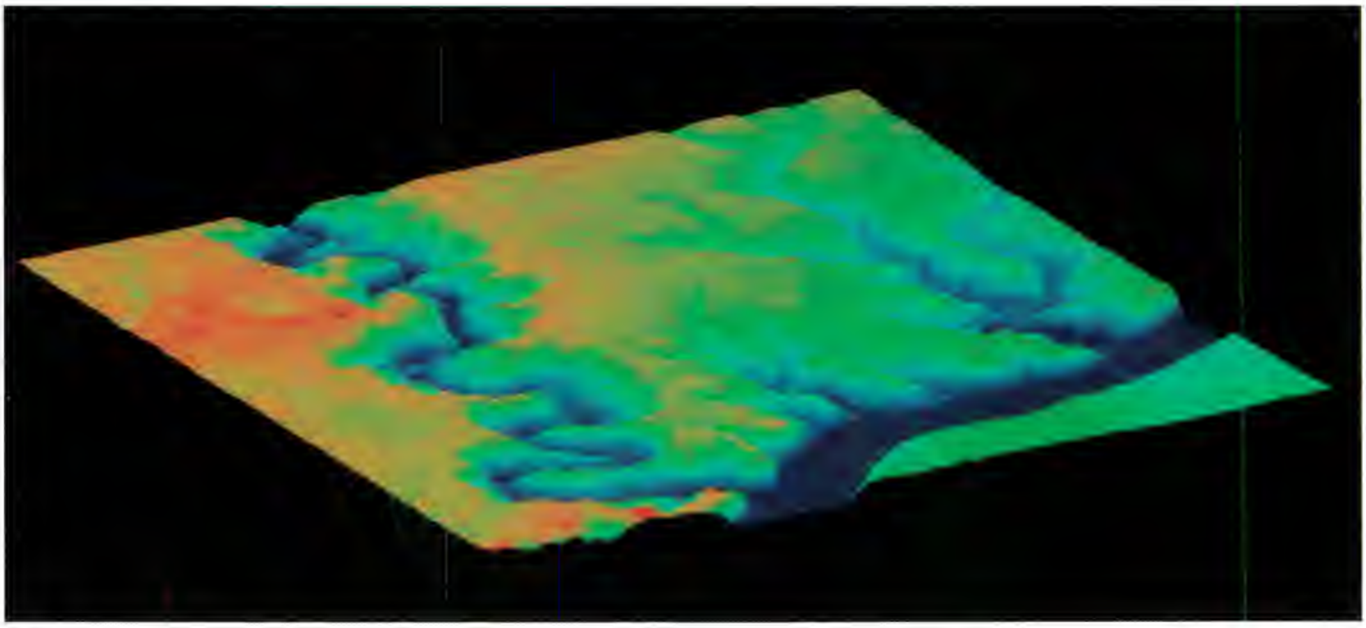

b

Figure 6.25 a,b. The technique of SAR interferometry can be used to provide digital elevation models. Figure a shows an interferometry image of an area in the Ukraine obtained from ERS-1 SAR data, together with a digital elevation model derived from the image (Fig. b). Elevation accuracies of the order of 1 m are achieved using this technique. Verification is difficult in this area because reference maps exhibiting such accuracy are very uncommon. The accuracies are assessed by taking independent interferometry images and producing further digital elevation models for consistency. Courtesy of D Massonnet, CNES, Toulouse; F Perlant, ISTAR, Toulouse, France.

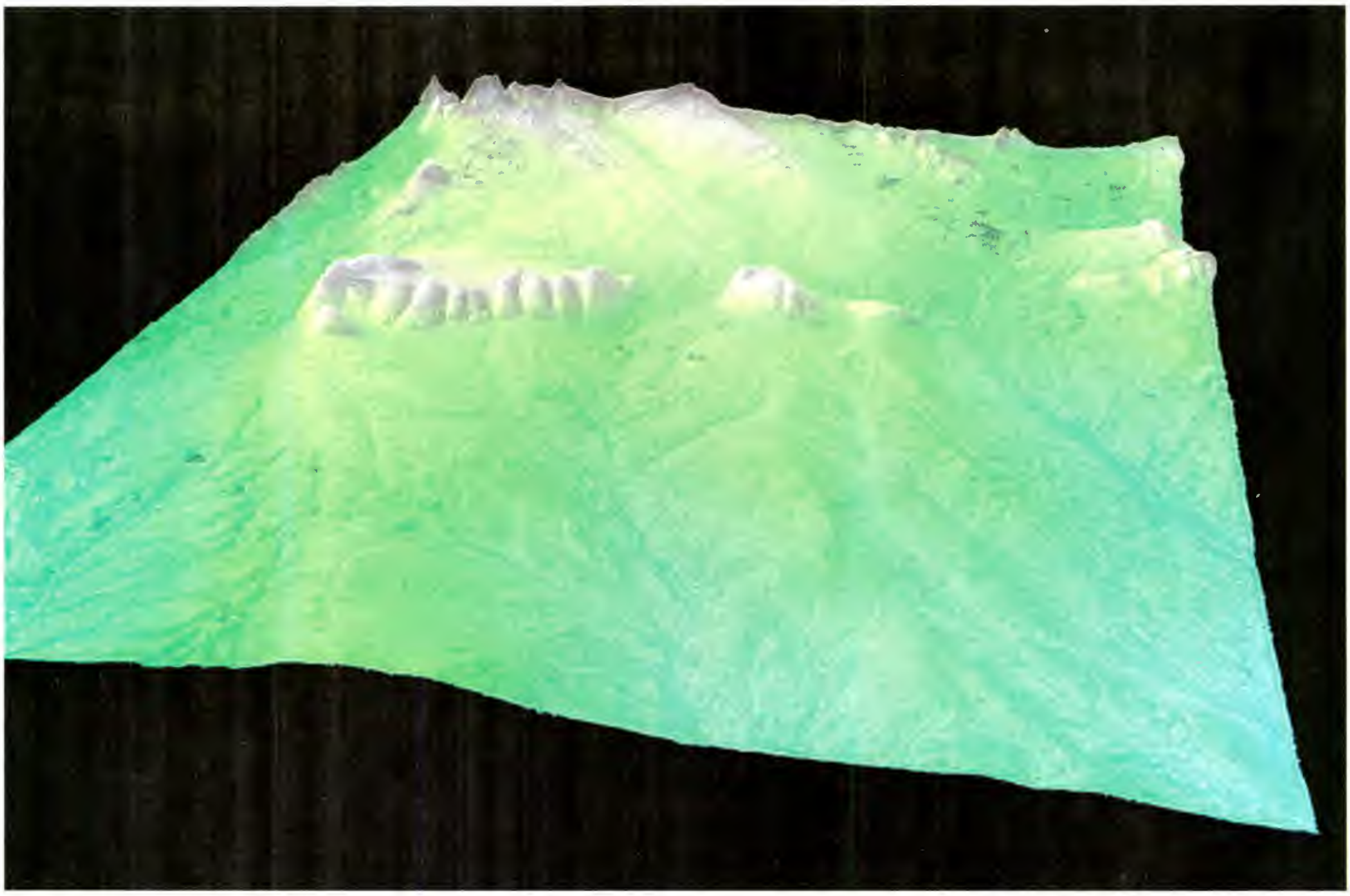

a

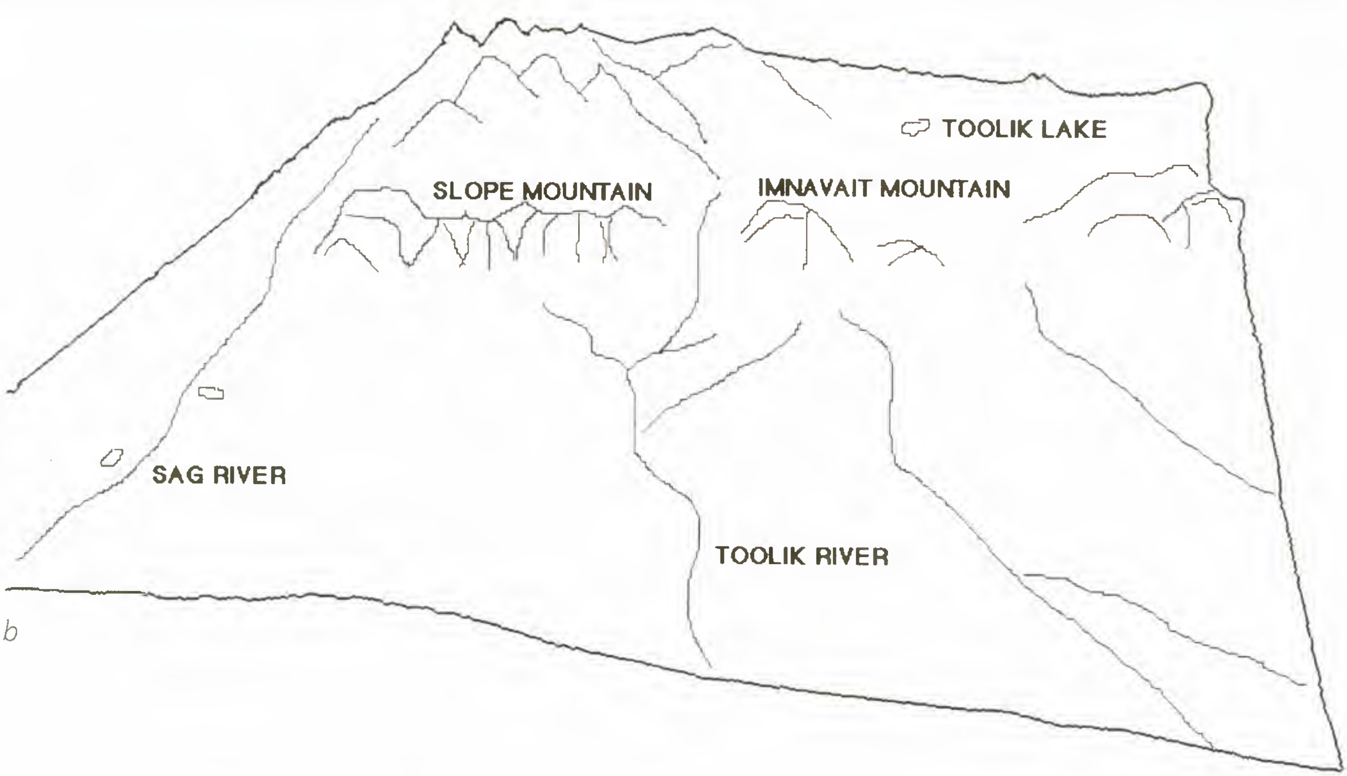

b

Figure 6.26 a,b. Topographic maps have been produced for three sites in Alaska using ERS-1 SAR data. This Figure shows the maps produced for the Toolik site. Figure a is a digital elevation model of the area shown in perspective. A sketch map is given in Figure b. These topographic maps have relative root mean square errors of 5 m or less and therefore provide a relatively inexpensive means of generating digital elevation models over regions of the Earth where little or no topographic data are available. Courtesy of H Zebker, C Werner, P Rosen, S Hensley, JPL, Pasadena, USA.

Figure 6.27. Precise ortho-images were derived from two sources of image data, ERS-1 SAR (blue) and Landsat TM (USA optical sensor) bands 7 (red) and 4 (green), and a digital elevation model. This integrated image has been used to study the structural geomorphology of a crater in the Charlevoix area of Quebec, Canada. The ERS-1 SAR/Landsat TM data integration is necessary to take advantage of the sensor complementarity, to enhance the specific characteristics of the SAR and to compensate for SAR weaknesses in lineament extraction due to shadow and layover in this specific context. Courtesy of D Deséve, R Desjardins, University of Quebec, Montreal; T Toutin, Canada Centre for Remote Sensing, Ottawa, Canada.

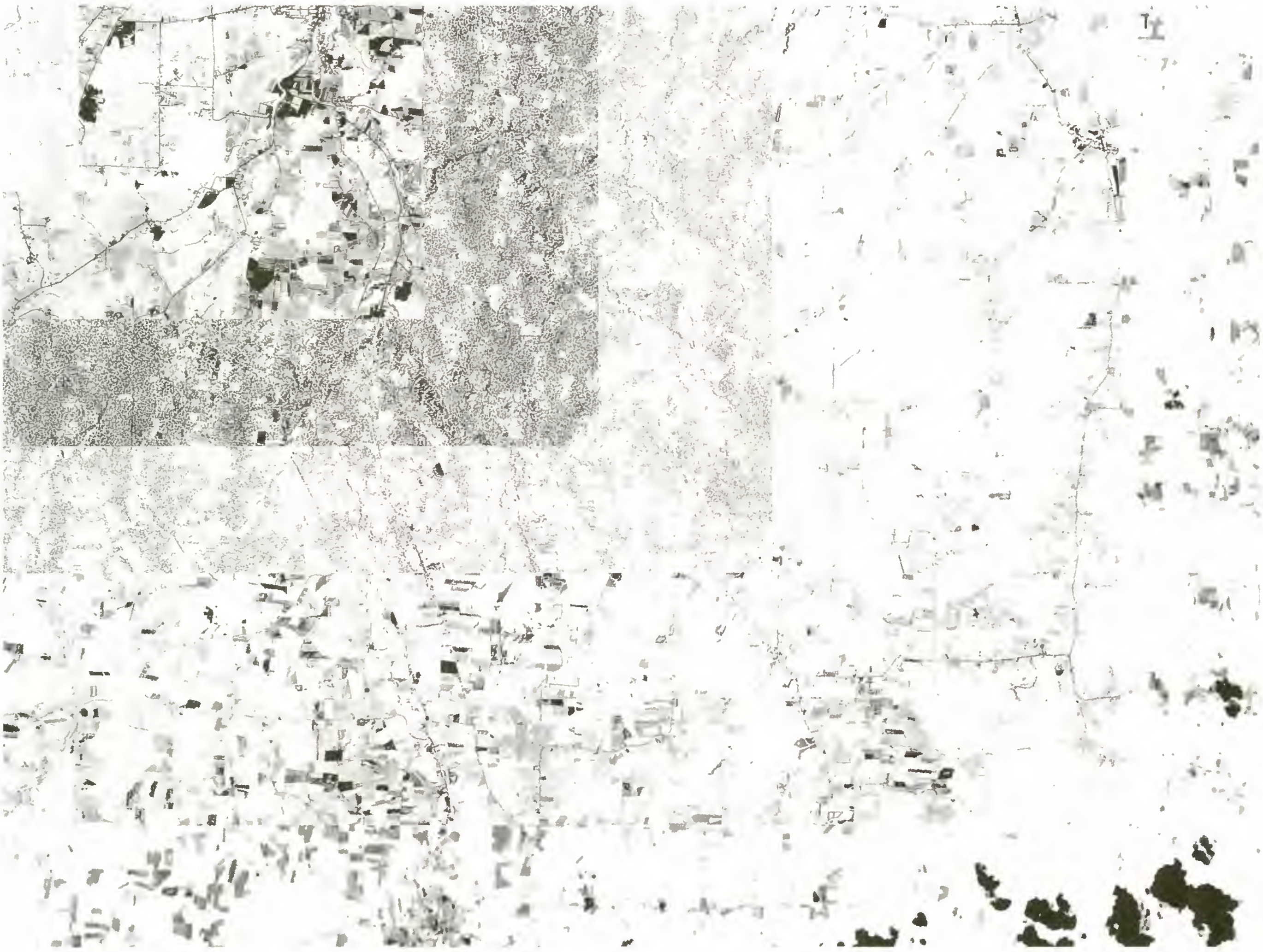

Figure 6.28. This image (covering an area of 39 × 29 km with a pixel size of 10 m) is a mosaic of eight different images which have been integrated with a digital elevation model. The following images are shown sequentially from the top left corner·

- *SAR (Canadian airborne).*
- *MEIS (Canadian airborne optical sensor);*
- *SPOT HRV panchromatic (French optical sensor);*
- *ERS-1 SAR;*
- *SEASAT SAR (USA);*
- *SPOT HRV multispectral;*
- *Landsat TM (USA optical sensor);*
- *MOS-MESSR (Japanese optical sensor).*

The absolute accuracy is 1/3 of a pixel for spaceborne visible infrared images and 1-2 pixels for airborne and SAR images. This mosaic shows qualitatively the results of the geometric correction process, and also the difference in the radiometric content and the thematic features which can be extracted from the different images as a function of the platform (airborne vs. spaceborne), of the sensor (visible/infrared vs. SAR) and of the resolution (4 m to 50 m). Courtesy of T Toutin, Canada Centre for Remote Sensing, Ottawa, Canada.

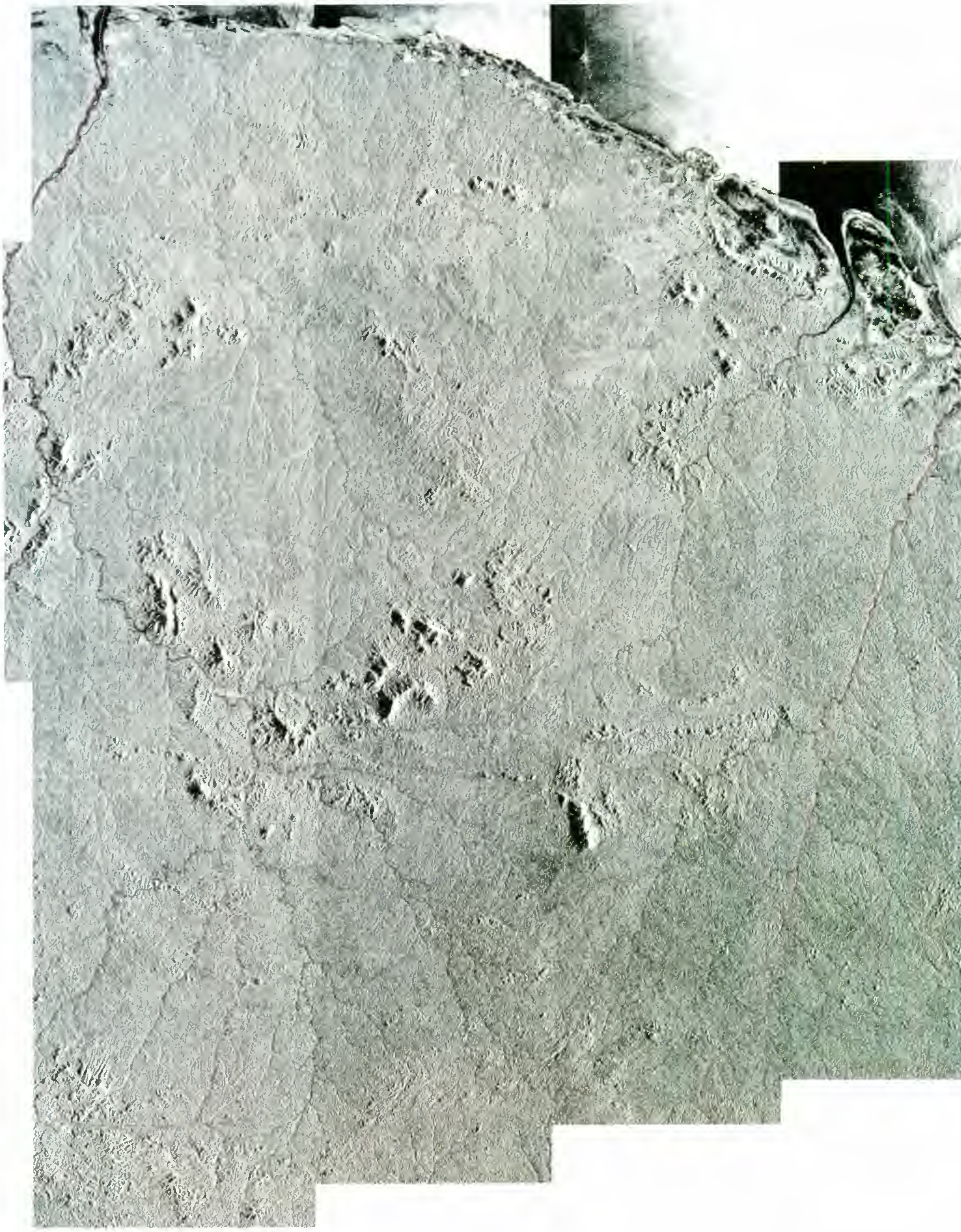

Figure 6.29. The first complete satellite coverage of French Guyana was obtained from 18 ERS-1 SAR images between April and December 1992. Several natural frontiers are clearly visible, including the Maroni river which forms the western border with Surinam and the Oyapock river which forms the eastern border with Brazil. This mosaic allows the study of large features such as geomorphological regions, river basins and forests which cannot be adequately analysed using single images. Courtesy of J-P Rudant, UPMC, H Maître, Telecom, Paris, France.

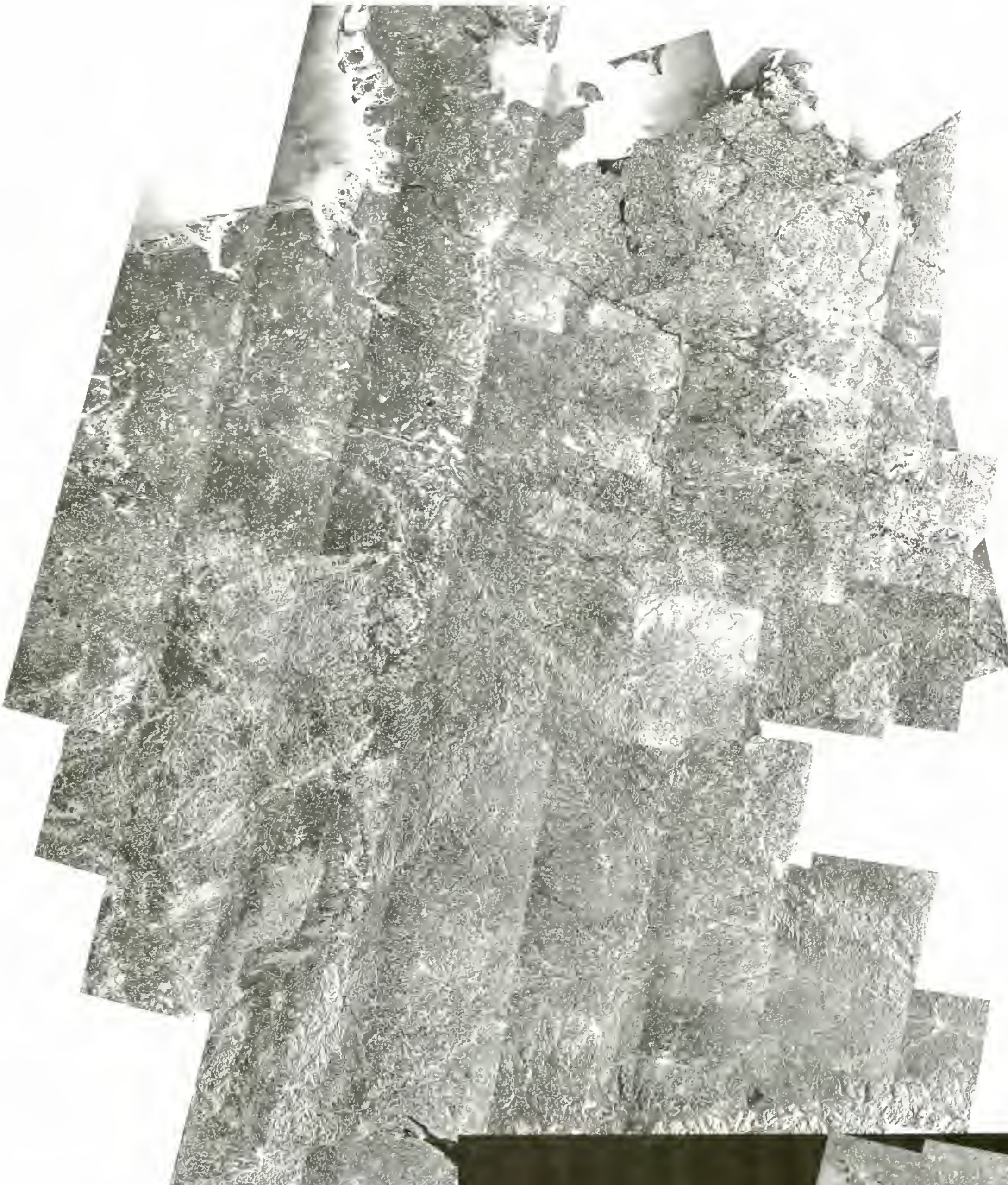

a

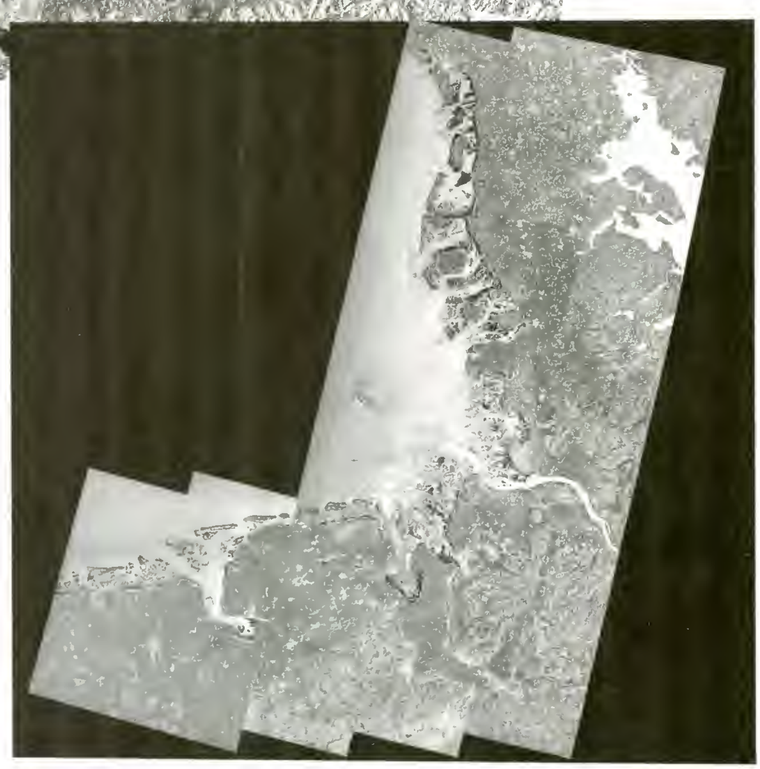

b

Figure 6.30 a,b. 150 ERS-1 SAR scenes have been mosaiced to produce a radar map of Germany (Fig. a). Processing is not yet fully complete but Figure b showing the German Baltic coast indicates the quality of the mosaic that will be available at the end of the project. The final mosaic will include 40 000 × 40 000 pixels and will be archived in an information system to which scientists will have easy access. Courtesy of R Winter, D Kosmann, DLR, Oberpfaffenhofen, Germany.

7. THE EARTH'S DYNAMIC CRUST

Within the Earth's crust and on its surface are traces of the Earth's formation, events that have helped to shape today's continents and oceans. These relics can provide clues to the future behaviour of the Earth and the location of its mineral deposits.

The Earth's crust is still in a dynamic state. Earthquakes and volcanoes create sudden, localised changes, sometimes with immediate and highly damaging results. Other changes occur over millions of years and can only be inferred rather than measured. In spite of their slow evolution, knowledge of the formation of the crust is important. It provides a valuable basis for hydrocarbon exploitation and contributes to our understanding of surface geology and geomorphology.

ERS-1 data are of key importance to five priority research areas:

- Improving the accuracy of maps of the Earth's shape and gravity field;
- Identifying unknown tectonic structures under sea ice;
- Improving the detail of tectonic structure mapping in areas under the ocean;
- Improving our understanding of land tectonic structures;
- Revealing the effects of earthquakes and volcanoes and thus providing new insights into their geology and processes.

Two of the ERS-1 instruments in particular are contributing to these studies:

- The radar altimeter, whose ability to measure sea surface topography is being used to identify the structures beneath the ocean. Combining ERS-1 data with those from other missions, notably Topex/Poseidon, provides high-accuracy assessments of the sea surface topography.
- The SAR, where differential interferometry based on multitemporal images provides the ability to detect small changes in the relative positions of areas of the Earth's surface. The technique is ideal for measuring crustal deformation, such as the displacements associated with earthquakes and volcanic eruptions.

7.1. Measuring the Earth's shape

Geodesy is the science of the measurement of the Earth's shape and gravitational field. The study of tectonics considers deformations within the Earth's crust and the structural effects that these may cause. The availability of satellite data, and in particular data from radar altimeters has made significant developments in these fields possible.

The ERS-1 coverage of latitudes between 82°N and 82°S represents a significant advance over previous missions which have been limited to latitudes between 72°N and 72°S at most. Also the very long duration of the mission, and variety of orbit patterns have provided a dataset of unprecedented density and size. By combining ERS-1 radar altimeter data over the ocean with those from Topex/Poseidon and Geosat, a detailed network of interlaced orbit tracks has been built up. This provides an opportunity for accurate intercalibration of the data and enables a finely spaced grid of accurate measurements to be obtained for the world's oceans. Using these data, global marine geoids and gravity fields have been determined at a higher resolution than ever produced before (0.1° grid). More recently data received during the geodetic phase of the ERS-1 mission have resulted in a quantum leap in the information available and maps are being produced with a 0.05° grid. As a result of this increase in resolution, new marine geophysical features have been discovered. For example, discontinuities along the mid-ocean ridges have been observed which have not previously been charted.

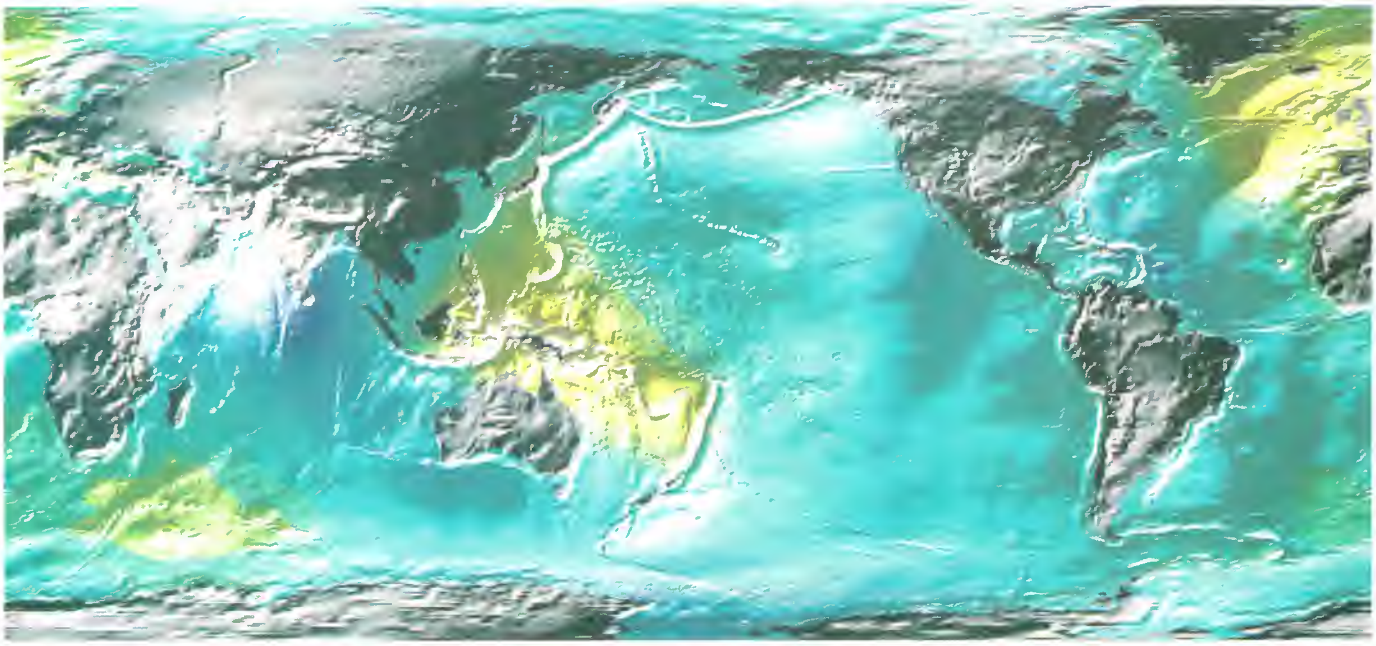

a

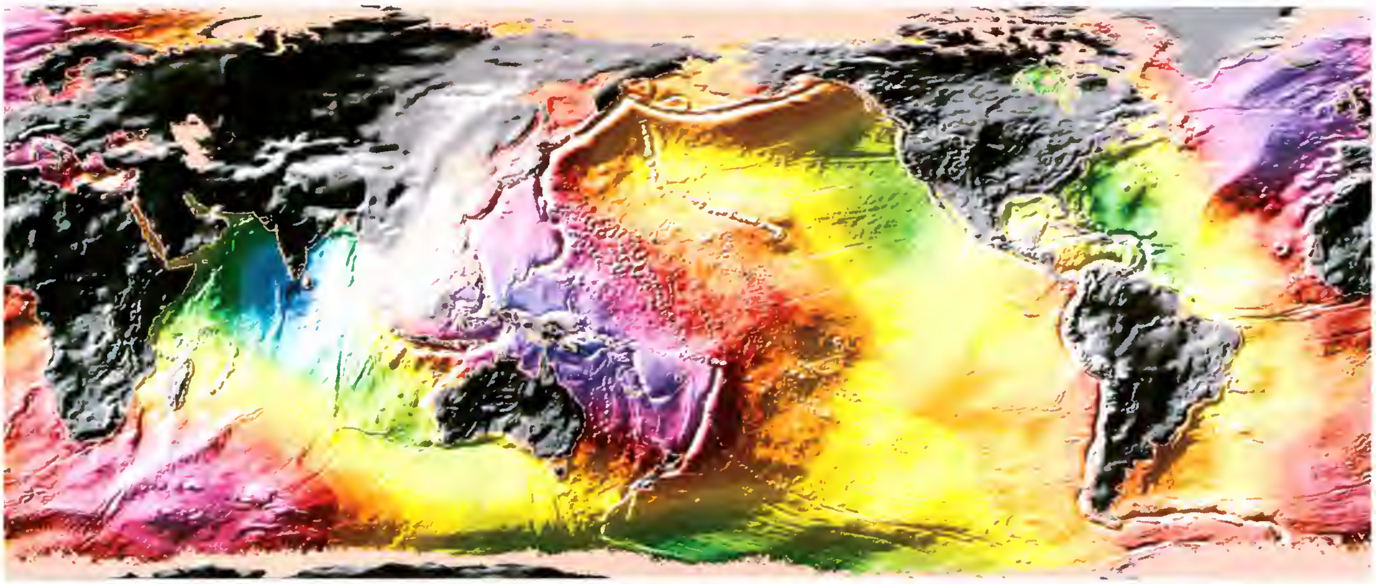

b

Figure 7.1 a,b. A sea surface height model was developed from the ERS-1 radar altimeter. The variations in the sea surface height reflect variations in the density of the Earth's mantle and the presence of tectonic features such as ridges, spreading centres, fractures and trenches on the ocean bottom. Figure a was derived from one year's data and is shown using a 0.1° grid, while Figure b was derived from the first 168-day cycle of ERS-1 (geodetic phase) and is shown using a 0.05° grid. The Figures are an exaggerated representation of the deviation from a reference ellipsoid. These deviations range from −105 m south of India to +85 m north of Australia. Clearly visible are the mid-Atlantic ridge between Europe and North America, the large circum-Pacific trenches and the Emperor Island chain including Hawaii on the left side of the image. The increased detail obtained during the geodetic phase of the mission (Fig. b) is clearly demonstrated. Courtesy of M Anzenhofer, GeoForschungsZentrum, Potsdam (GFZ), D-PAF, Oberpfaffenhofen, Germany.

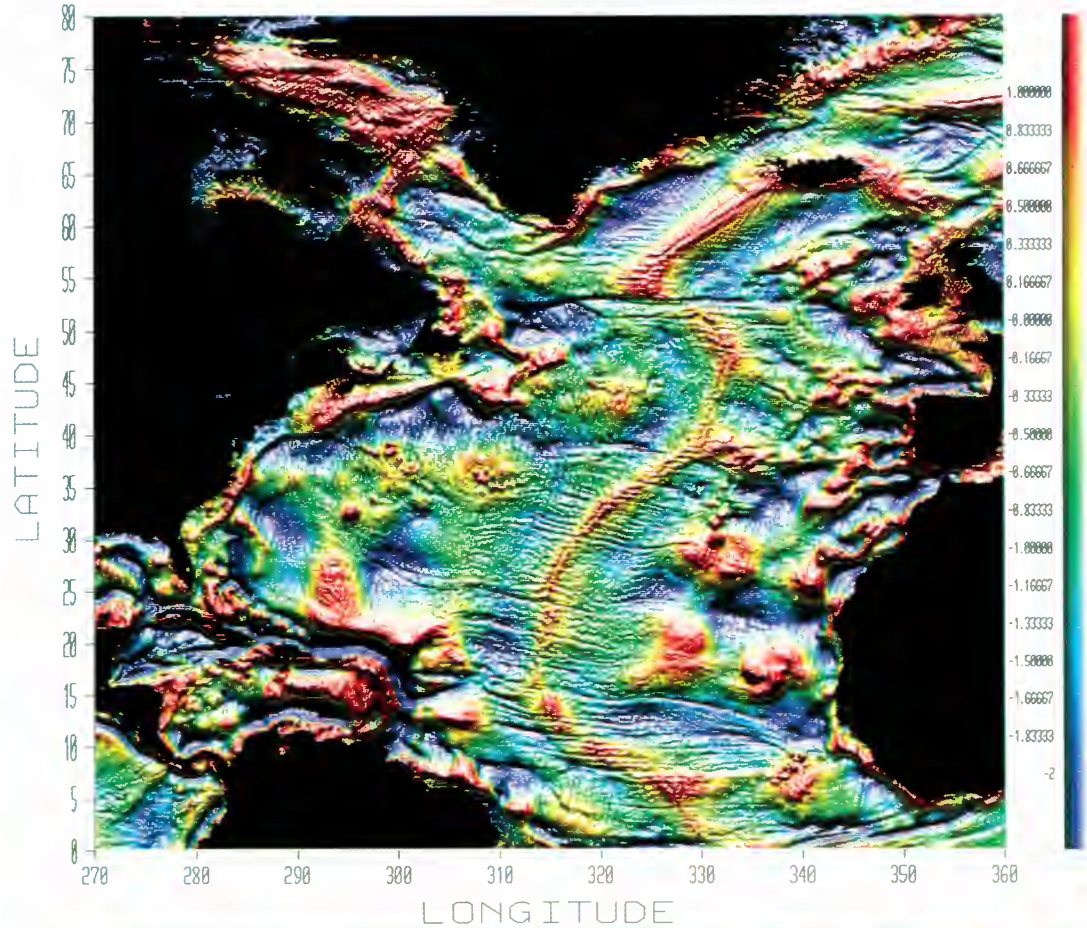

a

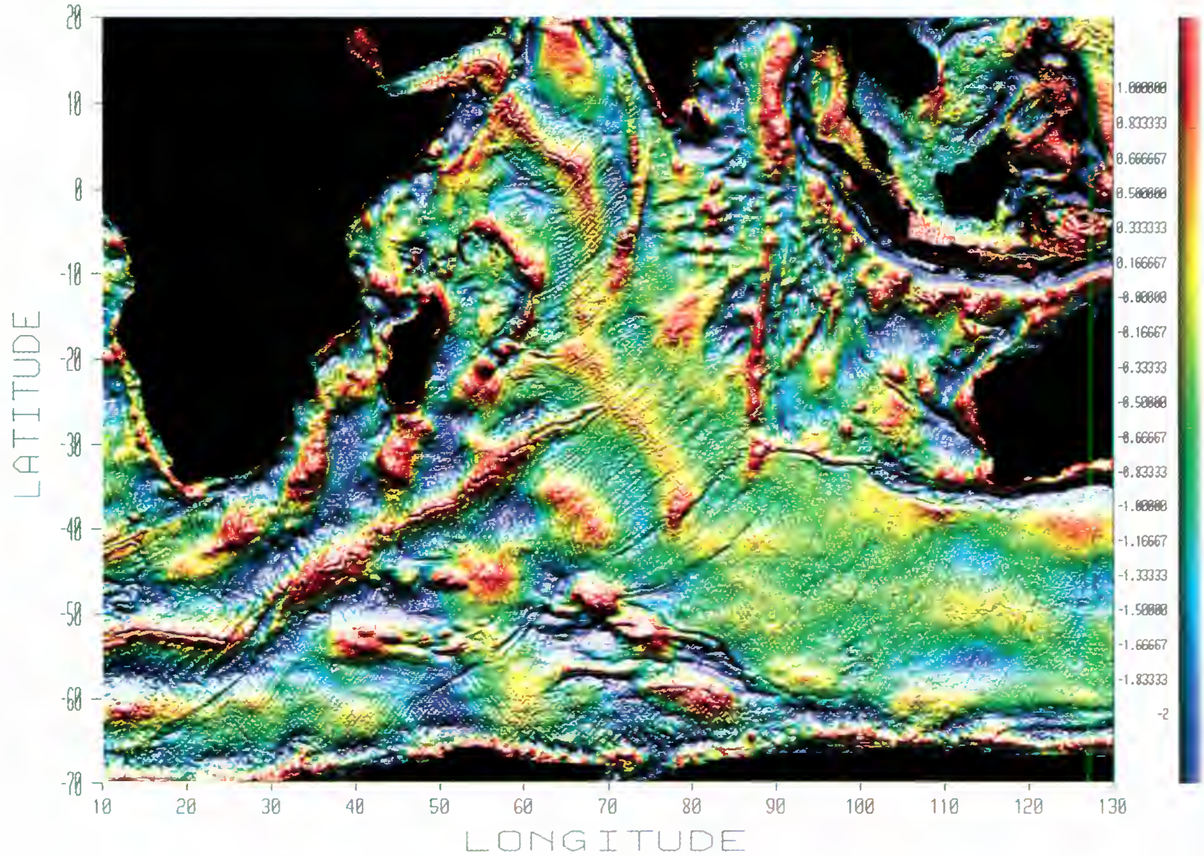

b

Figure 7.2 a,b,c. The marine geoid is presented as a relief map in a (North Atlantic), b (Indian Ocean) and c (Pacific Ocean). These data were recorded during the geodetic phase of the ERS-1 mission. The nature of the subsurface relief is inferred from the shape of the ocean surfaces, having removed the effects of such features as ocean tides and currents. Short-wavelength fractures and discontinuities that have not been observed before, particularly along mid-ocean ridges, can be seen. Courtesy of A Cazenave, GRGS-CNES, Toulouse, France.

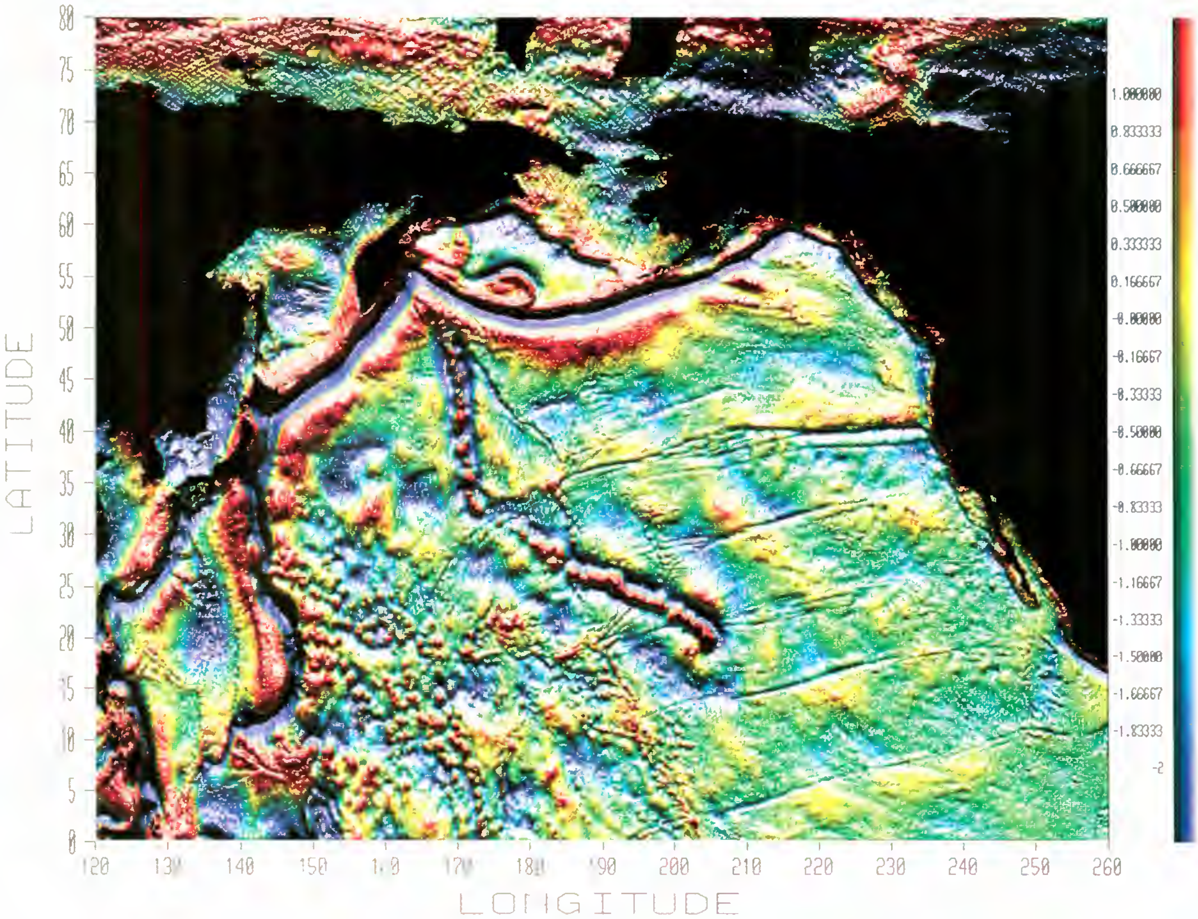

c

7.2. Tectonic structures under sea ice

The radar reflection from sea ice is very different from that of the ocean necessitating the development of new techniques to extract the geoid and marine gravity field over ice-covered oceans. This has been achieved for the first time with ERS-1, in part due to the availability of an improved altimeter tracking mode, but motivated by the significantly greater polar coverage which ERS-1 provides. As a result a unique map of the gravity field has been developed over the Arctic Ocean including regions permanently covered by ice.

Using the gravity maps derived from the polar oceans, major new discoveries have been made as a direct result of ERS-1. The formation of the Amerasian Basin has been a subject of debate for the past 30 years. ERS-1 gravity data have resolved the issue by revealing an extinct spreading ridge responsible for the development of this basin some 100 million years ago.

Studies in the Antarctic have shown the extent of crustal depression caused by the weight of the overlying ice sheets. This has led to the suggestion that the ice sheet was formerly much larger and that the crust is currently rising following the removal of the ice and its corresponding load.

Overall, ERS-1 has provided profound new insights into the underlying structures of the polar oceans.

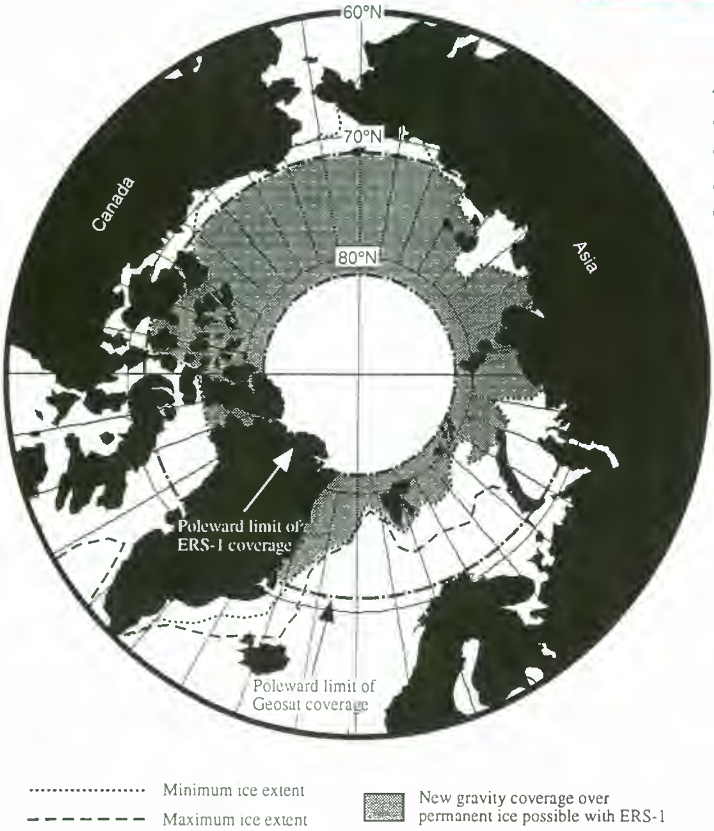

Figure 7.3. This Figure shows the regions of the Earth's geoid mapped for the first time by ERS-1 as a result of the orbital coverage extending to 82°N. ERS-1 is the first satellite carrying a radar altimeter to extend coverage to these regions. Courtesy of S Laxon, Mullard Space Science Laboratory, University College London, UK.

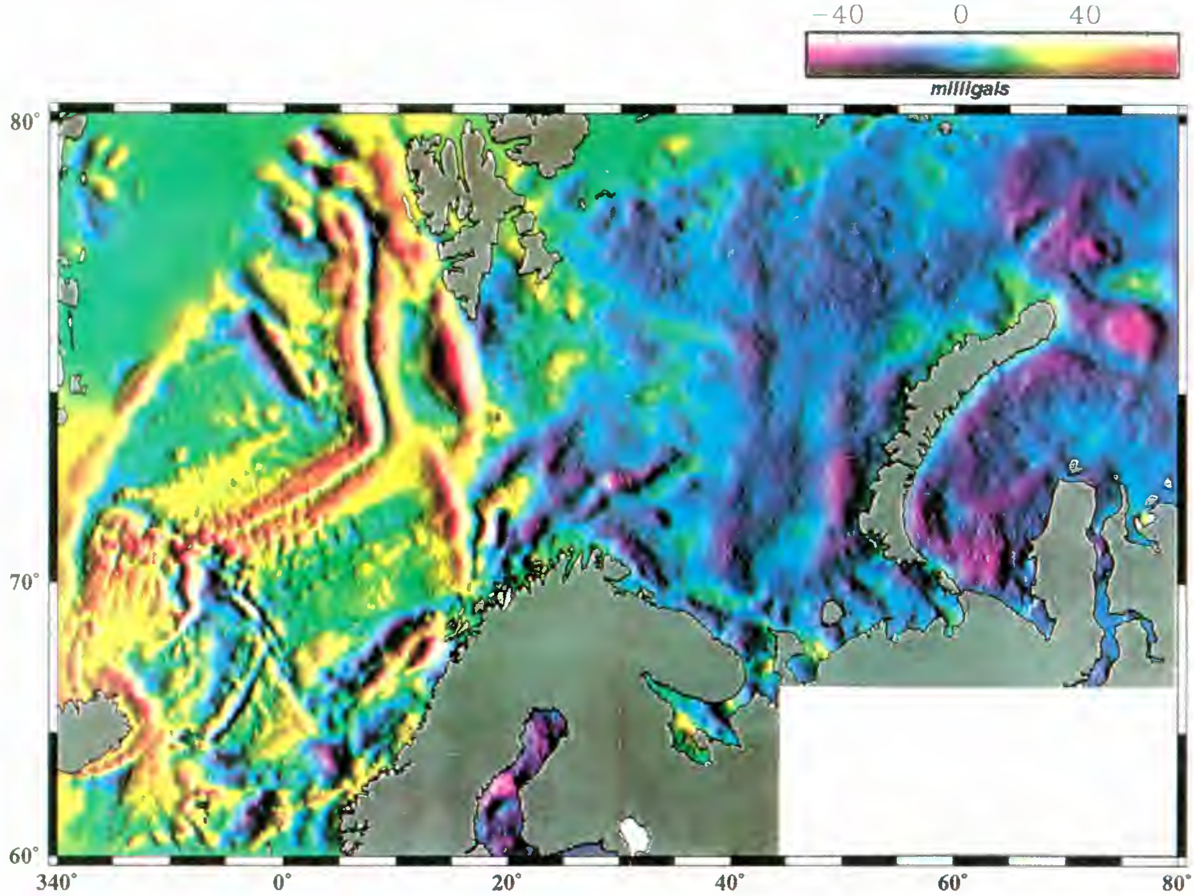

Figure 7.4. A gravity field for the Barents Sea has been determined using all available radar altimeter data. The largest gravity variations occur off the coast of Svalbard (top centre of the image) at the point of the first separation of Greenland from the Eurasian continent some 30 million years ago. An active spreading ridge leading north from Iceland and details of ancient dead rifts and old fragments of previously spreading ridges can be observed. These data are essential to understand the formation and ongoing dynamics of the Arctic Ocean. Courtesy of A Anderson, University of California, Santa Barbara, USA.

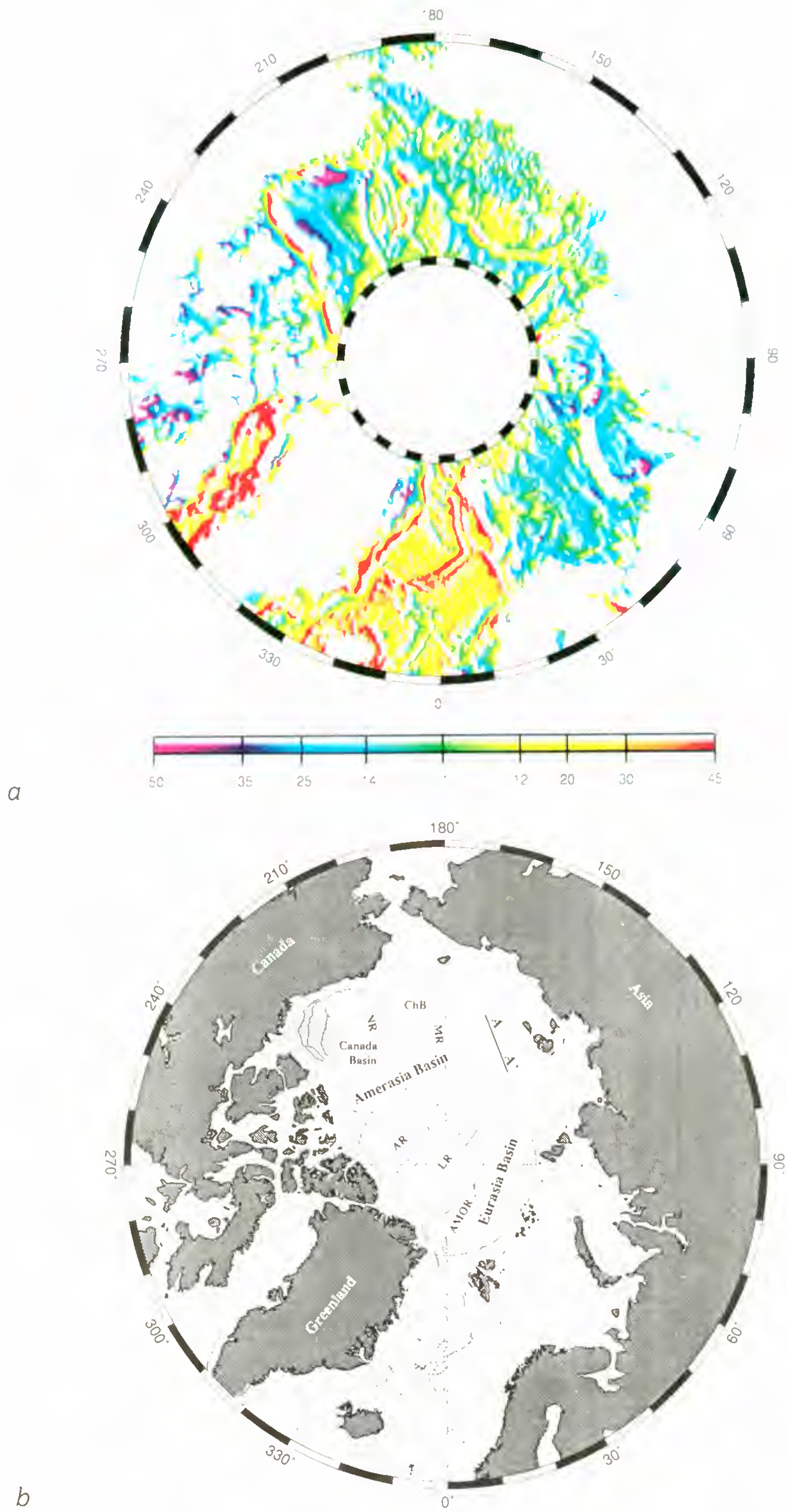

Figure 7.5 a,b. Several important tectonic features of the Amerasian Basin have been clearly demonstrated using ERS-1 radar altimeter data and are shown here. These include the Mendeleev Ridge, the Northwind Ridge and details of the Chukchi Borderland. Of greatest significance is a north-south trending, linear feature in the middle of the Canada Basin at 142°W that apparently represents an extinct spreading ridge that 'died' in the Mesozoic. At its southern end, this lineated gravity low appears to bend in a south easterly direction toward the MacKenzie Delta. This pattern provides evidence that the Canada Basin was formed by the rotation of Arctic Alaska away from the Canadian Arctic islands and by consequent sea floor spreading about a pole in the MacKenzie Delta. Courtesy of S Laxon, Mullard Space Science Laboratory, University College London, UK; D McAdoo, NOAA, Silver Spring, USA. (Published in *Science*, 29 July 1994, vol. 265, pp. 621-624).

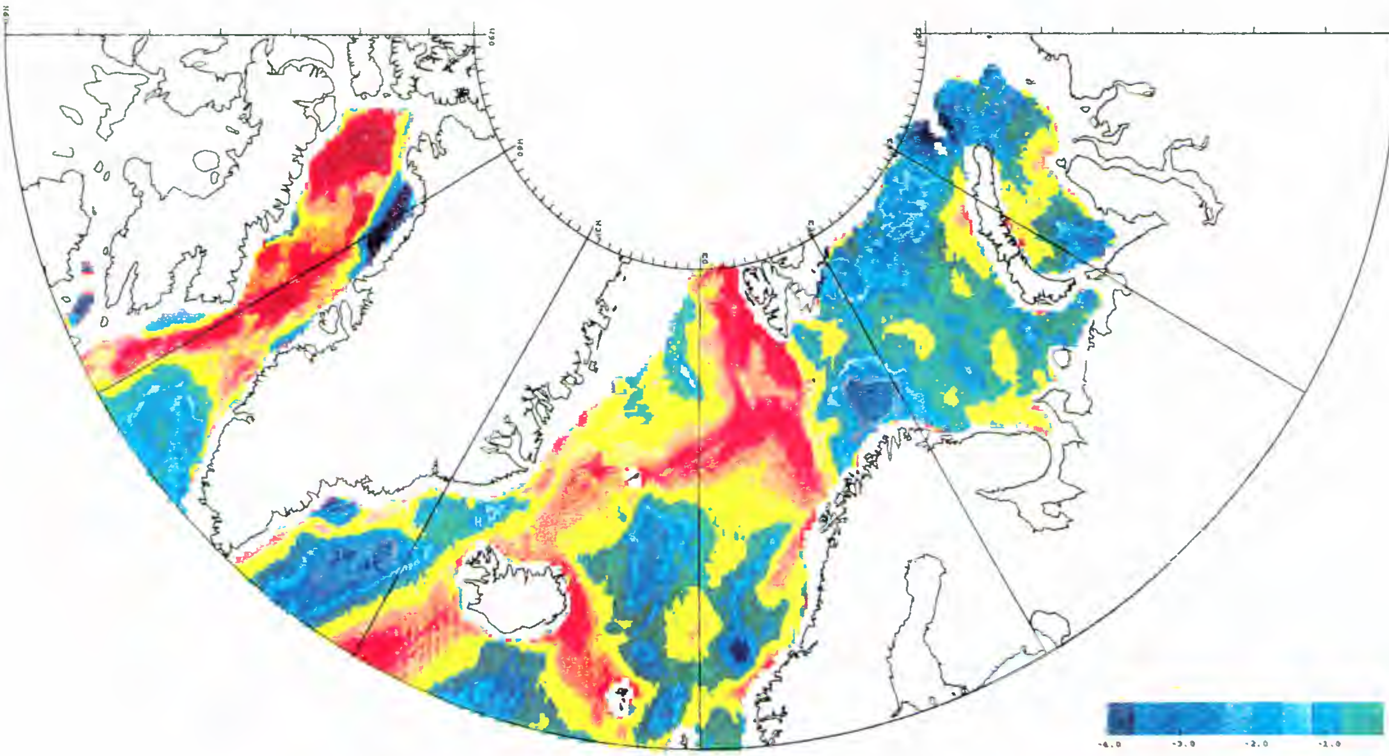

Figure 7.6. The geoid over the Arctic Ocean has been mapped and an interpretation in terms of the geology and geophysics has resulted in the contours of sedimentary basins in the Kara and Barents Seas being drawn. In the Kara Sea, a series of gravity lows can be observed which do not show up in other maps of sedimentary thicknesses. In the Barents Sea, the Hammerfest, Nordkapp, Olga and Sorkapp basins can be seen. These are some of the first maps of geological structures in the Arctic Ocean. Courtesy of F Blanc, CLS, Toulouse, France.

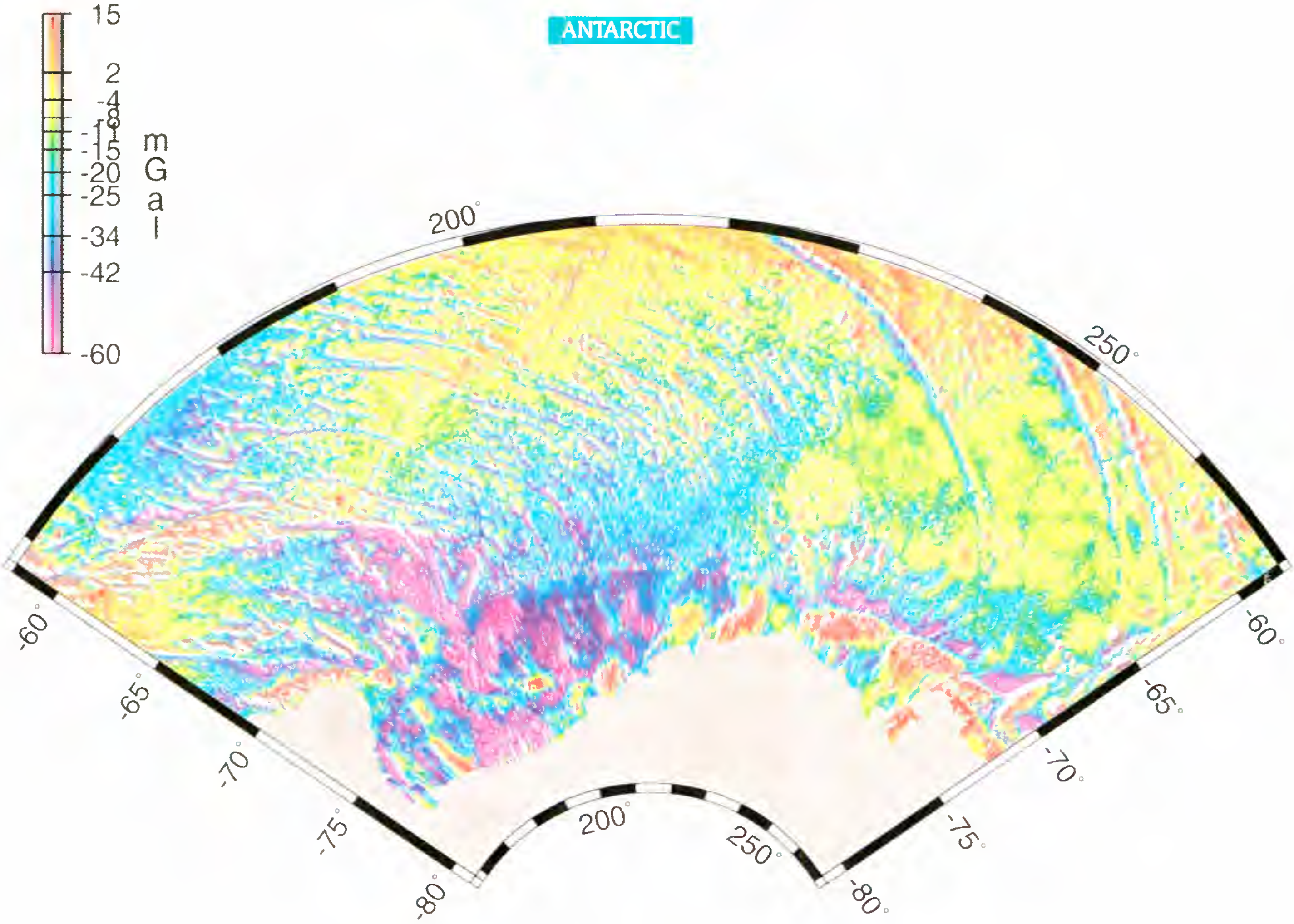

Figure 7.7. A high-resolution gravity field has been determined using Geosat and ERS-1 radar altimeter data for the Ross and Amundsen region of the Southern Ocean. A gravity low was observed in the Ross Sea which may constrain models of recent ice sheet history in the Ross Embayment. It is suggested that one-half of this gravity low could be attributed to the effect of the loading of the crust by the weight of a much larger sheet during the early Holocene (10 000 to 20 000 years ago). It is proposed that such an ice sheet may have covered most of the Ross Sea continental shelf extending north to the edge of the shelf and that the continental shelf in this region may still be rebounding toward a state of isostatic equilibrium. Courtesy of D McAdoo, NOAA, Silver Spring, USA

7.3. Tectonic structures under the ocean

In many of the polar areas, ERS-1 provides the only spaceborne altimeter data available. In other parts of the ocean, such data are available from the earlier Geosat mission and from the contemporary Topex/ Poseidon. Using the ERS-1 data with information from these satellites allows a gravity map with a 0.1° grid to be produced. Using the ERS-1 radar altimeter data from the geodetic phase a gravity map with a 0.05° grid has been produced, a much higher resolution than formerly available. As well as the large-scale features identified above, smaller-scale features have also been identified. Two examples are presented, one is a map showing continental spreading features in the Norwegian-Iceland-Greenland Sea related to the mid-Atlantic ridge, and the second shows gravitational features in smaller areas such as the North Sea.

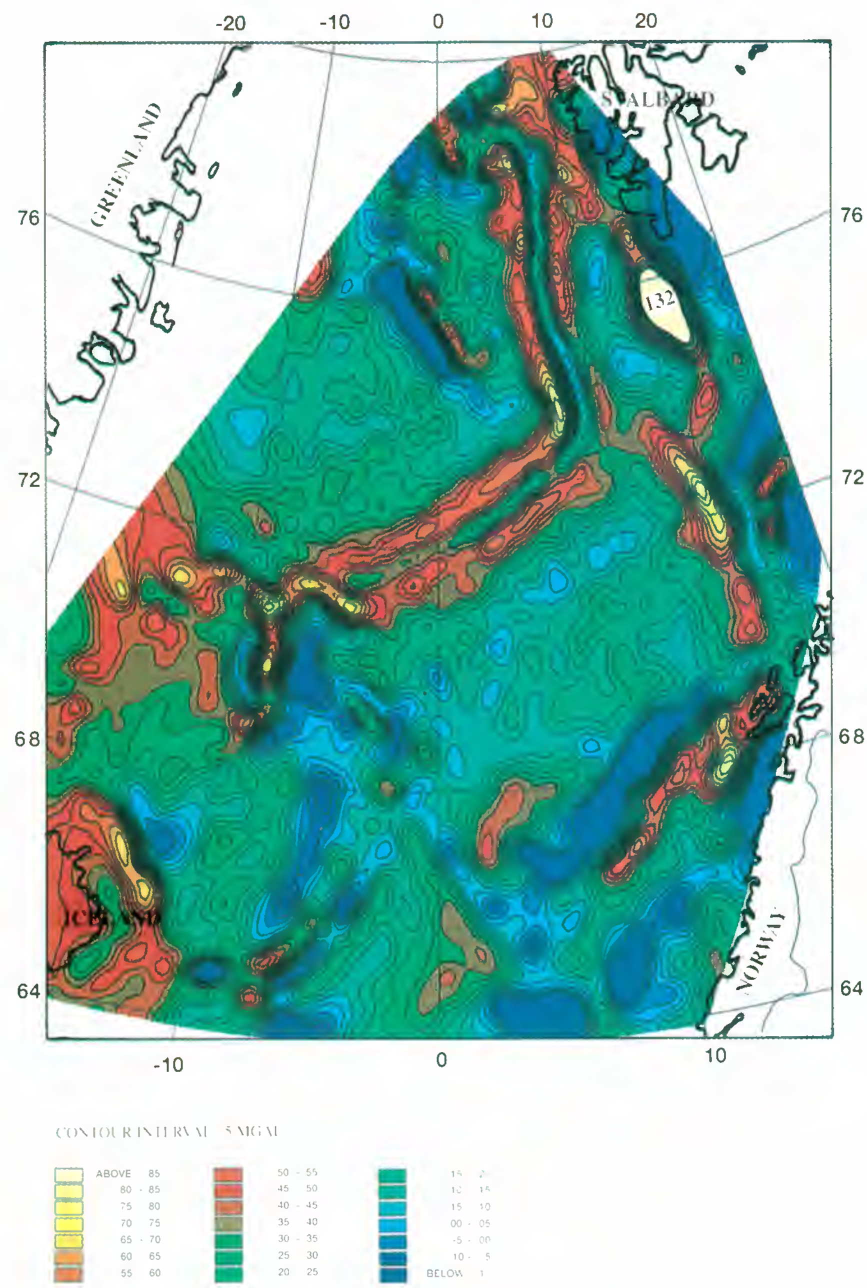

a

Figure 7.8 a,b,c. The gravity field in the Norwegian-Iceland-Greenland Sea has been mapped using ERS-1 radar altimeter data from the 35 day multi-disciplinary phase (Fig. a) and from the geodetic phase (Fig. b). The maps display many geological features relating to continental spreading along the extension of the mid-Atlantic ridge. The dense coverage of the geodetic phase has provided additional information on the fault and fracture zones associated with the three main segments of the ridge, the Kolbeinsey, the Mohns and the Knipovich ridges. Figure c is a location map of the area. Courtesy of P Knudsen, O Andersen, National Survey and Cadastre, Copenhagen; C Tscherning, University of Copenhagen, Denmark. (Figures 7.8 a and c published in *Geophys. Res. Letters*, Sept. 1992, vol. 19, No. 7, pp. 1795-1798).

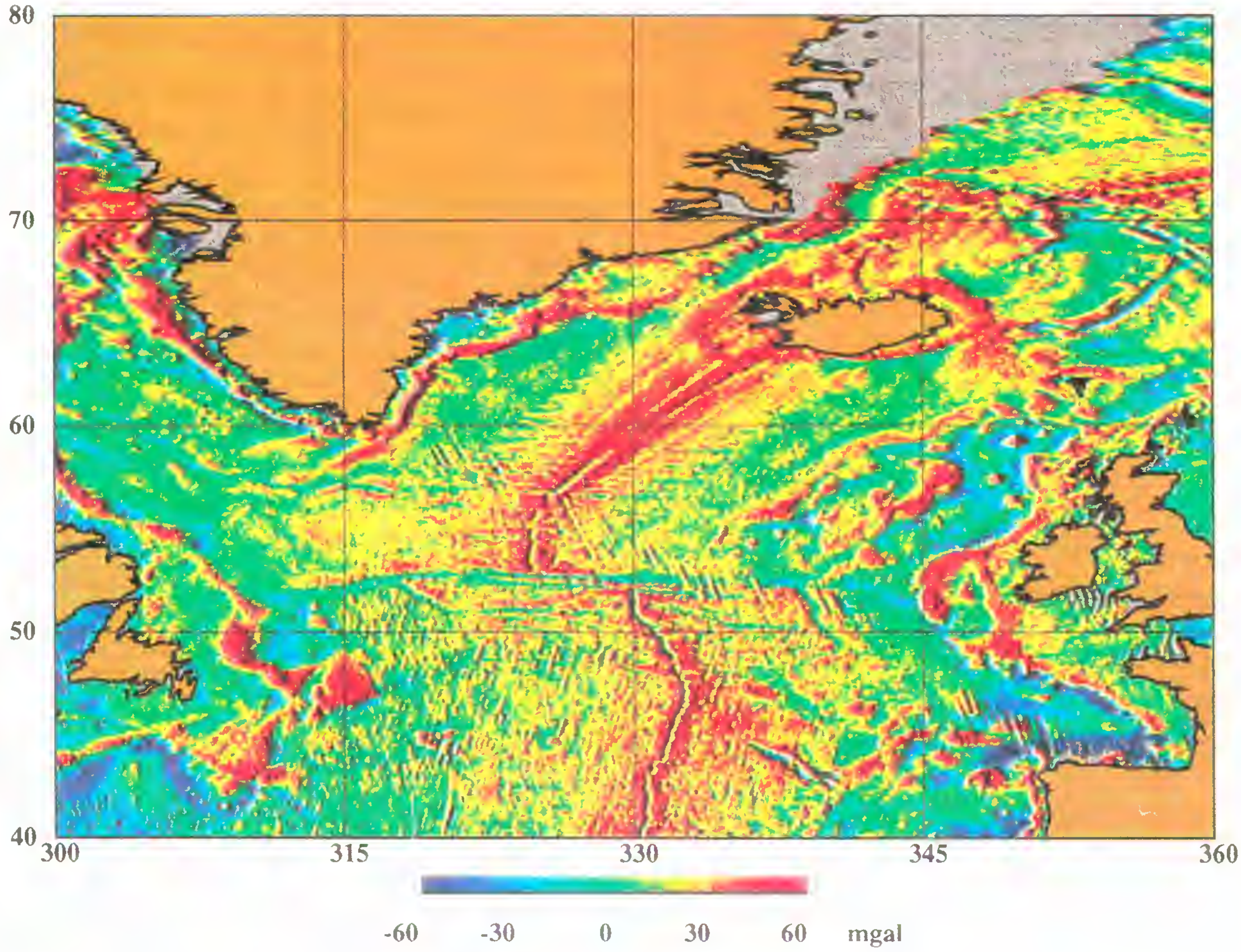
80
70
60
50
40
300
315
330
345
360
-60
-30
0
30
60
mgal

b


GREENLAND
SPITSB. FZ
MOLLOY R.
MOLLOY FZ
HORNSUND
SPITSBERGEN
Hovgaard FZ
BOREAS
BASIN
GREENLAND FZ
KNIPOVICH
RIDGE
G-ESCP
GREENLAND
BASIN
BARENTS SHELF
SENJA FZ
MOHNS RIDGE
W. JAN MAYEN
FZ
LOFOTEN
BASIN
Lofoten FZ
ICELAND
PLATEAU
EXT AX.
JAN MAYEN RIDGE
KOLBEINSEY RIDGE
Lofoten-Vesterålen
Vøring FZ
VØRING
VØRING P. ESCP
PLATEAU
E. JAN MAYEN FZ
JAN MAYEN F
NORWAY
AEGIR RIDGE
BASIN
DENMARK
STRAIT
ICELAND
LEGEND
Depth contour (100 m)
Plate boundary
Main structural feature
DSDP/ODP drill site
Marginal High
ICELAND
FAEROE RIGDE
FAEROE Is
F-SHETL ESCP
F-Shetl
Channel
NORTH
SEA
NORWAY

c

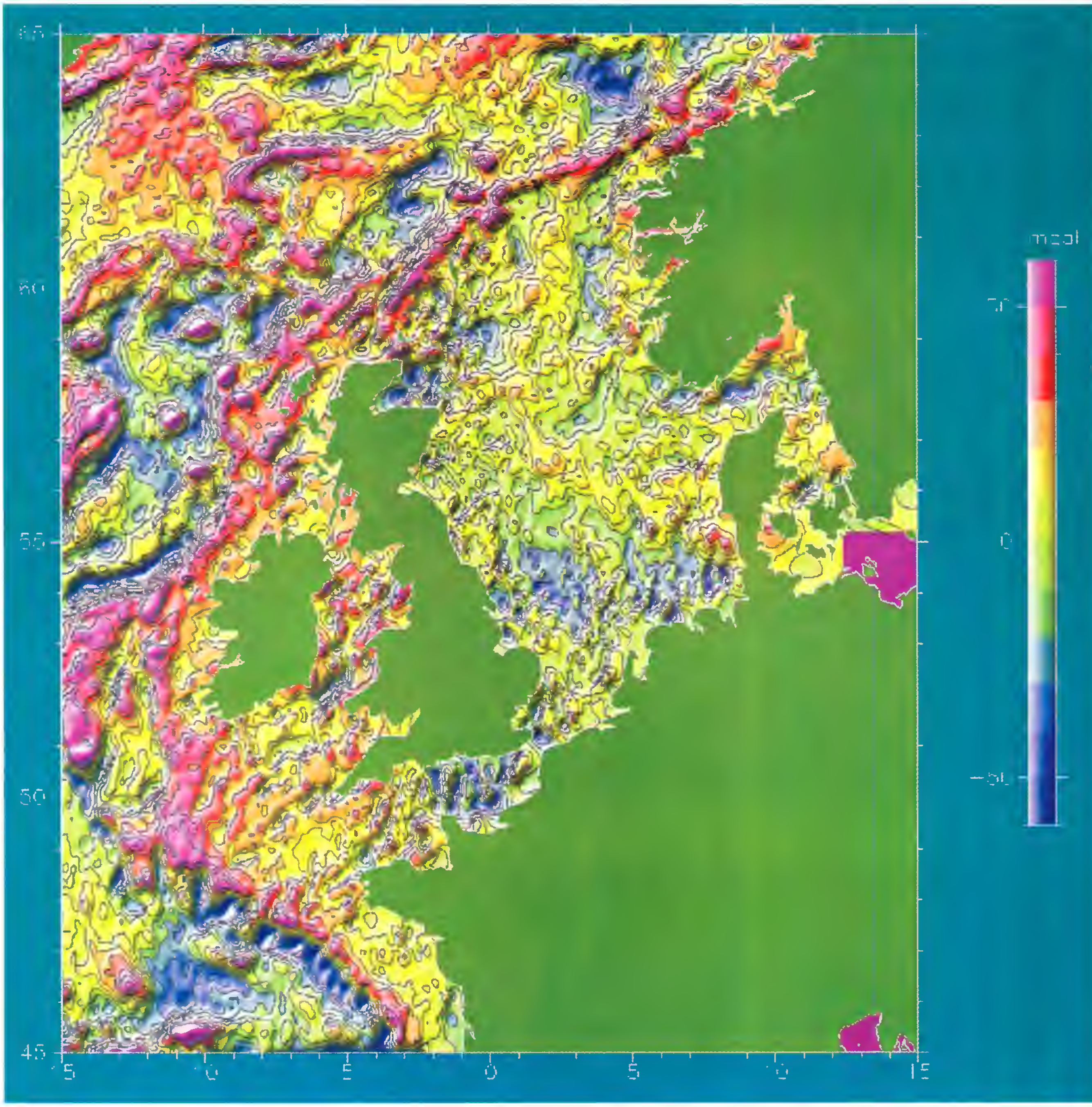

Figure 7.9. The Figure shows the mean sea surface over the Continental Shelf in the Northeast Atlantic. It is based on altimeter data from three satellites, namely Geosat (November 1986 – November 1989), ERS-1 (January 1992 – January 1993), and Topex/Poseidon (October 1992 – October 1993). In this area the mean sea surface largely coincides with the marine geoid because no strong currents are present. As a result the sea surface is due to the local mass concentration on and beneath the ocean floor. Linear structures known as 'Graben' can be observed to the southwest of Denmark. These are remnants of faults which originated when the North Sea was geologically much more active. Although these 'Graben' are presently filled with sediment and cannot be seen on bathymetric charts, they show as local disturbances in the gravity field.

The map derived from ERS-1 shows excellent correspondence with conventional gravity maps for this area thus proving the validity of this analysis in small, enclosed regions. It can now be expected that altimetry studies will be applied to further small regions and will permit the cost-effective production of gravity maps for geological study. Courtesy of M Naeije, Delft University of Technology, The Netherlands.

7.4. Tectonic structures on land

Imagery from the ERS-1 SAR have been used to identify fault lines in the land surface. The availability of SAR data for this purpose is very valuable as many of the areas of interest are covered either by cloud or vegetation, which make the use of alternative data sources difficult.

Two particular examples are presented, one for northern Turkey and the other for New Guinea. In both cases, displacement along a fault has been measured.

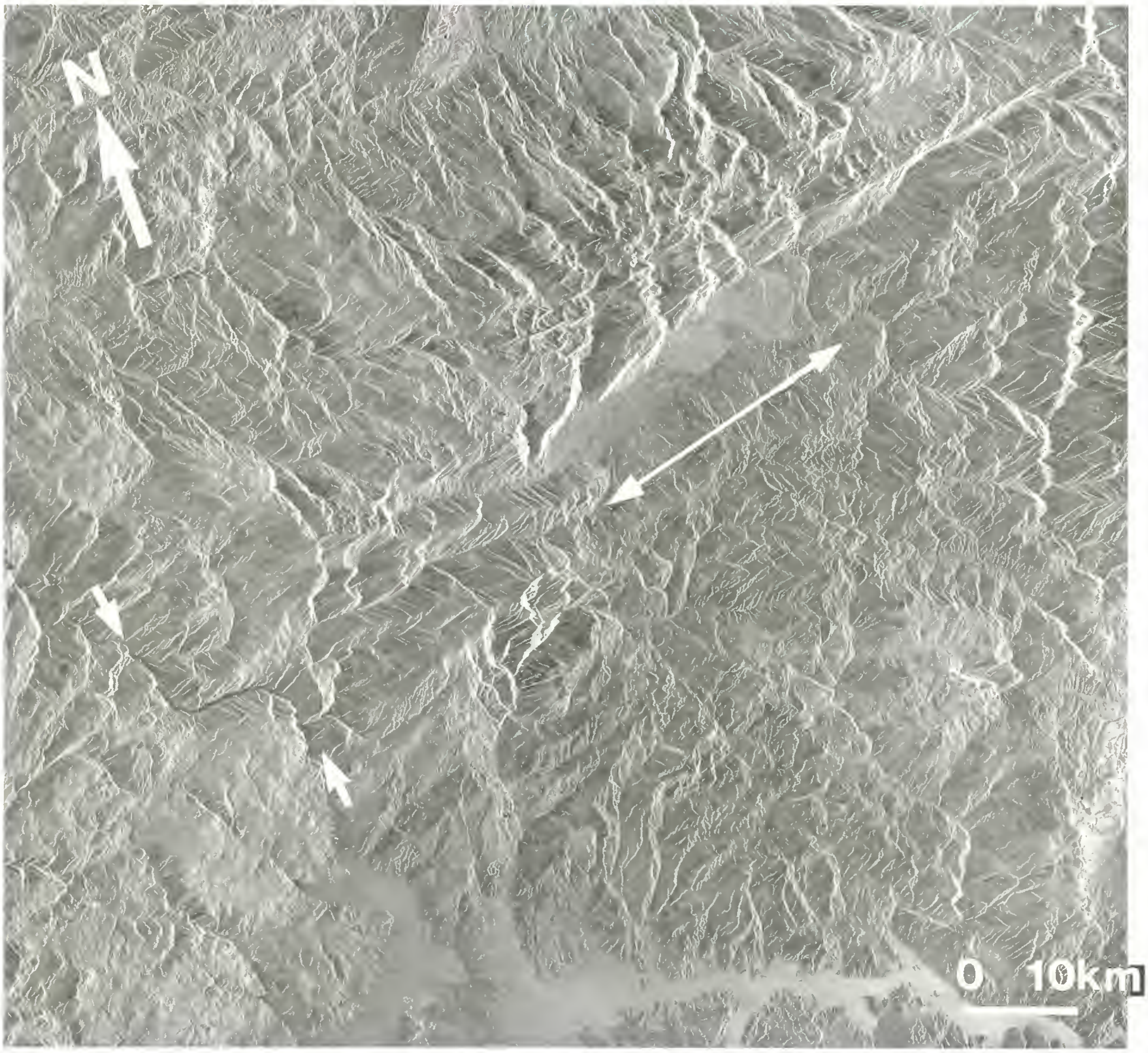

Figure 7.10. In the field of fundamental research in plate tectonics, it has been shown that ERS-1 SAR images can be used to measure horizontal displacements along active faults, in order to estimate the rate of movement of such faults. This type of study contributes to a better understanding of plate tectonic processes. This ERS-1 SAR image of northern Turkey shows the Ovacik fault. The fault crosses the image from NE to SW. Displacement of the Euphrates river is 9 km (see offset arrows). The length of the Ovacik basin is 20 km (see double arrow). Consequently the finite displacement for less than 13 million years is estimated between 9 and 20 km. Courtesy of J Chorowicz, University Pierre and Marie Curie, Paris, France.

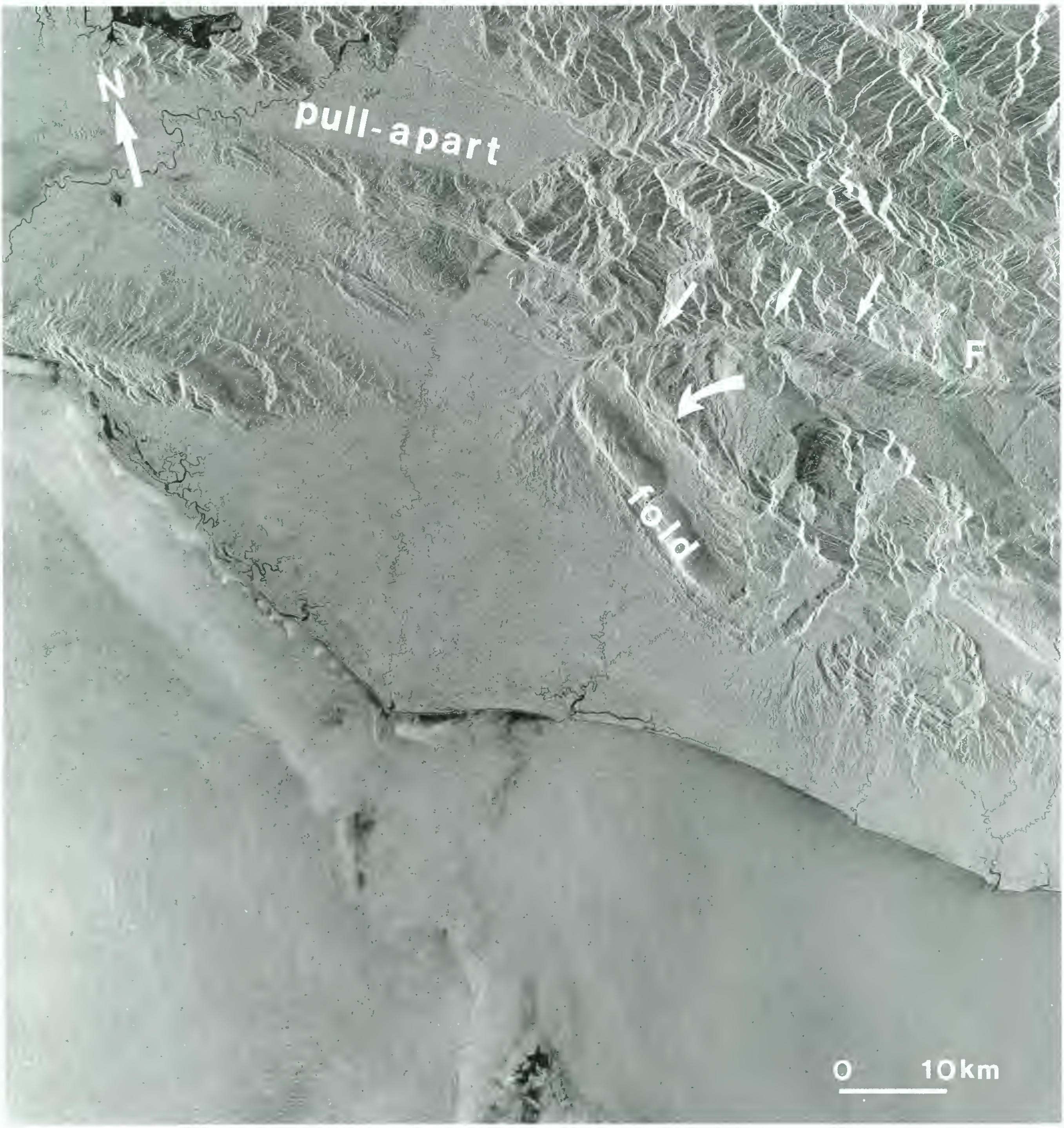

Figure 7.11. In New Guinea, in the southern flank of the Fold and Thrust belt of Irian Jaya, an active belt is developing along strike-slip faults, including pull apart basins. This ERS-1 SAR image has given evidence of the very beginning of lateral movement of a large block. Small arrows indicate specific morphological features called scarplets. These are not yet eroded sections of an active normal fault (F), related to gravitational movement towards the SW (large arrow) inducing folding and thrusting. Courtesy of M Pubellier, University Pierre and Marie Curie, Paris, France.

7.5. The effects of earthquakes and volcanoes

Detailed mapping of the structure of the Earth's surface and detection of relative surface changes can be used to examine the causes and effects of earthquakes. The ERS-1 SAR can achieve these objectives using interferometry.

SAR interferometry has been demonstrated with data from earlier SAR missions such as Seasat (USA) and SIR-B (Shuttle Imaging Radar). However, ERS-1 data have made major advances in the use of the method for measuring crustal motion. This contribution is mainly due to the very large number of images being generated which allow the mapping of large portions of the land surface, thus increasing the probability of spotting interesting events. The quality of the data and the precision of the track repetition is contributing by allowing a useful proportion of the acquired swaths to be combined with interferometry. Finally the long life achieved by ERS-1 SAR is allowing surveys over several years. No other past or present spaceborne system possesses this combination of attributes.

The advent and growth of differential SAR interferometry is, for the first time, permitting movements in the Earth's surface as small as a few centimetres to be detected and mapped over large areas. This provides the basis for detailed study of many dynamic features of the Earth's crust including earthquakes and volcanoes.

Even though interferometry was not included in the original specifications for ERS-1, the potential it has demonstrated for studying crustal deformation makes it one of the most dramatic new advances achieved by the mission.

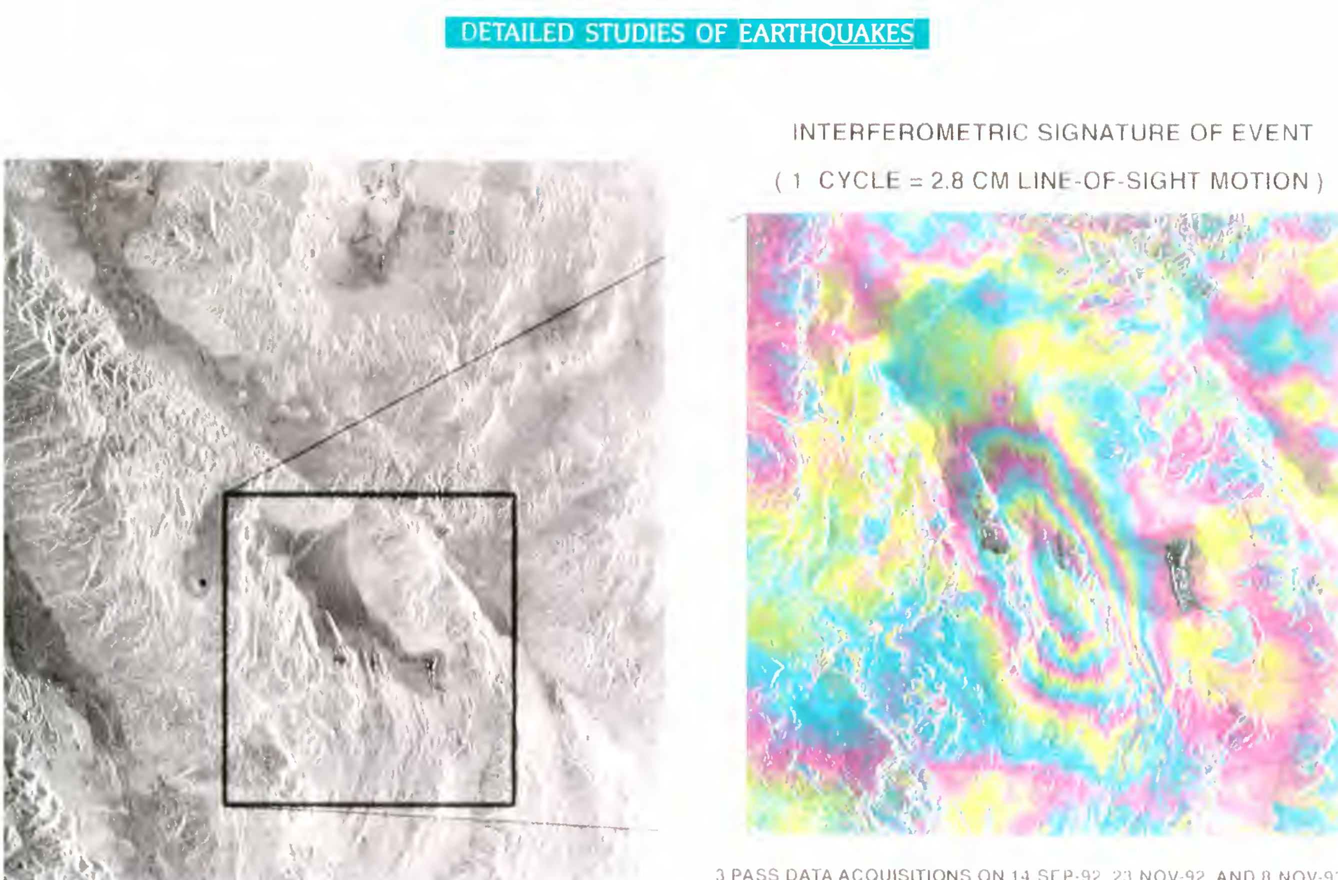

Figure 7.12. The 17 May 1993 earthquake in Eureka Valley, California (magnitude 6.1) was studied using SAR interferometry. The seismic record of the earthquake shows that it occurred on an approximate north to south normal fault plane, steeply dipping to the west. This ERS-1 SAR image is shown together with the interferogram which in this case was produced using three ERS-1 SAR images. The interferogram clearly depicts elongated, concentric ring-shaped fringes resulting from the subsidence of the fault block overlying the inclined fault surface, consistent with a normal fault mechanism. The maximum vertical displacement measured at the surface of the hanging wall is 10-12 cm. The Eureka Valley earthquake occurred in a remote region where no geodetic measurements were taken. The interferogram obtained with the ERS-1 SAR data provides the only geodetic information of the surface displacement associated with this earthquake. Courtesy of G Peltzer, JPL, Pasadena, USA.

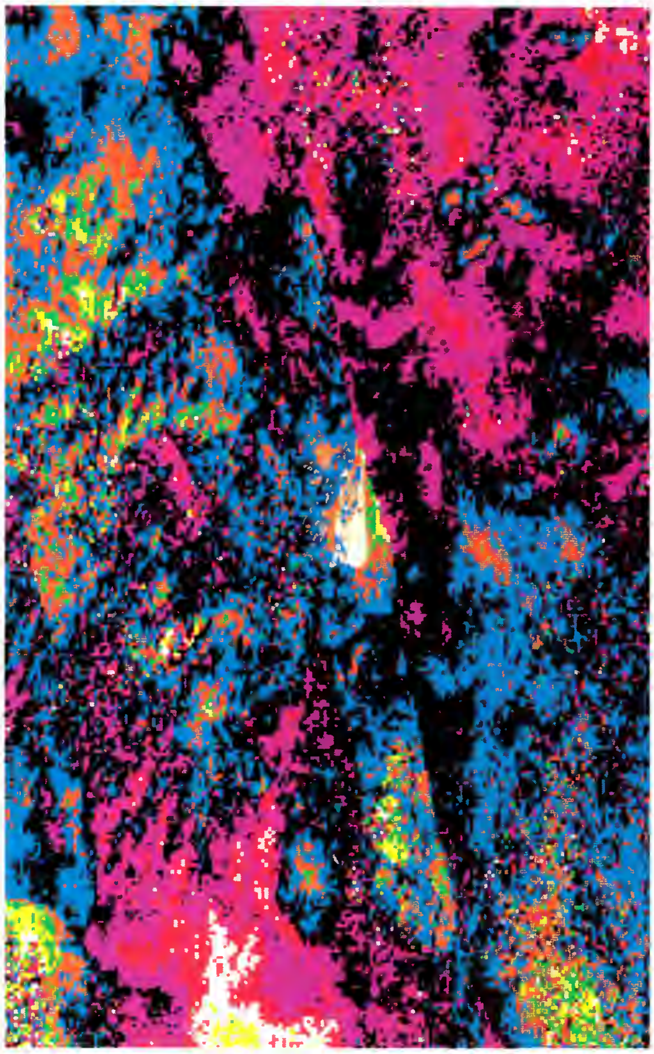

a

b

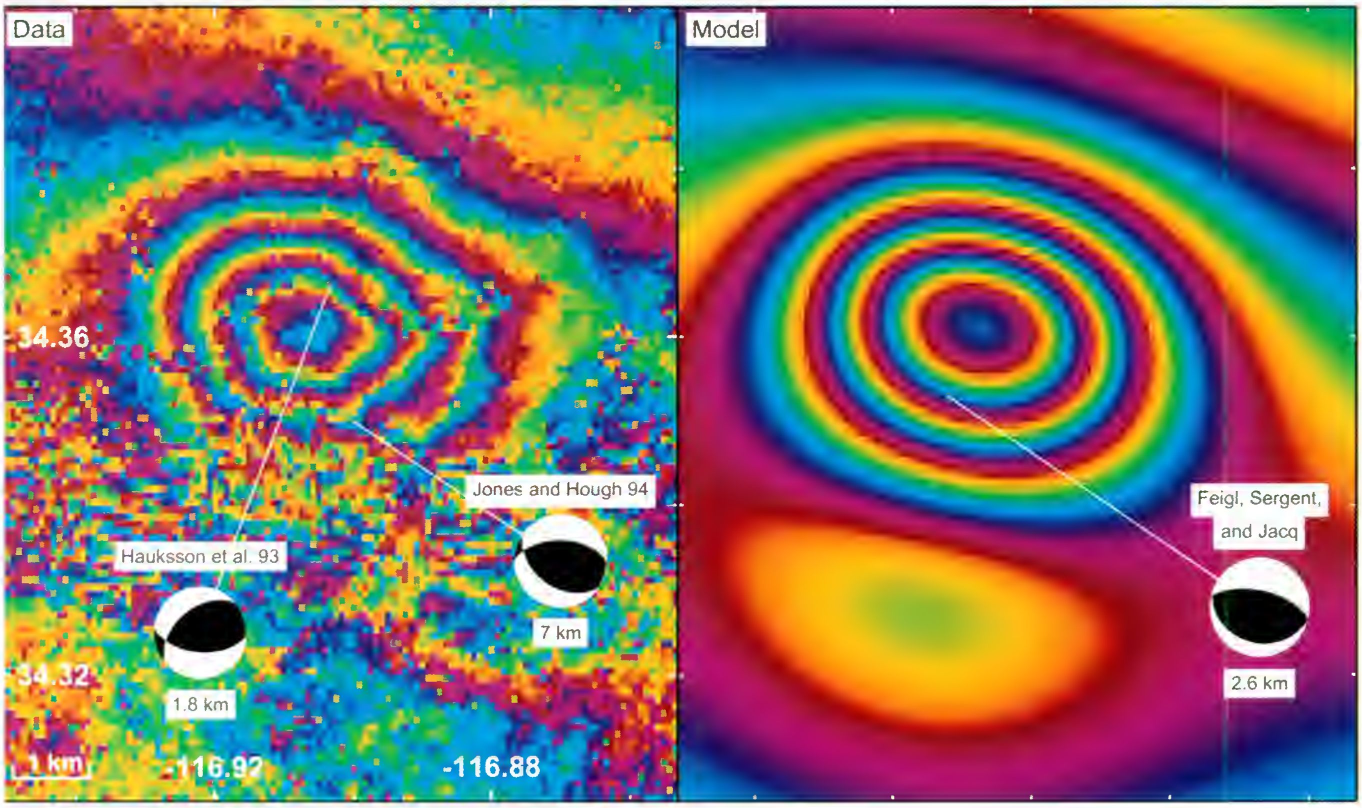

Figure 7.13 a,b. The 28 June 1992 Landers earthquake (magnitude 7.5) activated segments of the central Mojave fault zone in California. Field and seismological investigations show right lateral slips reaching maxima of 4 and 6 m, respectively 10 and 40 km north of the main shock.

The complete surface displacement in the range direction was mapped using ERS-1 SAR interferometry and fault ruptures have been measured with a precision better than 1 cm. Lines of discontinuity along three fault segments as far as 100 km from the main rupture were found. In the vicinity of the main break, the interferogram reveals complexities and dense patterns of fringes, attesting to large displacement gradients.

Figure a shows an example of a small movement along a fault to the north of the main Landers earthquake area. This image demonstrates the ability of the interferometry technique to locate small-scale movements. Figure b shows a comparison of an ERS-1 SAR interferogram with an equivalent prediction of fault movement from a theoretical model. The area of this movement is about 10 km across. The use of interferometry to validate models in this way allows improved understanding of earthquake mechanisms. Areas of model success can be confirmed and areas of disagreement explored to provide a more detailed understanding.

Figures a and b illustrate that ERS-1 SAR interferometry can identify not only the large-scale patterns but also smaller movements which could be difficult to locate using geodetic stations alone. Such measurements are needed to place the Landers earthquake sequence in the context of a recurring seismic cycle over California. The analysis of variations in the distribution of slip on the fault plane has brought new insights into fault geometry and slip distribution. Courtesy of D Massonnet, CNES, Toulouse, France.

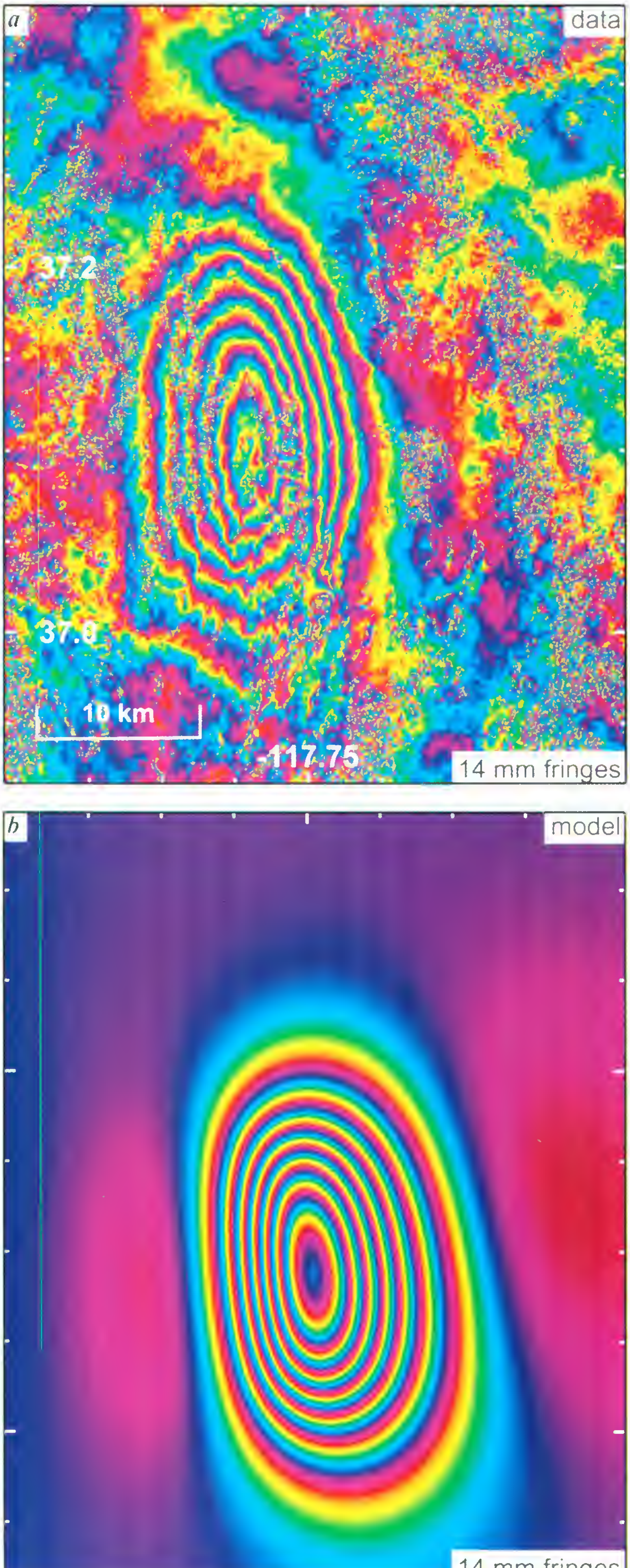

Figure 7.14 a,b. An interferogram for the Eureka Valley earthquake (17 May 1993), with a model prediction for the same event. In this example, the interferometry image was produced using two SAR images together with a digital elevation model of the local topography.

Clear similarities can be seen between the two images in terms of their overall shape. The differences between the images are also important since they highlight discrepancies and small-scale features requiring further investigation. Courtesy of D Massonnet, CNES, Toulouse, France.

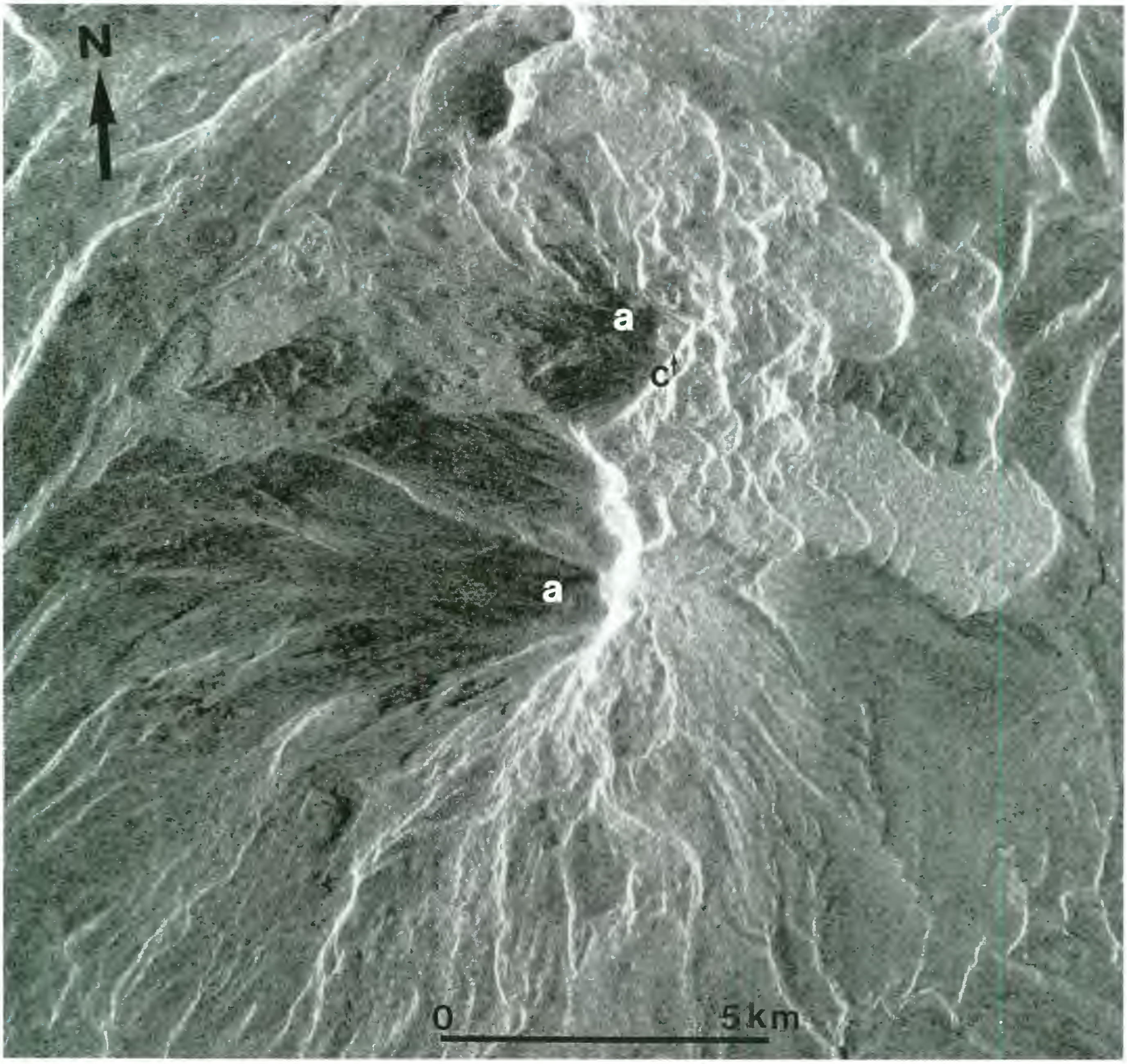

Figure 7.15. Few data have been collected while volcanoes are erupting due to the danger of collecting in-situ data and the large amount of cloud often associated with eruptions. ERS-1 SAR can penetrate through this cloud to provide data about the evolution of the eruption which can also be used for disaster monitoring. The information will also enable decisions to be made on the distribution of aid and the movement of population when volcanoes occur in heavily populated areas. The window taken from the SAR image is over the still erupting volcano Subancaya in southern Peru. The crater of the volcano (c) is rapidly changing with time. It is also possible to see the evolution of the ash cover (a) deposited on volcano Sabancaya and on the nearby larger Ampato volcano. The light grey lava flows belong to ancient eruptions. Courtesy of J Chorowicz, University Pierre and Marie Curie, Paris, France.

a

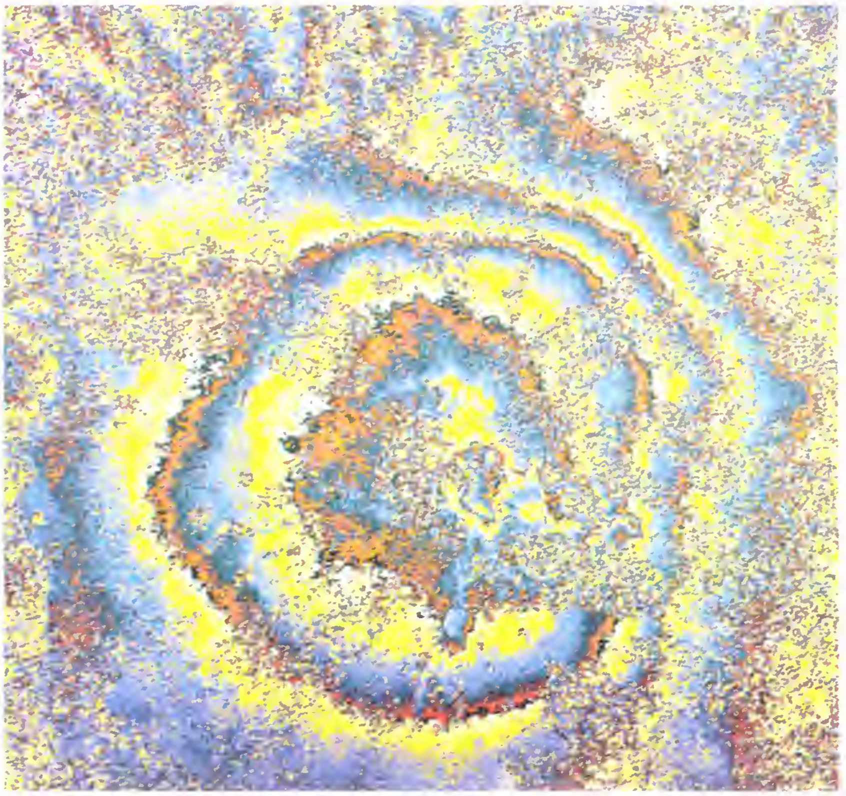

b

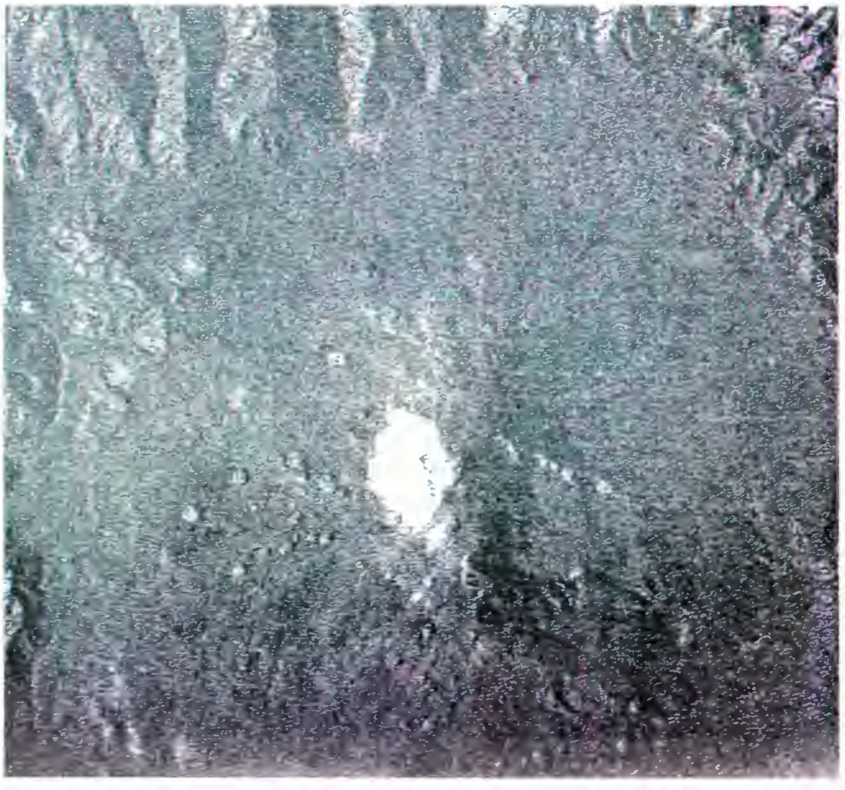

Figure 7.16 a,b. Initial work is being undertaken using interferometry for monitoring the shape of volcanoes. Figure a shows an example of an interferogram for Mount Etna, Sicily, together with a map projection of an ERS-1 SAR image (Fig. b). A topographic model of Mount Etna was used to eliminate the basic effects of topography from the image.

After processing for the effects of topography, the pattern of the fringes indicates a deflation of the structure of the volcano. This technique has the potential to provide new information about volcanoes to increase our understanding of the evolution and perhaps help in the predictions of eruptions.

Associated with this work, areas of landsliding have been noted close to the top of the volcano. Monitoring such small features with interferometry is difficult, and consequently this is an area of ongoing research in both this and other areas. Courtesy of D Massonnet, CNES, Toulouse, France.

Figure 7.17 a,b,c,d,e. ERS-1 SAR interferometry has been used to produce a map of Mount Vesuvius, Italy. The area covered by this image is 20 × 20 km. The height accuracy in the areas of optimum coherence is of the order of 6 m. (a): image of Vesuvius taken from a descending pass; (b): the associated interferometric fringes; (c): image from an ascending pass; (d): the interferometric fringes for image c; (e): an elevation map obtained from the combination of the two interferometric images. The elevation map was prepared to study subsidence in the Campanian area and has allowed the surveillance of small crustal movements. Courtesy of F Rocca, Polytechnic of Milan, Italy.

a

b

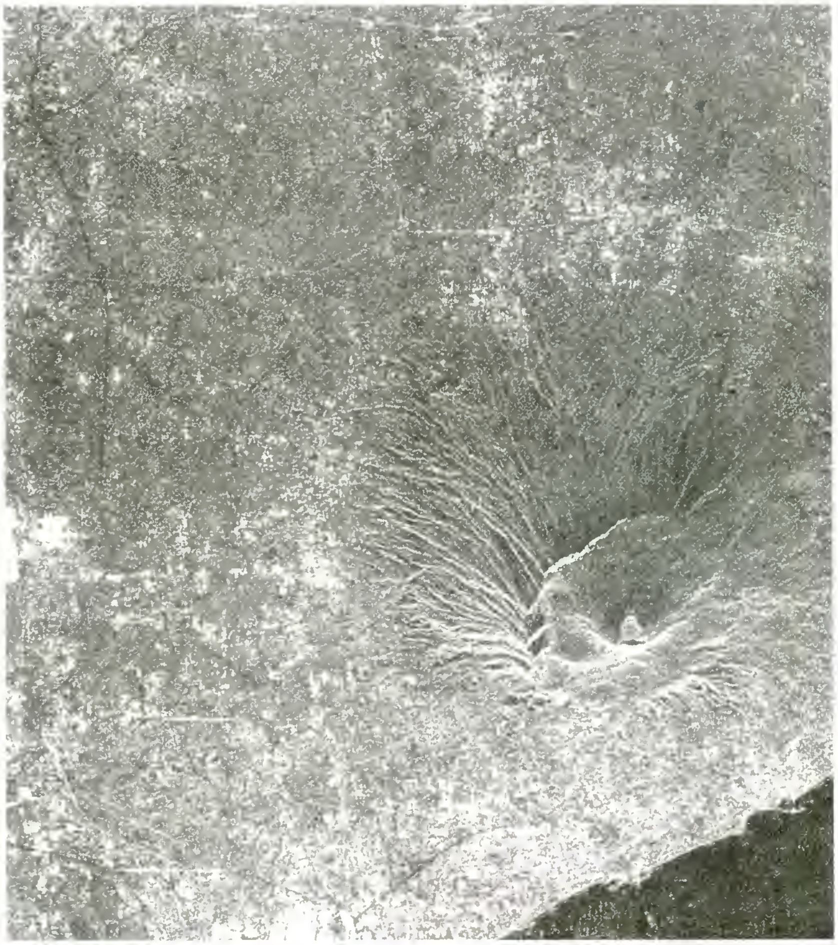

c

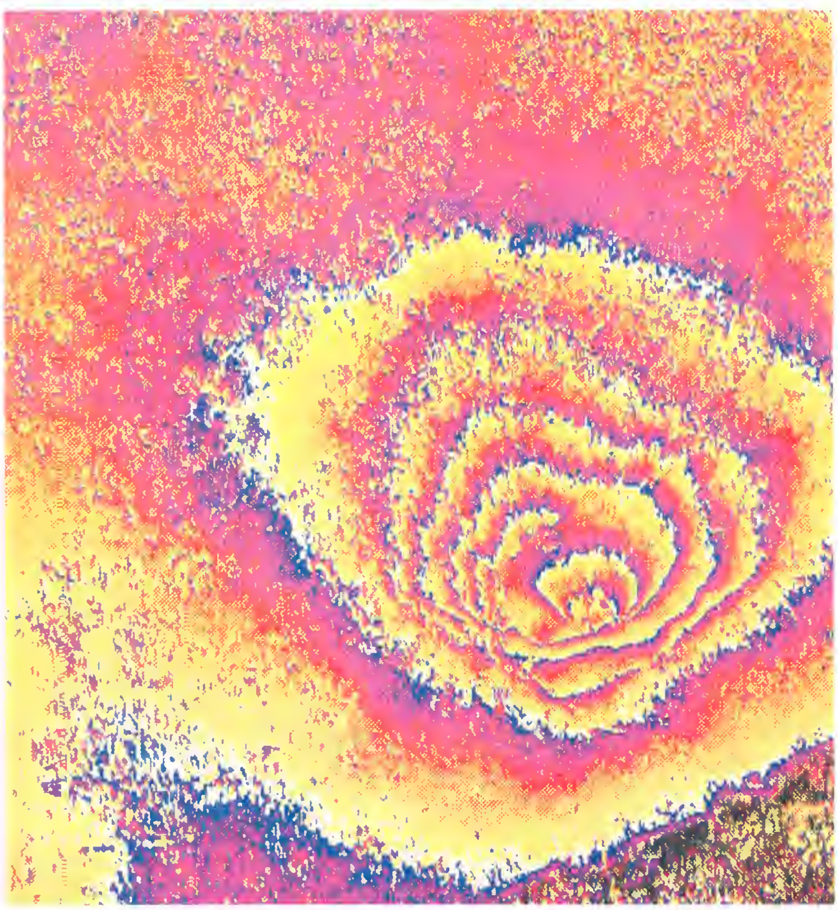

d

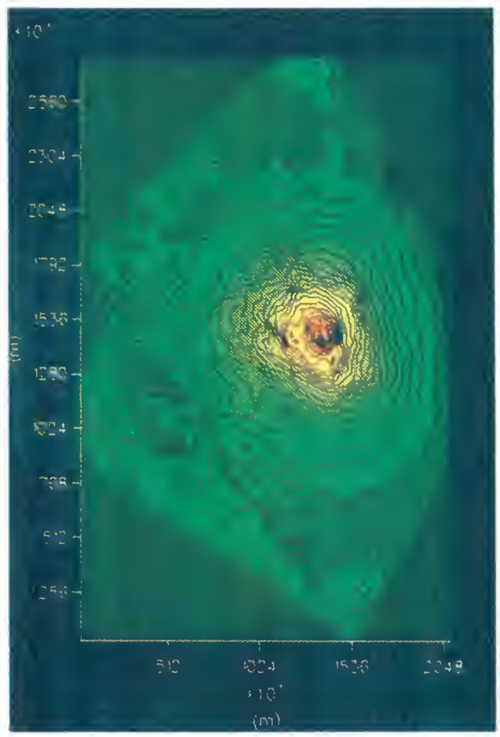
2560
2304
2048
1792
1536
1280
1024
768
512
256
(m)
512
1024
1536
2048
(m)

e

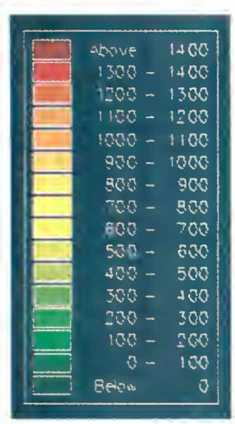
Above 1400
1300 - 1400
1200 - 1300
1100 - 1200
1000 - 1100
900 - 1000
800 - 900
700 - 800
600 - 700
500 - 600
400 - 500
300 - 400
200 - 300
100 - 200
0 - 100
Below 0

8. SUMMARY OF RESULTS AND OVERVIEW

8.1. A major scientific contribution

The examples of scientific research which have been presented in this document show that ERS-1 is making a major contribution to the measurement and monitoring of the Earth's surface. High standards of instrument performance and new levels of consistency, accuracy and coverage have been achieved. These are creating exciting new opportunities for scientific discovery.

Even though this document contains only a selection of research using ERS-1 data and many of these areas of research are still at an early stage, it is clear that a broad range of science is already benefiting from the data. As seen in Figure 8.1, progress is evident across many scientific disciplines in:

- Improving the accuracy of mapping environmental parameters;
- Performing localised studies from which a greater understanding of processes can be determined;
- Developing, testing or initialising models to generate more accurate forecasts.

Even within three and a half years of receiving the first data from ERS-1, the improved predictions for weather, ocean state and sea ice are already being applied to economic activities. This is demonstrating the operational potential of the mission. Volume II of this series of documents on ERS-1 achievements will explain how operational applications are taking place. In the land sciences, complex issues of variability and scale dependency, inherent in the terrestrial environment, mean that economic applications are less well developed.

The validation of forecasting models is a particularly important application for ERS-1 data. Systematic comparison of observations with model predictions gives scientists more confidence in the forecast. The use of ERS-1 data is also highlighting areas in which a greater understanding and modelling capability can be developed over the next 10 years.

A particularly good indicator of the high standards of scientific research which are being achieved is the range of articles accepted for publication in refereed scientific journals. Figure 8.2 shows a variety of scientific journals where the ERS-1 research is sufficiently important to feature.

Figure 8.1. Summary of the science achievements presented in this document.

AREA	Chapter 2 GLOBAL OCEAN AND ATMOSPHERE
MAPPING AND MONITORING	Ocean surface wind field Ocean surface waves Ocean topography Sea surface temperature Atmospheric aerosols
PROCESS UNDERSTANDING AND TREND DETECTION	Ocean / atmosphere interaction Ocean wave trends Ocean current processes anc variations Large scale phenomena (eg El Niño, Rossby waves)
MODELLING FOR FORECASTING AND PREDICTION	NWP - better ocean wind and wave fields Tides - better models in polar regions Climate - ocean current patterns, sea surface temperature, aerosol effects

Chapter 3 **REGIONAL OCEAN**	Chapter 4 **SEA ICE**	Chapter 5 **GLACIOLOGY AND SNOW**	Chapter 6 **LAND**	Chapter 7 **THE EARTH'S DYNAMIC CRUST**
cean surface wave patterns urface slicks	Sea ice extent, type, concentration and thickness Sea ice movement Iceberg movement	Ice elevation on major ice sheets Extent of major ice sheets Extent of small ice sheets and temperate glaciers Snow distributions	Global vegetation cover monitoring Crop cover and status Forest cover and status Soil moisture Surface water coverage Wetland vegetation cover Surface lithology Surface landforms Elevation and general land cover	Overall shape of the Earth (geoid) Regional geoid variations Earth's gravity field Land displacements resulting from earthquakes Changing shape of volcanoes during eruptions
egional & small scale atmospheric features, eg monsoons, cyclones cean dynamics - eddies, frontal boundaries	Mass balance of major ice sheets - ice thickness and movement at the edges Understanding structures within sea ice Heat fluxes within the ocean Ocean convective processes through sea ice patterns Ocean / atmosphere fluxes Effects of ocean current and associated temperature changes	Mass balances of major ice sheets - changes in thickness Mechanisms of ice movement within ice sheets Changes in ice sheet elevation patterns	Trends in global vegetation cover Regional soil moisture variation Local soil moisture patterns in relation to river flows	Tectonic structure under the oceans and sea ice Processes governing continental drift Effects of earthquakes on surrounding areas
egional circulation stuarine processes oastal sediment transport and erosion limate - better understanding of thresholds, land / atmosphere interactions, land ocean interactions	Wave modelling - better boundary conditions Climate - identification of possible thresholds for sea level rise	Modelling ice sheet dynamics - prediction of possible rapid changes, release of ice to the sea Climate - mass balance Hydrology - changing snow patterns, drainage basins within ice sheets	Climate - land / atmosphere interactions, land ocean interactions Hydrology and agriculture models - early stages of application	Tectonic models of continental and regional development Earthquake models

Figure 8.2 This mosaic features several of the covers of recent scientific journals which have published results from the use of ERS-1 data.

8.2. Current status of scientific understanding

GLOBAL OCEAN AND ATMOSPHERE

Advances in knowledge of the general ocean circulation and the major current and tidal systems of the world's oceans have been made using ERS-1 data in conjunction with Topex/Poseidon data. This is a critical element in global climate research. In particular, a deeper understanding of the evolution of the 1991-1993 Southern Oscillation (El Nio and La Nia) and the modelling of tides has been possible.

ERS-1 is providing an opportunity to study ocean winds and waves in a way not previously contemplated because of the lack of data, particularly in the Southern Ocean. This is helping to develop forecasting accuracy, applicable both for environmental research and economic activities. Features at the ocean/atmosphere interface have been detected which were not previously identified in the global forecasts.

Also at the ocean/atmosphere interface, improved accuracy in global sea surface temperature data is supporting investigations of the mechanics of climate change. Perhaps the most important application of these data in the long term is their contribution to the global climate record and the statistical detection of average changes in climate.

Measurement of atmospheric aerosols is also an important result. This has the potential to provide new data on the reflective properties and variability of atmospheric aerosols. Such data will be used, for example, in modelling investigations of the effect of aerosols on atmospheric and terrestrial heating and cooling rates. The ability to monitor the effects of high aerosol concentrations following volcanic eruptions is also important for climate studies.

REGIONAL OCEAN AND ATMOSPHERE

The ability to detect and measure regional atmospheric features is crucial for understanding processes as a basis for coupled ocean/atmosphere models. This is contributing to modelling climate response as well as understanding wind characteristics and their impacts in coastal zones.

Major ocean features such as eddies and internal waves can be discriminated, aiding our understanding of ocean circulation at regional and global scales. Important and promising contributions have been made in this area with the use of ERS-1 SAR to detect internal waves and surface slicks.

Along coastal boundaries and shelf regions, human activities are extensive. Pollution and environmental change have a significant impact. Monitoring of coastal erosion, sedimentation and shallow water bathymetry is providing promising results. This is an emerging area of science with a great need for improved forecasting. A key challenge is to acquire sufficient data on coastal hydrodynamics to develop a more in-depth understanding of the relationship between the forcing processes and erosion or deposition. The ability to collect high-resolution images giving near shore information on wind and wave regimes is expected to yield important insights into processes and current flow features in coastal and estuarine waters. This is essential to water quality monitoring and prediction.

SEA ICE

Although many important sea ice characteristics are known from other observations, ERS-1 SAR images provide a resolution which allows characteristics to be measured more accurately than with earlier instruments. Detailed phenomena such as leads, polynyas, multiyear ice floes, land fast ice, shear zones in the ice pack, ridges, ice edge eddies, ice tongues and wave propagation in the ice edge region have all been clearly visualised. The ERS-1 radar altimeter and ATSR have both been used successfully for mapping sea ice extent.

Valuable information has been gained on ice movement from ERS-1 SAR and scatterometer data, allowing the investigation of phenomena at the ice margin through sequential observations. Continental scale maps have been used to analyse large-scale changes in the ice, combined with information on winds and surface temperatures in the adjacent open water.

GLACIOLOGY AND SNOW

The contributions of ERS-1 to glaciological research have exceeded the original expectations of scientists. ERS-1 has demonstrated unique capabilities for observing the polar ice sheets and in providing data for mass balance assessments and modelling dynamics.

Repeat surveys of ice sheet topography by means of ERS-1 and ERS-2 altimetry will result in significant improvements in the estimation of the overall mass balance of the Greenland and Antarctic ice sheets, presently one of the main open questions in glaciology. The monitoring of ice boundaries and iceberg discharge by means of SAR will add to this assessment. Significant improvements will also be obtained for the mass balance of individual catchment basins, of outlet glaciers and of ice shelves. Together with the information on ice velocity fields, derived by means of SAR interferometry, this will help to improve modelling of ice dynamics and ice-atmosphere-ocean interactions. The development of a comprehensive model of the West Antarctic Ice Sheet and its ice streams to predict its future behaviour may then be feasible.

The regular survey of major glacier regions around the world during the lifetime of ERS-1 and ERS-2 will help to obtain a global picture of glacier variations and establish improved models of glacier-climate interaction.

The production of snow cover maps in mountainous areas and the detection of snow boundaries over temperate glaciers has also been greatly improved with ERS-1 data. Improved information on the extent and temporal dynamics of the snow cover are stimulating the development of physically based models for snow melt runoff, particularly tuned for the input of spatially distributed data. In the future, these models will provide new insights in the interaction mechanisms between atmospheric parameters and hydrological storage terms. The development of models for snowmelt runoff forecasting will follow from this.

LAND

A key stimulus to terrestrial applications is that due to their ability to penetrate cloud, the ERS-1 microwave instruments have enabled reliably timed imaging which has not been available from optical sensors. Descriptions of processes at the land surface are required to conduct research in climatology and to support economic activities.

Effective classifications of major land use types have been achieved at the global scale. At a more localised scale, initial work has commenced on classifying crop types, discriminating forest cover and retrieving hydrological variables. Preliminary results are encouraging: separation of different crop types has been demonstrated; indicators of soil moisture under specific conditions have been derived; and overbank water detected during flood events. Further scientific investigation remains to be undertaken. Processing of multitemporal data is a key technique in this area, where an accurate detection of change is critical.

Increasingly accurate topographic, geologic and other thematic maps are also now being produced using ERS-1 data. The coverage remains to be extended to meet global needs, although many maps of areas where information was previously unavailable are being used within the scientific community as well as by hydrocarbon and mineral exploration companies.

Techniques such as interferometry, made possible by the stability of the ERS-1 SAR instrument and its orbit characteristics, are producing accurate three-dimensional digital maps and detecting movements to an accuracy of a few centimetres. This stimulates exciting areas of science in geomorphology, geology and cartography and opens up opportunities for future economic applications. It can be expected that the coming years will show further major improvements in the applications of these advanced mapping and deformation monitoring methods.

THE EARTH'S DYNAMIC CRUST

Neither the mission objectives nor the instruments were originally designed primarily to conduct studies of the solid Earth. However, the excellence of the engineering and the innovation of the scientists has provided a range of benefits beyond the original expectations. The realisation of this potential resulted in the geodetic phase (168-day orbit), which has been a unique and invaluable opportunity to make significant advances in geodynamics. Unprecedented high spatial resolution is leading to improved measurements of the marine gravity field.

Mapping the polar ocean topography in zones covered by sea ice has not been possible prior to ERS-1. The new information is now leading to major new discoveries on the formation of the Arctic Basin and providing a new insight into the geology of this vast region.

Interferometry is providing a great potential for analysing earthquakes and changes in the shape of volcanoes. The ability to monitor even small movements at the surface across large areas is providing a unique dataset for process studies and model validation.

8.3. Maximising scientific return

The scientific use of ERS data continues to expand. For many disciplines, the data continuity which will be provided by the future ESA missions ERS-2 and Envisat, will enable processes to be more fully understood and conclusions to be drawn about environmental changes.

It is anticipated that to maximise the scientific return from ERS-1, ERS-2 and Envisat, and consequently to maximise economic and environmental policy benefits, three steps are needed:

1. The methods of data analysis and retrieval of geophysical parameters have to be further improved. Reliable and high-quality data must be made available to scientists. This task includes theoretical analysis, inter-comparisons of retrieval techniques developed at different institutes and laboratories and evaluation of the accuracy of retrieved geophysical

data. Based on commonly agreed methods, high-level datasets of geophysical parameters need to be generated, validated and made available for scientific investigation.

2. Validated geophysical data from ERS instruments then need to be intercalibrated and interpreted together with complementary data to maximise the spatial and temporal coverage. This enables features and processes to be measured in more detail.

   Even with the various complementary datasets provided by the ERS-1 mission itself, scientists are generally at the stage of single-instrument applications. The evolution of techniques for data synergy are a very important next step. For example, understanding the ocean and climate relationship will require the simultaneous use of all available information, including that from ERS, other Earth observation missions and in-situ instruments. This type of work is now being attempted, and results will become available over the next few years.

3. The development of improved models of the Earth system, adjusted to maximise the benefits of ERS data, is required. This development is being stimulated, particularly within numerical weather prediction modelling. As assimilation techniques and numerical weather prediction models improve, data from ERS-1 and ERS-2 will have an increasing impact on forecasts. For example, now that the value of the ERS-1 scatterometer data has been established, and their strengths and error characteristics are better known, the analysis used to produce initialisation data for models is being optimised to take full advantage of the ERS-1 data. The parallel development of new variational assimilation schemes will allow the ERS-1 scatterometer data to have a greater impact on forecast capability.

8.4. International Cooperation

More that 275 research groups worldwide, involving at least 2000 scientists are using ERS-1 data directly. A much larger number have access to the data as part of higher degrees within institutes and universities. Certainly within Europe, ERS-1 is stimulating an expanding range of remote sensing activities. This is providing an expanding resource base for operational applications development. Improved data, improved models and a growing pool of highly skilled professionals are all necessary to realise the value of economic applications of Earth observation data.

International cooperation within the science community has been enhanced by the provision of ERS-1 data. Participants in global research programmes such as the World Climate Research Programme (WCRP) and the International Geosphere and Biosphere Programme (IGBP) are deriving increased benefits from ERS-1 data. The provision of satellite data to these programmes is now a primary need which is being coordinated internationally through the Committee for Earth Observing Systems (CEOS).

In parallel, there is also a growing interest from developing and eastern European countries to use ERS-1 data to help address key environmental and resource management issues. New data acquisition facilities in developing countries, links with scientists in European and North American laboratories, training and pilot project initiatives supported by ESA, the European Union, the United Nations and other international bodies all contribute to increasing the effective use of data in these areas.

8.5. Future views of the Earth

ERS-1 is providing a global perspective for environmental science. Important scientific advances have been achieved worldwide in many national and international endeavours. ERS-2 will continue this data supply and also provide extended measurement capabilities through the incorporation of additional and improved instruments.

In the longer term, Envisat will provide the European element of the International Earth Observation System. Together with ADEOS from Japan and EOS from USA, this will provide the main information source for scientists to observe, monitor and understand Earth processes in the first part of the 21st century.

9. ACKNOWLEDGEMENTS

ESA is grateful to the following scientists who have provided expertise throughout this project.

Gudmandsen P	*Technical University of Denmark, Copenhagen, Denmark*
Hasselmann K	*Max Planck Institute for Meteorology, Hamburg, Germany*
Kerr Y	*LERTS/CESBIO, Toulouse, France*
Minster J-F	*CNES-CNRS/GRGS, Toulouse, France*
Rapley C	*International Geosphere Biosphere Programme, Stockholm, Sweden*
Robinson I	*University of Southampton, UK*
Rott H	*University of Innsbruck, Austria*
Wooding M	*Remote Sensing Applications Consultants, Alton, UK*

ESA would like to acknowledge the support of the following scientists who attended the review meeting at ESRIN on 6-7 October 1994, and also to those who provided information for the meeting.

Adragna F	*CNES, Toulouse, France*
Bruening C	*University of Hamburg, Germany*
Carsey F	*JPL, Pasadena, USA*
Chorowicz J	*University Pierre and Marie Curie, Paris, France*
Gudmandsen P	*Technical University of Denmark, Copenhagen, Denmark*
Johannessen J	*ESTEC Noordwijk, The Netherlands*
Kerr Y	*LERTS/CESBIO, Toulouse, France*
Kramer O	*GeoScan, Hildesheim, Germany*
Laxon S	*Mullard Space Science Laboratory University College London, UK*
Lichtenegger J	*ESRIN, Frascati, Italy*
McNutt L	*Alaska SAR Facility, Fairbanks, USA*
Rapley C	*International Geosphere Biosphere Programme, Stockholm, Sweden*
Rémy F	*GRGS-CNES, Toulouse, France*
Robinson I	*University of Southampton, UK*
Thompson T	*Swedish Meteorological & Hydrological Inst., Norrkoping, Sweden*

ESA would like to thank the following for providing the contributions used in this document.

Allen M	*Rutherford Appleton Laboratory, Didcot, UK*
Alpers W	*University of Hamburg, Germany*
Andersen O	*National Survey and Cadastre, Copenhagen, Denmark*
Anderson A	*University of California, Santa Barbara, USA*
Anzenhofer M	*GeoForschungsZentrum, Potsdam, Germany*
Aschbacher J	*Joint Research Centre, Ispra, Italy*
Askne J	*Chalmers University of Technology, Gothenberg, Sweden*
Atlas D	*NASA Goddard Space Flight Center, Greenbelt, USA*
Bakker J	*Synoptics, Wageningen, The Netherlands*
Bamber J	*Mullard Space Science Laboratory, University College London, UK*
Bhandari S	*Indian Space Research Organisation, Ahemedabad, India*
Bijker W	*Intl. Institute for Aerospace Survey & Earth Sciences, Enschede, The Netherlands*
Bindschlader R	*NASA Goddard Space Flight Center, Greenbelt, USA*
Blanc F	*CLS, Toulouse, France*
Blyth K	*Institute of Hydrology, Wallingford, UK*
Bourgez-Chavez L	*ERIM University of Michigan, Ann Arbor, USA*
Bruening C	*University of Hamburg, Germany*
Campbell W	*US Geological Survey, Tacoma, USA*
Carsey F	*Jet Propulsion Laboratory, Pasadena, USA*
Cavanie A	*Ifremer, Plouzane, France*
Cazenave A	*GRGS-CNES, Toulouse, France*
Cheney R	*NOAA, Silver Spring, USA*
Chidley T	*ISPAN, Flood Action Plan, Bangladesh*
Chorowicz J	*University Pierre and Marie Curie, Paris, France*
Colony R	*University of Washington, Seattle, USA*
Corves C	University of Edinburgh, UK
Cotton D	*James Rennell Centre for Ocean Circulation, Southampton, UK*
Deroin J-P	*French Geological Survey, BRGM, Orléans, France*
Deséve D	*University of Quebec, Montreal, Canada*
Desjardins R	*University of Quebec, Montreal, Canada*
Diament A	*Scott Polar Research Institute, Cambridge, UK*
Doake C	*British Antarctic Survey, Cambridge, UK*
Donlon C	*University of Southampton, UK*
Dowdeswell J	*Scott Polar Research Institute, Cambridge, UK*
Dowman I	*University College London, UK*
Dundas R	*University of Leicester, UK*
Durdan S	*Jet Propulsion Laboratory, Pasadena, USA*
Engelhardt H	*California Institute of Technology, Pasadena, USA*
Eyre J	*ECMWF, Reading, UK*
Fahnstock M	*NASA Goddard Space Flight Center, Greenbelt, USA*
Fatland D	*University of Alaska, Fairbanks, USA*

Font J	*Institut de Cinces del Mar CSIC, Barcelona, Spain*
Frison P	*CESR, Toulouse, France*
Frolich R	*British Antarctic Survey, Cambridge, UK*
Gaffard C	*ECMWF, Reading, UK*
Gagliardini D	*CONICET/CAERCEM, Buenos Aires, Argentina*
Gatto L	*US Army Corps of Engineers, Hannover, USA*
Gerreno M-C	*CNES-CNRS/GRGS, Toulouse, France*
Goldstein R	*Jet Propulsion Laboratory, Pasadena, USA*
Gower J	*University of British Colombia, Sidney, Canada*
Gudmandsen P	*Technical University of Denmark, Copenhagen, Denmark*
Guillaume A	*ECMWF, Reading, UK*
Guritz R	*University of Alaska, Fairbanks, USA*
Guymer T	*James Rennell Centre for Ocean Circulation, Southampton, UK*
Hagberg J	*Chalmers University of Technology, Gothenberg, Sweden*
Haines K	*University of Edinburgh, UK*
Halpern D	*Jet Propulsion Laboratory, Pasadena, USA*
Harms J	*Scot Conseil, Ramonville, France*
Hartl P	*University of Stuttgart, Germany*
Hasselmann S	*Max Planck Institute for Meteorology, Hamburg, Germany*
Henebry G	*University of Kansas, Manhatten, USA*
Hensley S	*Jet Propulsion Laboratory, Pasadena, USA*
Hoekman D	*Wageningen Agricultural University, The Netherlands*
Jezek K	*Byrd Polar Research Center, Ohio, USA*
Johannessen J	*ESTEC, Noordwijk, The Netherlands*
Johannessen O	*Nansen Environmental and Remote Sensing Centre, Bergen, Norway*
Jones M	*James Rennell Centre for Ocean Circulation, Southampton, UK*
Kamb B	*California Institute of Technology, Pasadena, USA*
Kasischke E	*Duke University, Durham, USA*
Kerr Y	*LERTS/CESBIO, Toulouse, France*
Knudsen P	*National Survey and Cadastre, Copenhagen, Denmark*
Koopmans B	*Intl. Inst. for Aerospace Survey & Earth Sciences, Enschede, The Netherlands*
Korsnes R	*Norsk Polarinstitut, Oslo, Norway*
Kosmann D	*DLR, Oberpfaffenhofen, Germany*
Kramer O	*GeoScan, Hildesheim, Germany*
Kux H	*INPE, Sao Paulo, Brazil*
Kwok R	*Jet Propulsion Laboratory, Pasadena, USA*
Laing A	*Nat. Inst. of Water & Atmosphere Res., Wellington, New Zealand*
Laxon S	*Mullard Space Science Laboratory, University College London, UK*
Le Toan T	*CESR, Toulouse, France*
Lehner S	*DLR, Oberpfaffenhofen, Germany*
Lemoine G	*Synoptics, Wageningen, The Netherlands*

Lingle C	*University of Alaska, Fairbanks, USA*
Liu A	*NASA Goddard Space Flight Center, Greenbelt, USA*
Livingston G	*NASA Ames Research Center, Moffett Field, USA*
Llewellyn-Jones D	*University of Leicester, UK*
Lorenc A	*UK Meteorological Office, Bracknell, UK*
Magagi R	*LERTS/CESBIO, Toulouse, France*
Mason D	*NUTIS University of Reading, UK*
Massonnet D	*CNES, Toulouse, France*
Matzler C	*University of Bern, Switzerland*
McAdoo D	*NOAA, Silver Spring, USA*
Miller L	*NOAA, Silver Spring, USA*
Minster J-F	*CNES-CNRS/GRGS, Toulouse, France*
Morley J	*Mullard Space Science Laboratory, University College London, UK*
Morrissey L	*NASA Ames Research Center, Moffett Field, USA*
Mougin E	*CESR, Toulouse, France*
Murray J	*Rutherford Appleton Laboratory, Didcot, UK*
Mutlow C	*Rutherford Appleton Laboratory, Didcot, UK*
Naeije M	*Delft University of Technology, The Netherlands*
Peltzer G	*Jet Propulsion Laboratory, Pasadena, USA*
Perlant F	*ISTAR, Toulouse, France*
Pubellier M	*University Pierre and Marie Curie, Paris, France*
Quilfen Y	*Ifremer, Plouzane, France*
Rees W	*Scott Polar Research Institute, Cambridge, UK*
Robinson I	*University of Southampton, UK*
Rocca F	*Polytechnic of Milan, Italy*
Röed L	*The Norwegian Meteorological Institute (DNMI), Oslo, Norway*
Roquet H	*ECMWF, Reading, UK*
Rosen P	*Jet Propulsion Laboratory, Pasadena, USA*
Roth R	*University of Hannover, Germany*
Rothrock A	*University of Washington, Seattle, USA*
Rott H	*University of Innsbruck, Austria*
Roush J	*University of Alaska, Fairbanks, USA*
Rudant J-P	*CEGN/UPMC, Paris, France*
Sandven S	*Nansen Environmental & Remote Sensing Centre, Bergen, Norway*
Saunders M	*Mullard Space Science Laboratory, University College London, UK*
Schweiger A	*University of Washington, Seattle, USA*
Shuchmann R	*ERIM, Ann Arbor, USA*
Shum C	*University of Texas at Austin, USA*
Sievers J	*Institut für Angewandte Geodasie, Frankfurt, Germany*
Stern H	*University of Washington, Seattle, USA*
Stoffelen A	*KNMI, AE de Bilt, The Netherlands*
Tapley B	*University of Texas at Austin, USA*
Thiel H	*University of Stuttgart, Germany*
Toutin T	*Canada Centre for Remote Sensing, Ottawa, Canada*

Tscherning C	*University of Copenhagen, Denmark*
Turner J	*British Antarctic Survey, Cambridge, UK*
Ulander L	*Chalmers University of Technology, Gothenberg, Sweden*
Vachon P	*Canada Centre for Remote Sensing, Ottawa, Canada*
Van Leeuwen H	*Wageningen Agricultural University, The Netherlands*
Vargas G	*University Pierre and Marie Curie, Paris, France*
Vogelzang J	*Rijkswaterstaat, Rijswijk, The Netherlands*
Wadge G	*NUTIS University of Reading, UK*
Wahl T	*Norwegian Defence Research Establishment, Kjeller, Norway*
Wiesmann A	*University of Bern, Switzerland*
Werner C	*Jet Propulsion Laboratory, Pasadena, USA*
Winter R	*DLR, Oberfpaffenhofen, Germany*
Wooding M	*Remote Sensing Applications Consultants, Alton, UK*
Wu X	*University of Stuttgart, Germany*
Zahel W	*University of Hamburg, Germany*
Zavody A	*Rutherford Appleton Laboratory, Didcot, UK*
Zebker H	*Jet Propulsion Laboratory, Pasadena, USA*